Distribution Agreement

In presenting this thesis or dissertation as a partial fulfillment of the requirements for an advanced degree from Emory University, I hereby grant to Emory University and its agents the non-exclusive license to archive, make accessible, and display my thesis or dissertation in whole or in part in all forms of media, now or hereafter known, including display on the world wide web. I understand that I may select some access restrictions as part of the online submission of this thesis or dissertation. I retain all ownership rights to the copyright of the thesis or dissertation. I also retain the right to use in future works (such as articles or books) all or part of this thesis or dissertation.

Signature:

_____   _____
Christina Lester   Date

The Development of VIP Antagonist (ANT) Peptide
Derivatives and Synthetic Approaches towards the Ryptide Macrocycle

By

Christina Lester

Doctor of Philosophy

Chemistry

_____
Simon B. Blakey, PhD.
Advisor

_____
Dennis Liotta, PhD.
Committee Member

_____
Monika Raj, PhD.
Committee Member

Accepted:

_____
Kimberly Jacob Arriola, Ph.D, MPH
Dean of the James T. Laney School of Graduate Studies

_____
Date

The Development of VIP Antagonist (ANT) Peptide
Derivatives and Synthetic Approaches towards the Ryptide Macrocycle

By

Christina Lester
B.S. East Tennessee State University, 2019

Advisor: Simon B. Blakey

An abstract of
A dissertation submitted to the Faculty of the
James T. Laney School of Graduate Studies of Emory University
in partial fulfillment of the requirements for the degree of
Doctor of Philosophy in Chemistry
2024

Abstract

The Development of VIP Antagonist (ANT) Peptide
Derivatives and Synthetic Approaches towards the Ryptide Macrocycle

By Christina Lester

 In part 1 of this dissertation, we will discuss the development of VIP antagonist peptide (ANTs) derivatives. ANTs improve T cell-dependent anti-tumor response in acute myeloid leukemia (AML) murine models. Despite this, peptide therapeutics tend to suffer from poor metabolic stability and subsequently short half-life circulation *in vivo*. We propose three modified ANT derivatives: Ac-ANT308, ANT308C13C17 stp, and ANT308-PEG with the purpose of improving their drug properties. *In vitro* studies found that Ac-ANT308 exhibited diminished T cell activation compared to parental ANT308, indicating N-terminus conservation was critical for antagonist activity. Furthermore, incorporation of cysteines at residues 13 & 17 to accommodate a staple resulted in diminished overall survival and increased tumor burden when dosed in leukemic mice. However, the incorporation of the staple at this position increased survival and reduced tumor burden relative to its unstapled counterpart. Notably, ANT308-PEG had a significant positive effect, and required significantly fewer doses to achieve comparable overall survival and tumor burden in leukemic mice dosed with parental ANT308. In part 2 of this dissertation, we will discuss our investigation of synthetic strategies to access the ribosomally post-translationally modified peptide (RiPP) Ryptide. To date, there is no known synthetic strategy to access the C-C cross-linked RRY macrocycle of the Ryptide family. We explored three synthetic routes to access this macrocycle: metallophotoredox cross-coupling, *ortho*-hydroxylation, and allylic amination. While the first two strategies were unsuccessful, we were able to access the key allylic guanidine tyrosine motif via the allylic amination strategy. Despite accessing the linear protected VGly-Arg-Tyr trimer, we were unable to effectuate ring closing metathesis (RCM) to complete the last major transformation prior to global deprotection to generate the Ryptide macrocycle.

**The Development of VIP Antagonist (ANT) Peptide
Derivatives and Synthetic Approaches towards the Ryptide Macrocycle**

By

Christina Lester
B.S. East Tennessee State University, 2019

Advisor: Simon B. Blakey

A dissertation submitted to the Faculty of the
James T. Laney School of Graduate Studies of Emory University
in partial fulfillment of the requirements for the degree of
Doctor of Philosophy in Chemistry
2024

Acknowledgements

I would like to begin with a big thanks to my advisor, Dr. Simon Blakey for your continued mentorship throughout my PhD. Thank you for being an incredibly supportive mentor and challenging me to become a better scientist. I would also like to thank my committee members, Dr. Dennis Liotta and Dr. Monika Raj for their continued support. Thank you Monika for always being so helpful and providing your expertise in peptide chemistry, your support has been invaluable to my projects and development as a chemist. Thank you Dennis for not just providing insight critical towards my development as a chemist, but providing insight towards alternative careers, and connecting me with the Tech Transfer office here at Emory. You all have been pivotal in my professional development over these past 5 years, and it has been a pleasure to get to know all of you.

Thank you to my lab members, current and past, for supporting my endeavors in lab and never failing to put a smile on my face. You all make the hardships of research worth it. Thank you Patrick for riding out this PhD with me, especially since our cohort was small and only became smaller post-pandemic. It has been awesome sitting next to you for (almost) 5 years. Thank you Keili for your contributions to our Ryptide project, it has been a pleasure working with you. Thank you to our collaborators Ned Waller, Yuou Wang, Jian-Ming Li, and Tenzin Passang for all your hard work on the murine studies on the ANT project. Not only have you all have taught me a great deal about science outside of chemistry, but your contributions also remind me of the reason why we do science: for the greater good of humanity. Thank you to my undergraduate mentors, Casey Elkins and Cassandra Eagle, for fueling my drive and dedication for science which led me to pursue a PhD.

Table of Contents

List of Figures

List of Schemes

List of Tables

Part 1: Chemical Modifications to enhance the Drug Properties of a VIP Antagonist (ANT) Peptide

Chapter 1: Background of VIP and the inception of the VIP antagonist peptides

In this chapter, we will first introduce VIP and its corresponding receptors. We will then discuss their physiological significance and role in various biological processes. After discussing the biological role of VIP, we will discuss the implications of aberrant VIP signaling in various disease states. From there we will discuss the structure activity relationship of VIP with its receptors, then highlight the various agonist/antagonist VIP derivatives that have been studied in the literature. In the second part of this chapter, we will introduce our antagonist VIP design and rationale. From there, we will highlight preliminary work by the Waller lab demonstrating the role of our VIP antagonist in T cell proliferation and activation across various disease models. We will conclude the chapter with an overview of the progression from native VIP to our VIP antagonist.

1.1 Introduction to VIP

1.1.1 VIP and its receptors: implications in physiological processes

Vasoactive intestinal polypeptide (VIP) is a 28-residue neuropeptide initially identified in the central and peripheral nervous systems by Said and Mutt.[1, 2] It has since been documented to be widely distributed throughout the body, serving as a neuromodulator in various organs and tissues including the heart,[3] lung,[4] intestines,[5] and the immune system.[6, 7] VIP belongs to the glucagon/secretin superfamily that regulate class B G-protein coupled receptors (GPCR), and includes related peptides such as pituitary adenylate cyclase activating peptide (PACAP), secretin, growth hormone-releasing factor (GRF), gastric inhibitory polypeptide (GIP), and glucagon-like peptides (GLP1 & GLP2).[8, 9]

PACAP and VIP have high sequence homology, sharing around 70% sequence identity. Studies have demonstrated that VIP acts on two isoforms of a receptor belonging to this family, named VIP/PACAP receptor (VPAC1 & VPAC2). While both VIP and PACAP can activate VPAC1 & VPAC2,[10] the PACAP receptor PAC1 has low affinity with regards to VIP.[11]
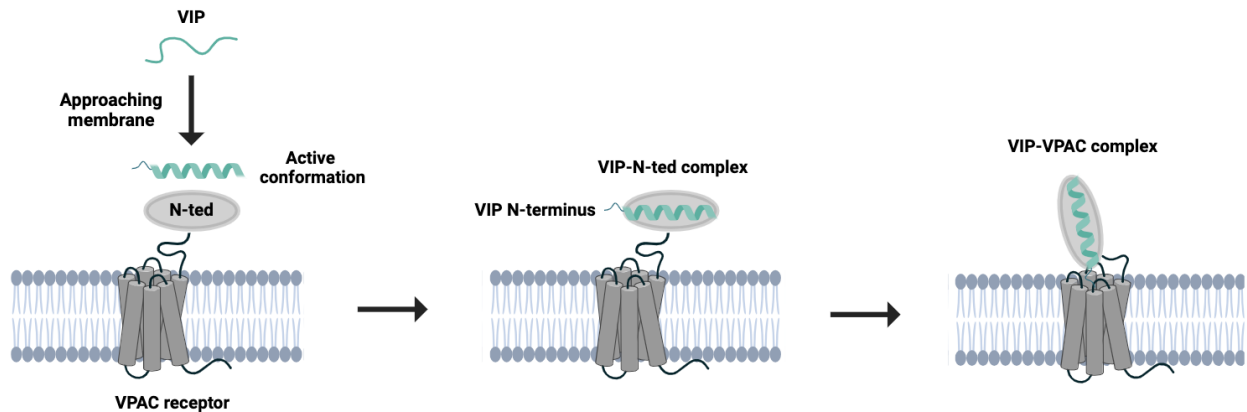
Figure 1.1 VIP docking and binding to its VPAC receptor. VIP folds into its active conformation upon approaching the lipophilic membrane, then binds to the N-ted of VPAC through its α-helix. VIP then interacts with VPAC through its N-terminal region.

The VIP/VPAC signaling pathway is potentiated by cAMP and cGMP-dependent pathways. The VPAC receptors possess 7 transmembrane helical domains typical of GPCRs, a large (>120 residues) and structured N-terminal ectodomain (N-ted) with three highly conserved cysteine disulfide bridges, and glycosylation sites. The N-ted of VPAC represents the major binding site for VIP (**Figure 1.1**). Although both isoforms have high affinity towards VIP, they only share around 55% sequence homology. Furthermore, VPAC1 and VPAC2 differ in their distribution in various organs and have different implications in various physiological processes.[12, 13] For instance, while VPAC1 is widely distributed in the brain and heavily localized in the cerebral cortex and hippocampus, VPAC2 is present mostly in the thalamus.[14, 15] With regards to the structure of the VPAC receptors, more recent

studies have revealed a cryo-EM derived structural elucidation of VPAC1 bound to PACAP27 and VIP.[16, 17] With regards to VIP's structure, the N-terminal region of VIP plays an important role in selective recognition of the VPAC receptors, while the C-terminal α-helical region is important in receptor binding.

In lymphocytes and other immune cell types, VIP modulates innate and adaptive immunity, and possesses anti-inflammatory/immunoregulatory properties. In response to ingesting noxious substances and pathogens, VIP serves to enhance the production of effector cytokines via intestinal type 2 and type 3 innate lymphoid cells (ILC2 & ILC3), leading to their activation. Consequently, VIP increases resistance to intestinal infection by various organisms.[18] Furthermore, VIP modulates the differentiation of CD4+ T helper (Th) cells, increasing host Th2 and T regulatory (Treg) subsets while decreasing pathogenic Th17 cells.[19] Both VPAC1 and VPAC2 modulate the profile of pathogenic memory Th cells, decreasing their expression of transcription factors and cytokine signaling.[19] While both receptors play a significant role in immunomodulation, VPAC1 is more prevalent in T cell profiles compared to VPAC2. For instance, VPAC1 is significantly expressed in resting CD4+ and CD8+ T cells, whereas VPAC2 is seldomly expressed or absent in unstimulated T cells.[20]

1.1.2 Implication of VIP and its receptors in disease states

Given VIP's anti-inflammatory and immunomodulatory functions (**Figure 1.2**), several studies sought to leverage VIP as a means to treat various disease states. Block and co-workers demonstrate the benefits of VIP treatment, of which its utility in the treatment of primary pulmonary hypertension patients led to decreased pulmonary artery pressure and substantial improvement of hemodynamic and prognostic parameters.[21] In patients with multiple sclerosis (MS), intraperitoneal administrations of mesenchymal stem cells (MSCs) as a vehicle to deliver VIP to peripheral immune organs resulted

in inhibited progression and reduced symptoms of MS.[22] In patients with Crohn's disease, Delgado and Gonzalez-Rey utilize VIP-induced regulatory dendritic cells (DC(VIP)) to down-regulate both inflammatory and Th1-drive autoimmune response, providing a new therapeutic perspective.[23] Additionally, more recent studies by Liu and co-workers demonstrated that in patients with type 2 diabetes, VIP stimulates glucose-dependent insulin secretion and has potential to serve as a hypoglycemic therapeutic.[24]
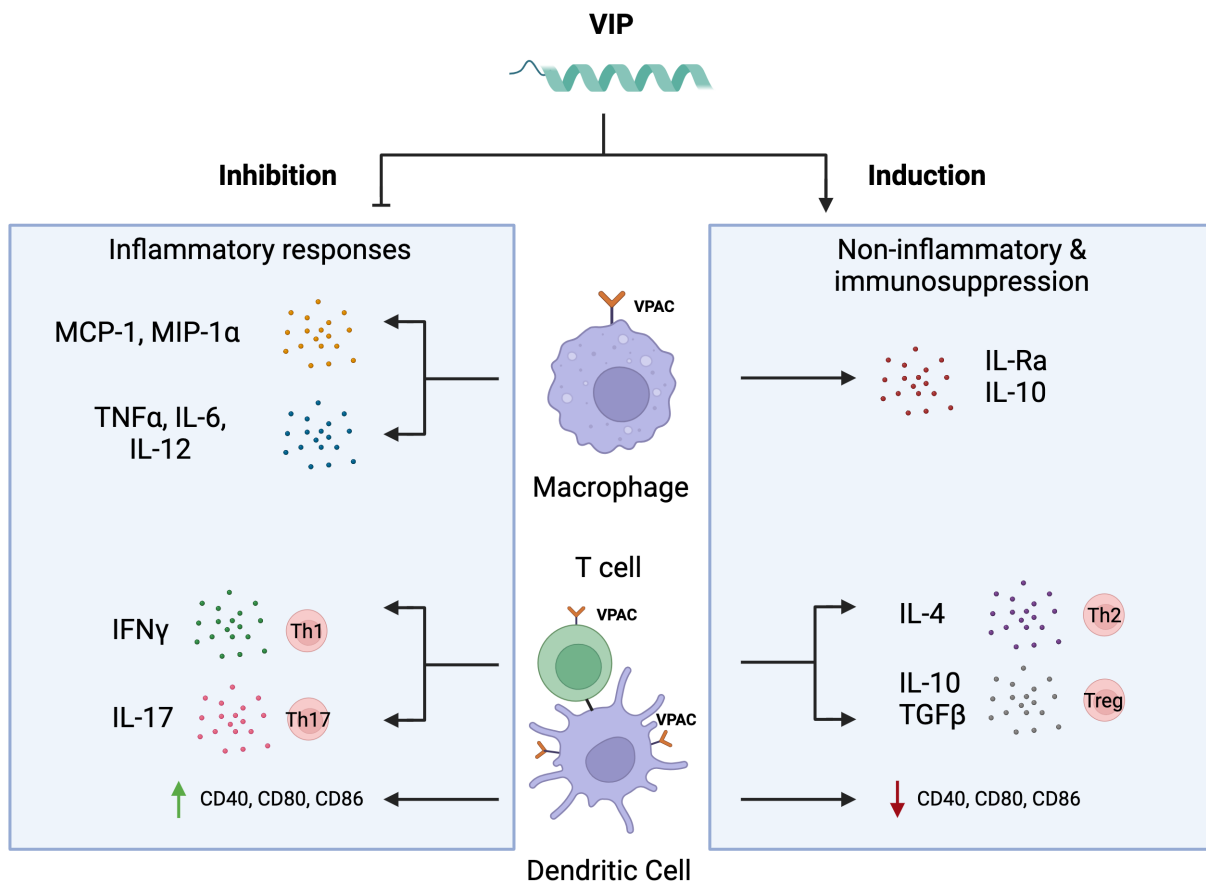
Figure 1.2 VIP plays an important role in immunomodulation. VPAC is expressed in innate (macrophages) and adaptive (T cells & dendritic cells) immunity. VIP inhibits proinflammatory cytokines (TNFα, IL-6, IL-12) and chemokines (MCP-1, MIP-1α), as well as T cells with Th1 and TH17 profiles that maintain inflammation. VIP further promotes production of anti-inflammatory

cytokines (IL-Ra, IL-10) by macrophages, as well as promotes suppressors of immune responses (Treg).[25]

In addition to the myriad of chronic inflammatory conditions alleviated by VIP treatment, VIP has also been investigated heavily in the literature as a proponent of cancer, including breast, bladder, colon, liver, lung, pancreatic, prostate, thyroid, and uterine cancers.[26, 27] These cancers broadly exhibit overexpression of VPAC1, whereas VPAC2 overexpression is typically limited in stromal tumors and neuroendocrine tumors.[27] Given that VIP overexpression is prevalent in a broad range of cancer types, aberrant VIP signaling is purported to play a significant role in tumor growth and differentiation. Furthermore, *in vitro* analysis of a broad range of cancer cell lines demonstrate that VIP stimulates tumor growth.[28] First identified in 1958, VIPomas are a malignant pancreatic neuroendocrine tumor that secretes VIP. Increased VIP serum levels contribute to both tumor formation and secretion of water from intestinal epithelial cells, resulting in symptoms such as watery diarrhea characteristic of the VIPoma syndrome (also known as Verner-Morrison Syndrome).[29-31] Furthermore, overexpression of VIP is associated with an increase in growth factors in prostate cancer tumors, and is believed to contribute towards prostate tumorgenesis.[32] Recent findings by Ago and co-workers suggest that VIP/VPAC2 signaling promotes breast cancer cell migration and metastatic growth.[33] Despite these findings, some literature demonstrate the beneficial effects of VIP in certain cancers, including small-cell lung and gastric cancers.[34, 35]

A deeper analysis of VIP's role in tumor progression reveals its function as an immunosuppressive agent, enabling tumor proliferation and rampant tumorgenesis. Studies have demonstrated that VIP promotes tumorgenesis and proliferation via inhibition of T cell proliferation and disruption of immune homeostatsis. Inhibition of VIP signaling has been shown to enhance CD8+ T cell proliferation in viral infections[36-38] and lymphoma.[6, 39] A recent study by Nishiyama and co-workers

found that in colon cancer models, VIP signaling inhibition enhanced M1 macrophage polarization and phagocytic function, resulting in tumor regression.[40]

1.2   Introduction to ANT peptide series

1.2.1   Historical perspective of VIP agonists

VIP & VIP agonists						
	1 . . . . 6	11 . . . . 16	21 . . . . 26 . . . 31			
VIP	HSDAV FTDNY	TRLRK QMAVK	KYLNS ILN			
Ro 25-1553	Ac-HSDAV FT**E**NY	**TK**LRK Q**Nle**A**A**K	**K***YLND* **LKKGGT**-NH$_2$			
LBT-3627	Ac-H*x*DA*x* FT**E***xy*	**TK**LRK **qNleAA***x*	KY*x*ND **LKkGgT**-NH$_2$			
Stp1*VIP-GK	HSDAV FTDNY	TR**X***RK Q**X***AVK	KYLNS ILN**GK**			

Figure 1.3 Sequence deviation of VIP agonists in literature. Bolded residues indicate amino acid deviation from VIP sequence. * represents incorporation of a staple. Bolded and lowercase represent β3-amino acids. Bolded & italicized lowercase represent cyclic β-amino acids. Nle = norleucine; X = (*S*)-2-(4-pentenyl)Ala-OH; x = cyclic β-amino acid.

In addition to the utility of VIP as a therapeutic agent, several VIP agonists have been developed in literature to enhance its therapeutic potential (**Figure 1.3**). VIP agonists have been developed to treat a myriad of diseases, including several respiratory diseases such as asthma and chronic obstructive pulmonary disease (COPD), Parkinson's disease (PD), and insulin secretion. In addition to VIP agonists, selective agonists towards VPAC1 or VPAC2 have also been developed. In 2003, Linden and co-workers utilize a VIP analog Ro 25-1553 developed by the Bolin group that selectively agonized VPAC2 to treat patients with asthma.[41, 42] This analog possessed both capped N- and C-termini, as well as sequence deviation at residues 8, 12, 17-19, 25-28. Key changes in this structure feature

replacement of Met with Nle, a modification commonly employed due its structural similarity and enhanced stability compared to Met.[43] Additionally, Ro 25-1553 possessed a residue change from Ser[25] to Asp[25] to accommodate an *i,i*+4 lactam staple with Lys[21] to enhance α-helicity. During their screening, most derivatives with staples poised in this location were found to be less potent than VIP; however, this placement in Ro 25-1553 did not affect potency and performed similarly to VIP *in vitro*. Circular dichroism (CD) studies demonstrated the enhanced α-helical character of Ro 25-1553 relative to VIP. It is worth noting that their previous studies found that lactam staples poised at the N-terminus of VIP were significantly less potent or completely inactive.[41]

In 2015, the Gendelman group developed a series of backbone-modified VIP agonists as neuroprotective agents for PD treatment. This derivative series was dubbed LBT, of which these derivatives demonstrated selectivity for VPAC1.[44] These analogs were developed via replacement of α-amino acids with their β-amino acid cognates to alter the covalent spacing between amide groups along the backbone. The aim of this modification was to disrupt protease recognition while retaining the native side chains and α-helical propensity.[45-48] The authors also developed the VPAC2-selective LBT-3627 derivative containing nine β-amino acid residues using Ro 25-1553 as a starting point. Furthermore, LBT-3627 demonstrated significant resistance to proteinase activities, which translated to an improved *in vivo* pharmacokinetic profile compared to previous LBT analogs and VIP. In 2019, the same group further elucidated the neuroprotective effects of LBT-3627 and demonstrated that LBT-3627 induced Tregs to afford neuroprotection.[49]

In 2013, Gill and co-workers sought to develop a VIP derivative for improved VPAC2 agonism and glucose-dependent insulin secretion.[50] Minor modifications to VIP were employed in their control, including transposition of M[17] with Ile to extend half-life circulation.[51] They also opted to incorporate

7

a C-terminal $G^{29} K^{30}$ extension as a means to neutralize the macrodipole and offer helix-capping hydrogen bonds. The authors ultimately sought to develop a series of stapled derivatives around this modified VIP, focused on residue replacement within the α-helical portion of the sequence (residues 10-23). Using GIP and its receptor as a model system, the authors used superimposition of the extracellular domains of GIP and VPAC2 to identify key residues in VIP to be essential to VPAC2 interaction. Of these essential residues, they identified V^{19}, Y^{22}, L^{23}, I^{26}, and L^{27} as essential and thus non-modifiable residues in their subsequent analogs of VIP. Through this study they also identified residues that could be modified with little impact on VPAC2 binding, including L^{13}, M^{17}, K^{21}, N^{24}, S^{25}, and N^{28}. The authors thus opted to design their stapled VIP derivatives around *i,i*+4 replacement of these non-essential residues to effectuate covalent staples and thus enhance rigidity and α-helicity. In addition to exploring lactam staples, they also sought to incorporate olefin non-canonical residues to generate hydrocarbon staples via ring closing metathesis (RCM). Through CD studies, they found that incorporation of lactam staples significantly enhanced α-helicity of the VIP derivatives compared to their non-cyclized forms. This contrasted the hydrocarbon stapled variants, of which both the non-cyclized and cyclized analogs possessed similar α-helicity, likely attributed to the inherent rigidity of the *S*(5)-pentenyl alanine residues. Furthermore, the cyclized lactam analogs possessed ~3-fold increase in estimated α-helicity compared to the cyclized hydrocarbon variants. In terms of functional VPAC2 agonism, employing a staple at positions 13-17, 17-21, and 21-25 led to higher potency for both staple types. Despite the lactam staple at all positions significantly enhancing helicity relative to the hydrocarbons staple, the hydrocarbon staple at positions 13-17 was the most potent analog, exhibiting sub nM EC_{50}. Additionally, this hydrocarbon stapled analog exhibits ~30-fold increase in potency relative to its unstapled cognate, despite possessing similar α-helicities (9.6 vs. 11.6%, respectively). Thus, it appears that α-helicity in this context plays a minor role in VPAC2 binding compared to staple interactions with the receptor, of which the authors propose that a favorable

hydrophobic interaction occurs between the staple at residues 13-17 and the receptor. The significantly more polar lactam staple poised in the same position expectedly yielded significantly lower potency compared to its aliphatic counterpart.

1.2.2 Historical perspective of VIP antagonists & design rationale for 1st generation VIP antagonist peptide

Figure 1.4 Sequence deviation of VIP antagonists in literature. Bolded residues indicate amino acid deviation from VIP sequence.

In contrast to VIP agonism, VIP antagonists have also been employed to address disease states where VIP signaling contributes to disease progression (**Figure 1.4**). VIP competitive antagonists were initially explored in the late 80's and early 90's and were developed to modulate neuronal survival in spinal cord cultures, as well as stimulate amylase release in the pancreas.[51, 52] One of these early antagonists was pioneered by Brenneman and co-workers, of which the antagonist comprised a VIP/neurotensin hybrid dubbed VIPhyb.[53] Hybridization with neurotensin, a 13-resiude neuropeptide, was initially sought to alter the membrane permeability of the VIP portion. Structurally, VIPhyb possesses residues 6 through 11 of neurotensin, replacing the first 6 residues at the N-terminus of VIP. The remaining residues of VIP are retained to preserve the binding capacity of the

C-terminal α-helical portion of VIP. Modification of the native N-terminus of VIP was found to ablate the agonist properties of VIP, effectively furnishing a competitive inhibitor.[54] As such, VIPhyb was found to be 10-fold more potent than VIP in the displacement of radiolabelled VIP. Furthermore, the accumulation of downstream cAMP from VIP signaling was significantly decreased in the presence of VIPhyb, demonstrating its ability to serve as a VIP antagonist. Since its inception, several reports have studied VIPhyb as a potential therapeutic in various disease states, as well as developed VIPhyb derivatives with improved drug properties.[40, 55, 56]

The Waller group initially demonstrated that VIP-knockout (VIP-KO) mice had enhanced cellular immune responses and increased survival post-infection with murine cytomegalovirus (mCMV).[57] Furthermore, they demonstrated that these VIP-KO mice were resistant to mCMV infection compared to their wild-type counterparts, suggesting that VIP signaling plays a role in immunosuppression, potentially via modulation of innate and/or adaptive antiviral immunity.[58] Additional studies revealed that VIPhyb increased the number of effector/memory CD8+ T cells and mature natural killer (NK) cells in mCMV-infected mice. In a later study, they further demonstrated that VIPhyb antagonism of VIP signaling resulted in a significant enhancement of a T cell dependent, autologous anti-leukemia response in murine models of acute myeloid leukemia (AML). Injections of VIPhyb reduced tumor burden in AML mice, as well as enhanced survival compared to controls, suggesting that VIP produced by tumors serves to promote tumor growth and progression.[36]

Given that VIP made by tumors is immunosuppressive, Waller and co-workers sought to perform a comparative study comprising VIP sequences identified across several human cancers, and using this rationale incorporated mutations in pursuit of a more potent VIPhyb. These VIPhyb-based antagonists, dubbed the ANT peptides, were extensively screened for their anti-leukemia activity and binding affinities towards VPAC1 and VPAC2. From this screen, two lead peptides were developed,

dubbed ANT08 and ANT308. The ANT series predominantly differs from VIPhyb with the residue change of L^{25} to S^{25}, as well as incorporation of a capped C-terminus. Furthermore, ANT308 deviates from ANT08 at residues 8 and 9, possessing S^8 and D^9 instead of D^8 and N^9. They demonstrate the efficacy of these ANT derivatives over VIPhyb in their AML models, wherein both peptides exhibit increased overall survival relative to VIPhyb. Furthermore, ANT308 demonstrated a significant increase in CD69 expression in CD4+ and CD8+ T cells and was also demonstrated to render 40% of the mice leukemia-free at day 60 compared to only 5% of mice treated with VIPhyb.[59] Outside of their AML studies, the Waller group also utilized the ANT peptides concomitant with aPD-1 immunotherapy to treat pancreatic ductal adenocarcinoma. In these studies, they found that treatment with ANT08 resulted in transformation of the tumor microenvironment, rendering them susceptible to immunotherapeutics. As such, they demonstrated that this combination therapy reduced tumor burden and increased overall survival of PDAC murine models.[60, 61]

1.3   Concluding Remarks

To conclude this chapter, we have introduced VIP and its receptors VPAC, as well as their ubiquitous role in various physiological processes. The anti-inflammatory properties of VIP have been extensively studied, wherein several studies demonstrate the therapeutic potential of VIP. In contrast, the immunosuppressive properties of VIP have significant consequences in aberrant VIP/VPAC signaling, enabling tumorigenesis and evasion of the immune system. We have discussed literature aimed at developing VIP agonists and antagonists, and highlighted the various modifications incorporated into these VIP derivatives. Finally, we introduce the background of the Waller lab's VIP antagonist ANT peptide series, highlighting their therapeutic potential. Because our objective is to modify the ANT peptides and improve their drug properties, we will discuss in the following chapter

the history of peptides in drug discovery and the subsequent modifications employed to improve their therapeutic potential.

1.4 References

(1) Said, S. I.; Rosenberg, R. N. Vasoactive Intestinal Polypeptide: Abundant Immunoreactivity in Neural Cell Lines and Normal Nervous Tissue. *Science* **1976**, *192* (4242), 907-908. DOI: doi:10.1126/science.1273576.

(2) Said, S. I.; Mutt, V. Polypeptide with Broad Biological Activity: Isolation from Small Intestine. *Science* **1970**, *169* (3951), 1217-1218. DOI: doi:10.1126/science.169.3951.1217.

(3) Henning, R. J.; Sawmiller, D. R. Vasoactive intestinal peptide: cardiovascular effects. *Cardiovascular Research* **2001**, *49* (1), 27-37. DOI: 10.1016/s0008-6363(00)00229-7 (acccessed 3/11/2024).

(4) Miotto, D.; Boschetto, P.; Bononi, I.; Zeni, E.; Cavallesco, G.; Fabbri, L. M.; Mapp, C. E. Vasoactive intestinal peptide receptors in the airways of smokers with chronic bronchitis. *European Respiratory Journal* **2004**, *24* (6), 958-963. DOI: 10.1183/09031936.04.10031504.

(5) Bains, M.; Laney, C.; Wolfe, A. E.; Orr, M.; Waschek, J. A.; Ericsson, A. C.; Dorsam, G. P. Vasoactive Intestinal Peptide Deficiency Is Associated With Altered Gut Microbiota Communities in Male and Female C57BL/6 Mice. *Frontiers in Microbiology* **2019**, *10*, Original Research. DOI: 10.3389/fmicb.2019.02689.

(6) Delgado, M.; Pozo, D.; Ganea, D. The significance of vasoactive intestinal peptide in immunomodulation. *Pharmacol Rev* **2004**, *56* (2), 249-290. DOI: 10.1124/pr.56.2.7   From NLM Medline.

(7) Ganea, D.; Hooper, K. M.; Kong, W. The neuropeptide vasoactive intestinal peptide: direct effects on immune cells and involvement in inflammatory and autoimmune diseases. *Acta Physiologica* **2015**, *213* (2), 442-452. DOI: https://doi.org/10.1111/apha.12427.

(8) Umetsu, Y.; Tenno, T.; Goda, N.; Shirakawa, M.; Ikegami, T.; Hiroaki, H. Structural difference of vasoactive intestinal peptide in two distinct membrane-mimicking environments. *Biochimica et Biophysica Acta (BBA) - Proteins and Proteomics* **2011**, *1814* (5), 724-730. DOI: https://doi.org/10.1016/j.bbapap.2011.03.009.

(9) Couvineau, A.; Laburthe, M. VPAC receptors: structure, molecular pharmacology and interaction with accessory proteins. *British Journal of Pharmacology* **2012**, *166* (1), 42-50. DOI: https://doi.org/10.1111/j.1476-5381.2011.01676.x.

(10) Gourlet, P.; de Neef, P.; Cnudde, J.; Waelbroeck, M.; Robberecht, P. In Vitro Properties of a High Affinity Selective Antagonist of the VIP1 Receptor. *Peptides* **1997**, *18* (10), 1555-1560. DOI: https://doi.org/10.1016/S0196-9781(97)00230-1.

(11) Pisegna, J. R.; Wank, S. A. Molecular cloning and functional expression of the pituitary adenylate cyclase-activating polypeptide type I receptor. *Proceedings of the National Academy of Sciences* **1993**, *90* (13), 6345-6349. DOI: doi:10.1073/pnas.90.13.6345.

(12) St. Hilaire, R.-C.; Murthy, S. N.; Kadowitz, P. J.; Jeter, J. R. Role of VPAC1 and VPAC2 in VIP mediated inhibition of rat pulmonary artery and aortic smooth muscle cell proliferation. *Peptides* **2010**, *31* (8), 1517-1522. DOI: https://doi.org/10.1016/j.peptides.2010.04.024.

(13) Couvineau, A.; Ceraudo, E.; Tan, Y. V.; Nicole, P.; Laburthe, M. The VPAC1 receptor: structure and function of a class B GPCR prototype. *Frontiers in Endocrinology* **2012**, *3*, Review. DOI: 10.3389/fendo.2012.00139.

(14) Usdin, T. B.; Bonner, T. I.; Mezey, E. Two receptors for vasoactive intestinal polypeptide with similar specificity and complementary distributions. *Endocrinology* **1994**, *135* (6), 2662-2680. DOI: 10.1210/endo.135.6.7988457 (acccessed 3/11/2024).

(15) Vertongen, P.; Schiffmann, S. N.; Gourlet, P.; Robberecht, P. Autoradiographic Visualization of the Receptor Subclasses for Vasoactive Intestinal Polypeptide (VIP) in Rat Brain. *Peptides* **1997**, *18* (10), 1547-1554. DOI: https://doi.org/10.1016/S0196-9781(97)00229-5.

(16) Piper, S. J.; Deganutti, G.; Lu, J.; Zhao, P.; Liang, Y.-L.; Lu, Y.; Fletcher, M. M.; Hossain, M. A.; Christopoulos, A.; Reynolds, C. A.; et al. Understanding VPAC receptor family peptide binding and selectivity. *Nature Communications* **2022**, *13* (1), 7013. DOI: 10.1038/s41467-022-34629-3.

(17) Duan, J.; Shen, D.-d.; Zhou, X. E.; Bi, P.; Liu, Q.-f.; Tan, Y.-x.; Zhuang, Y.-w.; Zhang, H.-b.; Xu, P.-y.; Huang, S.-J.; et al. Cryo-EM structure of an activated VIP1 receptor-G protein complex revealed by a NanoBiT tethering strategy. *Nature Communications* **2020**, *11* (1), 4121. DOI: 10.1038/s41467-020-17933-8.

(18) Pascal, M.; Kazakov, A.; Chevalier, G.; Dubrule, L.; Deyrat, J.; Dupin, A.; Saha, S.; Jagot, F.; Sailor, K.; Dulauroy, S.; et al. The neuropeptide VIP potentiates intestinal innate type 2 and type 3 immunity in response to feeding. *Mucosal Immunology* **2022**, *15* (4), 629-641. DOI: 10.1038/s41385-022-00516-9.

(19) Villanueva-Romero, R.; Gutiérrez-Cañas, I.; Carrión, M.; González-Álvaro, I.; Rodríguez-Frade, J. M.; Mellado, M.; Martínez, C.; Gomariz, R. P.; Juarranz, Y. Activation of Th lymphocytes alters pattern expression and cellular location of VIP receptors in healthy donors and early arthritis patients. *Scientific Reports* **2019**, *9* (1), 7383. DOI: 10.1038/s41598-019-43717-2.

(20) Sun, W.; Hong, J.; Zang, Y. C. Q.; Liu, X.; Zhang, J. Z. Altered expression of vasoactive intestinal peptide receptors in T lymphocytes and aberrant Th1 immunity in multiple sclerosis. *International Immunology* **2006**, *18* (12), 1691-1700. DOI: 10.1093/intimm/dxl103 (acccessed 3/11/2024).

(21) Petkov, V.; Mosgoeller, W.; Ziesche, R.; Raderer, M.; Stiebellehner, L.; Vonbank, K.; Funk, G.-C.; Hamilton, G.; Novotny, C.; Burian, B.; et al. Vasoactive intestinal peptide as a new drug for treatment of primary pulmonary hypertension. *The Journal of Clinical Investigation* **2003**, *111* (9), 1339-1346. DOI: 10.1172/JCI17500.

(22) Cobo, M.; Anderson, P.; Benabdellah, K.; Toscano, M. G.; Muñoz, P.; García-Pérez, A.; Gutierrez, I.; Delgado, M.; Martin, F. Mesenchymal Stem Cells Expressing Vasoactive Intestinal Peptide Ameliorate Symptoms in a Model of Chronic Multiple Sclerosis. *Cell Transplantation* **2013**, *22* (5), 839-854. DOI: 10.3727/096368912x657404.

(23) Gonzalez-Rey, E.; Delgado, M. Therapeutic treatment of experimental colitis with regulatory dendritic cells generated with vasoactive intestinal peptide. *Gastroenterology* **2006**, *131* (6), 1799-1811. DOI: 10.1053/j.gastro.2006.10.023 From NLM Medline.

(24) Hou, X.; Yang, D.; Yang, G.; Li, M.; Zhang, J.; Zhang, J.; Zhang, Y.; Liu, Y. Therapeutic potential of vasoactive intestinal peptide and its receptor VPAC2 in type 2 diabetes. *Frontiers in Endocrinology* **2022**, *13*, Review. DOI: 10.3389/fendo.2022.984198.

(25) Abad, C.; Tan, Y.-V. Immunomodulatory Roles of PACAP and VIP: Lessons from Knockout Mice. *Journal of Molecular Neuroscience* **2018**, *66* (1), 102-113. DOI: 10.1007/s12031-018-1150-y.

(26) Iwasaki, M.; Akiba, Y.; Kaunitz, J. Recent advances in vasoactive intestinal peptide physiology and pathophysiology: focus on the gastrointestinal system [version 1; peer review: 4 approved]. *F1000Research* **2019**, *8* (1629). DOI: 10.12688/f1000research.18039.1.

(27) Reubi, J. C.; Läderach, U.; Waser, B.; Gebbers, J.-O.; Robberecht, P.; Laissue, J. A. Vasoactive Intestinal Peptide/Pituitary Adenylate Cyclase-activating Peptide Receptor Subtypes in Human Tumors and Their Tissues of Origin1. *Cancer Research* **2000**, *60* (11), 3105-3112. (acccessed 3/12/2024).

(28) Moody, T. W.; Nuche-Berenguer, B.; Jensen, R. T. Vasoactive intestinal peptide/pituitary adenylate cyclase activating polypeptide, and their receptors and cancer. *Curr Opin Endocrinol Diabetes Obes* **2016**, *23* (1), 38-47. DOI: 10.1097/MED.0000000000000218 From NLM Medline.

(29) Azizian, A.; König, A.; Ghadimi, M. Treatment options of metastatic and nonmetastatic VIPoma: a review. *Langenbeck's Archives of Surgery* **2022**, *407* (7), 2629-2636. DOI: 10.1007/s00423-022-02620-7.

(30) Belei, O.; Basaca, D.-G.; Heredea, E. R.; Iacob, E. R.; Olariu, L.; Folescu, R.; Motoc, A. G. M.; Nanu, A.-M.; Mărginean, O. Chronic Diarrhea Caused by Vasoactive Intestinal Peptide-Secreting Tumor. *Life* **2023**, *13* (10), 1974.

(31) Verner, J. V.; Morrison, A. B. Islet cell tumor and a syndrome of refractory watery diarrhea and hypokalemia. *Am J Med* **1958**, *25* (3), 374-380. DOI: 10.1016/0002-9343(58)90075-5   From NLM Medline.

(32) Fernandez-Martinez, A. B.; Bajo, A. M.; Valdehita, A.; Isabel Arenas, M.; Sanchez-Chapado, M.; Carmena, M. J.; Prieto, J. C. Multifunctional role of VIP in prostate cancer progression in a xenograft model: suppression by curcumin and COX-2 inhibitor NS-398. *Peptides* **2009**, *30* (12), 2357-2364. DOI: 10.1016/j.peptides.2009.09.018   From NLM Medline.

(33) Asano, S.; Yamasaka, M.; Ozasa, K.; Sakamoto, K.; Hayata-Takano, A.; Nakazawa, T.; Hashimoto, H.; Waschek, J. A.; Ago, Y. Vasoactive intestinal peptide–VIPR2 signaling regulates tumor cell migration. *Frontiers in Oncology* **2022**, *12*, Original Research. DOI: 10.3389/fonc.2022.852358.

(34) Chen, L.; Yuan, W.; Chen, Z.; Wu, S.; Ge, J.; Chen, J.; Chen, Z. Vasoactive intestinal peptide represses activation of tumor-associated macrophages in gastric cancer via regulation of TNFalpha, IL-6, IL-12 and iNOS. *Int J Oncol* **2015**, *47* (4), 1361-1370. DOI: 10.3892/ijo.2015.3126   From NLM Medline.

(35) Maruno, K.; Absood, A.; Said, S. I. Vasoactive intestinal peptide inhibits human small-cell lung cancer proliferation *in vitro* and *in vivo*. *Proceedings of the National Academy of Sciences* **1998**, *95* (24), 14373-14378. DOI: doi:10.1073/pnas.95.24.14373.

(36) Petersen, C. T.; Li, J. M.; Waller, E. K. Administration of a vasoactive intestinal peptide antagonist enhances the autologous anti-leukemia T cell response in murine models of acute leukemia. *Oncoimmunology* **2017**, *6* (5), e1304336. DOI: 10.1080/2162402X.2017.1304336 From NLM PubMed-not-MEDLINE.

(37) Li, J.-M.; Hossain, M. S.; Southerland, L.; Waller, E. K. Pharmacological inhibition of VIP signaling enhances antiviral immunity and improves survival in murine cytomegalovirus-infected allogeneic bone marrow transplant recipients. *Blood* **2013**, *121* (12), 2347-2351. DOI: 10.1182/blood-2012-06-437640 (acccessed 3/12/2024).

(38) Youssef, J. G.; Lavin, P.; Schoenfeld, D. A.; Lee, R. A.; Lenhardt, R.; Park, D. J.; Fernandez, J. P.; Morganroth, M. L.; Javitt, J. C.; Jayaweera, D. The Use of IV Vasoactive Intestinal Peptide (Aviptadil) in Patients With Critical COVID-19 Respiratory Failure: Results of a 60-Day Randomized Controlled Trial*. *Critical Care Medicine* **2022**, *50* (11), 1545-1554. DOI: 10.1097/ccm.0000000000005660.

(39) Varela, N.; Chorny, A.; Gonzalez-Rey, E.; Delgado, M. Tuning inflammation with anti-inflammatory neuropeptides. *Expert Opinion on Biological Therapy* **2007**, *7* (4), 461-478. DOI: 10.1517/14712598.7.4.461.

(40) Kittikulsuth, W.; Nakano, D.; Kitada, K.; Uyama, T.; Ueda, N.; Asano, E.; Okano, K.; Matsuda, Y.; Nishiyama, A. Vasoactive intestinal peptide blockade suppresses tumor growth by regulating macrophage polarization and function in CT26 tumor-bearing mice. *Scientific Reports* **2023**, *13* (1), 927. DOI: 10.1038/s41598-023-28073-6.

(41) Bolin, D. R.; Michalewsky, J.; Wasserman, M. A.; O'Donnell, M. Design and development of a vasoactive intestinal peptide analog as a novel therapeutic for bronchial asthma. *Biopolymers* **1995**, *37* (2), 57-66. DOI: https://doi.org/10.1002/bip.360370203.

(42) Lindén, A.; Hansson, L.; Andersson, A.; Palmqvist, M.; Arvidsson, P.; Löfdahl, C.-G.; Larsson, P.; Lötvall, J. Bronchodilation by an inhaled $VPAC_2$ receptor agonist in patients with stable asthma. *Thorax* **2003**, *58* (3), 217-221. DOI: 10.1136/thorax.58.3.217.

(43) Randhawa, Z. I.; Witkowska, H. E.; Cone, J.; Wilkins, J. A.; Hughes, P.; Yamanishi, K.; Yasuda, S.; Masui, Y.; Arthur, P. Incorporation of Norleucine at Methionine Positions in Recombinant Human Macrophage Colony Stimulating Factor (M-CSF, 4-153) Expressed in Escherichia coli: Structural Analysis. *Biochemistry* **1994**, *33* (14), 4352-4362. DOI: 10.1021/bi00180a032.

(44) Olson, K. E.; Kosloski-Bilek, L. M.; Anderson, K. M.; Diggs, B. J.; Clark, B. E.; John M. Gledhill, J.; Shandler, S. J.; Mosley, R. L.; Gendelman, H. E. Selective VIP Receptor Agonists Facilitate Immune Transformation for Dopaminergic Neuroprotection in MPTP-Intoxicated Mice. *The Journal of Neuroscience* **2015**, *35* (50), 16463-16478. DOI: 10.1523/jneurosci.2131-15.2015.

(45) Horne, W. S.; Price, J. L.; Gellman, S. H. Interplay among side chain sequence, backbone composition, and residue rigidification in polypeptide folding and assembly. *Proceedings of the National Academy of Sciences* **2008**, *105* (27), 9151-9156. DOI: doi:10.1073/pnas.0801135105.

(46) Boersma, M. D.; Haase, H. S.; Peterson-Kaufman, K. J.; Lee, E. F.; Clarke, O. B.; Colman, P. M.; Smith, B. J.; Horne, W. S.; Fairlie, W. D.; Gellman, S. H. Evaluation of Diverse α/β-Backbone Patterns

for Functional α-Helix Mimicry: Analogues of the Bim BH3 Domain. *Journal of the American Chemical Society* **2012**, *134* (1), 315-323. DOI: 10.1021/ja207148m.

(47) Cheloha, R. W.; Maeda, A.; Dean, T.; Gardella, T. J.; Gellman, S. H. Backbone modification of a polypeptide drug alters duration of action in vivo. *Nature Biotechnology* **2014**, *32* (7), 653-655. DOI: 10.1038/nbt.2920.

(48) Johnson, L. M.; Barrick, S.; Hager, M. V.; McFedries, A.; Homan, E. A.; Rabaglia, M. E.; Keller, M. P.; Attie, A. D.; Saghatelian, A.; Bisello, A.; et al. A Potent α/β-Peptide Analogue of GLP-1 with Prolonged Action in Vivo. *Journal of the American Chemical Society* **2014**, *136* (37), 12848-12851. DOI: 10.1021/ja507168t.

(49) Mosley, R. L.; Lu, Y.; Olson, K. E.; Machhi, J.; Yan, W.; Namminga, K. L.; Smith, J. R.; Shandler, S. J.; Gendelman, H. E. A Synthetic Agonist to Vasoactive Intestinal Peptide Receptor-2 Induces Regulatory T Cell Neuroprotective Activities in Models of Parkinson's Disease. *Frontiers in Cellular Neuroscience* **2019**, *13*, Original Research. DOI: 10.3389/fncel.2019.00421.

(50) Giordanetto, F.; Revell, J. D.; Knerr, L.; Hostettler, M.; Paunovic, A.; Priest, C.; Janefeldt, A.; Gill, A. Stapled Vasoactive Intestinal Peptide (VIP) Derivatives Improve VPAC2 Agonism and Glucose-Dependent Insulin Secretion. *ACS Med Chem Lett* **2013**, *4* (12), 1163-1168. DOI: 10.1021/ml400257h.

(51) Gozes, I.; Bardea, A.; Reshef, A.; Zamostiano, R.; Zhukovsky, S.; Rubinraut, S.; Fridkin, M.; Brenneman, D. E. Neuroprotective strategy for Alzheimer disease: intranasal administration of a fatty

neuropeptide. *Proceedings of the National Academy of Sciences* **1996**, *93* (1), 427-432. DOI: doi:10.1073/pnas.93.1.427.

(52) Pandol, S. J.; Dharmsathaphorn, K.; Schoeffield, M. S.; Vale, W.; Rivier, J. Vasoactive intestinal peptide receptor antagonist [4Cl-D-Phe6, Leu17] VIP. *American Journal of Physiology-Gastrointestinal and Liver Physiology* **1986**, *250* (4), G553-G557. DOI: 10.1152/ajpgi.1986.250.4.G553.

(53) Gozes, I.; McCune, S. K.; Jacobson, L.; Warren, D.; Moody, T. W.; Fridkin, M.; Brenneman, D. E. An antagonist to vasoactive intestinal peptide affects cellular functions in the central nervous system. *J Pharmacol Exp Ther* **1991**, *257* (3), 959-966. From NLM Medline.

(54) Gozes, I.; Fridkin, M.; Brenneman, D. E. A VIP hybrid antagonist: From developmental neurobiology to clinical applications. *Cellular and Molecular Neurobiology* **1995**, *15* (6), 675-687. DOI: 10.1007/BF02071131.

(55) Zia, H.; Leyton, J.; Casibang, M.; Hau, V.; Brenneman, D.; Fridkin, M.; Gozes, I.; Moody, T. W. (N)-Stearyl, Norleucine17) VIP hybrid inhibits the growth of pancreatic cancer cell lines. *Life Sciences* **1999**, *66* (5), 379-387. DOI: https://doi.org/10.1016/S0024-3205(99)00604-9.

(56) Moody, T. W.; Jensen, R. T.; Fridkin, M.; Gozes, I. (N-stearyl, norleucine17) VIPhybrid is a broad spectrum vasoactive intestinal peptide receptor antagonist. *Journal of Molecular Neuroscience* **2002**, *18* (1), 29-35. DOI: 10.1385/JMN:18:1-2:29.

(57) Li, J.-M.; Southerland, L.; Hossain, M. S.; Giver, C. R.; Wang, Y.; Darlak, K.; Harris, W.; Waschek, J.; Waller, E. K. Absence of Vasoactive Intestinal Peptide Expression in Hematopoietic Cells

Enhances Th1 Polarization and Antiviral Immunity in Mice. *The Journal of Immunology* **2011**, *187* (2), 1057-1065. DOI: 10.4049/jimmunol.1100686 (acccessed 3/13/2024).

(58) Li, J. M.; Darlak, K. A.; Southerland, L.; Hossain, M. S.; Jaye, D. L.; Josephson, C. D.; Rosenthal, H.; Waller, E. K. VIPhyb, an antagonist of vasoactive intestinal peptide receptor, enhances cellular antiviral immunity in murine cytomegalovirus infected mice. *PLoS One* **2013**, *8* (5), e63381. DOI: 10.1371/journal.pone.0063381 From NLM Medline.

(59) Fnu, T. P.; Li, J. M.; Ravindranathan, S.; Waller, E. K. Inhibition of Vasoactive Intestinal Peptide Signaling with More Potent Inhibitors Augments T-Cell Activation and Prolongs Survival in Leukemic Mice. *Blood* **2021**, *138*, 1868-+. DOI: 10.1182/blood-2021-151879.

(60) Ravindranathan, S.; Tenzin, P.; Chandrasekaran, S.; Ware, B.; Zaidi, M.; Wang, S.; Dhamsania, R.; Zhu, J.; Thomas, S.; Majumdar, A.; et al. 819 Targeting vasoactive intestinal peptide receptor signaling: a novel approach to enhance anti-tumor response in pancreatic ductal adenocarcinoma. *Journal for ImmunoTherapy of Cancer* **2020**, *8* (Suppl 3), A489-A491. DOI: 10.1136/jitc-2020-SITC2020.0819.

(61) Ravindranathan, S.; Passang, T.; Li, J.-M.; Wang, S.; Dhamsania, R.; Ware, M. B.; Zaidi, M. Y.; Zhu, J.; Cardenas, M.; Liu, Y.; et al. Targeting vasoactive intestinal peptide-mediated signaling enhances response to immune checkpoint therapy in pancreatic ductal adenocarcinoma. *Nature Communications* **2022**, *13* (1), 6418. DOI: 10.1038/s41467-022-34242-4.

Chapter 2: Introduction to peptide therapeutics & peptide modifications

In this chapter, we will discuss the emergence of peptides as therapeutic targets in drug discovery, highlighting their advantageous properties relative to small molecules and biologics, as well as their ability to target receptors previously classified as "undruggable" by traditional small molecule design. We will further discuss limitations hindering the realization of peptide therapeutics, introducing the concept of peptidomimetics and other modifications. We will finally discuss the various methods developed and utilized by synthetic chemists to enhance the drug properties of peptides, with particular attention towards metabolic stability and half-life circulation.

2.1 Historical perspective and applications of peptide therapeutics

2.1.1 Protein targets in drug discovery

Proteins are large biomolecules consisting of amino acids and are essential to cellular function. Proteins comprise a wide range of biological function, ranging from catalyzing metabolic reactions, DNA replication, and modulating downstream signaling. Proteins are inherently flexible, enabling conformational changes to execute their functions. The chief characteristic of proteins is their ability to bind to other molecules with high specificity and selectivity. The region at which molecules bind to the protein is referred to as the binding site, which conventionally take the form of a depression or pocket.[1] Protein receptors that possess defined binding sites have been attractive targets in drug discovery due to their ability to accommodate small molecule therapeutics (**Figure 2.1A**). This class

of therapeutics generally requires well-defined, hydrophobic binding sites to achieve sufficient affinity for the corresponding receptor. Proteins that possess well-defined binding sites in their inactive form are generally referred to as "druggable" targets, of which a significant class of proteins with cryptic binding or flat, undefined binding sites have historically been referred to as "undruggable" targets.[2] The inability to develop therapeutics targeting the "undruggable" class represents a significant limitation in drug development, limiting the discovery of new therapeutic modalities (**Figure 2.1B**).[3]
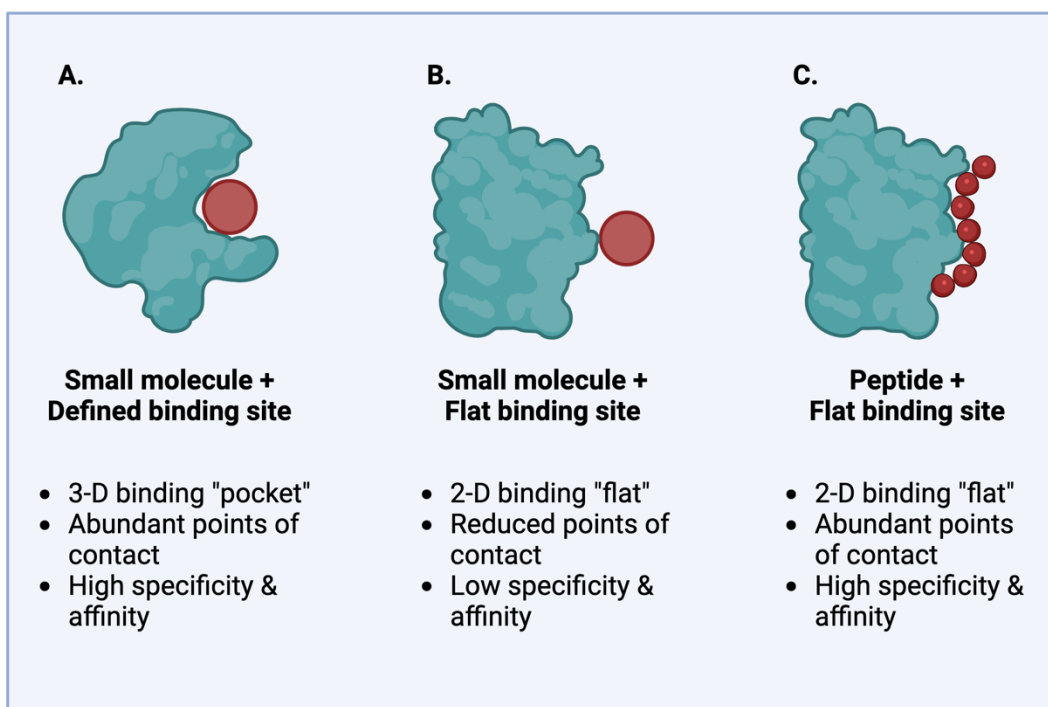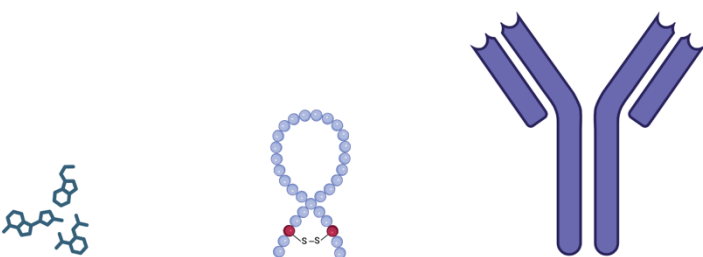
Figure 2.1 A-C Comparison of small molecule vs. peptide properties when binding to shallow vs. defined binding sites. A. Small molecules are designed to target traditional receptors with deep pocket binding sites, enabling high specificity and affinity for these targets. **B.** Small molecules are unable to engage receptors with shallow binding sites in a selective manner with high specificity. **C.** Peptides can engage the extended interface of shallow binding sites, enabling high specificity and affinity for these non-conventional targets.

Protein-protein interactions (PPI) are physical contacts of high specificity between at least two proteins, and are typified by electrostatic forces, hydrogen bonding, and hydrophobic effects, as well as their lack of endogenous small molecular ligands. PPIs form a complex network within cells dubbed the interactome, which is vital in physiological and pathological processes including signal transduction, cell proliferation, differentiation, growth, and apoptosis.[4] The intricacy of this network is further emphasized by the abundance of PPIs, wherein an estimated 130,000-650,000 types of PPIs comprise the human interactome.[5-7] Given their abundance and importance in cellular function, aberrant PPIs are associated with a wide range of disease states, including cancer,[8] infectious,[9] and neurodegenerative diseases,[10] and have been the target of drug discovery for many years. However, due to their relatively flat and shallow binding pockets, utility of traditional small molecule therapeutics is insufficient due to their low affinity and specificity towards these receptors. For instance, the interface area for PPI typically ranges around 1000-2000 Å, much larger than the typical interface of a defined receptor-ligand contact domain at around 300-500 Å.[11] Although small molecule drugs have been developed for PPI in various clinical trial stages, these small molecules possess unusually large molecular weights (>400 Da) compared to traditional small molecules (200-500 Da).[4, 12]

2.1.2 Emergence of peptide therapeutics and their associated challenges

	Small molecule	Peptides	Biologics
Molecular weight	< 500 Da	>700 Da, <1600 Da	150,000 Da
Oral availability	Available	Available	Not available
Can target intracellular receptors?	Yes	Yes	Difficult
Can target PPI?	Difficult	Yes	Yes
Toxicity	High	Low	Low
Metabolic stability	High	Low	Low

Table 2.1 Peptides possess advantageous drug profiles of both small molecules and biologics.

Therapeutic peptides are a distinct class of pharmaceutical agents that typically possess molecular weights exceeding 500 Da but smaller than that of most proteins (<5000 Da).[13] Therapeutic peptides possess an intermediate drug profile between small molecules and biologics, making them attractive targets in drug discovery (**Table 2.1**). Like proteins, endogenous peptides play critical roles in various biological processes, functioning as hormones and other signaling molecules. Unlike traditional small molecules, endogenous peptides can interact with proteins possessing flat and shallow binding sites with high affinity, making them attractive candidates for accessing these "undruggable" targets (**Figure 2.1 C**).[14, 15] Initial research in the utility of peptides as therapeutic agents began in the first half of the 20th century, wherein several bioactive peptides were discovered and isolated. Of note, the

discovery and synthesis of insulin, a large peptide comprised of 51 amino acids, represents a monumental scientific and medical advancement.[16] The discovery of these essential therapeutic peptides catalyzed the development and discovery of other peptide hormones up to the turn of the 21st century.[17] These efforts were further supported by simultaneous advancements in protein purification and synthesis, automated peptide synthesis,[18] structure elucidation,[15] and sequencing[19, 20] during this time. Entering the 21st century, the rapid advancements in peptide drug discovery research established their place as an emergent and competent class of therapeutics. For example, since 2000, the reliance on recombinant insulin was negated by the emergence of 33 non-insulin peptide drugs.[13] To date, therapeutic peptides account for a significant proportion of the pharmaceutical market, with more than 170 peptides in clinical development.[15, 21]

2.2 Introduction to peptidomimetics and peptide modifications

2.2.1 Historical perspective of peptide modifications

Therapeutic peptides are not without their challenges. Similar to biologics, peptides tend to suffer from poor *in vivo* stability, succumbing to endogenous peptidases and other metabolic processes. Thus, peptides suffer from poor half-life circulation; coupled with their poor oral bioavailability, these factors represent significant challenges for oral administration and require frequent intravenous (IV) administration. Additionally, while the large size of peptides enables increased likelihood of binding to hotspots on flat protein surfaces, this feature poses limitations on cell permeability for intracellular protein targets.[22] In order to address these challenges and improve their drug properties, several synthetic modifications have been developed to improve metabolic stability and thus half-life circulation.

27

2.2.2 D-amino acid substitutions

Almost all of the 20 canonical amino acids (except achiral glycine) adopt two conformations due to the presence of the chiral α-carbon. Thus, they exist in either L- or D-configuration (*S* or *R*, respectively). The evolution of biological organisms is predicated on the foundation that enzymes and receptors almost exclusively recognize proteins and peptides derived from the *L*-conformation of amino acids. In contrast, D-amino acids have long been considered unnatural and their occurrence in living organisms is significantly more rare.[23] Nevertheless, research has found that D-amino acids do exist in body fluids and organs of mammals, including humans.[24] Because L-derived enzymes struggle to engage proteins and peptides comprised of D-amino acids, researchers sought to leverage this feature to generate D-amino acid substituted peptides that are more resistant to enzymatic degradation. Additionally, these modified peptides retain the same functional group scaffold, thus maintaining the overall hydrophilicity, charge, and hydrogen bonding capability required of the native peptide for receptor binding and affinity. Overall, the incorporation of D-amino acids enhances metabolic stability and half-life circulation, as well as exhibiting low immunogenicity.[25]

L-peptides
(Right-handed helix)

D-peptides
(Left-handed helix)

L-amino acid
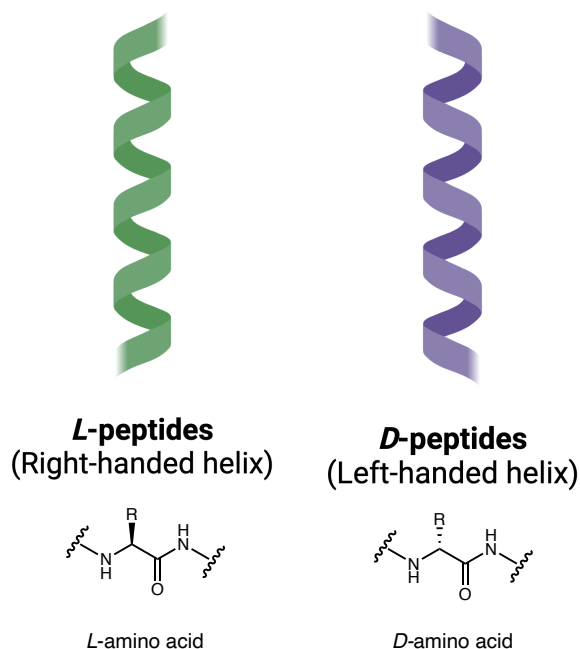
D-amino acid

Figure 2.2 Implications of D-amino acids on peptide secondary structure. Peptides comprised of *L*-amino acids may form a right-handed helix, whereas peptides comprised of *D*-amino acids may form the inverse left-handed helix due to inversion of the stereocenter.

Incorporation of D-amino acids also has significant implications in peptide folding and secondary structure. For instance, D-amino acid substitution is known to disrupt helix formation when poised in the helical portion of a peptide sequence.[26, 27] This strategy has been used to perform structure-activity studies between conformational domains and bioactivity.[28-30] While changes in side chain orientation are beneficial for the lack of D-peptide recognition by enzymes, this also poses a drawback in regard to recognition by the receptor of interest. Retro-inversion was designed to address this consequence and was utilized to preserve the native side chain orientation. In addition to full substitution, the sequence of the D-peptide is reversed, thus restoring the L-amino acid side chain angles. While L-peptides traditionally adopt a right-handed helix, D-peptides adopt a left-handed helix (**Figure 2.2**).[31] Thus, the retro-inverted peptide retains the left-handed helix characteristic of D-

peptides, and as such fail to maintain the secondary structure topology required in specific-protein interactions. Therefore, this strategy is typically limited to unordered peptides that do not possess secondary structures. An alternative method is mirror image phage display (MIPD), a technique used to identify D-peptides that bind to endogenous protein domains. This method involves screening a phage display library of L-peptides with activity towards a D-protein, and then generating the mirror image D-peptides, which bind to the corresponding mirror image L-protein of interest. Limitations to produce recombinant transmembrane domains for testing and limitations in (D)-protein target size represent significant drawbacks of this technique. Current research is underway to develop methods that address these limitations, including a recent report that developed a general protein engineering platform (D)-PDB.[31] As a proof of concept, they developed D-analogs of GLP and PTH1 receptors with increased half-life that retains potency of its natural counterpart.

Several reports have demonstrated the beneficial effects of D-substitution in peptide therapeutics. Lee and co-workers demonstrated that anti-microbial depsipeptide KSLK derivatives containing partial D-amino acid substitution significantly enhanced the stability of the peptide serum.[32] Additionally, replacement of all residues with D-amino acids resulted in a left-hand helical structure that maintained anti-microbial activity. They found that the helical structure was important to activity, wherein replacement of internal residues disrupted helical formation and thus diminished activity. Using structure-assisted design, the Kay group developed a potent trimeric D-peptide inhibitor of HIV-1 entry, demonstrating the ability for D-peptides to interact with high specificity and affinity with natural protein targets.[33] Wu and co-workers utilized mirror image phage display to develop D-peptide MDM2 and MDMX antagonists for the treatment of aberrant p53-associated tumors. Although their D-peptides were resistant to proteolysis, they were unable to transverse the cell membrane and required ligation to a cell penetrating peptide (CPP) for entry.[34] A recent report by Funke and co-workers utilize

both phage display and retro-inversion to develop potent D-peptide Tau fibrilization inhibitors (ISAD$_1$ & ISAD$_{1rev}$, respectively) for the treatment of Alzheimer's disease (AD).[35] Both ISAD$_1$ and ISAD$_{1rev}$ were protease stable and less immunogenic than their native counterparts. Despite the promise of D-amino acid substitution to improve peptide therapeutics, there is currently no D-peptides that have reached the market.[25] Additional efforts to expand screening methods and protein targets have significant promise to enable the development of D-peptide therapeutics.

2.2.3 Macrocyclization of peptides
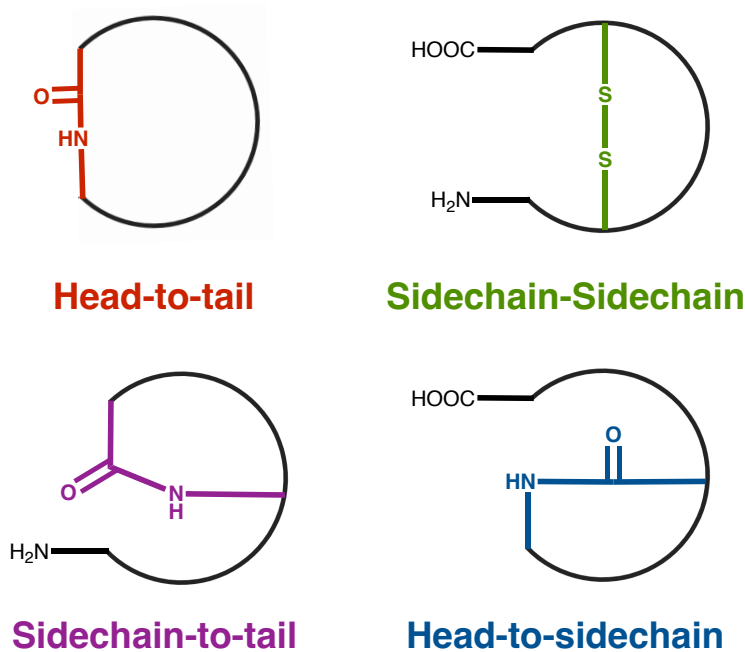
Figure 2.3 Different types of peptide macrocycles. The most common macrocyclic peptides include head-to-tail, sidechain stapling, head-to-sidechain, and sidechain-to-tail. Multiple iterations can be employed to generate multicyclic scaffolds.

Macrocyclic peptides have emerged as an attractive class of drug candidates due to the significant advantages imposed by macrocyclization, including synthetic accessibility, high degree of specific

binding, increased membrane permeability, and increased metabolic stability compared to their linear counterparts.[36, 37] Peptide macrocyclization can be broadly categorized by location of the cyclic element, namely: head-to-tail, sidechain-sidechain "stapling", head-to-sidechain, and sidechain-to-tail (**Figure 2.3**).

A.

B.
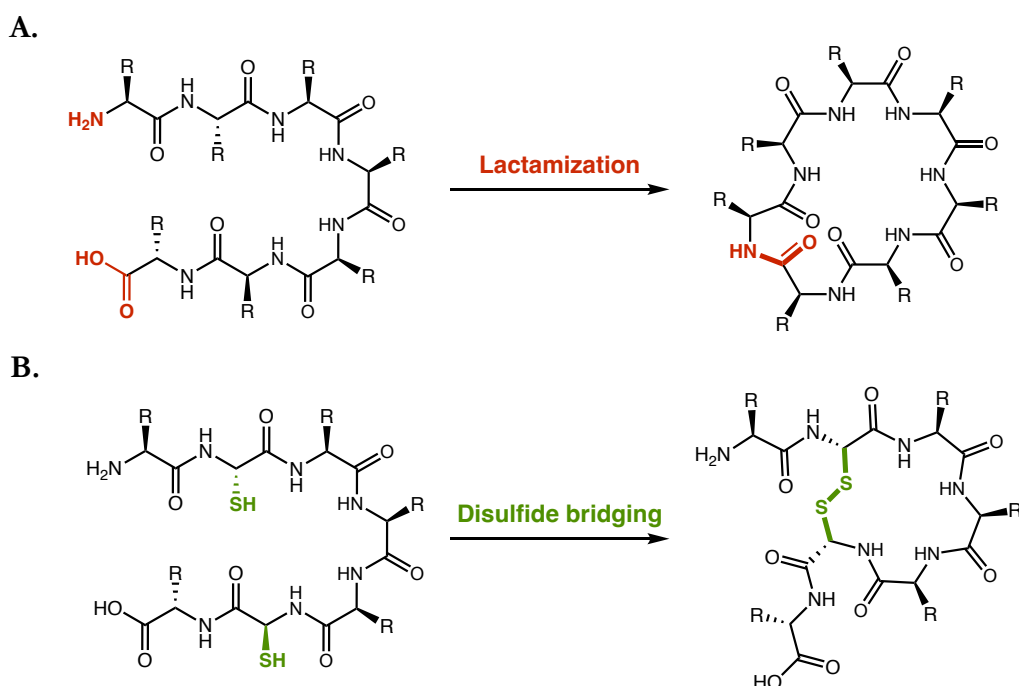
Scheme 2.1 A&B Lactamization and disulfide bridging are common methods that leverage the native functionalities of amino acids. Lactamization is commonly employed in head-to-tail cyclization, as well as side-chain to side-chain cyclization via Lys/Orn and Glu/Asp.

Several synthetic methods have been developed to access these cyclic scaffolds chemoselectively. Lactamization (**Scheme 2.1A**) is a common method used to access macrocycles, especially head-to-tail and side-chain stapling cyclizations.[38] Lactamization relies on the amine and carboxylic acid functionalities inherent of amino acids. Additionally, lactamization can occur either in solution phase or on resin-bound sequences in solid phase synthesis; these features contribute to this method's significant accessibility, making lactamization one of the most commonly employed cyclization

strategy. Disulfide bridging (**Scheme 2.1B**) is another common chemoselective cyclization strategy, utilized both by nature and researchers alike. In biological processes, disulfide bridging is essential to protein folding and stabilizing tertiary or higher order structures.[39] Disulfide bridging occurs via oxidation of cysteine, a relatively rare amino acid with thiol sidechains.[40] This method's ease of accessibility has enabled its use in DNA-encoded libraries, where it serves as a final step in the combinatorial synthesis of cyclic peptides.[41] Although widely accessible, disulfide bridges are considered more transient compared to other cyclization methods, primarily due to their relative weakness and susceptibility towards enzymatic reduction *in vivo*.[42] Inspired by the exquisite reactivity and chemoselectivity afforded through cysteine chemistry, a myriad of other thioether forming synthetic methods have been employed in macrocyclization reactions.[43-46]
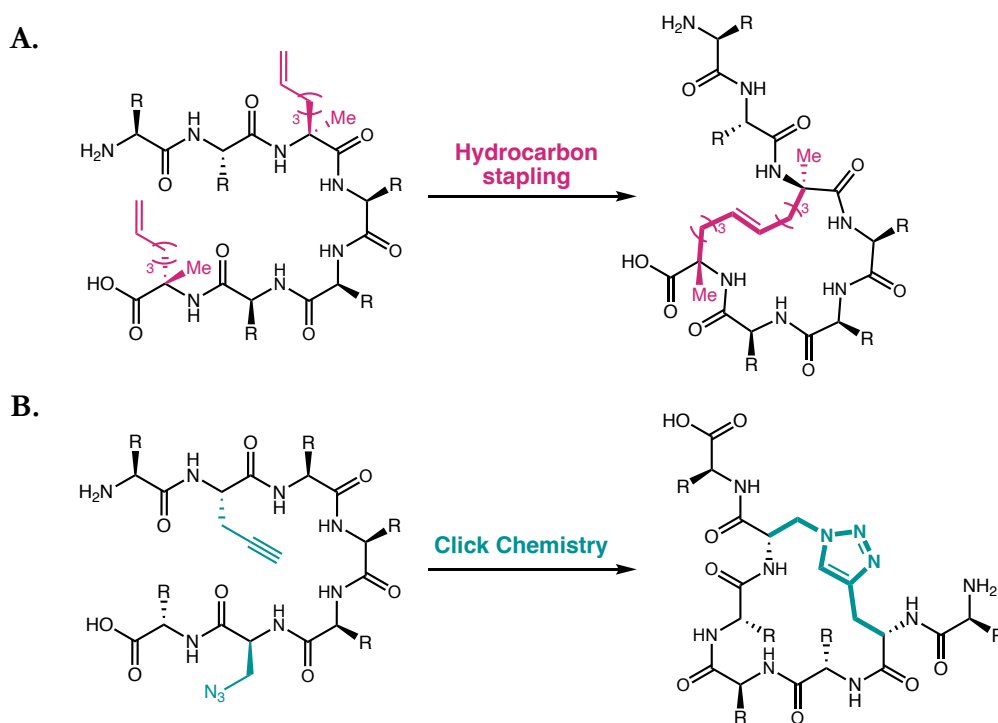
Scheme 2.2 A&B Hydrocarbon stapling and Click chemistry utilize non-canonical residues to effectuate chemoselective cyclizations.

Although the utility of native amino acid functionalities is readily accessible, they are typically limited to cysteine for chemoselective transformations. Furthermore, incorporation of cysteine residues during peptide synthesis requires the utility of noxious thiol reducing agents to prevent deleterious side reactions. The incorporation of non-canonical amino acids expands chemoselective transformations beyond cysteine, allowing for a diverse array of covalent linkers (**Scheme 2.2A&B**). Seminal work by Verdine and co-workers implemented an all-hydrocarbon linker to stabilize and induce α-helical structures in peptides.[47] To effectuate their hydrocarbon staple, they developed a modified α,α-disubstituted alanine residue, of which the α-methyl moiety provided additional rigidity via the helix-stabilization effect. In addition to the methyl, the modified alanine also possessed an aliphatic terminal olefin for ring closing metathesis.[48] While significantly more expensive than canonical residues, the highly stable C-C macrocyclic linker is advantageous over weak disulfide bonds afforded from cysteine. Korsmeyer and co-workers demonstrate the significant potential of this staple type in their seminal work towards a stapled BH_3 peptide, wherein hydrocarbon stapled derivatives (SAHBs) exhibited dramatically enhanced α-helicity, protease-resistance, cell-permeability, and potency towards leukemia cells compared to native BH_3.[49, 50] In addition to 1 turn of the α-helix (*i, i*+4), various linker lengths of the α,α-disubstituted alanine have been developed, accommodating 2 turns (*i, i*+7) and 3 turns (*i, i*+11). Since its introduction, hydrocarbon stapling (**Scheme 2.2A**) has become an essential tool to access various macrocyclic peptides, especially sidechain stapled adducts.[51, 52]
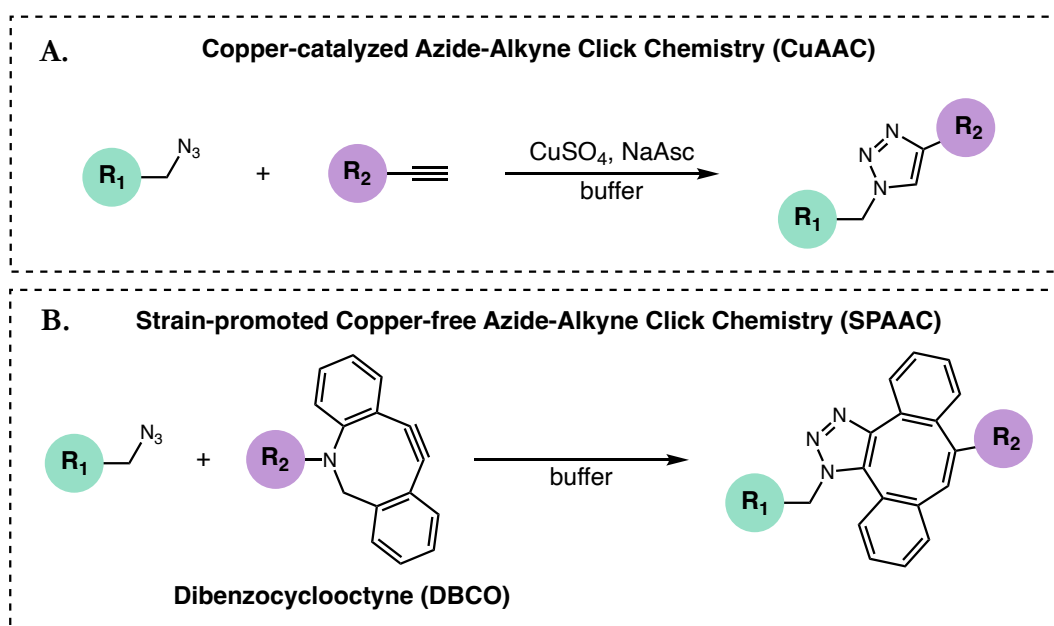
Scheme 2.3 A&B Utility of copper & copper-free click chemistry. In contrast to CuAAC, SPAAC leverages strain to circumvent the need for cytotoxic copper catalysts when generating the triazole linker.

Developed by Sharpless and colleagues in 2001, azide-alkyne "click" chemistry (**Scheme 2.3A**) has revolutionized both chemistry and biology alike.[53] Boasting exquisite chemoselectivity, high yields, minimal to no byproducts, and simplistic setup, it is no surprise that click chemistry would find broad utility in the field of peptide macrocyclization. To date, several amino acids possessing moieties required for click chemistry have become readily accessible, including azido-lysine/azido-ornithine and corresponding alkynylated amino acids. Additionally, dibenzylcyclooctyne (DBCO) amino acids have also been utilized to engage copper-free click macrocyclizations (**Scheme 2.3B**).[54] Further research has revealed that the triazole linker formed from click chemistry can serve as a bioisostere of amide bonds, providing a more stable surrogate to lactam linkers susceptible to peptidases.[55, 56]

2.2.4 Peptoid and other backbone modifications
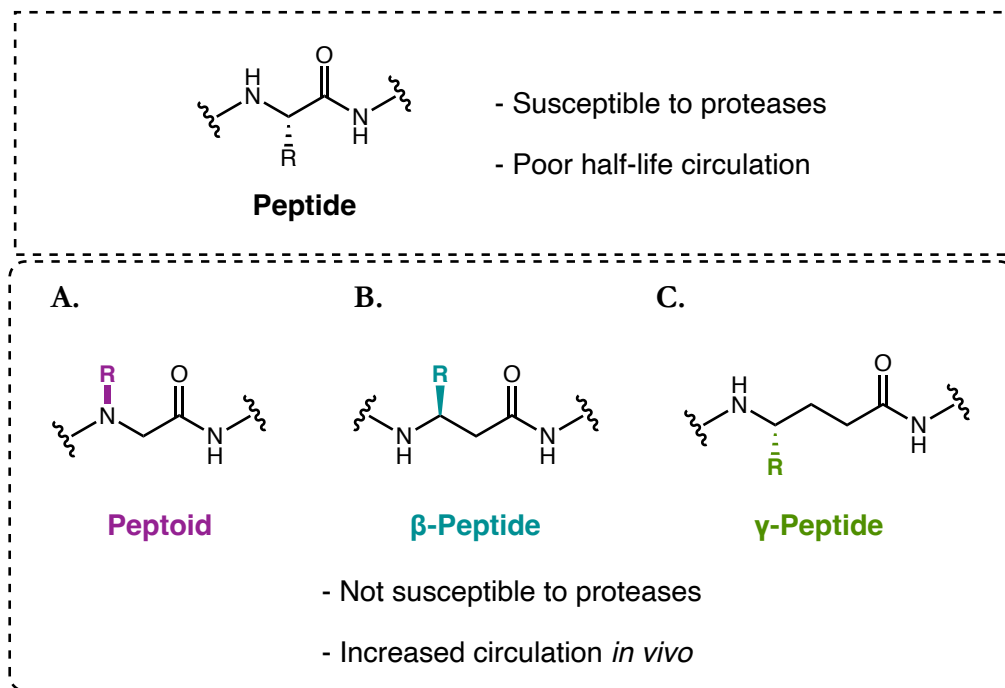
Figure 2.4 A-C Different classes of peptidomimetics possessing modified peptide backbones.
β- & γ-residues incorporate additional carbon units along the backbone, whereas peptoids are characterized by tertiary amides incorporating the side chain. Inclusion of peptidomimetics increases proteolytic resistance, thereby increasing half-life circulation *in vivo*.

Similar to D-amino acids, peptidomimetics aim to enhance proteolytic stability while retaining the native side chains of the parental amino acid. Instead of inverting the 3-D conformation of the amino acid, this class of modification incorporates the side chain at different locations along the peptide backbone. Oligo-*N*-substituted glycines, dubbed peptoids (**Figure 2.4A**), are perhaps the most well-studied and commonly employed peptidomimetic, and have been utilized in the development of therapeutics and diagnostics.[57, 58] Peptoids possess side chains at the amide nitrogen rather than the α-carbon, generating pseudo-glycine derivatives that lack stereocenters unlike their native cognates. These oligo-tertiary amides are resistant to enzymatic degradation. Furthermore, the ablation of the

amide proton along the backbone imparts significant flexibility due to the lack of hydrogen bonding networks critical to secondary structure formation. The backbone tertiary amides can adopt *cis-* or *trans-*conformations, of which secondary structures are derived exclusively from steric and/or electronic interactions.[59] Thus, peptoids are resistant to denaturing under changes to solvent or temperatures compared to their peptide counterparts.
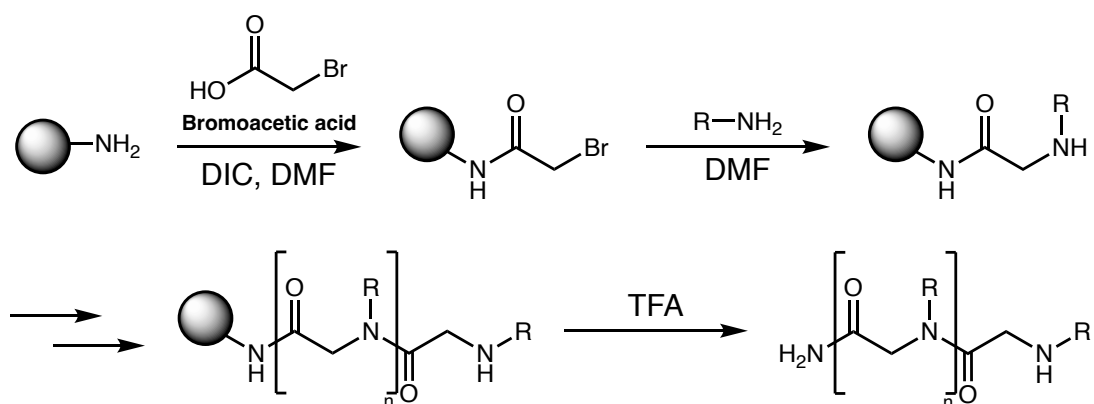
Scheme 2.4 Solid phase synthesis of *N*-glycine peptoids. Synthesis begins with peptide coupling between the amine-bound resin and bromoacetic acid. SN$_2$ displacement with the desired primary amine generates the peptoid monomer. This process is repeated until the desired length is achieved, then cleaved from resin to deliver the peptoid.

Zuckermann et al. have adapted solid phase synthesis to accommodate peptoid bulding blocks (**Scheme 2.4**).[60] This synthetic method is comprised of two principal steps: first, acylation using a haloacetic acid, followed by displacement with a primary amine. In addition to peptoids, other classes of peptidomimetics have been studied and demonstrated to serve as enhanced mimetics, including β-peptides (**Figure 2.4B**)[61, 62] and γ-amino acid derivatives (**Figure 2.4C**).[63, 64] In an effort to develop peptide therapeutics with improved drug properties, peptoids have been employed along with additional modifications, including cyclization and the formation of chimeras with peptides.[65-67]

2.2.5 Peptide-biomolecule conjugates
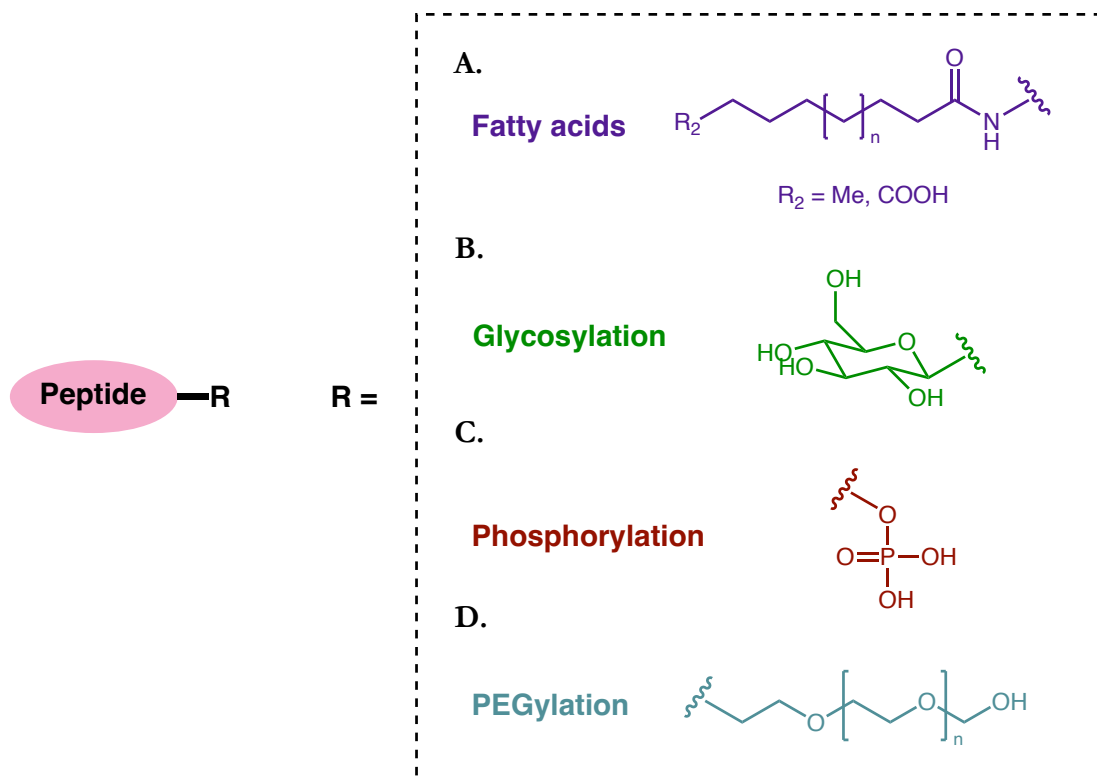
Figure 2.5 A-D Different classes of biomolecules employed in therapeutic peptide conjugates.

Bioconjugation of various molecules onto therapeutics is a common method to improve multiple parameters in drug development, including stability, targetability, and potency.[68] For peptide therapeutics, inclusion of fatty acid chains (**Figure 2.5A**) is commonly employed to improve drug solubility, absorption, and half-life circulation. Incorporation of lipophilic elements enhances interactions of the peptides with membrane-bound targets due to the lipophilic properties of the phospholipid membrane, increasing target affinity.[69] Furthermore, the inert fatty acid chains delay enzymatic degradation, increasing the longevity of the peptide conjugate.[70] Incorporation of fatty acids

have been used to develop a next-generation insulin derivative, Levemir, with improved solubility and duration of action.[71] In addition to the improvement of pharmacokinetic properties, incorporation of fatty acids has been demonstrated to improve antimicrobial activity of antibacterial peptides. For example, a study by Uhl et al. demonstrated that medium length fatty acid replacement of the hydrophobic motif of Pep19-4LF enhanced its antimicrobial activity.[72] Importantly, the fatty acid replacement not only enhanced activity but also increased solubility and decreased aggregation in biological media compared to the original hydrophobic motif of Pep19-4LF.

Glycosylation (**Figure 2.5B**) and phosphorylation (**Figure 2.5C**) are post-translational enzymatic modifications that play a critical role in mediating physiological processes. The incorporation of phosphoryl or glycosyl units onto proteins serve various functions, including regulation of protein function, signaling, localization, and triggering events such as protein folding and apoptosis.[73, 74] Due to their ubiquitous presence in cell signaling and function, their incorporation in peptide therapeutics has been utilized to improve biodistribution and target specificity. Additionally, incorporation of these moieties has been demonstrated to enhance bioavailability, metabolic stability, and reduce aggregation & denaturation.[75, 76] Phosphorylated immunopeptides have been implicated as promising immunotherapy anti-cancer targets, and glycopeptides comprise an important class of last-resort antibiotics, including vancomycin and telavancin.[77, 78]

Polyethylene glycol (PEG) is a non-immunogenic biomolecule that has traditionally been utilized as a spacer in a wide array of peptide drug conjugates (**Figure 2.5D**). However, PEG has also been leveraged for its unique properties in the pursuit of enhanced peptide therapeutics, of which its hydrophilic and inert functionalities modulate solubility and increase metabolic stability. Since the approval of Adagen in the 90's, several PEGylated compounds have been developed and approved

for therapeutic use, including small molecules, biologics and lipid nanoparticles.[79] PEGylation has also been extensively studied in peptides.[80] For example, PEGylation of the antimicrobial peptide LyeTx I-b resulted in a derivative with decreased tissue toxicity and increased metabolic stability *in vivo* without compromising antimicrobial activity.[81] PEG size plays a significant role in the modulation of peptide stability and function, wherein larger PEG moieties impart reduced renal clearance and increased half-life circulation, but with a greater risk of interference and thus reduced efficacy. Nevertheless, PEGylation remains a popular approach to modulate the pharmacokinetic properties of various therapeutic classes.

2.3 Concluding remarks

In conclusion, the emergence of peptide-based therapeutics has great potential to address protein targets previously classified as undruggable due to their shallow binding interface. These protein-protein interactions are ubiquitous to a wide range of physiological processes, and thus yield great potential for developing therapeutics with novel modalities. Despite their promise, peptide therapeutics suffer from limitations including poor metabolic stability and thus half-life circulation. To address these issues and improve the pharmacokinetic profiles of peptides, several classes of modifications have been developed, including but not limited to: D-amino acid substitution, macrocyclization, and biomolecule conjugation. In the subsequent chapter, we will discuss our strategy to modify and improve the drug properties of the VIP peptide antagonist ANT308.

2.4 References

(1) Stank, A.; Kokh, D. B.; Fuller, J. C.; Wade, R. C. Protein Binding Pocket Dynamics. *Accounts of Chemical Research* **2016**, *49* (5), 809-815. DOI: 10.1021/acs.accounts.5b00516.

(2) Shan, Y.; Mysore, V. P.; Leffler, A. E.; Kim, E. T.; Sagawa, S.; Shaw, D. E. How does a small molecule bind at a cryptic binding site? *PLoS Comput Biol* **2022**, *18* (3), e1009817. DOI: 10.1371/journal.pcbi.1009817 From NLM Medline.

(3) Xie, X.; Yu, T.; Li, X.; Zhang, N.; Foster, L. J.; Peng, C.; Huang, W.; He, G. Recent advances in targeting the "undruggable" proteins: from drug discovery to clinical trials. *Signal Transduction and Targeted Therapy* **2023**, *8* (1), 335. DOI: 10.1038/s41392-023-01589-z.

(4) Lu, H.; Zhou, Q.; He, J.; Jiang, Z.; Peng, C.; Tong, R.; Shi, J. Recent advances in the development of protein–protein interactions modulators: mechanisms and clinical trials. *Signal Transduction and Targeted Therapy* **2020**, *5* (1), 213. DOI: 10.1038/s41392-020-00315-3.

(5) Venkatesan, K.; Rual, J.-F.; Vazquez, A.; Stelzl, U.; Lemmens, I.; Hirozane-Kishikawa, T.; Hao, T.; Zenkner, M.; Xin, X.; Goh, K.-I.; et al. An empirical framework for binary interactome mapping. *Nature Methods* **2009**, *6* (1), 83-90. DOI: 10.1038/nmeth.1280.

(6) Nero, T. L.; Morton, C. J.; Holien, J. K.; Wielens, J.; Parker, M. W. Oncogenic protein interfaces: small molecules, big challenges. *Nature Reviews Cancer* **2014**, *14* (4), 248-262. DOI: 10.1038/nrc3690.

(7) Stumpf, M. P. H.; Thorne, T.; de Silva, E.; Stewart, R.; An, H. J.; Lappe, M.; Wiuf, C. Estimating the size of the human interactome. *Proceedings of the National Academy of Sciences* **2008**, *105* (19), 6959-6964. DOI: doi:10.1073/pnas.0708078105.

(8) Cheng, S.-S.; Yang, G.-J.; Wang, W.; Leung, C.-H.; Ma, D.-L. The design and development of covalent protein-protein interaction inhibitors for cancer treatment. *Journal of Hematology & Oncology* **2020**, *13* (1), 26. DOI: 10.1186/s13045-020-00850-0.

(9) Li, S.; Zhou, W.; Li, D.; Pan, T.; Guo, J.; Zou, H.; Tian, Z.; Li, K.; Xu, J.; Li, X.; et al. Comprehensive characterization of human–virus protein-protein interactions reveals disease comorbidities and potential antiviral drugs. *Computational and Structural Biotechnology Journal* **2022**, *20*, 1244-1253. DOI: https://doi.org/10.1016/j.csbj.2022.03.002.

(10) Calabrese, G.; Molzahn, C.; Mayor, T. Protein interaction networks in neurodegenerative diseases: From physiological function to aggregation. *J Biol Chem* **2022**, *298* (7), 102062. DOI: 10.1016/j.jbc.2022.102062 From NLM Medline.

(11) Ran, X.; Gestwicki, J. E. Inhibitors of protein–protein interactions (PPIs): an analysis of scaffold choices and buried surface area. *Current Opinion in Chemical Biology* **2018**, *44*, 75-86. DOI: https://doi.org/10.1016/j.cbpa.2018.06.004.

(12) Scott, D. E.; Bayly, A. R.; Abell, C.; Skidmore, J. Small molecules, big targets: drug discovery faces the protein–protein interaction challenge. *Nature Reviews Drug Discovery* **2016**, *15* (8), 533-550. DOI: 10.1038/nrd.2016.29.

(13) Wang, L.; Wang, N.; Zhang, W.; Cheng, X.; Yan, Z.; Shao, G.; Wang, X.; Wang, R.; Fu, C. Therapeutic peptides: current applications and future directions. *Signal Transduct Target Ther* **2022**, *7* (1), 48. DOI: 10.1038/s41392-022-00904-4 From NLM Medline.

(14) Wang, X.; Ni, D.; Liu, Y.; Lu, S. Rational Design of Peptide-Based Inhibitors Disrupting Protein-Protein Interactions. *Frontiers in Chemistry* **2021**, *9*, Review. DOI: 10.3389/fchem.2021.682675.

(15) Lau, J. L.; Dunn, M. K. Therapeutic peptides: Historical perspectives, current development trends, and future directions. *Bioorganic & Medicinal Chemistry* **2018**, *26* (10), 2700-2707. DOI: https://doi.org/10.1016/j.bmc.2017.06.052.

(16) Vecchio, I.; Tornali, C.; Bragazzi, N. L.; Martini, M. The Discovery of Insulin: An Important Milestone in the History of Medicine. *Front Endocrinol (Lausanne)* **2018**, *9*, 613. DOI: 10.3389/fendo.2018.00613 From NLM PubMed-not-MEDLINE.

(17) Muttenthaler, M.; King, G. F.; Adams, D. J.; Alewood, P. F. Trends in peptide drug discovery. *Nature Reviews Drug Discovery* **2021**, *20* (4), 309-325. DOI: 10.1038/s41573-020-00135-8.

(18) Merrifield, R. B. Solid Phase Peptide Synthesis. I. The Synthesis of a Tetrapeptide. *Journal of the American Chemical Society* **1963**, *85* (14), 2149-2154. DOI: 10.1021/ja00897a025.

(19) Sanger, F.; Tuppy, H. The amino-acid sequence in the phenylalanyl chain of insulin. I. The identification of lower peptides from partial hydrolysates. *Biochem J* **1951**, *49* (4), 463-481. DOI: 10.1042/bj0490463 From NLM Medline.

(20) Sanger, F.; Thompson, E. O. The amino-acid sequence in the glycyl chain of insulin. II. The investigation of peptides from enzymic hydrolysates. *Biochem J* **1953**, *53* (3), 366-374. DOI: 10.1042/bj0530366 From NLM Medline.

(21) Henninot, A.; Collins, J. C.; Nuss, J. M. The Current State of Peptide Drug Discovery: Back to the Future? *Journal of Medicinal Chemistry* **2018**, *61* (4), 1382-1414. DOI: 10.1021/acs.jmedchem.7b00318.

(22) Rossino, G.; Marchese, E.; Galli, G.; Verde, F.; Finizio, M.; Serra, M.; Linciano, P.; Collina, S. Peptides as Therapeutic Agents: Challenges and Opportunities in the Green Transition Era. *Molecules* **2023**, *28* (20). DOI: 10.3390/molecules28207165 From NLM Medline.

(23) Kreil, G. d-AMINO ACIDS IN ANIMAL PEPTIDES. *Annual Review of Biochemistry* **1997**, *66* (1), 337-345. DOI: 10.1146/annurev.biochem.66.1.337.

(24) Souza, I. N. O.; Roychaudhuri, R.; de Belleroche, J.; Mothet, J. P. d-Amino acids: new clinical pathways for brain diseases. *Trends Mol Med* **2023**, *29* (12), 1014-1028. DOI: 10.1016/j.molmed.2023.09.001 From NLM Medline.

(25) Lander, A. J.; Jin, Y.; Luk, L. Y. P. D-Peptide and D-Protein Technology: Recent Advances, Challenges, and Opportunities**. *ChemBioChem* **2023**, *24* (4), e202200537. DOI: https://doi.org/10.1002/cbic.202200537.

(26) Fairman, R.; Anthony-Cahill, S. J.; DeGrado, W. F. The helix-forming propensity of D-alanine in a right-handed .alpha.-helix. *Journal of the American Chemical Society* **1992**, *114* (13), 5458-5459. DOI: 10.1021/ja00039a086.

(27) Krause, E.; Bienert, M.; Schmieder, P.; Wenschuh, H. The Helix-Destabilizing Propensity Scale of d-Amino Acids: The Influence of Side Chain Steric Effects. *Journal of the American Chemical Society* **2000**, *122* (20), 4865-4870. DOI: 10.1021/ja9940524.

(28) Pouny, Y.; Shai, Y. Interaction of D-amino acid incorporated analogues of pardaxin with membranes. *Biochemistry* **1992**, *31* (39), 9482-9490. DOI: 10.1021/bi00154a022 From NLM Medline.

(29) BECK-SICKINGER, A. G.; GAIDA, W.; SCHNORRENBERG, G.; LANG, R.; JUNG, G. Neuropeptide Y: identification of the binding site. *International Journal of Peptide and Protein Research* **1990**, *36* (6), 522-530. DOI: https://doi.org/10.1111/j.1399-3011.1990.tb00991.x.

(30) Grundemar, L.; Kahl, U.; Callréus, T.; Langel, Ü.; Bienert, M.; Beyermann, M. Ligand binding and functional effects of systematic double d-amino acid residue substituted neuropeptide Y analogs on Y1 and Y2 receptor types. *Regulatory Peptides* **1996**, *62* (2), 131-136. DOI: https://doi.org/10.1016/0167-0115(96)00011-0.

(31) Garton, M.; Nim, S.; Stone, T. A.; Wang, K. E.; Deber, C. M.; Kim, P. M. Method to generate highly stable D-amino acid analogs of bioactive helical peptides using a mirror image of the entire PDB. *Proceedings of the National Academy of Sciences* **2018**, *115* (7), 1505-1510. DOI: doi:10.1073/pnas.1711837115.

(32) Hong, S. Y.; Oh, J. E.; Lee, K.-H. Effect of d-amino acid substitution on the stability, the secondary structure, and the activity of membrane-active peptide. *Biochemical Pharmacology* **1999**, *58* (11), 1775-1780. DOI: https://doi.org/10.1016/S0006-2952(99)00259-2.

(33) Welch, B. D.; VanDemark, A. P.; Heroux, A.; Hill, C. P.; Kay, M. S. Potent D-peptide inhibitors of HIV-1 entry. *Proceedings of the National Academy of Sciences* **2007**, *104* (43), 16828-16833. DOI: doi:10.1073/pnas.0708109104.

(34) Liu, M.; Li, C.; Pazgier, M.; Li, C.; Mao, Y.; Lv, Y.; Gu, B.; Wei, G.; Yuan, W.; Zhan, C.; et al. D-peptide inhibitors of the p53–MDM2 interaction for targeted molecular therapy of malignant neoplasms. *Proceedings of the National Academy of Sciences* **2010**, *107* (32), 14321-14326. DOI: doi:10.1073/pnas.1008930107.

(35) Aillaud, I.; Kaniyappan, S.; Chandupatla, R. R.; Ramirez, L. M.; Alkhashrom, S.; Eichler, J.; Horn, A. H. C.; Zweckstetter, M.; Mandelkow, E.; Sticht, H.; et al. A novel D-amino acid peptide with therapeutic potential (ISAD1) inhibits aggregation of neurotoxic disease-relevant mutant Tau and prevents Tau toxicity in vitro. *Alzheimer's Research & Therapy* **2022**, *14* (1), 15. DOI: 10.1186/s13195-022-00959-z.

(36) Bechtler, C.; Lamers, C. Macrocyclization strategies for cyclic peptides and peptidomimetics. *RSC Medicinal Chemistry* **2021**, *12* (8), 1325-1351, 10.1039/D1MD00083G. DOI: 10.1039/D1MD00083G.

(37) Vinogradov, A. A.; Yin, Y.; Suga, H. Macrocyclic Peptides as Drug Candidates: Recent Progress and Remaining Challenges. *J Am Chem Soc* **2019**, *141* (10), 4167-4181. DOI: 10.1021/jacs.8b13178.

(38) Posada, L.; Serra, G. Three Methods for Peptide Cyclization Via Lactamization. *Methods Mol Biol* **2022**, *2371*, 3-17. DOI: 10.1007/978-1-0716-1689-5_1 From NLM Medline.

(39) Bechtel, T. J.; Weerapana, E. From structure to redox: The diverse functional roles of disulfides and implications in disease. *Proteomics* **2017**, *17* (6). DOI: 10.1002/pmic.201600391 From NLM Medline.

(40) Poole, L. B. The basics of thiols and cysteines in redox biology and chemistry. *Free Radic Biol Med* **2015**, *80*, 148-157. DOI: 10.1016/j.freeradbiomed.2014.11.013 From NLM Medline.

(41) Pham, M. V.; Bergeron-Brlek, M.; Heinis, C. Synthesis of DNA-Encoded Disulfide- and Thioether-Cyclized Peptides. *ChemBioChem* **2020**, *21* (4), 543-549. DOI: https://doi.org/10.1002/cbic.201900390.

(42) Arunachalam, B.; Phan, U. T.; Geuze, H. J.; Cresswell, P. Enzymatic reduction of disulfide bonds in lysosomes: Characterization of a Gamma-interferon-inducible lysosomal thiol reductase (GILT). *Proceedings of the National Academy of Sciences* **2000**, *97* (2), 745-750. DOI: doi:10.1073/pnas.97.2.745.

(43) Meng, G.; Pu, J.; Li, Y.; Han, A.; Tian, Y.; Xu, W.; Zhang, T.; Li, X.; Lu, L.; Wang, C.; et al. Design and Biological Evaluation of m-Xylene Thioether-Stapled Short Helical Peptides Targeting the HIV-1 gp41 Hexameric Coiled–Coil Fusion Complex. *Journal of Medicinal Chemistry* **2019**, *62* (19), 8773-8783. DOI: 10.1021/acs.jmedchem.9b00882.

(44) Ji, P.; Zhang, Y.; Wei, Y.; Huang, H.; Hu, W.; Mariano, P. A.; Wang, W. Visible-Light-Mediated, Chemo- and Stereoselective Radical Process for the Synthesis of C-Glycoamino Acids. *Org Lett* **2019**, *21* (9), 3086-3092. DOI: 10.1021/acs.orglett.9b00724 From NLM PubMed-not-MEDLINE.

(45) Morewood, R.; Nitsche, C. A biocompatible stapling reaction for in situ generation of constrained peptides. *Chemical Science* **2021**, *12* (2), 669-674, 10.1039/D0SC05125J. DOI: 10.1039/D0SC05125J.

(46) Tu, L.; Wang, D.; Li, Z. Design and Synthetic Strategies for Helical Peptides. In *Cyclic Peptide Design*, Goetz, G. Ed.; Springer New York, 2019; pp 107-131.

(47) Schafmeister, C. E.; Po, J.; Verdine, G. L. An all-hydrocarbon cross-linking system for enhancing the helicity and metabolic stability of peptides. *Journal of the American Chemical Society* **2000**, *122* (24), 5891-5892. DOI: DOI 10.1021/ja000563a.

(48) Miller, S. J.; Blackwell, H. E.; Grubbs, R. H. Application of Ring-Closing Metathesis to the Synthesis of Rigidified Amino Acids and Peptides. *Journal of the American Chemical Society* **1996**, *118* (40), 9606-9614. DOI: 10.1021/ja961626l.

(49) Walensky, L. D.; Kung, A. L.; Escher, I.; Malia, T. J.; Barbuto, S.; Wright, R. D.; Wagner, G.; Verdine, G. L.; Korsmeyer, S. J. Activation of Apoptosis in Vivo by a Hydrocarbon-Stapled BH3 Helix. *Science* **2004**, *305* (5689), 1466-1470. DOI: doi:10.1126/science.1099191.

(50) Walensky, L. D.; Bird, G. H. Hydrocarbon-Stapled Peptides: Principles, Practice, and Progress. *Journal of Medicinal Chemistry* **2014**, *57* (15), 6275-6288. DOI: 10.1021/jm4011675.

(51) Xie, X.; Gao, L.; Shull, A. Y.; Teng, Y. Stapled peptides: providing the best of both worlds in drug development. *Future Medicinal Chemistry* **2016**, *8* (16), 1969-1980. DOI: 10.4155/fmc-2016-0102.

(52) Migoń, D.; Neubauer, D.; Kamysz, W. Hydrocarbon Stapled Antimicrobial Peptides. *The Protein Journal* **2018**, *37* (1), 2-12. DOI: 10.1007/s10930-018-9755-0.

(53) Rostovtsev, V. V.; Green, L. G.; Fokin, V. V.; Sharpless, K. B. A Stepwise Huisgen Cycloaddition Process: Copper(I)-Catalyzed Regioselective "Ligation" of Azides and Terminal Alkynes. *Angewandte Chemie International Edition* **2002**, *41* (14), 2596-2599. DOI: https://doi.org/10.1002/1521-3773(20020715)41:14<2596::AID-ANIE2596>3.0.CO;2-4.

(54) Agard, N. J.; Prescher, J. A.; Bertozzi, C. R. A strain-promoted [3 + 2] azide-alkyne cycloaddition for covalent modification of biomolecules in living systems. *J Am Chem Soc* **2004**, *126* (46), 15046-15047. DOI: 10.1021/ja044996f From NLM Medline.

(55) Hou, J.; Liu, X.; Shen, J.; Zhao, G.; Wang, P. G. The impact of click chemistry in medicinal chemistry. *Expert Opinion on Drug Discovery* **2012**, *7* (6), 489-501. DOI: 10.1517/17460441.2012.682725.

(56) Li, H.; Aneja, R.; Chaiken, I. Click Chemistry in Peptide-Based Drug Design. *Molecules* **2013**, *18* (8), 9797-9817.

(57) Simon, R. J.; Kania, R. S.; Zuckermann, R. N.; Huebner, V. D.; Jewell, D. A.; Banville, S.; Ng, S.; Wang, L.; Rosenberg, S.; Marlowe, C. K.; et al. Peptoids: a modular approach to drug discovery. *Proc Natl Acad Sci U S A* **1992**, *89* (20), 9367-9371. DOI: 10.1073/pnas.89.20.9367.

(58) Giorgio, A.; Del Gatto, A.; Pennacchio, S.; Saviano, M.; Zaccaro, L. Peptoids: Smart and Emerging Candidates for the Diagnosis of Cancer, Neurological and Autoimmune Disorders. *Int J Mol Sci* **2023**, *24* (22). DOI: 10.3390/ijms242216333 From NLM Medline.

(59) Miller, S. M.; Simon, R. J.; Ng, S.; Zuckermann, R. N.; Kerr, J. M.; Moos, W. H. Proteolytic studies of homologous peptide and N-substituted glycine peptoid oligomers. *Bioorganic & Medicinal Chemistry Letters* **1994**, *4* (22), 2657-2662. DOI: https://doi.org/10.1016/S0960-894X(01)80691-0.

(60) Zuckermann, R. N.; Kerr, J. M.; Kent, S. B. H.; Moos, W. H. Efficient Method for the Preparation of Peptoids [Oligo(N-Substituted Glycines)] by Submonomer Solid-Phase Synthesis. *Journal of the American Chemical Society* **1992**, *114* (26), 10646-10647. DOI: DOI 10.1021/ja00052a076.

(61) Cheng, R. P.; Gellman, S. H.; DeGrado, W. F. β-Peptides: From Structure to Function. *Chemical Reviews* **2001**, *101* (10), 3219-3232. DOI: 10.1021/cr000045i.

(62) Cabrele, C.; Martinek, T. A.; Reiser, O.; Berlicki, Ł. Peptides Containing β-Amino Acid Patterns: Challenges and Successes in Medicinal Chemistry. *Journal of Medicinal Chemistry* **2014**, *57* (23), 9718-9739. DOI: 10.1021/jm5010896.

(63) Teng, P.; Shi, Y.; Sang, P.; Cai, J. gamma-AApeptides as a New Class of Peptidomimetics. *Chemistry* **2016**, *22* (16), 5458-5466. DOI: 10.1002/chem.201504936 From NLM Medline.

(64) Miura, T.; Malla, T. R.; Owen, C. D.; Tumber, A.; Brewitz, L.; McDonough, M. A.; Salah, E.; Terasaka, N.; Katoh, T.; Lukacik, P.; et al. In vitro selection of macrocyclic peptide inhibitors

containing cyclic γ2,4-amino acids targeting the SARS-CoV-2 main protease. *Nature Chemistry* **2023**, *15* (7), 998-1005. DOI: 10.1038/s41557-023-01205-1.

(65) Kawakami, T.; Ogawa, K.; Hatta, T.; Goshima, N.; Natsume, T. Directed Evolution of a Cyclized Peptoid–Peptide Chimera against a Cell-Free Expressed Protein and Proteomic Profiling of the Interacting Proteins to Create a Protein–Protein Interaction Inhibitor. *ACS Chemical Biology* **2016**, *11* (6), 1569-1577. DOI: 10.1021/acschembio.5b01014.

(66) Herlan, C. N.; Meschkov, A.; Schepers, U.; Bräse, S. Cyclic Peptoid-Peptide Hybrids as Versatile Molecular Transporters. *Frontiers in Chemistry* **2021**, *9*, Original Research. DOI: 10.3389/fchem.2021.696957.

(67) Araszczuk, A. M.; D'Amato, A.; Schettini, R.; Costabile, C.; Della Sala, G.; Pierri, G.; Tedesco, C.; De Riccardis, F.; Izzo, I. Macrocyclic Triazolopeptoids: A Promising Class of Extended Cyclic Peptoids. *Organic Letters* **2022**, *24* (42), 7752-7756. DOI: 10.1021/acs.orglett.2c03062.

(68) Li, Y.; Wang, Y.; Wei, Q.; Zheng, X.; Tang, L.; Kong, D.; Gong, M. Variant fatty acid-like molecules Conjugation, novel approaches for extending the stability of therapeutic peptides. *Scientific Reports* **2015**, *5* (1), 18039. DOI: 10.1038/srep18039.

(69) Bhat, M.; Jatyan, R.; Mittal, A.; Mahato, R. I.; Chitkara, D. Opportunities and challenges of fatty acid conjugated therapeutics. *Chemistry and Physics of Lipids* **2021**, *236*, 105053. DOI: https://doi.org/10.1016/j.chemphyslip.2021.105053.

(70) Lim, S. I.; Mizuta, Y.; Takasu, A.; Hahn, Y. S.; Kim, Y. H.; Kwon, I. Site-specific fatty acid-conjugation to prolong protein half-life in vivo. *Journal of Controlled Release* **2013**, *170* (2), 219-225. DOI: https://doi.org/10.1016/j.jconrel.2013.05.023.

(71) Kurtzhals, P. Pharmacology of Insulin Detemir. *Endocrinology and Metabolism Clinics of North America* **2007**, *36*, 14-20. DOI: https://doi.org/10.1016/S0889-8529(07)80004-1.

(72) Storck, P.; Umstätter, F.; Wohlfart, S.; Domhan, C.; Kleist, C.; Werner, J.; Brandenburg, K.; Zimmermann, S.; Haberkorn, U.; Mier, W.; et al. Fatty Acid Conjugation Leads to Length-Dependent Antimicrobial Activity of a Synthetic Antibacterial Peptide (Pep19-4LF). *Antibiotics* **2020**, *9* (12), 844.

(73) Reily, C.; Stewart, T. J.; Renfrow, M. B.; Novak, J. Glycosylation in health and disease. *Nature Reviews Nephrology* **2019**, *15* (6), 346-366. DOI: 10.1038/s41581-019-0129-4.

(74) Ardito, F.; Giuliani, M.; Perrone, D.; Troiano, G.; Lo Muzio, L. The crucial role of protein phosphorylation in cell signaling and its use as targeted therapy (Review). *Int J Mol Med* **2017**, *40* (2), 271-280. DOI: 10.3892/ijmm.2017.3036.

(75) Moradi, S. V.; Hussein, W. M.; Varamini, P.; Simerska, P.; Toth, I. Glycosylation, an effective synthetic strategy to improve the bioavailability of therapeutic peptides. *Chem Sci* **2016**, *7* (4), 2492-2500. DOI: 10.1039/c5sc04392a From NLM PubMed-not-MEDLINE.

(76) Chandrashekar, C.; Hossain, M. A.; Wade, J. D. Chemical Glycosylation and Its Application to Glucose Homeostasis-Regulating Peptides. *Frontiers in Chemistry* **2021**, *9*, Mini Review. DOI: 10.3389/fchem.2021.650025.

(77) Nova, I. C.; Ritmejeris, J.; Brinkerhoff, H.; Koenig, T. J. R.; Gundlach, J. H.; Dekker, C. Detection of phosphorylation post-translational modifications along single peptides with nanopores. *Nature Biotechnology* **2023**. DOI: 10.1038/s41587-023-01839-z.

(78) Zeng, D.; Debabov, D.; Hartsell, T. L.; Cano, R. J.; Adams, S.; Schuyler, J. A.; McMillan, R.; Pace, J. L. Approved Glycopeptide Antibacterial Drugs: Mechanism of Action and Resistance. *Cold Spring Harb Perspect Med* **2016**, *6* (12). DOI: 10.1101/cshperspect.a026989 From NLM Medline.

(79) Gao, Y.; Joshi, M.; Zhao, Z.; Mitragotri, S. PEGylated therapeutics in the clinic. *Bioeng Transl Med* **2024**, *9* (1), e10600. DOI: 10.1002/btm2.10600 From NLM PubMed-not-MEDLINE.

(80) Li, C.; Li, T.; Tian, X.; An, W.; Wang, Z.; Han, B.; Tao, H.; Wang, J.; Wang, X. Research progress on the PEGylation of therapeutic proteins and peptides (TPPs). *Frontiers in Pharmacology* **2024**, *15*, Review. DOI: 10.3389/fphar.2024.1353626.

(81) Moreira Brito, J. C.; Carvalho, L. R.; Neves de Souza, A.; Carneiro, G.; Magalhães, P. P.; Farias, L. M.; Guimarães, N. R.; Verly, R. M.; Resende, J. M.; Elena de Lima, M. PEGylation of the antimicrobial peptide LyeTx I-b maintains structure-related biological properties and improves selectivity. *Frontiers in Molecular Biosciences* **2022**, *9*, Original Research. DOI: 10.3389/fmolb.2022.1001508.

Chapter 3: Development of ANT308 derivatives & their performance in T cell studies of AML murine models

In this chapter, we will introduce our modified ANT308 derivatives as well as the rationale behind each modification. We will describe our strategies to access each modification, as well as the challenges that we overcame to generate our ANT308 derivatives. We will then discuss the implications of these derivatives for T cell activation and proliferation relative to unmodified ANT308 *in vitro*. After our initial analyses, we will discuss the implications of these peptide derivatives in AML murine model studies, evaluating their ability to increase overall survival and reduce tumor burden. Finally, we will discuss the challenges faced during plasma stability studies, as well as future directions in our pursuit of a modified ANT308 target with enhanced drug properties.

3.1 Derivatizations of ANT peptides

3.1.1 Introduction to ANT derivatives

In collaboration with the Waller lab, we sought to develop modified variants of their lead ANT peptide ANT308 to improve their drug properties, given that peptide therapeutics tend to suffer from poor metabolic stability and half-life circulation.[1] In pursuit of modified derivatives, we proposed three modifications: N-terminus capping, peptide stapling, and C-terminus PEGylation. Because the termini of peptides are susceptible to exopeptidases,[2] we hypothesized that acetylation of the N-terminus will impart stability towards proteolytic activity. Because native VIP adopts an α-helical structure when

binding to the N-ted domain of the VPAC receptors,[3] we proposed that incorporation of a covalent restraint in the ANT308 α-helical sequence will enhance stability by masking the proteolytically sensitive amide bonds. Additionally, we propose that the staple will enhance binding affinity by pre-emptively conforming the peptide into its active conformation, thus reducing the entropic penalty of folding as the peptide approaches the transmembrane VPAC. Because the C-terminus of VIP is solvent exposed,[4] we proposed that incorporation of a large, inert polyethylene glycol (PEG) could extend the longevity of ANT308 by reducing renal clearance.

3.2 Peptide stapling of ANT308

3.2.1 Incorporation of a covalent staple in ANT308

In our pursuit of a stapled ANT308 derivative, there were two major considerations essential to our design: staple location and staple type. As mentioned in the previous chapter, Gill and co-workers employed lactam and hydrocarbon staples onto VIP.[5] Their most optimal stapled peptide contained a hydrocarbon staple at positions 13 and 17. Furthermore, they found that a hydrocarbon staple poised at this position performed better than its lactam cognate, attributed to potential interactions with a hydrophobic interface of the receptor. Given that ANT308 deviates minimally from VIP in the α-helical region of their sequence, we proposed that L^{13} and M^{17} are optimal for replacement in our system.
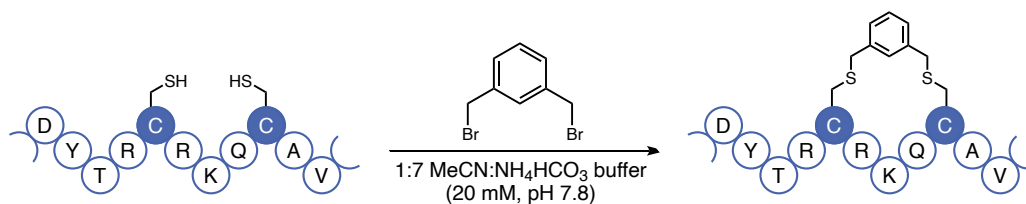
Figure 3.1 *m*-xylene bisalkylation to generate stapled ANT308.

Although hydrocarbon staples are attractive to effectuate hydrophobic constraints, we were concerned with this method for several reasons: the non-canonical residues required for hydrocarbon stapling

are expensive and difficult to incorporate in SPPS due to the sterically encumbered α-carbon. Additionally, the complete removal of Grubb's catalyst represents a significant drawback of this method, inhibiting their utility in downstream *in vivo* assays. Thus, we opted to employ the bisalkylation strategy developed by Meng and co-workers (**Figure 3.1**).[6] This strategy is advantageous because of the facile incorporation of cysteine residues and the lack of metal-mediated transformations. Additionally, this strategy enables the incorporation of a hydrophobic constraint, similar to the incorporation of a hydrocarbon staple in VIP.

3.2.2 Peptide stapling effects on secondary structure of ANT308

Circular Dichroism
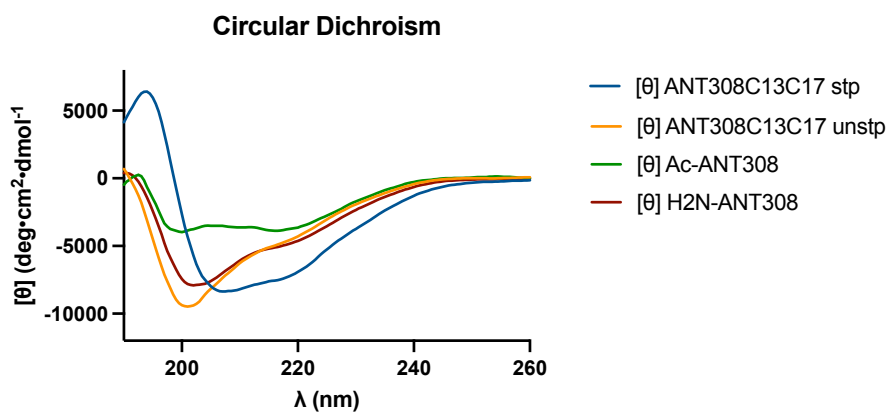
Figure 3.2 Circular dichroism spectra for ANT308 and ANT308 derivatives.

Peptide	α Helicity %
ANT308	5.30
Ac-ANT308	2.90
ANT308C13C17 unstp	4.84
ANT308C13C17 stp	10.6

Table 3.1 Calculated helicity values of ANT308 and ANT308 derivatives.

After incorporating the *m*-xylene staple into ANT308, we examined the influence of the staple on secondary structure via circular dichroism (CD) analysis (**Figure 3.2**). The parent ANT308 and the

unstapled control ANT308C13C17 unstp exhibit comparable spectra and α-helicity. In contrast, ANT308C13C17 stp yields a spectrum resembling that of α-helices, including a maximum ~190 nm and minima ~210 and 220 nm. Furthermore, the incorporation of the staple doubled in helicity compared to the unstapled and native ANT308 (**Table 3.1**). In comparison to the hydrocarbon-stapled VIP at residues 13 and 17, ANT308C13C17 stp exhibits similar helicity (9.6 vs. 10.6%, respectively).[5] These results are consistent with literature, of which the *m*-xylene staple has been demonstrated to impart slight to moderate helix induction and allows for a degree of flexibility in aqueous media.[7, 8]

3.3 PEGylation of ANT308
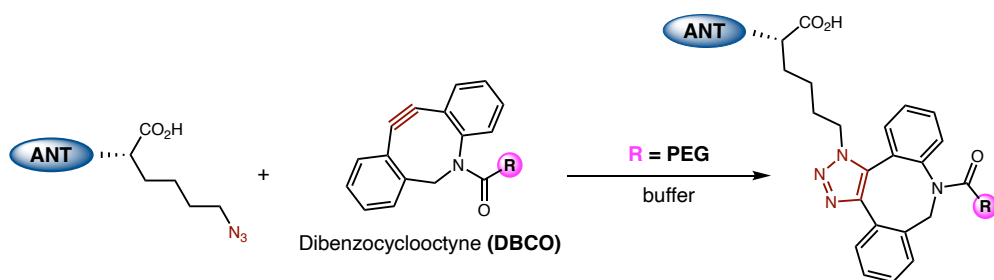
Figure 3.3 Generation of ANT308-PEG via strain-promoted copper-free click chemistry.

After developing our stapled ANT308 derivative, we then turned our attention towards PEGylated ANT308. As discussed in chapter 2, a previous report by Derome and co-workers found that a 22 kDa PEG linker could be attached to the C-terminus of VIP without affecting binding affinity to VPAC1.[4] Although these VIP-PEG conjugates were generated via cysteine-maleimide chemistry, we were worried about their stability in our downstream *in vivo* assays, primarily their susceptibility to retro-Micahel addition in the presence of exogenous thiols.[9] Thus, we opted to generate our ANT308-PEG conjugates via strain-promoted copper-free click chemistry (**Figure 3.3**). We chose to

incorporate an azido-lysine onto the C-terminus of ANT308 during SPPS, followed by reaction with a DBCO-PEG 20 kDa under mild aqueous conditions. In our pursuit of the ANT308-PEG precursor ANT308K$_{N3}$, we found that modification of the cleavage cocktail to include DTT in place of EDT was required to prevent reduction of the azide, while sufficiently suppressing acid-mediated methionine oxidation.[10]

Although synthesis of the ANT308-PEG conjugate was facile, the subsequent purification to remove excess PEG was significantly more challenging due to their comparable sizes. Initially, we developed a strategy around resin-bound azide incubation in PBS. Through gel quantitation and BaCl$_2$/iodide staining, we determined that 95% of free PEG was removed in our control studies. Thus, this purification strategy was robust, mild, and required minimal input from the user. Unfortunately, this strategy faced reproducibility issues, and successful removals varied significantly between batches of resin from different vendors. Thus, we sought to develop a new purification strategy with significant reliability.

We rationalized that because PEG is neutral, we could purify the ANT308-PEG via cation exchange chromatography. Given that ANT308 is very basic (pI ~11.65) we optimized purification conditions around 100 mM CAPS equilibration buffer, pH 10.6 and Sepharose resin. 250 mM NaCl additive was enough to sufficiently remove ANT308-PEG from resin within a couple column volumes. To confirm that excess PEG was removed in the flow through, we utilized 5% (w/v) BaCl$_2$/0.1 N iodide solution to fix and stain precipitated PEG. Lanes containing free PEG would be confirmed by their lack of staining in Coomassie. This strategy was also translatable to the FPLC, of which UV signature was sufficient to monitor PEG and ANT308-PEG removal.

3.4 *in vitro* T-cell proliferation studies
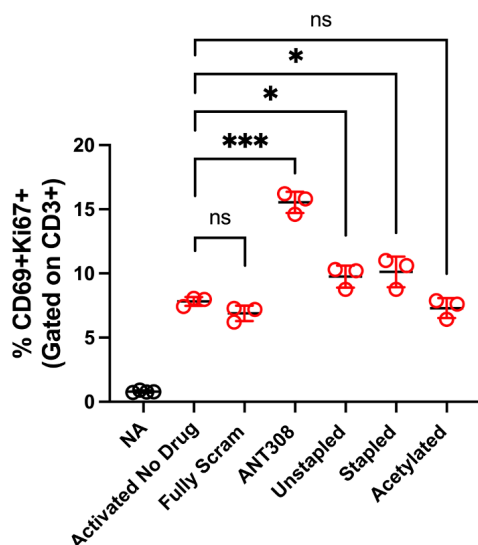
Figure 3.4 *in vitro* T-cell activation study of acetylated and stapled ANT308. Isolated T cells from 4 healthy donor PMBCs were pooled and plated in triplicate wells for the assay. T cells were activated with CD3/CD28/CD2 soluble activator in the absence or presence of peptides for 48 hours and assessed for CD69 and Ki67 expression following culture. The graphs are presented +/- standard deviation. For statistical analysis, unpaired T-test was used. $*p<0.05$, $**p<0.01$, and $***p<0.001$.

After developing our ANT308 derivatives, we performed initial studies investigating the ability of Ac-ANT308 and ANT308C13C17 stp to enhance T cell proliferation *in vitro* (**Figure 3.4**). The acetylated derivative Ac-ANT308 yielded no change in T cell proliferation relative to the controls. This indicates that conservation of the N-terminus of ANT308 is critical towards its antagonist ability. Additionally, the unstapled and stapled derivatives ANT308C13C17 unstp & ANT308C13C17 stp yielded diminished T cell proliferation relative to ANT308, only slightly enhancing proliferation relative to the controls. This suggests that modification of residues 13 and 17 is non-trivial and has significant implications in ANT308, contrary to analogous findings in VIP.[5]

A

Non activated
6.05%   4.36%

Activated
36.2%   20.2%

Activated +1μM ANT308
34.8%   18.9%

Activated +10μM ANT308
44.7%   23.3%

Activated +1μM ANT308K-PEG
41.4%   24.0%

Activated +10μM ANT308K-PEG
47.9%   24.1%

CD69+

CD8+

B

%CD4+ CD69+

ns
***
**
**
****   ****   ****
ns

C

%CD8+ CD69+

*
*
*
****   *
ns   ns

Non activated
Activated No Drug
Activated+ANT308 1μM
Activated+ANT308 10μM
Activated+ANT308K-PEG 1μM
Activated+ANT308K-PEG 10μM

D

Granzyme B

Non activated
1.88%   3.66%

Activated
5.81%   11.1%

Activated +1μM ANT308
8.42%   13.1%

Activated +1μM ANT308K-PEG
13.2%   17.2%

CD8+

E

Ki67+

Non activated
1.42%   1.01%

Activated
6.27%   3.74%

Activated +1μM ANT308
6.7%   4.13%

Activated +1μM ANT308K-PEG
9.81%   6.54%

CD8+

F

%CD4+ Granzyme B+

*
**   *
***

Non activated
Activated plate1
ANT308 1μM
ANT308K-PEG 1μM

G

%CD8+ Granzyme B+

*
ns   ns
***

Non activated
Activated plate1
ANT308 1μM
ANT308K-PEG 1μM

H

%CD4+ Ki67+

*
ns   *
****

Non activated
Activated No drug
ANT308 1μM
ANT308K-PEG 1μM

I

%CD8+ Ki67+

*
ns   *
****

Non activated
Activated No drug
ANT308 1μM
ANT308K-PEG 1μM

60

Figures 3.5A-I: ANT308 & ANT308-PEG activate human T cells. A-C. 1 or 10 μM ANT308 or ANT308-PEG were mixed with isolated & pooled human T cells with the presence of αCD3/CD28 activator & 50 IU/mL IL-2. 48 hours following activation, CD4+ & CD8+ T cell subsets were examined for CD69 expressions. One-way ANOVA analysis. **D-I.** 1 μM ANT308 or ANT308-PEG were incubated with pooled human T cells for 48 hours, CD4+ & CD8+ T cell subsets were examined for Granzyme B & Ki67 expressions. Representative flow cytometry plots & graphical representations were shown. Two to three replicates each, mean with SEM shown, unpaired t test, $*p<0.05$, $**p<0.01$, and $***p<0.001$.

We next assessed ANT308-PEG for human T cell activation *in vitro* (**Figure 3.5 A-I**). Both native ANT308 and ANT308-PEG significantly enhanced CD69 expression in CD4+ and CD8+ T cells (**Figure 3.5 A-C**). However, at low concentration (1 μM), only ANT308-PEG significantly increased CD69+ populations. Interestingly, while a 10-fold increase in ANT308 concentration correlates to an increase in T cell activation, ANT308-PEG exhibits similar proliferation regardless of dose. In addition to CD69 expression, we also tested ANT308-PEG for its ability to enhance other T cell expression markers (**Figure 3.5 D-I**). Granzyme B is a serine protease stored in the secretory granules of cytotoxic T lymphocytes (CTL) and natural killer (NK) cells, with important functions in antitumor immunity. Additionally, Ki67 is a T cell proliferation marker strongly associated with tumor cell proliferation and growth.[11-13] ANT308-PEG better enhanced Ki67 and Granzyme B expression in CD4+ and CD8+ T cells compared to native ANT308, indicating that PEGylation improves antagonist function.

3.5 *in vivo* AML murine studies

3.5.1 AML: an unmet need for clinical therapeutic development

As discussed in chapter 1, previous studies by the Waller lab demonstrated that VIPhyb and the ANT peptides resulted in significant enhancement of a T cell dependent, anti-leukemia response in murine models of acute myeloid leukemia (AML).[14, 15] In addition to their findings, AML has been identified as an excellent clinical target for VIP antagonism, due to several factors. For one, AML is an aggressive cancer with increasing incidence and a low survival rate, of which less than 1/3 of patients survive 5 years.[16] Of those who enter remission post-treatment, around 40% relapse, making relapsed AML a common scenario.[17, 18] This highlights a need to develop therapies that not only address tumor growth and proliferation, but also modulate T cell memory for long-term eradication. These factors taken together indicate that the ANT308 derivatives have strong therapeutic potential to treat AML. Thus, we opted to perform *in vivo* analysis of our ANT308 derivatives in AML murine models.

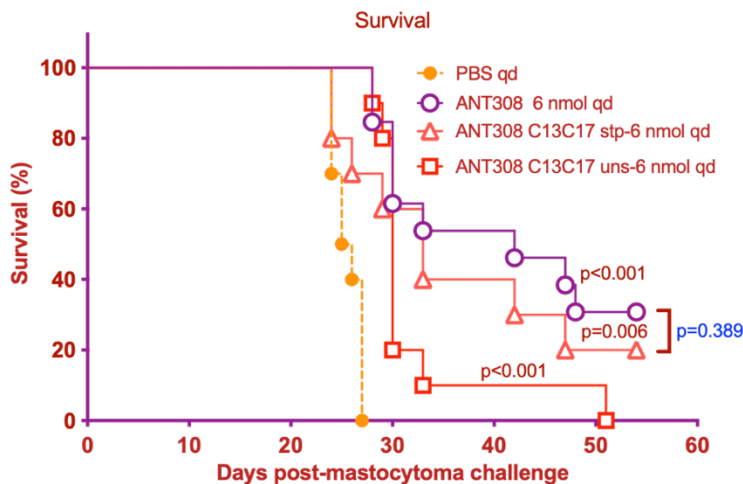### 3.5.2 Survival challenge studies of ANT308 derivatives

Figure 3.6: In myeloid sarcoma murine models, ten doses of ANT308C13C17 stp had similar prolonged survival of tumor burden mice as ten doses of ANT308, compared to control mice.

100000 P815 tumor cells (in 100 μL PBS) were subcutaneously injected into the right flank after shaving fur. Seven days later, the mouse was subcutaneously injected with 6 nmol ANT308, 6 nmol ANT308C13C17 unstp, 6 nmol ANT308C13C17 stp, or 200 μL PBS once daily for 10 days. Median survival day (MSD): ANT308 – 42 days, ANT308C13C17 unstp – 30 days, ANT308C13C17 stp – 33 days, PBS – 26 days.
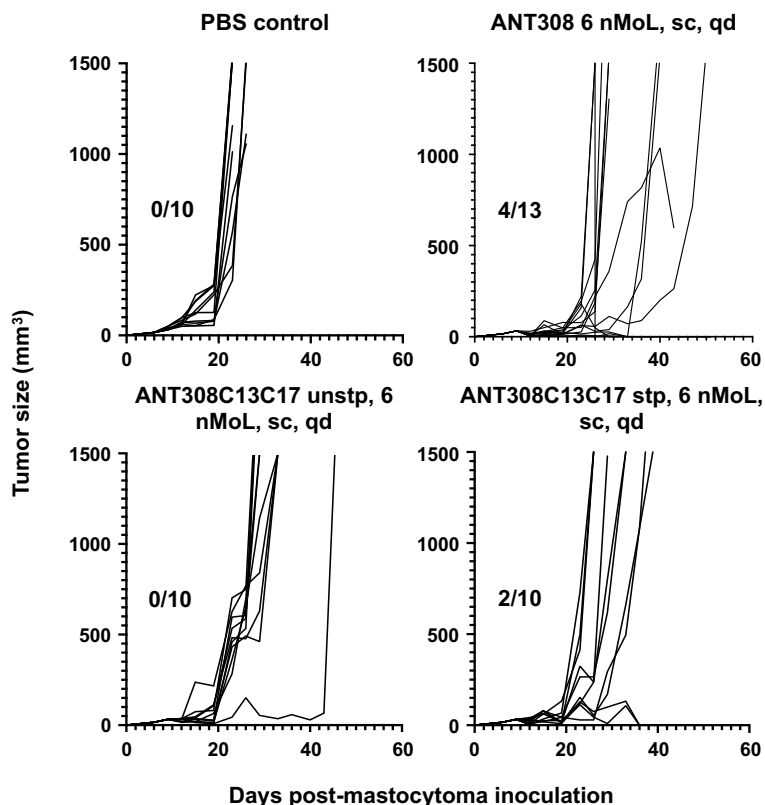
Figure 3.7: In myeloid sarcoma murine models, ten doses of ANT308 control and ANT308C13C17 stp prolonged tumor burden suppression relative to ANT308C13C17 unstp and control mice. 100000 P815 tumor cells (in 100 μL PBS) were subcutaneously injected into the right flank after shaving fur. Seven days later, the mouse was subcutaneously injected with 6 nmol ANT308, 6 nmol ANT308C13C17 unstp, 6 nmol ANT308C13C17 stp, or 200 μL PBS once daily for 10 days. (divisor, number on the left of the division slash, is survival mouse number; dividend, number on the right of the division dash, is total mouse number in the group).

Barring Ac-ANT308, we examined the tumor burden and overall survival of AML mice dosed with our unstapled and stapled derivatives relative to native ANT308 (**Figure 3.6 & 3.7**). Mice treated with ANT308 exhibited significantly higher survival rates and lower tumor burden relative to the PBS control. In contrast, treatment with ANT308C13C17 unstp resulted in significantly lower survival rates and tumor burden, leading to marginal to no enhancement relative to the PBS control. This further corroborates the results from the *in vitro* studies, indicating that residue change was detrimental to antagonist ability. In contrast, ANT308C13C17 stp exhibits better overall survival and tumor burden compared to its linear counterpart, demonstrating that incorporation of the covalent staple rescues antagonist activity. Despite this, ANT308C13C17 stp does not outperform native ANT308 in our *in vivo* studies.

Figure 3.8: Four doses of ANT308-PEG significantly prolonged survival tumor burden mice as fourteen doses of ANT308, compared with control mice. 100000 P815 tumor cells (in 100 µL PBS) were subcutaneously injected into the right flank after shaving fur. Seven days later the mouse was subcutaneously injected with 3 nmol ANT308 once daily, 3 nmol ANT308-PEG once every three

days, or VIP full scramble control once daily for 14 days. Median survival day (MSD): ANT308 – 26 days, ANT308-PEG – 29 days, Scramble – 19 days.
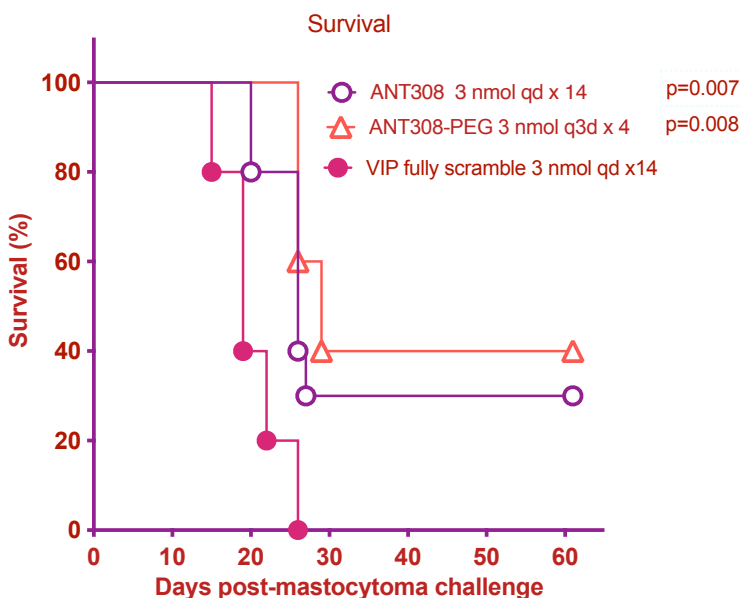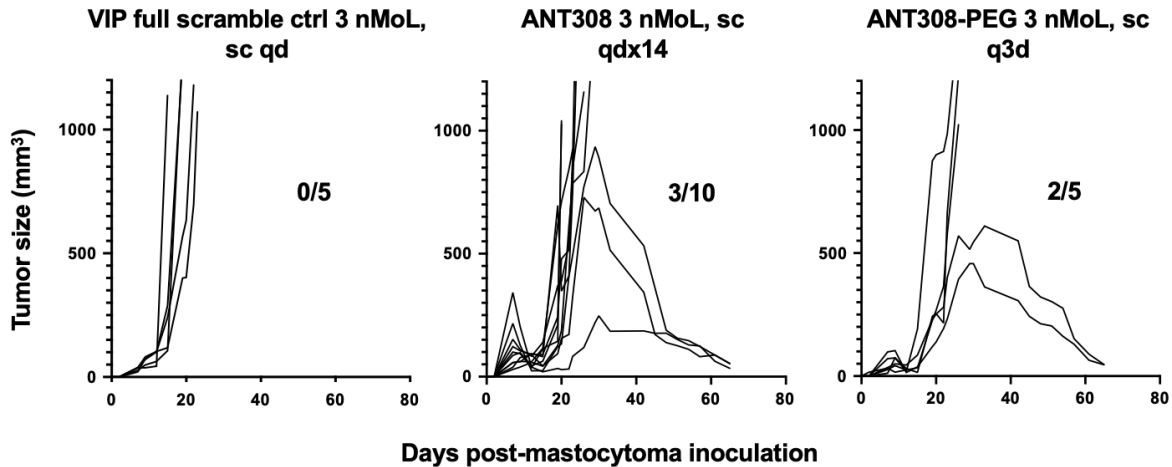

Figure 3.9: Four doses of ANT308-PEG significantly prolonged tumor burden suppression relative to fourteen doses of ANT308 and control mice. 100000 P815 tumor cells (in 100 μL PBS) were subcutaneously injected into the right flank after shaving fur. Seven days later the mouse was subcutaneously injected with 3 nmol ANT308 once daily, 3 nmol ANT308-PEG once every three days, or VIP full scramble control once daily for 14 days. (divisor, number on the left of the division slash, is survival mouse number; dividend, number on the right of the division dash, is total mouse number in the group.)

We next examined the effects of ANT308-PEG on AML murine model tumor burden and overall survival (**Figures 3.8 & 3.9**). Mice treated with both ANT308 and ANT308-PEG showed significant enhancement in overall survival and reduction in tumor burden compared to the PBS control. Additionally, we were pleased to find that significantly fewer doses (3.5x) of ANT308-PEG achieved comparable overall survival and tumor burden relative to ANT308, suggesting that incorporation of PEG increases the longevity of the peptide and its subsequent potency.

3.6 Plasma stability assay of ANT308 derivatives

In order to properly examine the efficacy of our derivatizations on peptide stability, we attempted to perform plasma stability assays on our modified ANT308 peptides. Using a protocol from Payne et al.,[19] we employed and adapted this method for our own analysis, using propantheline bromide as the control. We were able to successfully develop our own method to effectuate the stability study, as shown in **figure 3.10** & **table 3.2**:
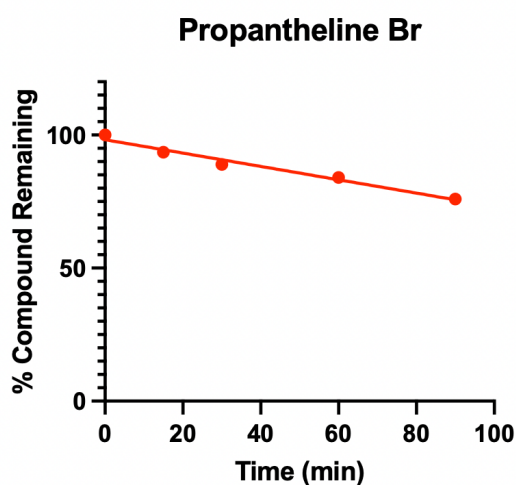
Figure 3.10 Control study monitoring propantheline bromide degradation.

Area under curve for 326.2, 368.3					
Aliquot	0 min	15 min	30 min	60 min	90 min
1	7.14E+06	6.73E+06	6.62E+06	6.05E+06	5.45E+06
2	7.24E+06	6.84E+06	5.65E+05	6.29E+06	5.52E+06
3	6.62E+06	6.61E+06	6.17E+06	5.80E+06	5.42E+06
AVG	7.19E+06	6.73E+06	6.39E+06	6.05E+06	5.46E+06
%	100%	93.5%	88.9%	84.0%	75.9%

Table 3.2 Area under the curve replicate averaged to quantitate remaining intact control. Values in red were considered outliers and removed from the average. Percent remaining was calculated by comparing averages to average at time 0.

After establishing conditions for our control, we moved on towards testing our derivatives in our study, starting with ANT308K$_{N3}$. In our initial attempt, we obtained significant variance amongst replicates for all timepoints and noted that we were seeing almost complete consumption of peptide even at time 0. Literature of VIP in human plasma stability studies indicate that it has a half-life of ~1 minute.[20-22] Plasma concentrations of VIP in literature are measured using radioimmunoassays, which possess exquisite sensitivity down to the low pmol/L range not capable by our analysis.[21, 22] Given that ANT308 is relatively conserved in sequence to VIP (68% similarity), we concluded that ANT308 and its derivatives likely have a similar half-life to VIP. Given these challenges, we chose not to pursue further analysis of the other ANT308 derivatives in our plasma stability assay. The Waller lab have pursued a variation of this study with ANT308 and ANT308-PEG, wherein they monitored their ability to activate T cells *in vitro* post-incubation at various timepoints in human plasma. Interestingly, preliminary data demonstrates that these peptides continue to exhibit T cell activation comparable to time 0 up to 96 hours. This may potentially indicate that ANT308 degradation products possess antagonist activity, although further testing is required.

3.7 Concluding Remarks

In summary, we have developed three key ANT308 derivatives in an attempt to enhance the drug properties of the VIP antagonist. We demonstrated that N-terminus conservation is critical to antagonist activity, of which acetylation of the N-terminus shut down T cell activation *in vitro*. Furthermore, we demonstrated that changes in residues 13 and 17 to cysteines negatively impacted antagonist activity of ANT308, resulting in decreased overall survival and increased tumor burden relative to parental ANT308. However, incorporation of the covalent staple rescued activity and enabled comparable results to parental ANT308 in the *in vivo* studies. Finally, we demonstrated the significance of PEG incorporation at the C-terminus of ANT308, which provided comparable results

to parental ANT308 at significantly lower dosage. Additionally, ANT308-PEG also exhibited an increase in Ki67 and Granzyme B proliferation at lower concentration than ANT308. Taken together, these results indicate that PEGylation increased the longevity of ANT308, enabling comparable potency to ANT308 at a lower dosage. Additional studies are underway to determine its relative stability compared to parental ANT308.

3.8 References

(1) Wang, L.; Wang, N.; Zhang, W.; Cheng, X.; Yan, Z.; Shao, G.; Wang, X.; Wang, R.; Fu, C. Therapeutic peptides: current applications and future directions. *Signal Transduct Target Ther* **2022**, *7* (1), 48. DOI: 10.1038/s41392-022-00904-4 From NLM Medline.

(2) Jayawardene, D. S.; Dass, C. The effect of N-terminal acetylation and the inhibition activity of acetylated enkephalins on the aminopeptidase M-catalyzed hydrolysis of enkephalins. *Peptides* **1999**, *20* (8), 963-970. DOI: 10.1016/s0196-9781(99)00089-3 From NLM Medline.

(3) Couvineau, A.; Ceraudo, E.; Tan, Y. V.; Nicole, P.; Laburthe, M. The VPAC1 receptor: structure and function of a class B GPCR prototype. *Frontiers in Endocrinology* **2012**, *3*, Review. DOI: 10.3389/fendo.2012.00139.

(4) Pan, C. Q.; Hamren, S.; Roczniak, S.; Tom, I.; DeRome, M. Generation of PEGylated VPAC1-selective antagonists that inhibit proliferation of a lung cancer cell line. *Peptides* **2008**, *29* (3), 479-486. DOI: 10.1016/j.peptides.2007.09.003.

(5) Giordanetto, F.; Revell, J. D.; Knerr, L.; Hostettler, M.; Paunovic, A.; Priest, C.; Janefeldt, A.; Gill, A. Stapled Vasoactive Intestinal Peptide (VIP) Derivatives Improve VPAC2 Agonism and Glucose-Dependent Insulin Secretion. *ACS Med Chem Lett* **2013**, *4* (12), 1163-1168. DOI: 10.1021/ml400257h.

(6) Meng, G.; Pu, J.; Li, Y.; Han, A.; Tian, Y.; Xu, W.; Zhang, T.; Li, X.; Lu, L.; Wang, C.; et al. Design and Biological Evaluation of m-Xylene Thioether-Stapled Short Helical Peptides Targeting the HIV-1 gp41 Hexameric Coiled-Coil Fusion Complex. *J Med Chem* **2019**, *62* (19), 8773-8783. DOI: 10.1021/acs.jmedchem.9b00882.

(7) Tian, Y.; Jiang, Y.; Li, J.; Wang, D.; Zhao, H.; Li, Z. Effect of Stapling Architecture on Physiochemical Properties and Cell Permeability of Stapled alpha-Helical Peptides: A Comparative Study. *Chembiochem* **2017**, *18* (21), 2087-2093. DOI: 10.1002/cbic.201700352 From NLM Medline.

(8) de Araujo, A. D.; Hoang, H. N.; Kok, W. M.; Diness, F.; Gupta, P.; Hill, T. A.; Driver, R. W.; Price, D. A.; Liras, S.; Fairlie, D. P. Comparative alpha-helicity of cyclic pentapeptides in water. *Angew Chem Int Ed Engl* **2014**, *53* (27), 6965-6969. DOI: 10.1002/anie.201310245 From NLM Medline.

(9) Fontaine, S. D.; Reid, R.; Robinson, L.; Ashley, G. W.; Santi, D. V. Long-Term Stabilization of Maleimide–Thiol Conjugates. *Bioconjugate Chemistry* **2015**, *26* (1), 145-152. DOI: 10.1021/bc5005262.

(10) Schneggenburger, P. E.; Worbs, B.; Diederichsen, U. Azide reduction during peptide cleavage from solid support-the choice of thioscavenger? *J Pept Sci* **2010**, *16* (1), 10-14. DOI: 10.1002/psc.1202 From NLM Medline.

(11) Ida, H.; Utz, P. J.; Anderson, P.; Eguchi, K. Granzyme B and natural killer (NK) cell death. *Modern Rheumatology* **2005**, *15* (5), 315-322. DOI: 10.3109/s10165-005-0426-6 (acccessed 3/20/2024).

(12) Li, L. T.; Jiang, G.; Chen, Q.; Zheng, J. N. Ki67 is a promising molecular target in the diagnosis of cancer (Review). *Mol Med Rep* **2015**, *11* (3), 1566-1572. DOI: 10.3892/mmr.2014.2914.

(13) Sun, X.; Kaufman, P. D. Ki-67: more than a proliferation marker. *Chromosoma* **2018**, *127* (2), 175-186. DOI: 10.1007/s00412-018-0659-8.

(14) Fnu, T. P.; Li, J. M.; Ravindranathan, S.; Waller, E. K. Inhibition of Vasoactive Intestinal Peptide Signaling with More Potent Inhibitors Augments T-Cell Activation and Prolongs Survival in Leukemic Mice. *Blood* **2021**, *138*, 1868-+. DOI: 10.1182/blood-2021-151879.

(15) Petersen, C. T.; Li, J. M.; Waller, E. K. Administration of a vasoactive intestinal peptide antagonist enhances the autologous anti-leukemia T cell response in murine models of acute leukemia. *Oncoimmunology* **2017**, *6* (5), e1304336. DOI: 10.1080/2162402X.2017.1304336 From NLM PubMed-not-MEDLINE.

(16) Kantarjian, H.; Kadia, T.; DiNardo, C.; Daver, N.; Borthakur, G.; Jabbour, E.; Garcia-Manero, G.; Konopleva, M.; Ravandi, F. Acute myeloid leukemia: current progress and future directions. *Blood Cancer Journal* **2021**, *11* (2), 41. DOI: 10.1038/s41408-021-00425-3.

(17) Thol, F.; Ganser, A. Treatment of Relapsed Acute Myeloid Leukemia. *Current Treatment Options in Oncology* **2020**, *21* (8), 66. DOI: 10.1007/s11864-020-00765-5.

(18) Arfons, L. M.; Tomblyn, M.; Rocha, V.; Lazarus, H. M. Second hematopoietic stem cell transplantation in myeloid malignancies. *Current Opinion in Hematology* **2009**, *16* (2), 112-123. DOI: 10.1097/MOH.0b013e3283257a87.

(19) Johansen-Leete, J.; Passioura, T.; Foster, S. R.; Bhusal, R. P.; Ford, D. J.; Liu, M.; Jongkees, S. A. K.; Suga, H.; Stone, M. J.; Payne, R. J. Discovery of Potent Cyclic Sulfopeptide Chemokine Inhibitors via Reprogrammed Genetic Code mRNA Display. *Journal of the American Chemical Society* **2020**, *142* (20), 9141-9146. DOI: 10.1021/jacs.0c03152.

(20) Cui, X.; Cao, D.; Qu, C.; Zhang, X.; Zheng, A. A study of the chemical and biological stability of vasoactive intestinal peptide. *Drug Development and Industrial Pharmacy* **2013**, *39* (12), 1907-1910. DOI: 10.3109/03639045.2012.693503.

(21) Domschke, S.; Domschke, W.; Bloom, S. R.; Mitznegg, P.; Mitchell, S. J.; Lux, G.; Strunz, U. Vasoactive intestinal peptide in man: pharmacokinetics, metabolic and circulatory effects. *Gut* **1978**, *19* (11), 1049-1053. DOI: 10.1136/gut.19.11.1049.

(22) Henning, R. J.; Sawmiller, D. R. Vasoactive intestinal peptide: cardiovascular effects. *Cardiovascular Research* **2001**, *49* (1), 27-37. DOI: 10.1016/s0008-6363(00)00229-7 (acccessed 3/11/2024).

(23) Micsonai, A.; Wien, F.; Kernya, L.; Lee, Y. H.; Goto, Y.; Refregiers, M.; Kardos, J. Accurate secondary structure prediction and fold recognition for circular dichroism spectroscopy. *Proc Natl Acad Sci U S A* **2015**, *112* (24), E3095-3103. DOI: 10.1073/pnas.1500851112 From NLM Medline.

3.9 Supporting information

3.9.1 Materials

Canonical N-α-Fmoc-*L*-amino acids were obtained from Oakwood Chemical, Estill, USA. Fmoc-Lys(N₃)-OH was purchased from Aapptec, Louisville, USA and Fmoc-Asp(OMpe)-OH was purchased from Combi-Blocks, San Diego, USA. NovaSyn® TGR resin was obtained from Novabiochem, Merck Biosciences, Darmstadt, Germany. All peptides were prepared by solid-phase automated synthesis (CEM Liberty Blue) using standard Fmoc protocol. Asparagine (N), cysteine (C), and glutamine (Q) were incorporated with Trt protected side chains. Aspartic acid (D) was incorporated with OMpe protected side chain. Arginine (R) was incorporated with Pbf protected side chain. Lysine (K) was incorporated with Boc protected side chain. Serine (S), threonine (T), and tyrosine (Y) were incorporated with *t*Bu protected side chains. DBCO-mPEG, 20 kDa was purchased from Click Chemistry Tools, Scottsdale, USA. Synthetic reagents and solvent were purchased from MilliporeSigma, Darmstadt, Germany of the highest grade and used without further purification. Gel-electrophoresis materials were purchased from BioRad, Hercules, USA.

3.9.2 Linear peptide synthesis

All peptides were prepared as carboxamides at the C-terminus on NovaSyn® TGR resin (0.24 mmol/g). 0.2 M amino acid stock solutions were used, along with 1.0 M Oxyma Pure and 1.0 M DIC. All stock solutions were prepared using HPLC-grade DMF. For Fmoc-deprotection, 20% (v/v) piperidine solution in DMF was prepared. For N-terminus acetylation, 20% (v/v) acetic anhydride in DMF was used. Syntheses were carried out under 0.1 mmol scale. All amino acids were singly coupled at 90°C for 2 minutes except for arginine, which was doubly coupled. The instrument was set to deliver 6 equivalents of amino acid, etc. N-terminus acetylation was performed using 4 iterative couplings at 60°C.

3.9.3 Cleavage and Purification of Crude Peptides

Crude peptides without methionine or cysteine were cleaved under air using a cocktail of TFA. For peptides containing methionine or cysteine, cleavage was performed under nitrogen using a cocktail of 94% HPLC-grade TFA, 2.5% H_2O, 2.5% EDT, 1% TIPS for 2 hours. For peptides containing azidolysine, cleavage was performed under nitrogen using a cocktail of 92.5:2.5:2.5:2.5 (w/w/w/w) TFA:H_2O:TIPS:DTT for 2 hours [10]. The crude peptide solution was triturated with 10 CV of cold Et_2O. The white solid was centrifuged at 4000 rpm for 10 min to form a pellet. After removal of Et_2O, the solid was resuspended twice with Et_2O then dried under a stream of nitrogen. The crude material was reconstituted in 20% MeCN in H_2O (0.1% TFA) and filtered via 0.45 μm syringe filter (PTFE). The crude solution was purified on an Agilent 1260 preparatory RP-HPLC using a Pursuit C18 column (21.2 x 250 mm, 5 μm) at 20 mL/min. The peptides were purified using H_2O (solvent A) and MeCN (solvent B) with 0.1% TFA co-solvent under the following gradient in **table 3.3**:

Time (min)	Solvent A (%)	Solvent B (%)
0	79	21
5	74	26
19	67	33
24	25	75

Table 3.3 HPLC gradient for ANT peptide purification

Peptide elution was monitored via UV absorption at 220 nm. The desired fractions were collected and lyophilized to yield purified product as a white powder, stored at -20°C.

3.9.4 Peptide stapling and purification

Cysteine-derived peptides were prepared as a 10 mg/mL stock solution in 1:7 MeCN: 20 mM NH_4HCO_3 buffer (pH 7.8). Reactions were performed using 1 mL aliquots and 5 equivalents of 1,3-

bis(bromomethyl)benzene. The peptide solutions were stirred at room temperature under nitrogen. Starting material consumption was monitored using an Agilent 1260 LC-MS using a Zorbax C18 column. After reaction completion, the crude material was purified on an Agilent 1260 semi-preparatory RP-HPLC using a Pursuit C18 column (10 x 250 mm, 5 µm) at 10 mL/min. Crude stapled peptide was purified using a gradient of 25-75% MeCN (0.1% TFA) over 25 minutes. The desired fractions were collected and lyophilized to yield purified stapled product as a white powder, stored at -20°C.

3.9.5 Synthesis and purification of peptide-PEG conjugates

Azido-lysine-derived peptides were prepared as a 1 mg/mL solution in 1xPBS buffer (pH 7.4). 2 equivalents of DBCO-mPEG, 20 kDa were added to the peptide solution and allowed to stir at room temperature for 24 hours. Reaction completion was confirmed via 4-20% SDS-PAGE and stained with Coomassie Bio-safe™. Peptide-PEG conjugates were dialyzed (2 kDa MWCO) into 100 mM CAPS buffer (pH 10.6) then purified on a Bio-Rad FPLC (NGC 10) via CEX using a HiTrap® SP Sepharose FF column (Cytiva, Marlborough, USA). After eluting free PEG, the desired PEG-peptide was eluted using 100 mM CAPS buffer (pH 10.6) with 250 mM NaCl. Peptide-PEG elution was monitored via UV absorption at 220 nm. Fractions containing PEG-peptide were distinguished from free PEG via Coomassie stain. The desired fractions were collected and lyophilized to yield product as a white powder, stored at -20°C.

3.9.6 Peptide analysis and characterization

Purified peptides were characterized by single quadrupolar LCMS using an Agilent 1260 series instrument or by Agilent 6545XT LC-QTOF. The mass-to-charge ratios were used to determine the experimental mass of the peptide, which were verified against the calculated mass. Analytical RP-

HPLC spectra were obtained using an Agilent 1260 series with a Pursuit C18 column (4.6 x 250 mm, 5 µm). Purified peptides were prepared in 5% MeCN in H_2O (0.1% TFA) then run on a 5-95% MeCN gradient (0.1% TFA) over 10 minutes at 1 mL/min. Peptide purity was determined to be >95% via integration at 220 nm.

3.9.7 Circular Dichroism Spectroscopy

Circular dichroism spectra were obtained using a Jasco J-1500 spectrometer measuring from 260-190 nm in 20 mM sodium phosphate buffer (pH 7.0) at 20°C. A 0.1 mm path length quartz cuvette was used, and spectra were obtained with 0.5 nm data pitch, 100 nm/min scan speed, a time constant (D.I.T.) of 1 second, and a mean (n=3) accumulation for each spectrum. Peptides were prepared as 5 mg/mL stock solutions in buffer. A blank of 20 mM sodium phosphate buffer was used to subtract the background from the peptide spectra. Raw data was processed to reveal mean residue ellipticity [θ].

3.9.8 α-helical Content

Estimation of peptide secondary structure from circular dichroism spectra was performed using the web-based application BeStSel [23], a freely accessible tool for estimation of peptide helicity. The α-helical content of the peptides qualitatively correlated with the CD spectra reported in this study.

3.9.9 Plasma stability assay

Using a protocol developed by Payne et al., the peptides or control (propantheline bromide) were prepared as 5 mM stock in 50 mM MOPS buffer and were added to human plasma (Sigma Aldrich, citrate added as an anticoagulant) to a final concentration of 200 µM. The peptides or control were incubated at 37°C for 0, 15, 30, 60, or 90 minutes before being quenched with three volumes of 1:1 (v/v) MeOH: MeCN. The samples post-quench were centrifuged at 13,500 rpm for 5 minutes before removing an aliquot of the supernatant (20 µL) and diluting it with one volume of MiliQ water (20

μL). The subsequent analysis was performed using a reverse-phase UHPLC-QTOF mass spectrometer. The area under the starting peptide peak (normalized to total area under the chromatogram) was used to quantify the amount of parent peptide remaining post-incubation.

3.9.10 *in vitro* T cell studies

Work performed by Yuou Wang and Tenzin Passang in the Waller lab. Leukapheresis product containing peripheral blood mononuclear cells (PBMC) from multiple healthy donors were obtained from Stem Cell Technologies. T cells were isolated from PBMC using human pan-T cell isolation kit according to manufacturer's protocol (Miltenyi Biotec, Catalog No. 130-096-535). Isolated T cells from 4-5 donors were pooled and seeded at a density of 1×10^6/mL in a 96-well plate, activated with 1.5 μL/mL CD3/CD28 T cell activator (ImmunoCult) in the presence of 30 IU interleukin 2 (IL2). Pooled T-cells were activated in the presence or absence of peptides (scrambled, ANT308 or modified ANT308) and cultured for 48 hours. Leukocyte Activation Cocktail with Golgi Plug (BD) was added 4 hours prior to cell harvesting to assess Granzyme B expression in CD4+ and CD8+ T cells. Briefly, cells were stained with Fixable Aqua live/dead viability stain for 5 minutes at room temperature (RT). Surface antibodies (**Table 3.4**) were added to the cells at the desired concentration and left to stain for 30 minutes at 4°C. Following surface staining, cells were subsequently fixed and permeabilized for intracellular Granzyme B detection. Antibody targeting Granzyme B (Cat. 515408, BioLegend) was added and left to stain for 45 minutes at RT. Stained samples were run on five-laser Cytek Aurora cytometer for subsequent analysis.

Target	Fluorochrome	Vendor	Catalog No.
CD3	PE/Cyanine 5	BioLegend	300410
CD4	APC-Cy7	BD	557871
CD8	Alexa Fluor 700	BD	557945
CD69	Brilliant Violet 650	BioLegend	310934
4-1BB	Brilliant Violet 650	BioLegend	309828

Table 3.4 List of antibodies used for flow cytometry
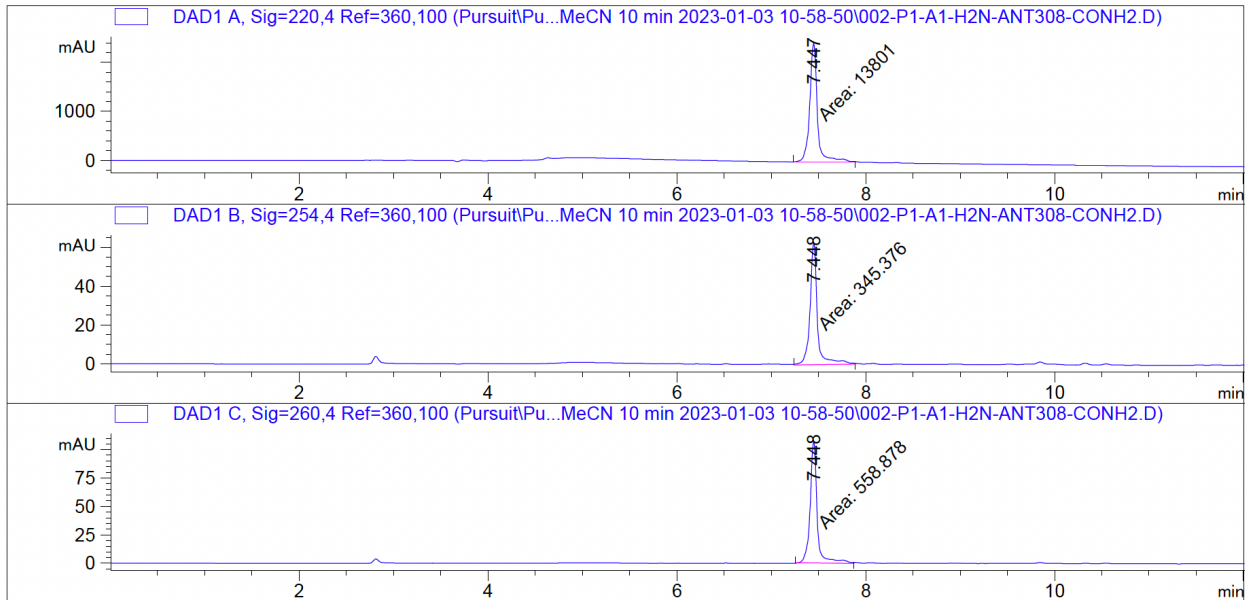
3.9.11 *in vivo* **AML studies**

Work performed by Jian-Ming Li in the Waller lab. P815-mastocytoma/myeloid leukemia cell line was obtained from ATCC. DBA/2j (H-2K^d) mice were purchased from Jackson Laboratory (Bar Harbor, Maine). The mice were maintained by Emory University facilities. Both male and female mice were 8-10 weeks old. On day 0, DBA/2j mice were injected subcutaneously with 1×10^5 P815 cells. The treatments were injected subcutaneously and started from day 7 once daily (ANT308, ANT308C13C17 stp, ANT308C13C17 unstp, and VIP-fully scramble, sc) and once every three days (ANT308-PEG, sc) for 10 days or 14 days. Lymphocyte kinetics were analyzed weekly through pterygoid venous plexus blood collection from the recipients. DBA mice were measured with tumor size by caliper, twice weekly. Either condition was reached or moribund, mice would be euthanized, the dead would be counted on the next day: when tumor size was over 20 mm on any side, or tumor ulceration was >10 mm/infection/necrosis, mouse ability was impaired, unable to eat/drink, or mouse was emaciated. Data were analyzed using Prism version 9 and SPSS statistics 23 are presented as mean ± SD of all evaluable samples if not otherwise specified. Survival differences among groups were calculated with the Kaplan-Meier log-rank test in a pair-wise fashion. Other data were compared using 1-way analysis of variance. A p-value of <0.05 was considered significant. Animal studies were approved by the Institutional Animal Care & Use Committee (IACUC).
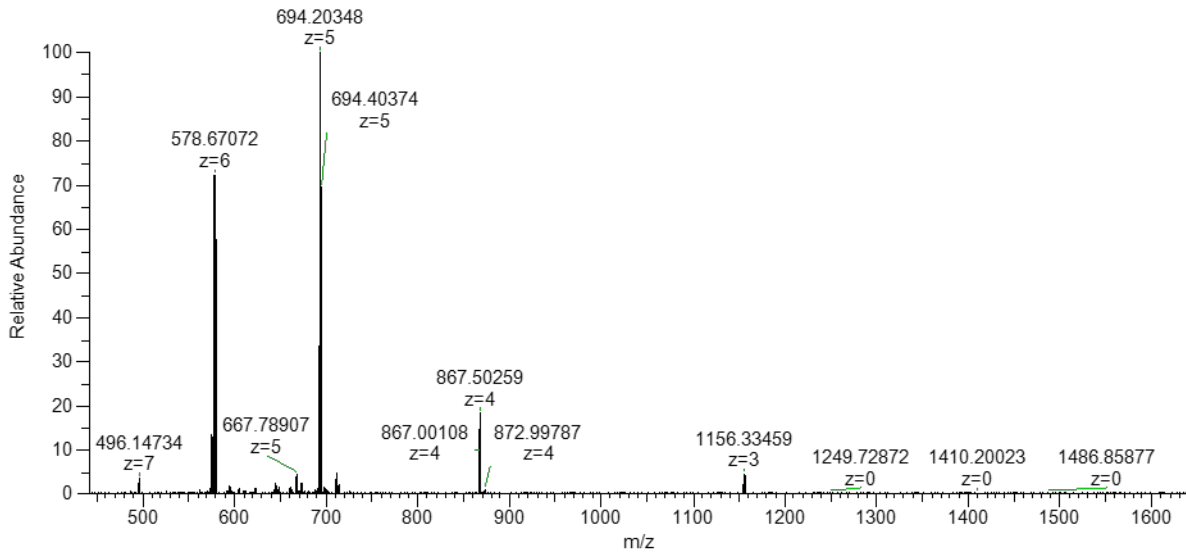
3.9.12 HPLC & MS Spectra

Peptide	MW	6M^{6+} calc	6M^{6+} exp	5M^{5+} calc	5M^{5+} exp	4M^{4+} calc	4M^{4+} exp	3M^{3+} calc	3M^{3+} calc
ANT308	3463.98	578.67	578.6	694.20	693.9	867.50	867.7	1156.33	1156.0
AcANT308	3505.98	585.71	585.67	702.66	702.60	878.07	878.00	1170.42	1170.33
ANT308K	3620.27	604.39	604.35	725.06	725.02	906.07	906.02	1207.76	1207.70
ANT308C13C17	3425.86	571.98	572.0	686.18	686.5	857.47	857.6	1142.96	1143.3
ANT308C13C17stp	3527.92	589.33	589.5	706.99	706.9	883.50	883.3	1177.65	1177.6

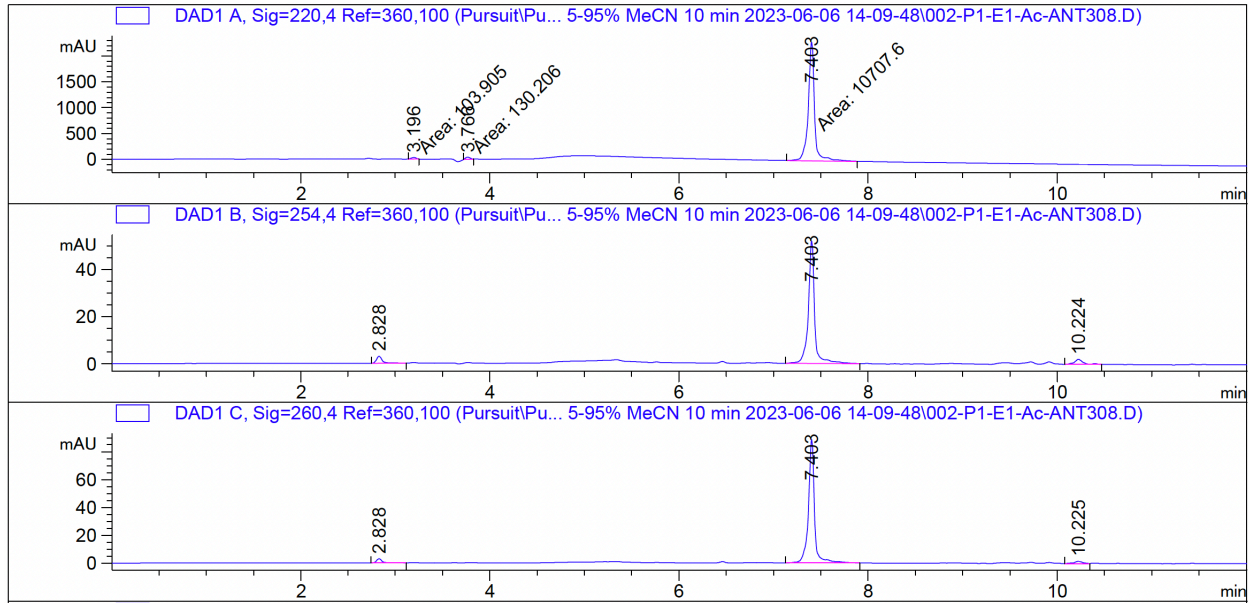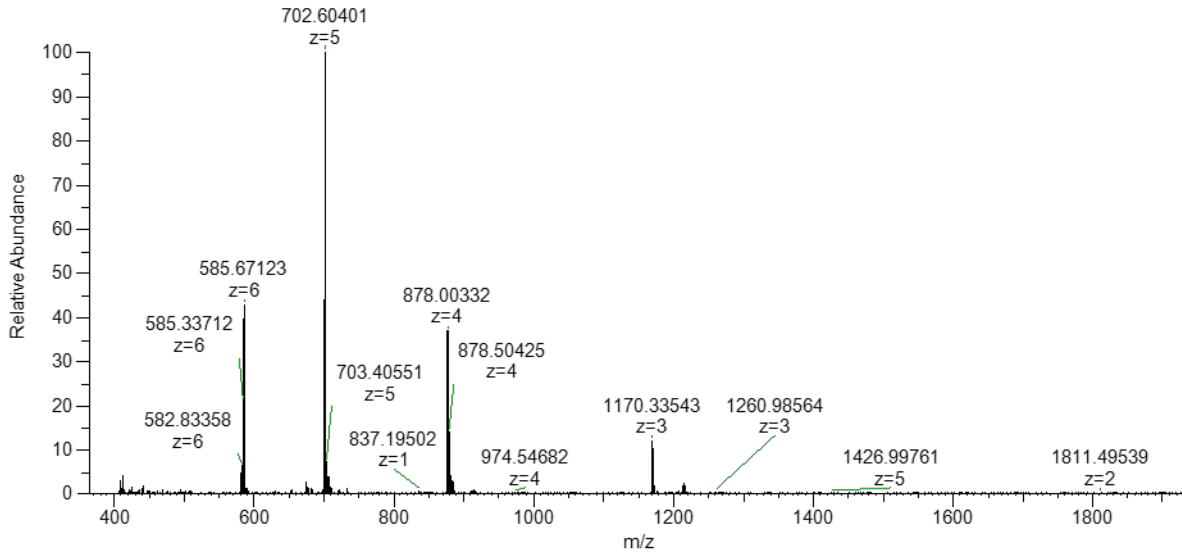**Table 3.5 Comparison of calculated & experimental *m/z***

ANT308

DAD1 A, Sig=220,4 Ref=360,100 (Pursuit\Pu...MeCN 10 min 2023-01-03 10-58-50\002-P1-A1-H2N-ANT308-CONH2.D)

7.447
Area: 13801

DAD1 B, Sig=254,4 Ref=360,100 (Pursuit\Pu...MeCN 10 min 2023-01-03 10-58-50\002-P1-A1-H2N-ANT308-CONH2.D)

7.448
Area: 345.376

DAD1 C, Sig=260,4 Ref=360,100 (Pursuit\Pu...MeCN 10 min 2023-01-03 10-58-50\002-P1-A1-H2N-ANT308-CONH2.D)

7.448
Area: 558.878

EX2995 #18-536 RT: 0.16-4.68 AV: 519 NL: 6.39E+007
T: FTMS + p ESI Full ms [300.0000-4000.0000]

694.20348
z=5

694.40374
z=5

578.67072
z=6

867.50259
z=4

496.14734
z=7

667.78907
z=5

867.00108
z=4

872.99787
z=4

1156.33459
z=3

1249.72872
z=0

1410.20023
z=0

1486.85877
z=0

Ac-ANT308

DAD1 A, Sig=220,4 Ref=360,100 (Pursuit\Pu... 5-95% MeCN 10 min 2023-06-06 14-09-48\002-P1-E1-Ac-ANT308.D)

DAD1 B, Sig=254,4 Ref=360,100 (Pursuit\Pu... 5-95% MeCN 10 min 2023-06-06 14-09-48\002-P1-E1-Ac-ANT308.D)

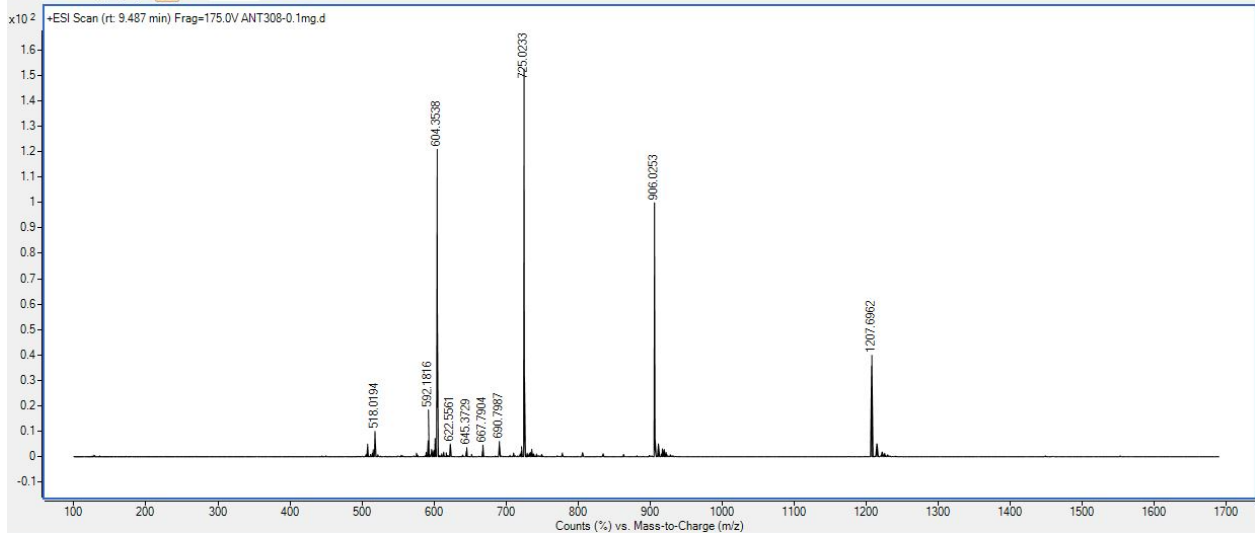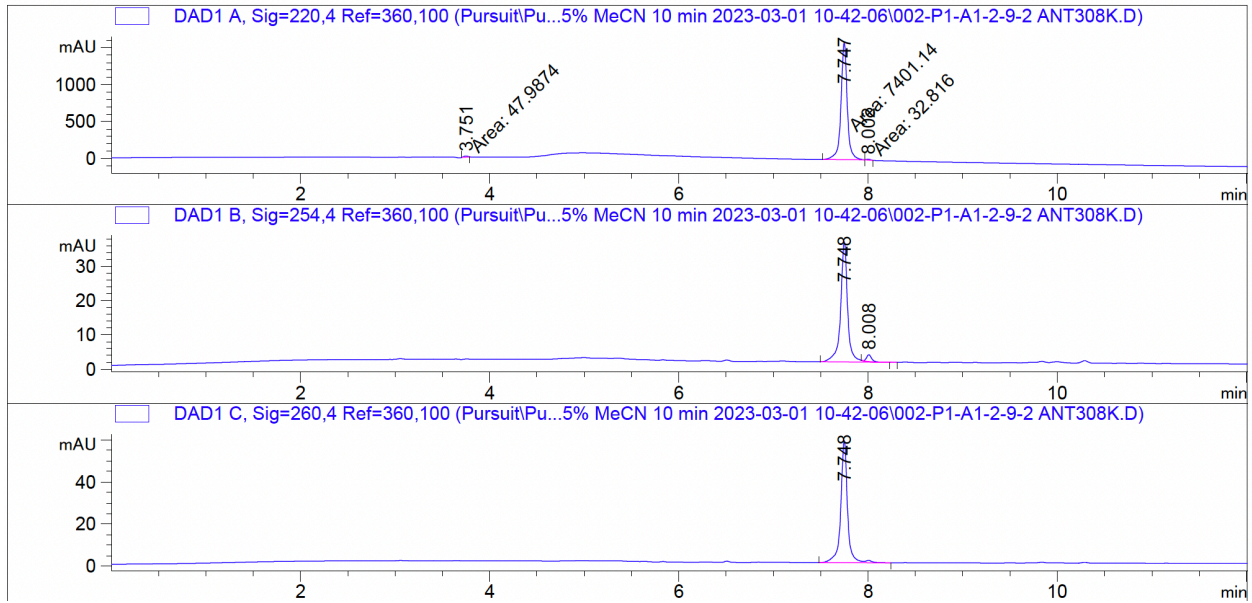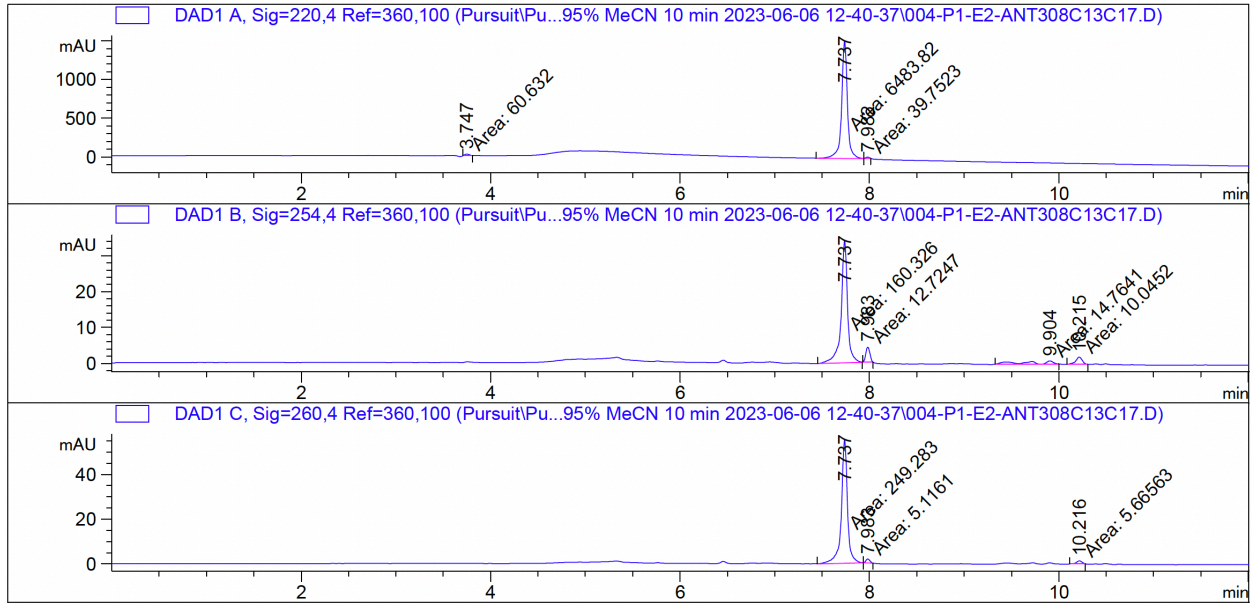DAD1 C, Sig=260,4 Ref=360,100 (Pursuit\Pu... 5-95% MeCN 10 min 2023-06-06 14-09-48\002-P1-E1-Ac-ANT308.D)

EX28423 #3-91 RT: 0.03-0.79 AV: 89 NL: 6.01E+007
T: FTMS + p ESI Full ms [400.0000-4000.0000]

ANT308K_{N3}

DAD1 A, Sig=220,4 Ref=360,100 (Pursuit\Pu...5% MeCN 10 min 2023-03-01 10-42-06\002-P1-A1-2-9-2 ANT308K.D)

DAD1 B, Sig=254,4 Ref=360,100 (Pursuit\Pu...5% MeCN 10 min 2023-03-01 10-42-06\002-P1-A1-2-9-2 ANT308K.D)

DAD1 C, Sig=260,4 Ref=360,100 (Pursuit\Pu...5% MeCN 10 min 2023-03-01 10-42-06\002-P1-A1-2-9-2 ANT308K.D)

+ESI Scan (rt: 9.487 min) Frag=175.0V ANT308-0.1mg.d

ANT308C13C17 unstp

DAD1 A, Sig=220,4 Ref=360,100 (Pursuit\Pu...95% MeCN 10 min 2023-06-06 12-40-37\004-P1-E2-ANT308C13C17.D)

DAD1 B, Sig=254,4 Ref=360,100 (Pursuit\Pu...95% MeCN 10 min 2023-06-06 12-40-37\004-P1-E2-ANT308C13C17.D)

DAD1 C, Sig=260,4 Ref=360,100 (Pursuit\Pu...95% MeCN 10 min 2023-06-06 12-40-37\004-P1-E2-ANT308C13C17.D)

EX3248_20210908122621 #3-54 RT: 0.03-0.47 AV: 52 NL: 5.43E7
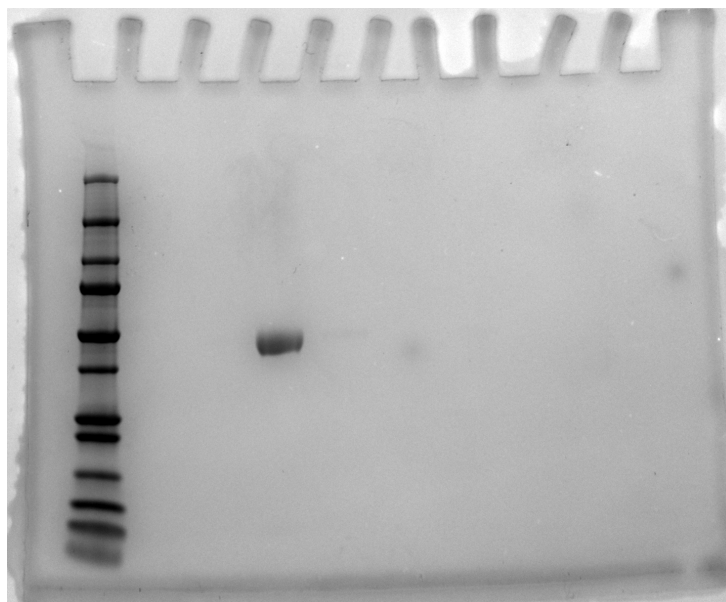T: FTMS + p ESI Full ms [300.0000-2000.0000]
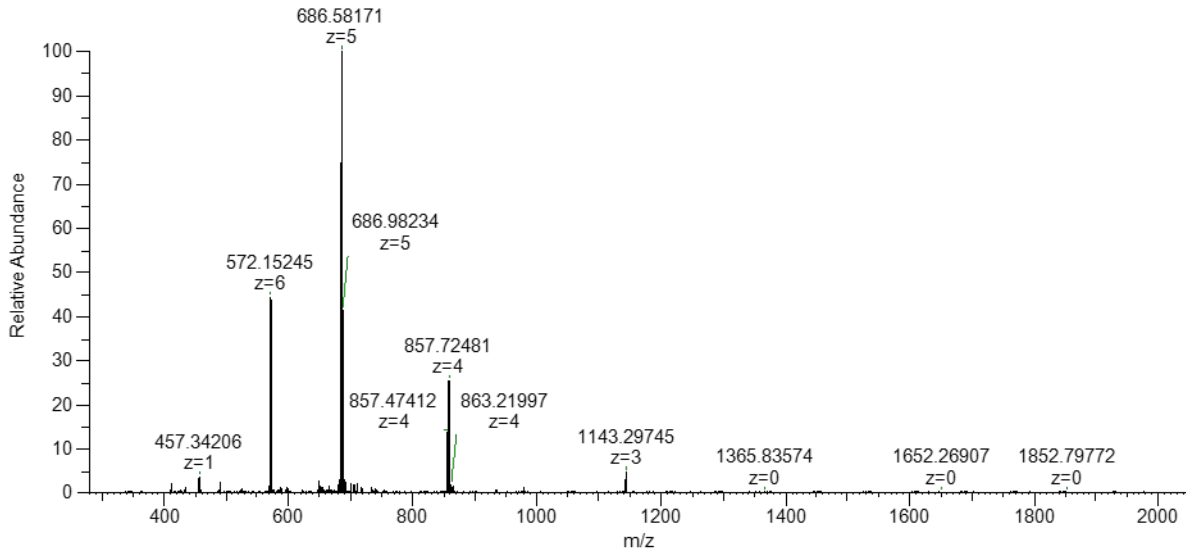
ANT308C13C17 stp
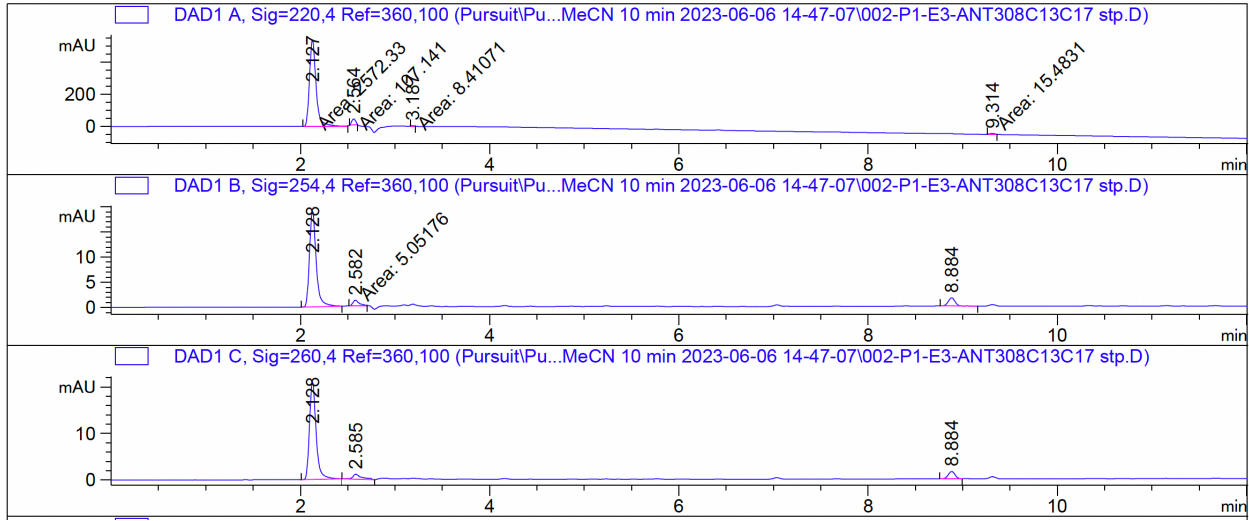
EX3291 #3-126 RT: 0.03-1.1 AV: 124 NL: 3.92E7
T: FTMS + p ESI Full ms [400.0000-2000.0000]
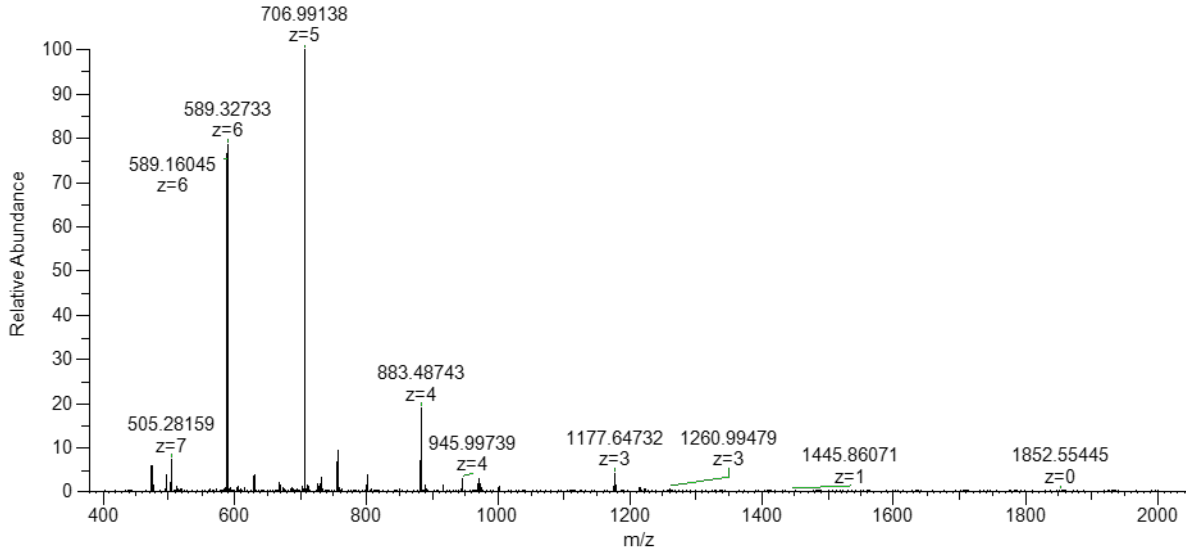
3.9.13 Peptide-PEG Analysis and Characterization

Lane	Sample
1	ladder
4	ANT308-PEG

Table 3.6 SDS-PAGE analysis of purified ANT308-PEG.

Part 2: Synthetic strategies to access ryptide

Chapter 4: Introduction to RiPP macrocyclic peptides

4.1 Introduction to macrocyclic peptides in drug discovery

In this chapter, we will discuss the historical significance of natural products in drug discovery, and the importance of genome mining for the discovery of new classes of natural products. Furthermore, we will discuss the emergence of naturally occurring macrocyclic peptides with novel cross-links and their therapeutic potential. This chapter will also investigate current synthetic strategies to access these cross-links, particularly those that focus on tyrosine and arginine C-C crosslinks.

4.1.1 Historical perspective of natural products in drug discovery – Introduction of Ribosomally synthesized and post-translationally modified peptides (RiPPs)

Throughout history, natural products have played a pivotal role in drug discovery, providing a fount of therapeutics to treat cancer and infectious diseases. Natural products possess several advantageous features relative to conventional synthetic molecules, such as significant scaffold diversity, structural complexity, and molecular rigidity.[1, 2] While most synthetic molecules have traditionally fallen under Lipinski's rule of five, there is an increasing demand for non-conforming therapeutics as evident by the increase in approval of high-molecular weight drugs.[3] Furthermore, natural products comprise a major source of oral drugs that extend beyond this rule.

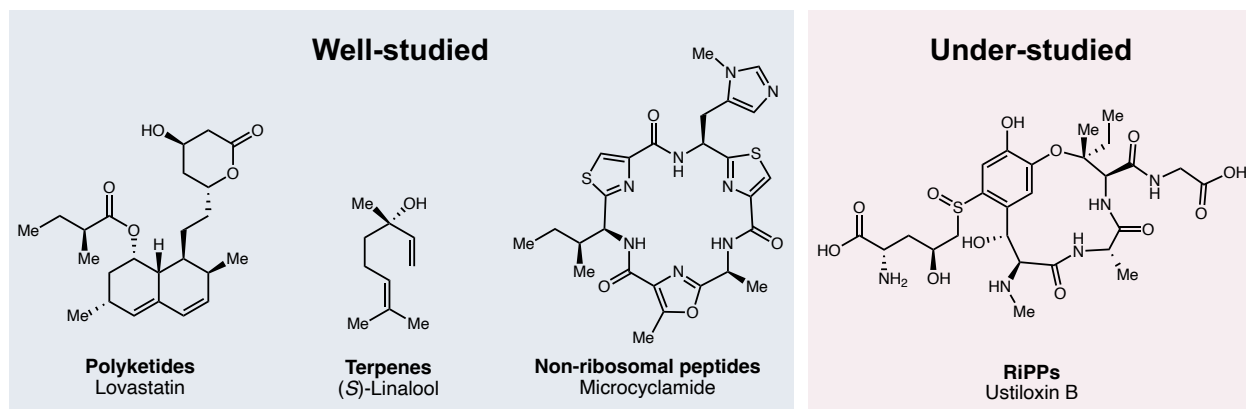## Classes of Natural Products

Figure 4.1 The emergence of the RiPP subclass. While polyketides, terpenes, and non-ribosomal peptides have been well-documented in literature, the chemical diversity of peptides of ribosomal origin (RiPPs) have only recently been uncovered.

Research in the 20th century has uncovered several prevalent classes of natural products, namely polyketides, terpenoids, alkaloids, and non-ribosomal peptides (**Figure 4.1**). The prevalence of genome sequencing in the 21st century has enabled the discovery and expansion of new classes of natural products, including ribosomally synthesized and post-translationally modified peptides (RiPPs).[1] RiPPs are a broad class of macrocyclic peptides with diverse bioactivies and structural complexity. They are distinct from non-ribosomal peptides, wherein RiPPs are not known to incorporate amino acids beyond the canonical 20 proteinogenic amino acids. Despite this, post-translational modification of this class enables a broad range of structural complexity with an expansive diversity of molecular scaffolds. Furthermore, there is growing interest in RiPP natural products due to their significant therapeutic potential, including antibacterial, antifungal, antiviral, and antitumor activities.
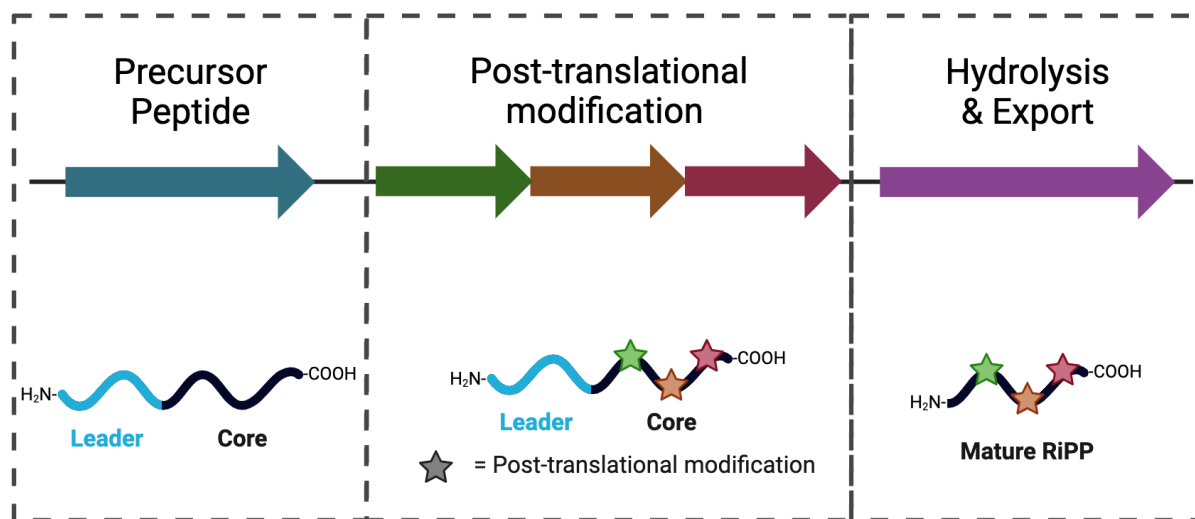
4.1.2 Genome sequencing and biosynthesis of RiPPs

Figure 4.2 General biosynthetic pathway towards generation of RiPPs. In the precursor peptide, the leader sequence recruits biosynthetic enzymes that modify the core sequence. The modified core sequence is cleaved from the leader sequence, furnishing the mature RiPP product.

RiPPs are typically subdivided based on their biosynthesis but can also be classified based on their producing organism or bioactivities. RiPP biosynthesis (**Figure 4.2**) is initiated upon ribosomal translation of mRNA encoding a precursor peptide and completed upon modification via post-translational modification (PTM) enzymes and cleavage from the leader sequence. The precursor peptide contains an N-terminal leader sequence and a C-terminal core region, which contains sites for PTM. Recognition sites may also be present in the C-terminus region when required in the biosynthesis. The leader sequence functions to recruit the biosynthetic enzymes that implement PTMs on the core region. After modification, the leader sequence is cleaved from the core region via peptidases to furnish the final product. In some cases, additional modifications may ensue concomitant or post leader sequence cleavage, including head-to-tail cyclization or additional PTMs.

In some cases, a signal sequence precedes the leader sequence, and serves to direct the precursor peptide to the organelle where it will undergo modification.

4.2 Synthetic approaches towards RiPP peptides

4.2.1 Synthetic approaches towards RiPPs with C-C crosslinks to Tyrosine

A common PTM found in RiPPs includes macrocyclization, which impart an increase in metabolic stability and a decrease in conformational flexibility. While some macrocyclization classes are easily realized from a synthetic perspective (i.e. N- to C- cyclization or disulfide bridging), many RiPPs contain unique cross-links that are synthetically difficult to access. Some of the more synthetically challenging cross-links include aryl-alkyl C-C linkages to various canonical amino acid side chains, including tryptophan, phenylalanine, and tyrosine. Furthermore, alkyl-alkyl C-C linkages are prevalent, particularly forming the complex non-canonical amino acids labionin, lanthionin, and avionin predominant in class III lanthipeptides. In preparation for developing a synthetic strategy towards ryptide, we will introduce RiPPs containing C-C cross-links to tyrosine, then discuss synthetic strategies that have been utilized to access these RiPPs.

Several classes of RiPPs contain various linkages to the side chain of tyrosine, including C-O, C-N, and C-C cross-links (**Figure 4.3**). Those that incorporate cross-links to tyrosine include dikaritins, pyrroloqinoline quinones (PQQ), and cittilins. Dikaritins are a class of fungal RiPPs that consist of phomopsins, ustiloxins, and asperipins, which all contain C-O linkages to tyrosine.[4] Biarylitides are a class of RiPPs that possess a conserved YYH or YFH core.[5] Biarylitides comprise a C-N linkage between the side chains of tyrosine and histidine. Tryptorubin A is a bicyclic RiPP derived from *Streptomyces* that contains a C-N linkage between the side chain of tyrosine and tryptophan.[6, 7]
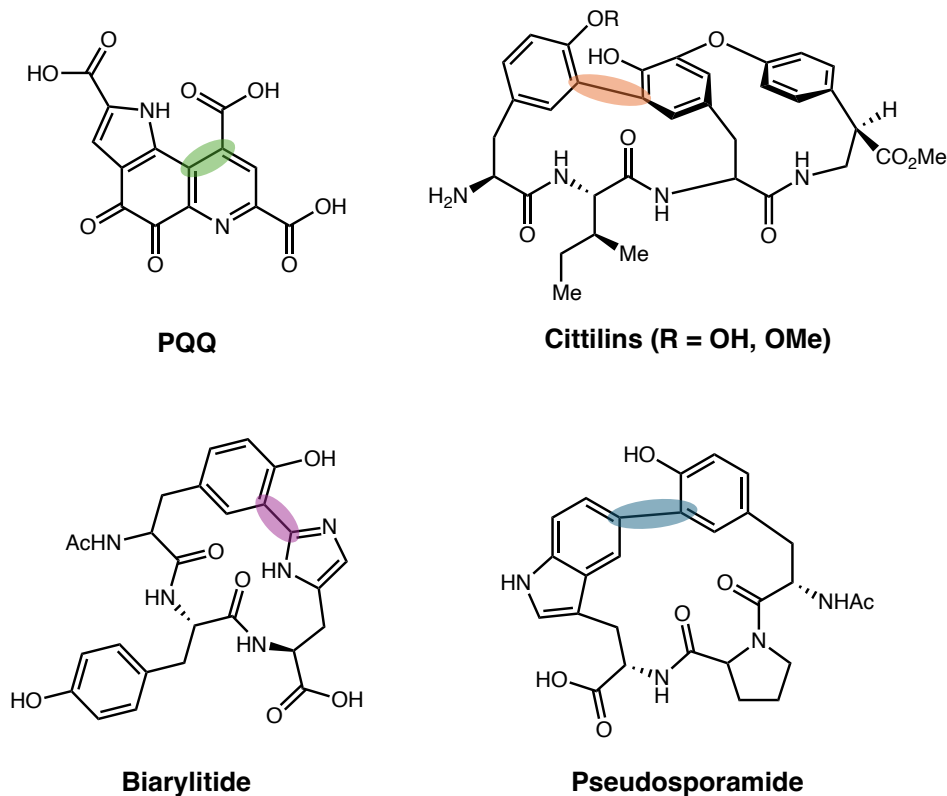
Figure 4.3 Different RiPP subclasses containing C-C crosslinks to tyrosine.

PQQ (or methoxatin) is a redox cofactor for bacterial dehydrogenases and possesses a PTM of glutamic acid and tyrosine. Since its discovery in 1979[8], PQQ has been extensively studied and demonstrated to provide neuroprotective effects.[9] A C-C cross-link between glutamic acid and tyrosine occurs during the biosynthesis of PQQ via radical *S*-adenosylmethionine-dependent enzyme (SAM), and the resulting intermediate undergoes additional enzymatic modification to furnish the cyclized PQQ.[10] There have been multiple reported syntheses of PQQ, of which the first syntheses were reported by the Weinreb and Corey groups in the early 80's.[11, 12]

Weinreb, 1981
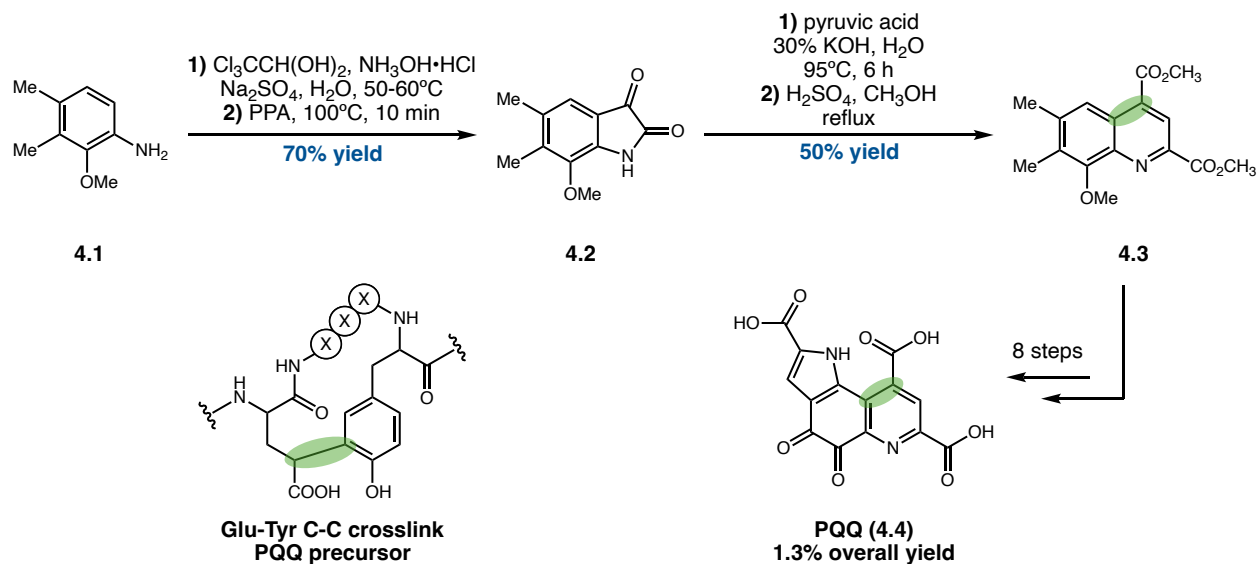
Scheme 4.1 Weinreb synthesis of PQQ. The biosynthesis of PQQ involves a C-C crosslink between glutamic acid and tyrosine.

The strategy utilized by Weinreb and co-workers focused on establishing the desired C-C cross-link early in the synthesis (**Scheme 4.1**). They leveraged a Sandmeyer isatin synthesis to generate a precursor to the desired quinoline core. Starting from an aniline (**4.1**), an aza-Michael addition with *in situ* nitrosoalkene furnished an oxime intermediate, which upon cyclization generates the isatin precursor (**4.2**). The Pfitzinger ring-condensation of isatin[13] with pyruvic acid affords the desired quinoline core (**4.3**), and 8 additional steps furnishes PQQ (**4.4**) in 1.3% overall yield.

Corey, 1981
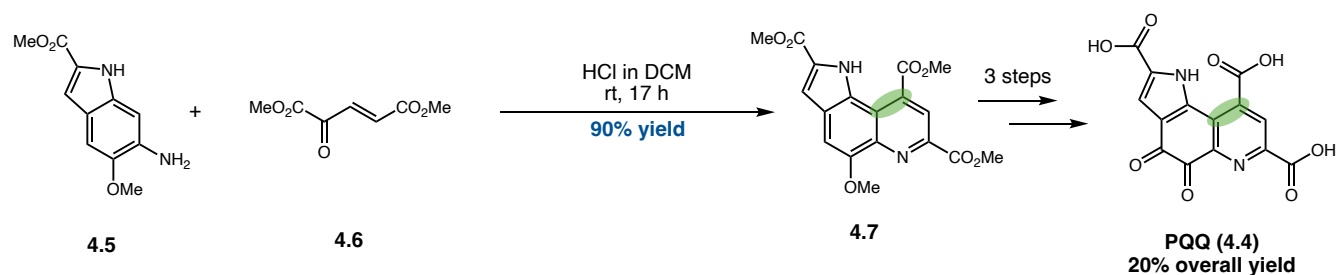
Scheme 4.2 Corey synthesis of PQQ.

The strategy employed by Corey and co-workers (**Scheme 4.2**) focused on generating a substituted indole core (**4.5**) in 5 steps, followed by a Doebner-Miller cyclization.[14] Aza-Michael addition of the indole into oxaglutaconate (**4.6**) followed by intramolecular aryl addition and subsequent dehydration afforded the quinoline core with the desired C-C crosslink (**4.7**) in excellent yield. 3 additional steps furnished PQQ (**4.4**) in a 20% overall yield. Syntheses of PQQ since the seminal work by Corey and Weinreb have focused on modifications of the Doebner-Miller cyclization, and include efforts from the Rees group.[15]

Hendrickson, 1982
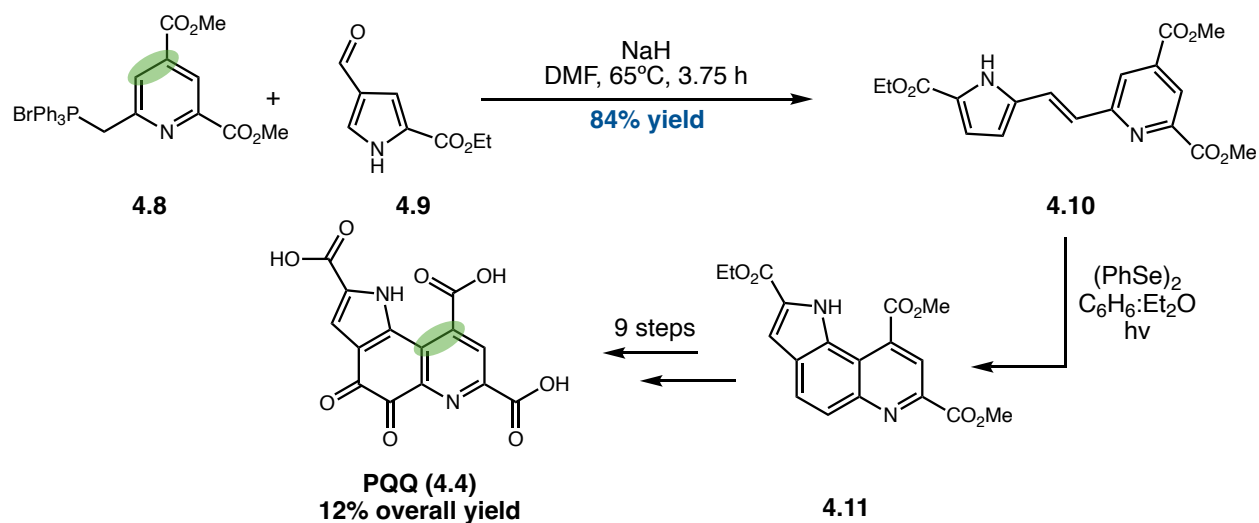
Scheme 4.3 Hendrickson synthesis of PQQ.

In the early-mid-80's, several other groups also contributed to the synthesis of PQQ.[16-19] The strategy leveraged by Hendrickson and co-workers (**Scheme 4.3**) involved a convergent synthesis of PQQ via pyrrole and pyridine ligation and photocyclization to forge the quinoline core. Initially, the pyridine fragment (**4.8**) containing the desired C-C cross-link underwent Wittig coupling with an aldehyde-substituted pyrrole (**4.9**) in excellent yield. The cross-linked pyridine-pyrrole (**4.10**) underwent a stilbene-type photocyclization to generate the desired quinoline core (**4.11**) in moderate yield, and after 9 steps furnished PQQ (**4.4**) in a 12% overall yield.
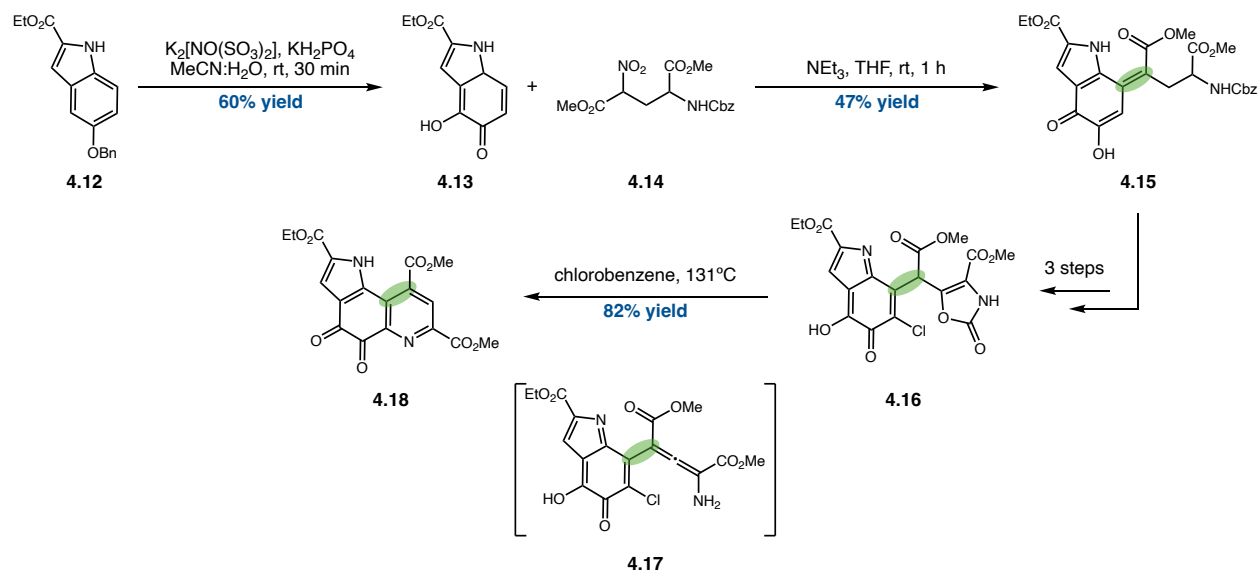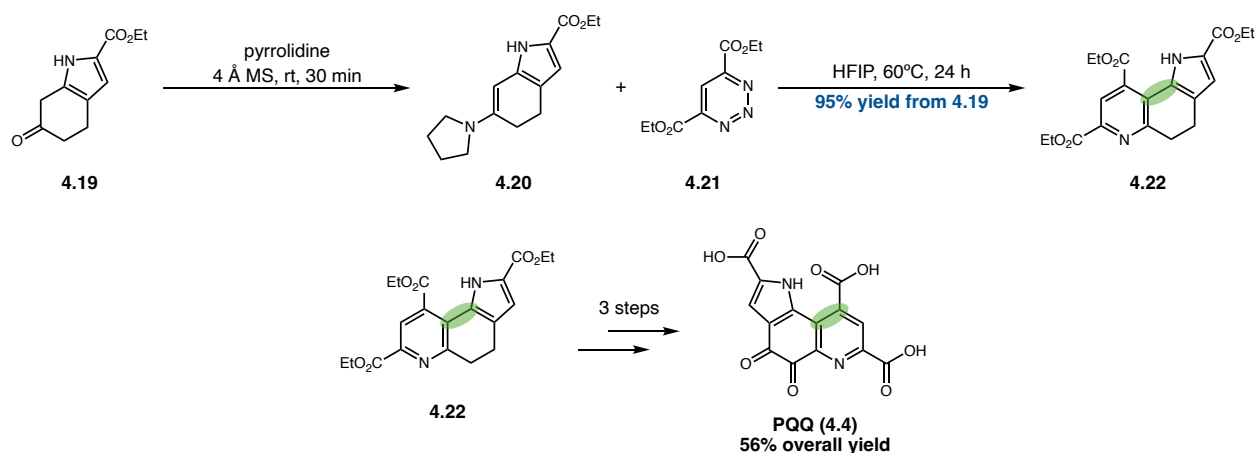
Scheme 4.4 Büchi synthesis of PQQ.

Similar to the Corey group's synthesis of PQQ, Büchi and co-workers (**Scheme 4.4**) envisaged indole as a starting fragment to access the PQQ core. Debenzylation of indole (**4.12**) generates the intermediate **4.13**, which undergoes a Michael addition/elimination sequence with **4.14** to generate the advanced intermediate (**4.15**). Additional transformations followed by thermal-mediated cyclization of tricycle (**4.16**) via a postulated allene intermediate (**4.17**) generated protected PQQ (**4.18**). Subsequent hydrolysis afforded PQQ in a 14-18% overall yield in seven steps total.

Boger, 2016

Scheme 4.5 Boger synthesis of PQQ

In 2016, the Boger group (**Scheme 4.5**) reported a concise synthesis of PQQ in 4 steps and in 56% overall yield.[20] Their synthetic approach featured an intermolecular hetero Diels-Alder cycloaddition. The starting ketone (**4.19**) is first transformed into enamine **4.20**, which undergoes cycloaddition with triazine (**4.21**). Ablation of nitrogen gas followed by pyrrolidine protonation and aromatization formed tricycle (**4.22**) in excellent yields. Important to the synthesis is the use of perfluoronated solvent to activate the electron-deficient heterocyclic azadienes, as well as serve as a mild acid catalyst for promoting loss of pyrrolidine to deliver the aromatized product. Subsequent oxidation and hydrolysis afforded PQQ (**4.4**).

Cittilin A[21] and B[22] are secondary metabolites derived from *Myxococcus* and *Streptomyces* bacterial strains, respectively. They consist of three tyrosines and an isoleucine forming a bicyclic tetrapeptide scaffold.[23] This class of RiPP undergoes PTM via P450 enzymes, and contains a central tyrosine 2 that is difunctionalized at carbons 3 & 5 on the tyrosine side chain. Thus, cittilins contain both an aryl C-C cross-link to tyrosine 1 (western macrocycle), and a C-O cross-link to tyrosine 3 (eastern macrocycle).

Synthetic efforts were initially focused towards accessing the western macrocycle and were developed by the Zhu group.[24] Eventually the Zhu group was able to complete the total synthesis of cittilin B.[25]

Zhu, 2001
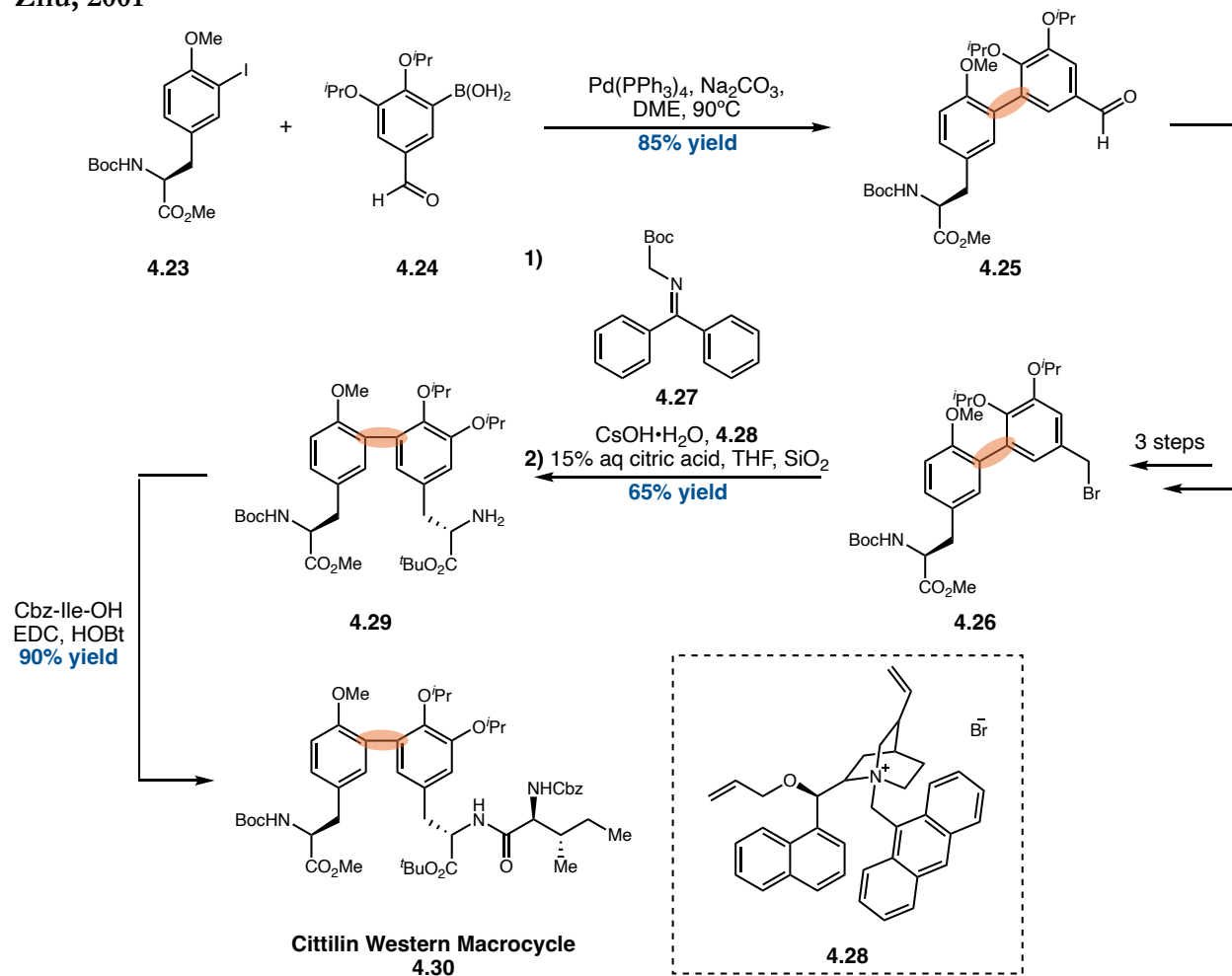
Scheme 4.6 Zhu synthesis of the Cittilin western macrocycle.

The western macrocycle was first completed by Zhu and co-workers in 2001 (**Scheme 4.6**). Key to their strategy was the synthesis of an aryl boronic acid (**4.24**), which was utilized in a palladium-catalyzed Suzuki coupling with iodinated protected-tyrosine (**4.23**) to forge the biaryl intermediate (**4.25**). To furnish the amino acid backbone of the central tyrosine, the aldehyde moiety was reduced and protected with a mesyl group, followed by Finklestein bromination. This intermediate (**4.26**)

underwent Corey's enantioselective alkylation using catalytic **4.28** with *N*-(diphenylmethylene)glycine *t*-butyl ester (**4.27**) to furnish the linear dipeptide (**4.29**). After a single peptide coupling the western macrocycle was complete (**4.30**). Zhu and co-workers observed a single atropisomer but did not disclose absolute configuration or axial chirality.

Zhu, 2003
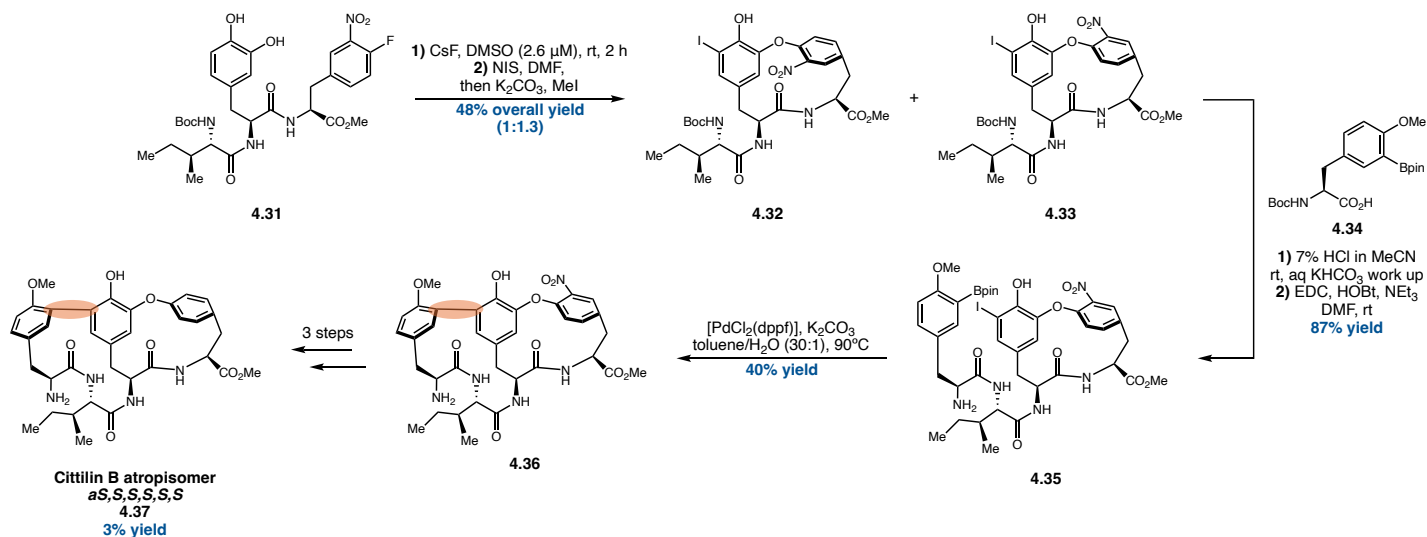
Scheme 4.7 Zhu total synthesis of Cittilin B atropisomer

The Zhu group subsequently explored conditions to furnish the C-O cross-link in the eastern macrocycle (**Scheme 4.7**), which was accomplished via an intramolecular S_NAr between a fluorinated phenylalanine and a hydroxylated tyrosine.[26] In their total synthesis of Cittilin B, Zhu and co-workers first constructed the eastern macrocycle, then furnished the western macrocycle via Suzuki-Miyaura coupling. A linear tripeptide was first formed via peptide couplings of isoleucine, 3-hydroxytyrosine, and 3-fluoro-4-nitrotyrosine to generate linear trimer **4.31**. The eastern macrocycle was then furnished using the intramolecular S_NAr conditions developed previously, forming two atropisomers (**4.32** & **4.33**) that were both carried forward. With the eastern macrocycle complete, a peptide coupling on the N-terminus of the trimer with a boronic acid tyrosine (**4.34**) derivative forged the cyclic tetramer **4.35**. Finally, Suzuki-Miyaura coupling completed the western macrocycle, completing synthesis of the

bicyclic scaffold (**4.36**). Global deprotection and removal of the nitro group forged a single

atropisomer (*aS,S,S,S,S,S*) of cittilin B (**4.37**) in a 3% overall yield. Additional characterization studies

of cittilin B revealed its configuration to be (*aR,S,S,S,S,S*).

Boger, 2003
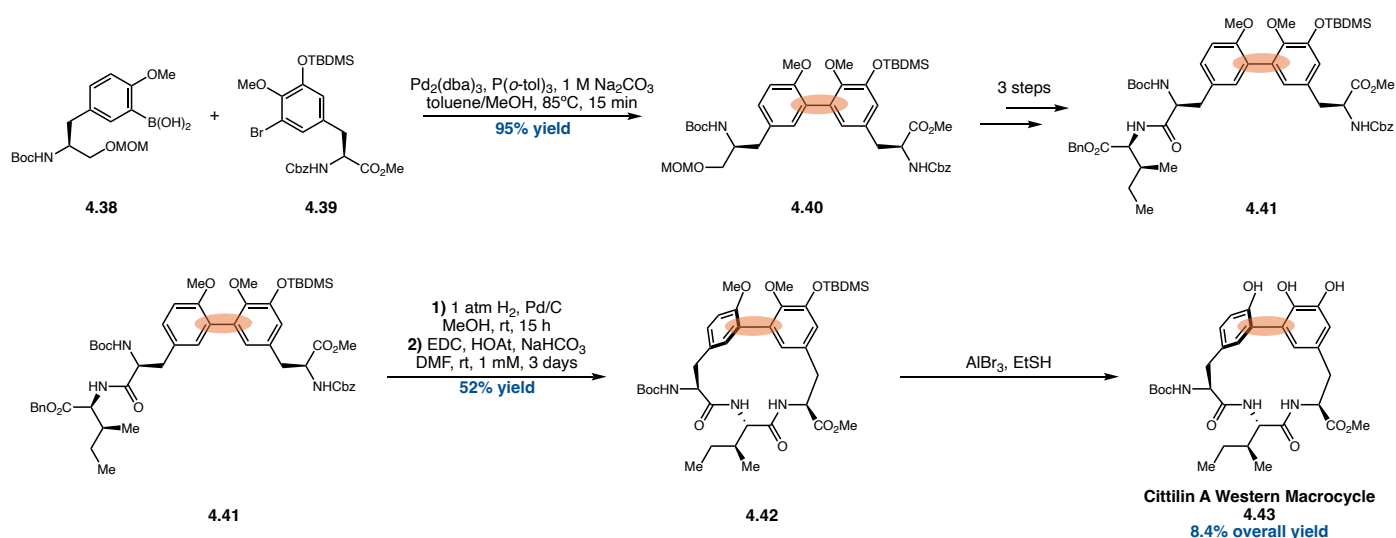
Scheme 4.8 Boger synthesis of the eastern macrocycle of Cittilin B

Since the reveal of cittilin B's configuration, Boger and co-workers developed a synthetic strategy to

access the correct atropisomer of the eastern macrocycle using a similar strategy to Zhu's synthesis of

the western macrocycle (**Scheme 4.8**). Suzuki coupling of **4.38** and **4.39** forged dimer **4.40**, followed

by deprotection, oxidation, and peptide coupling to isoleucine to furnish the cyclic trimer (**4.41**). The

TBDMS protecting group on the central tyrosine of Cittilin increased the energy barrier around the

aryl-aryl bond and slowed their interconversion. Deprotection and lactamization forged the eastern

macrocycle of Cittilin B (**4.43**) in an 8.4% overall yield.

While synthetic strategies have been explored for PQQ and cittilins, emergent classes of RiPPs containing C-C tyrosine cross-links have yet to be synthetically realized. A subclass of biarylitides have recently been identified to contain an unusual Tyr1-His3 C-C bridging.[27, 28] Pseudosporamide was recently reported to contain a C-C linkage between the side chains of tyrosine and tryptophan.[29]

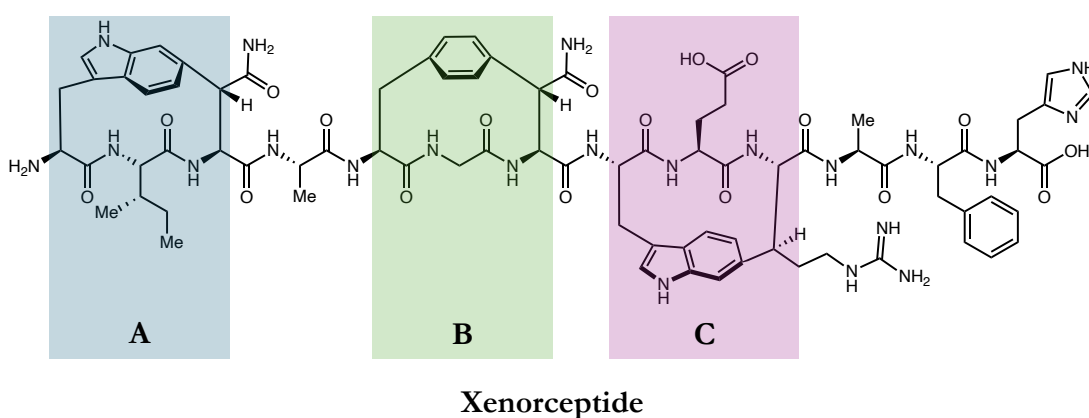**4.2.2 Synthetic approaches towards RiPPs with C-C crosslinks of Arg (Xenorceptide)**

Xenorceptide

Figure 4.4: Structure of Xenorceptide. The tricyclic peptide contains three macrocyclic links forming rings A-C. Ring C contains a C-C cross-link to the β-position of Arg.

PTM of arginine residues in RiPPs is significantly more scarce compared to other amino acids. Xenorceptide was recently discovered to possess such a modification and was first isolated from *Xenorhabdus* bacterial strains.[30] Xenorceptide is a 13-residue tricyclic peptide, comprising C-C linkages between Trp-1/Asn-3 (ring A), Phe-5/Asn-7 (ring B), and Trp-8/Arg-10 (ring C) (**Figure 4.4**). Although a partial synthesis of the B ring has been reported,[30] there is currently no total synthesis or partial synthesis of ring C.

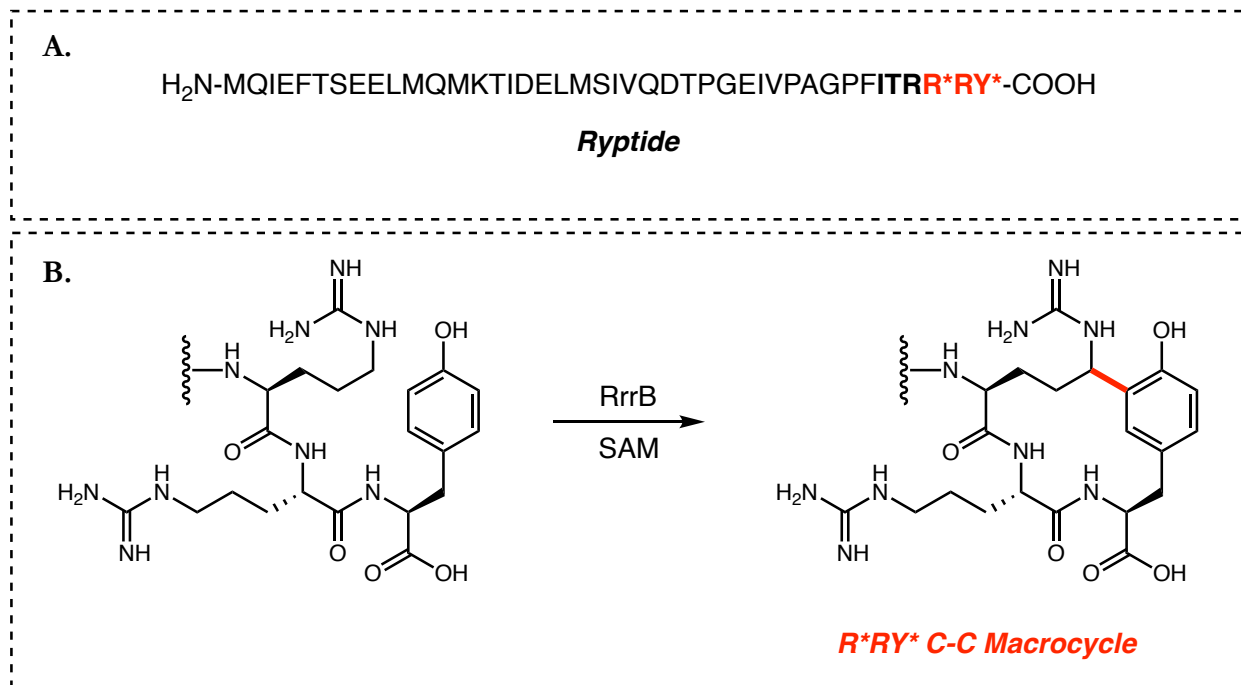### 4.2.3 Introduction to Ryptide & Retrosynthetic Analysis

Figure 4.5 A&B Structure of Ryptide. A. Precursor 42-mer sequence of Ryptide. Bolded residues are conserved residues in the RRR subfamily. Residues in red comprise the macrocycle of ryptide. * represents residues that have been modified to accommodate the macrocycle. **B.** C-C cross-link between Arg and Tyr furnishes the post-translational modification of ryptide.

The ryptide class was initially discovered in 2019 by Seyedsayamost and co-workers, and comprises a 42-mer peptide (**Figure 4.5A**).[31] Genome mining efforts revealed the biosynthetic gene cluster *rrr* that encodes for RaS enzymes. One such enzyme catalyzes a cross-link between the δ-position of arginine and the *o*-hydroxy position of tyrosine (**Figure 4.5B**). Ryptides possess a conserved RRY sequence that contain this C-C cross-link. To this date, no natural product of the ryptide class has been fully characterized, with only elucidation of the tricyclic moiety. Additionally, the configurational

assignment of the C-C cross-link remains unknown. To realize potential biological activities of this class, we sought to develop synthetic strategies to access both potential diastereomers of the ryptide RRY core, initially focusing on (*S,S,S*)-RRY.
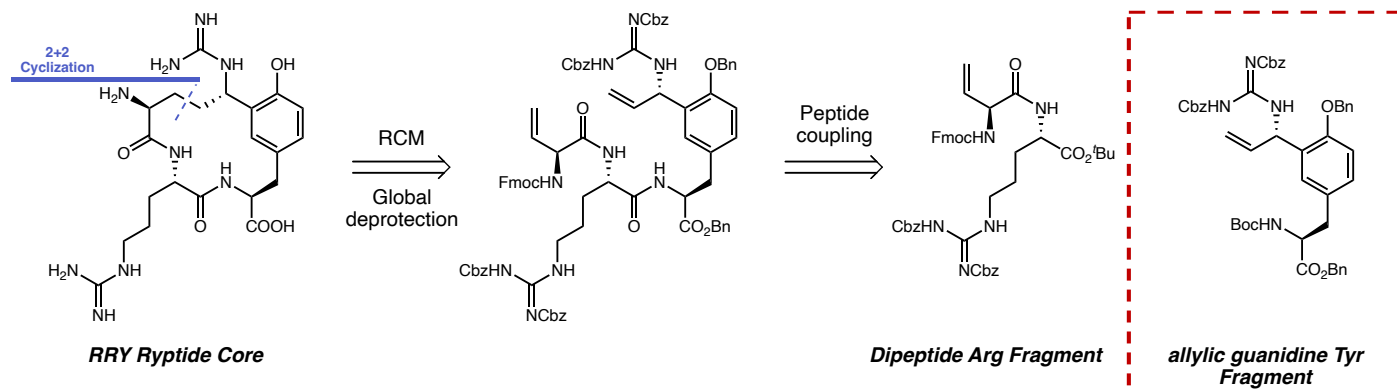
Scheme 4.9 Retrosynthetic analysis of Ryptide.

In our idealized retrosynthetic pathway (**Scheme 4.9**), we envisaged closing the macrocycle via ring closing metathesis, and coupling a vinylglycine (VGly)-Arg dipeptide (**4.45**) with an allylic guanidine tyrosine (**4.46**) to furnish the linear trimer (**4.44**). In the subsequent chapter, we will discuss our attempts to access the tyrosine fragment via: 1) metallophotoredox cross-coupling; 2) *ortho*-hydroxylation; and 3) stereoselective allylic amination.

4.3 Concluding Remarks

Natural products are the cornerstone of drug discovery, providing significant structural diversity and bioactivities that can be leveraged in therapeutic development. RiPPs are an emergent class of natural products with unique bioactivities that have been enabled by advances in bioinformatics and genome

sequencing. Many RiPPs contain rigid scaffolds predicated on C-C cross-links, enabled by radical SAM. Several RiPPs containing C-C cross-links to tyrosine have been identified, and subsequently several synthetic strategies have been developed to access this subclass of RiPPs. In contrast, very few RiPPs are known containing C-C cross-links to arginine, including the Ryptide subclass. In the subsequent chapter, we will discuss our synthetic strategies towards the synthesis of the Rytide macrocyclic RRY scaffold.

4.5 References

(1) Atanasov, A. G.; Zotchev, S. B.; Dirsch, V. M.; Orhan, I. E.; Banach, M.; Rollinger, J. M.; Barreca, D.; Weckwerth, W.; Bauer, R.; Bayer, E. A.; et al. Natural products in drug discovery: advances and opportunities. *Nature Reviews Drug Discovery* **2021**, *20* (3), 200-216. DOI: 10.1038/s41573-020-00114-z.

(2) Aware, C. B.; Patil, D. N.; Suryawanshi, S. S.; Mali, P. R.; Rane, M. R.; Gurav, R. G.; Jadhav, J. P. Natural bioactive products as promising therapeutics: A review of natural product-based drug development. *South African Journal of Botany* **2022**, *151*, 512-528. DOI: https://doi.org/10.1016/j.sajb.2022.05.028.

(3) Stegemann, S.; Moreton, C.; Svanbäck, S.; Box, K.; Motte, G.; Paudel, A. Trends in oral small-molecule drug discovery and product development based on product launches before and after the Rule of Five. *Drug Discovery Today* **2023**, *28* (2), 103344. DOI: https://doi.org/10.1016/j.drudis.2022.103344.

(4) Ford, R. E.; Foster, G. D.; Bailey, A. M. Exploring fungal RiPPs from the perspective of chemical ecology. *Fungal Biol Biotechnol* **2022**, *9* (1), 12. DOI: 10.1186/s40694-022-00144-9 From NLM PubMed-not-MEDLINE.

(5) Hug, J. J.; Frank, N. A.; Walt, C.; Senica, P.; Panter, F.; Muller, R. Genome-Guided Discovery of the First Myxobacterial Biarylitide Myxarylin Reveals Distinct C-N Biaryl Crosslinking in RiPP Biosynthesis. *Molecules* **2021**, *26* (24). DOI: 10.3390/molecules26247483 From NLM Medline.

(6) Wyche, T. P.; Ruzzini, A. C.; Schwab, L.; Currie, C. R.; Clardy, J. Tryptorubin A: A Polycyclic Peptide from a Fungus-Derived Streptomycete. *Journal of the American Chemical Society* **2017**, *139* (37), 12899-12902. DOI: 10.1021/jacs.7b06176.

(7) Reisberg, S. H.; Gao, Y.; Walker, A. S.; Helfrich, E. J. N.; Clardy, J.; Baran, P. S. Total synthesis reveals atypical atropisomerism in a small-molecule natural product, tryptorubin A. *Science* **2020**, *367* (6476), 458-463. DOI: 10.1126/science.aay9981 (acccessed 2024/02/15).

(8) Salisbury, S. A.; Forrest, H. S.; Cruse, W. B.; Kennard, O. A novel coenzyme from bacterial primary alcohol dehydrogenases. *Nature* **1979**, *280* (5725), 843-844. DOI: 10.1038/280843a0 From NLM Medline.

(9) Zhou, X. Q.; Yao, Z. W.; Peng, Y.; Mao, S. S.; Xu, D.; Qin, X. F.; Zhang, R. J. PQQ ameliorates D-galactose induced cognitive impairments by reducing glutamate neurotoxicity via the GSK-3beta/Akt signaling pathway in mouse. *Sci Rep* **2018**, *8* (1), 8894. DOI: 10.1038/s41598-018-26962-9 From NLM Medline.

(10) Zhu, W.; Klinman, J. P. Biogenesis of the peptide-derived redox cofactor pyrroloquinoline quinone. *Curr Opin Chem Biol* **2020**, *59*, 93-103. DOI: 10.1016/j.cbpa.2020.05.001 From NLM Medline.

(11) Gainor, J. A.; Weinreb, S. M. Total synthesis of methoxatin, the coenzyme of methanol dehydrogenase and glucose dehydrogenase. *The Journal of Organic Chemistry* **1981**, *46* (21), 4317-4319. DOI: 10.1021/jo00334a053.

(12) Corey, E. J.; Tramontano, A. Total synthesis of the quinonoid alcohol dehydrogenase coenzyme (1) of methylotrophic bacteria. *Journal of the American Chemical Society* **1981**, *103* (18), 5599-5600. DOI: 10.1021/ja00408a067.

(13) Knight, J. A.; Porter, H. K.; Calaway, P. K. The Synthesis of Quinolines by the Pfitzinger Reaction. *Journal of the American Chemical Society* **1944**, *66* (11), 1893-1894. DOI: 10.1021/ja01239a029.

(14) Denmark, S. E.; Venkatraman, S. On the Mechanism of the Skraup−Doebner−Von Miller Quinoline Synthesis. *The Journal of Organic Chemistry* **2006**, *71* (4), 1668-1676. DOI: 10.1021/jo052410h.

(15) MacKenzie, A. R.; Moody, C. J.; Rees, C. W. Synthesis of the bacterial coenzyme methoxatin. *Journal of the Chemical Society, Chemical Communications* **1983**, (22), 1372-1373, 10.1039/C39830001372. DOI: 10.1039/C39830001372.

(16) Hendrickson, J. B.; DeVries, J. G. A convergent total synthesis of methoxatin. *The Journal of Organic Chemistry* **1982**, *47* (6), 1148-1150. DOI: 10.1021/jo00345a057.

(17) Buchi, G.; Botkin, J. H.; Lee, G. C. M.; Yakushijin, K. A synthesis of methoxatin. *Journal of the American Chemical Society* **1985**, *107* (19), 5555-5556. DOI: 10.1021/ja00305a055.

(18) Schröder, B.; Gaich, T. Methoxatin as a Target in Total Synthesis. *Synthesis* **2017**, *49* (08), 1746-1756. DOI: 10.1055/s-0036-1589492.

(19) Laws, D., III; Plouch, E. V.; Blakey, S. B. Synthesis of Ribosomally Synthesized and Post-Translationally Modified Peptides Containing C–C Cross-Links. *Journal of Natural Products* **2022**, *85* (10), 2519-2539. DOI: 10.1021/acs.jnatprod.2c00508.

(20) Glinkerman, C. M.; Boger, D. L. Catalysis of Heterocyclic Azadiene Cycloaddition Reactions by Solvent Hydrogen Bonding: Concise Total Synthesis of Methoxatin. *Journal of the American Chemical Society* **2016**, *138* (38), 12408-12413. DOI: 10.1021/jacs.6b05438.

(21) Irschik, H.; Trowitzsch-Kienast, W.; Gerth, K.; Hofle, G.; Reichenbach, H. Saframycin Mx1, a new natural saframycin isolated from a myxobacterium. *J Antibiot (Tokyo)* **1988**, *41* (8), 993-998. DOI: 10.7164/antibiotics.41.993 From NLM Medline.

(22) Helynck, G.; Dubertret, C.; Frechet, D.; Leboul, J. Isolation of RP 66453, a new secondary peptide metabolite from Streptomyces sp. useful as a lead for neurotensin antagonists. *J Antibiot (Tokyo)* **1998**, *51* (5), 512-514. DOI: 10.7164/antibiotics.51.512 From NLM Medline.

(23) Hug, J. J.; Dastbaz, J.; Adam, S.; Revermann, O.; Koehnke, J.; Krug, D.; Müller, R. Biosynthesis of Cittilins, Unusual Ribosomally Synthesized and Post-translationally Modified Peptides from

Myxococcus xanthus. *ACS Chemical Biology* **2020**, *15* (8), 2221-2231. DOI:

10.1021/acschembio.0c00430.

(24) Boisnard, S.; Carbonnelle, A.-C.; Zhu, J. Studies on the Total Synthesis of RP 66453: Synthesis

of Fully Functionalized 15-Membered Biaryl-Containing Macrocycle. *Organic Letters* **2001**, *3* (13),

2061-2064. DOI: 10.1021/ol016021v.

(25) Bois-Choussy, M.; Cristau, P.; Zhu, J. Total Synthesis of an Atropdiastereomer of RP-66453

and Determination of Its Absolute Configuration. *Angewandte Chemie International Edition* **2003**, *42*

(35), 4238-4241. DOI: https://doi.org/10.1002/anie.200351996 (acccessed 2024/02/15).

(26) Boisnard, S.; Zhu, J. Studies toward the total synthesis of RP-66453. *Tetrahedron Letters* **2002**, *43*

(14), 2577-2580. DOI: https://doi.org/10.1016/S0040-4039(02)00307-6.

(27) Zdouc, M. M.; Alanjary, M. M.; Zarazua, G. S.; Maffioli, S. I.; Crusemann, M.; Medema, M. H.;

Donadio, S.; Sosio, M. A biaryl-linked tripeptide from Planomonospora reveals a widespread class of

minimal RiPP gene clusters. *Cell Chem Biol* **2021**, *28* (5), 733-739 e734. DOI:

10.1016/j.chembiol.2020.11.009 From NLM Medline.

(28) Nam, H.; An, J. S.; Lee, J.; Yun, Y.; Lee, H.; Park, H.; Jung, Y.; Oh, K.-B.; Oh, D.-C.; Kim, S.

Exploring the Diverse Landscape of Biaryl-Containing Peptides Generated by Cytochrome P450

Macrocyclases. *Journal of the American Chemical Society* **2023**, *145* (40), 22047-22057. DOI:

10.1021/jacs.3c07140.

(29) Saito, S.; Atsumi, K.; Zhou, T.; Fukaya, K.; Urabe, D.; Oku, N.; Karim, M. R. U.; Komaki, H.; Igarashi, Y. A cyclopeptide and three oligomycin-class polyketides produced by an underexplored actinomycete of the genus Pseudosporangium. *Beilstein J Org Chem* **2020**, *16*, 1100-1110. DOI: 10.3762/bjoc.16.97 From NLM PubMed-not-MEDLINE.

(30) Nguyen, T. Q. N.; Tooh, Y. W.; Sugiyama, R.; Nguyen, T. P. D.; Purushothaman, M.; Leow, L. C.; Hanif, K.; Yong, R. H. S.; Agatha, I.; Winnerdy, F. R.; et al. Post-translational formation of strained cyclophanes in bacteria. *Nature Chemistry* **2020**, *12* (11), 1042-1053. DOI: 10.1038/s41557-020-0519-z.

(31) Caruso, A.; Martinie, R. J.; Bushin, L. B.; Seyedsayamdost, M. R. Macrocyclization via an Arginine-Tyrosine Crosslink Broadens the Reaction Scope of Radical S-Adenosylmethionine Enzymes. *Journal of the American Chemical Society* **2019**, *141* (42), 16610-16614. DOI: 10.1021/jacs.9b09210.

Chapter 5: Progress towards the synthesis of Ryptide

5.1 Synthetic strategies leveraging metallophotoredox cross-coupling to access Tyr fragment

In this chapter, we will discuss the importance of transition metal catalysis in natural product syntheses, with particular focus on key methodologies that we explored in our efforts towards ryptide, including metallophotoredox, *ortho*-hydroxylation, and allylic amination chemistry. Furthermore, we will discuss our implementation of these methodologies into our synthetic routes. With regards to our synthetic efforts, the ryptide RRY macrocyclic core will be divided in three parts: 1) the tyrosine fragment 2) the precursor RR dimer fragment 3) late-stage macrocyclization. For each of these parts we will discuss challenges/limitations associated with these fragments, as well as solutions/workarounds we explored. We will finish the chapter with a discussion of the next steps towards our ryptide synthetic strategy.

5.1.1 Historical perspective of metallophotoredox chemistry of amino acids

Catalysis is ubiquitous in modern chemical transformations, of which 90% of commercial chemicals involve at least one catalytic step in their synthesis.[1] Since the turn of the century, transition metal catalysis has been extensively utilized as a reliable and modular way to construct complex frameworks from simple feedstock chemicals. Recognition of this feat has culminated in several Nobel Prizes, particularly in stereoselective catalysis,[2-4] olefin metathesis,[5-7] and palladium-catalyzed cross-coupling.[8-10] In contrast, light-mediated transformations have not seen broad adoption in the synthetic field due

to its use of harsh high-energy light and significant variation in absorption properties of organic substrates. Despite this, photoredox catalysis has gained significant popularity in the past decade. Key to the success of photoredox chemistry is the discovery of absorptive organic and organometallic complexes, enabling photochemical transformations without regard of the photophysical properties of the starting materials. The merging of these two powerful platforms, dubbed metallophotoredox, provides an opportunity to leverage transition-metal substrate control with excited-state chemistry, enabling a wide array of reactivity and access to novel disconnections.

Although classic palladium-mediated transformations can forge bonds to $C(sp^2)$ carbon centers, they are significantly limited in their ability to couple sp^3-hybridized fragments. Research in nickel-mediated catalysis has enabled this difficult transformation, of which nickel more readily undergoes oxidative addition into alkyl electrophiles and has a lower propensity to undergo β-hydride elimination than palladium.[11] In an effort to expand the scope of coupling partners to simpler and more abundant building blocks, nickel has also seen extensive use in metallophotoredox chemistry. An attractive class of substrates for metallophotoredox chemistry includes halide electrophiles, which are amongst the most common feedstock chemicals utilized in synthetic chemistry due to their abundance and bench stability. In addition to halide electrophiles, amino acids are cheap and widely abundant building blocks, of which decarboxylative cross-coupling of amino acids has emerged as a powerful strategy to forge C-C bonds. Thus, metallophotoredox cross-couplings aims to take advantage of these simple and widely available chemicals to generate molecular complexity.
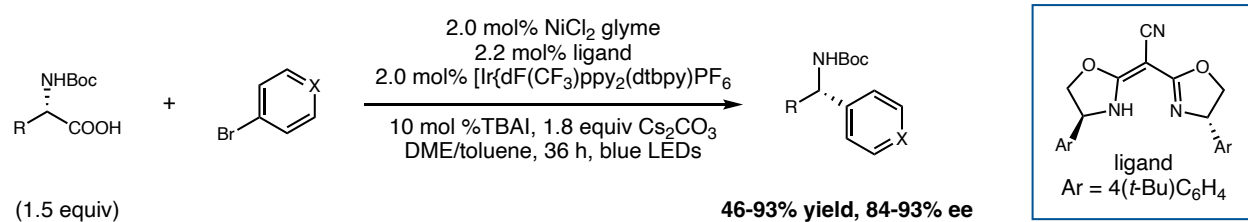
Scheme 5.1: General strategy leveraged by Macmillan and co-workers to forge stereoselective C-C crosslinks via decarboxylative α-amino radical formation.

Within the past decade, metallophotoredox cross-couplings have enabled the synthesis of unique C-C bonds. Seminal work by Macmillan and co-workers developed a synergistic dual catalytic strategy to access $C(sp^3\text{-}sp^2)$ bond formations not possible by transition metal or photoredox catalysis alone.[12] The nickel cycle orchestrates C-C bond formation, whereas the photocatalytic cycle generates the radical intermediate and turns over the nickel cycle. The same group later published an asymmetric transformation by leveraging chiral bisoxazoline (BOX) ligands (**Scheme 5.1**).[13] For our initial attempt of the tyrosine fragment, we aimed to utilize this chemistry to forge the key C-C crosslink in the ryptide core (**Scheme 5.2**).
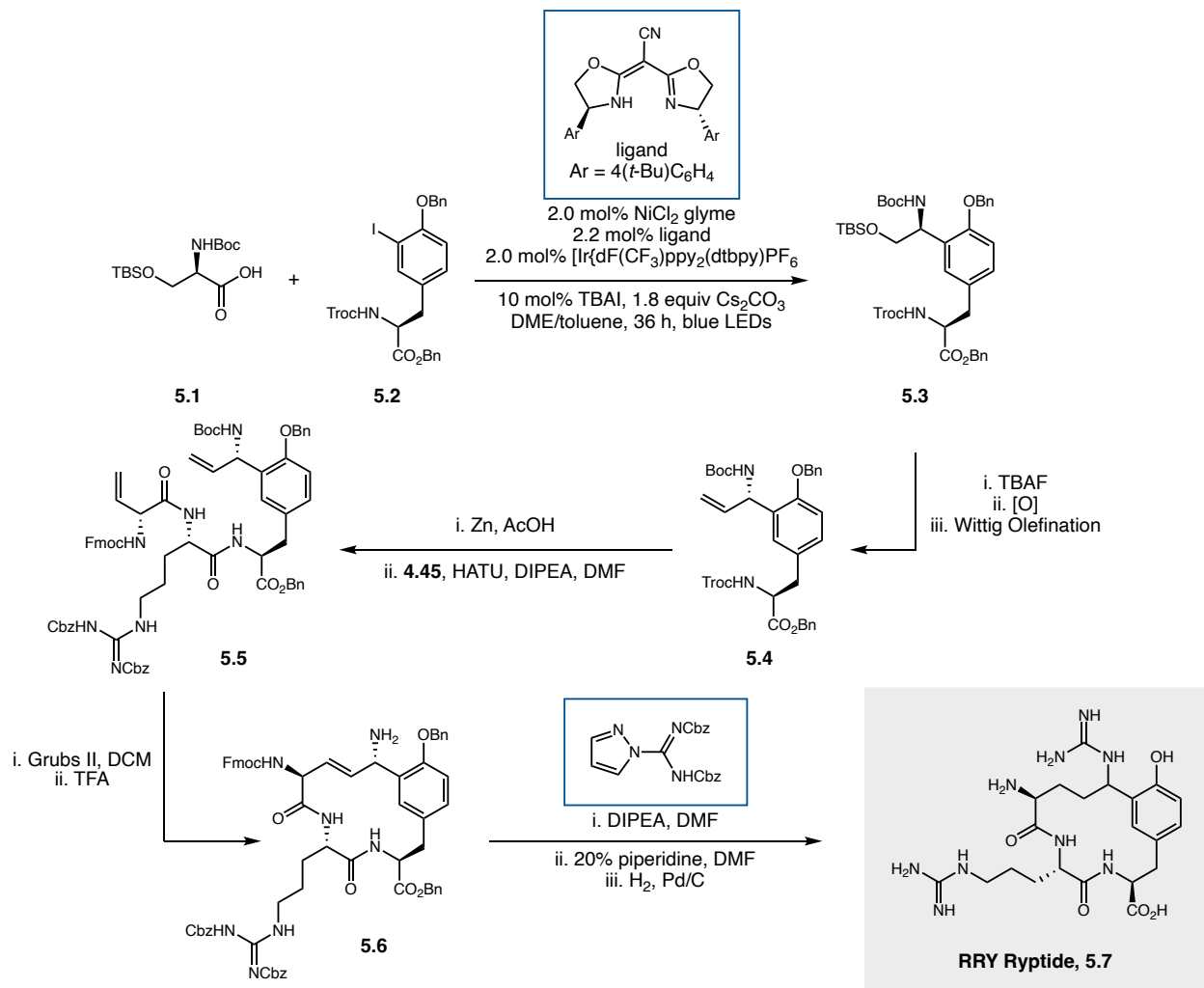
Scheme 5.2 Forward synthesis leveraging metallophotoredox cross-coupling.

Starting from protected serine (**5.1**) and 3-iodo-tyrosine (**5.2**), an asymmetric metallophotoredox decarboxylative cross-coupling would furnish the C-C cross-link of the ryptide core (**5.3**). The ensuing alcohol deprotection and oxidation would enable a Wittig olefination to generate a handle for RCM (**5.4**). Troc deprotection and peptide coupling with VGly-Arg dimer (**4.45**) would furnish the linear trimer (**5.5**). After macrocyclization to **5.6**, guanidinylation followed by global deprotection would generate the ryptide RRY core (**5.7**).

5.1.2 Metallophotoredox chemistry towards ryptide core
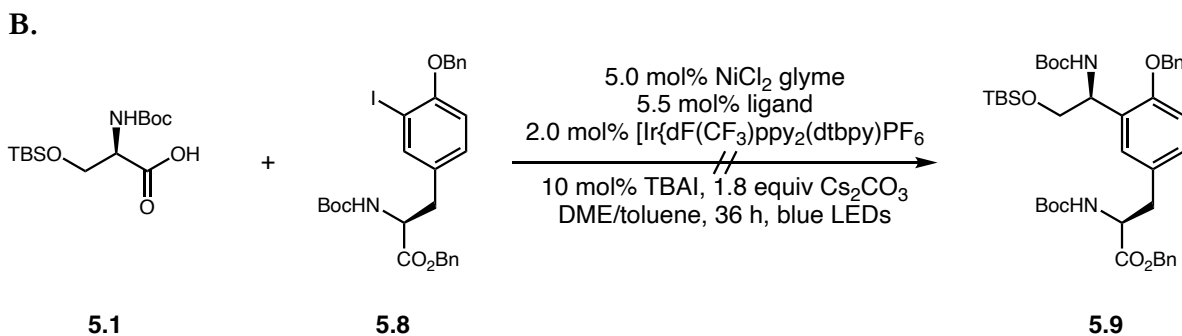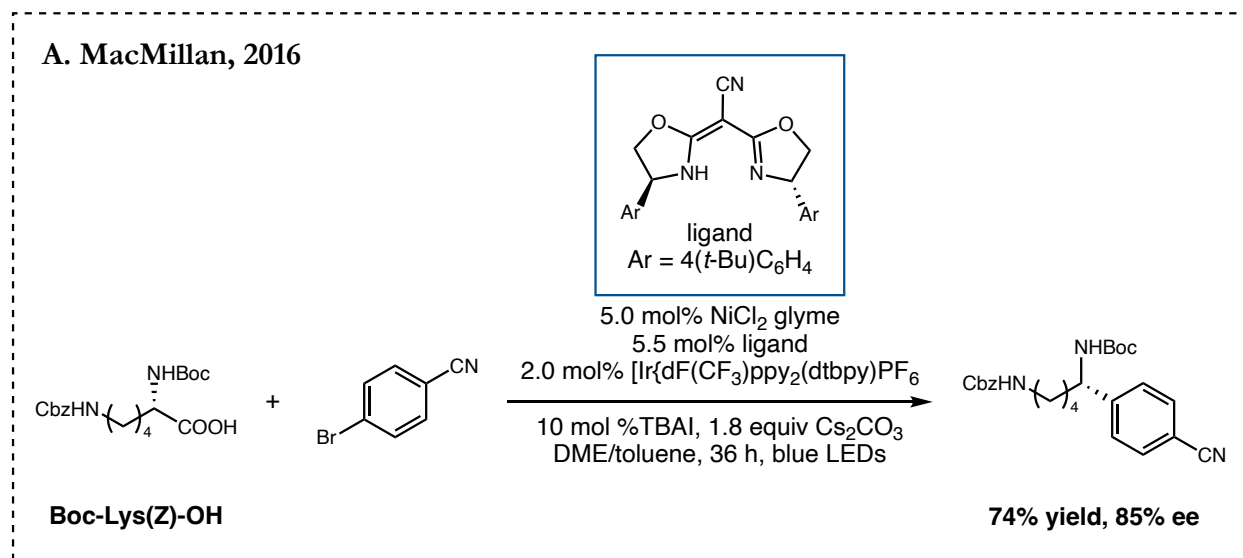
Scheme 5.3 A&B Asymmetric decarboxylative metallophotoredox cross-couplings. **A.** Model reaction in precedent. **B.** Unsuccessful attempt to cross-couple Ser and Tyr.

Initial attempts to generate **5.3** via asymmetric metallophotoredox cross coupling were unsuccessful. Our initial studies revealed that Troc deprotection occurs under these conditions, and thus we opted for Boc-protected tyrosine **5.8** (**Scheme 5.3 A&B**). We observed no product formation (**5.9**) and recovered tyrosine starting material. We also observed serine protodecarboxylation side product by mass spectrometry. From this attempt, we hypothesized that serine undergoes facile radical

decarboxylation while tyrosine oxidative addition is challenging, resulting in a rate mismatch. Furthermore, the strategy developed by Macmillan and co-workers is limited to electron-deficient arenes, with no examples of ortho-substituted arenes, further suggesting that oxidative addition of hindered/electron-rich arenes is challenging.

A. MacMillan, 2014

10.0 mol% NiCl₂ glyme
15.0 mol% dtbbpy
1.0 mol% [Ir{dF(CF₃)ppy₂(dtbpy)PF₆

1.8 equiv Cs₂CO₃
DMF, 72 h, blue LEDs

± 74% yield

B.

10.0 mol% NiCl₂ glyme
15.0 mol% dtbbpy
1.0 mol% [Ir{dF(CF₃)ppy₂(dtbpy)PF₆

1.8 equiv Cs₂CO₃
DMF, 72 h, blue LEDs

5.10   5.11   5.12
± 58% yield
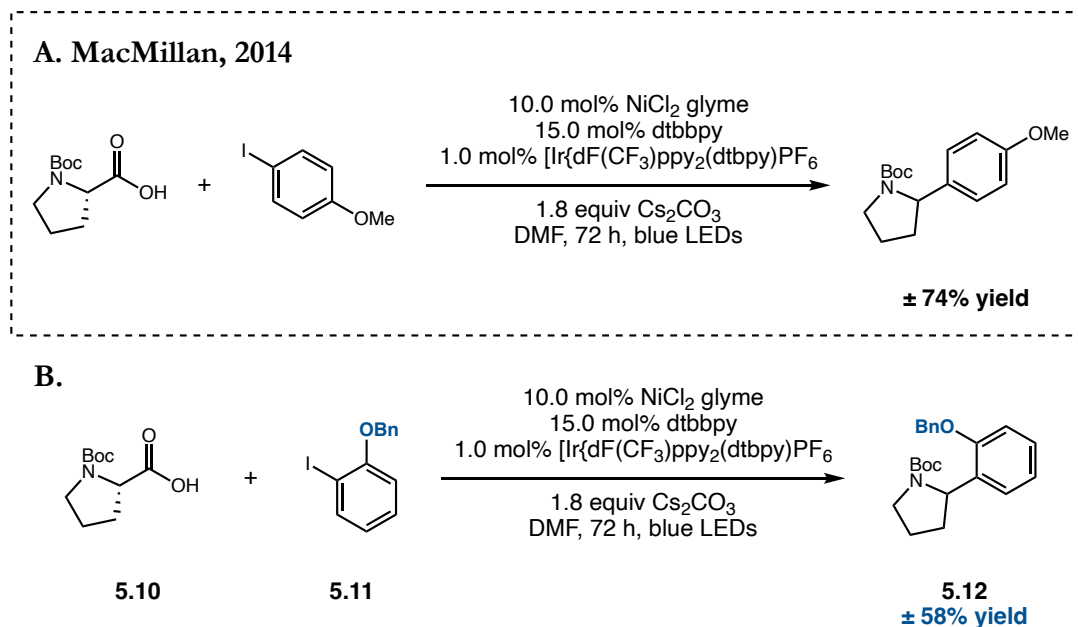
Scheme 5.4 A&B Racemic ligand model systems. **A.** Model reaction precedent. **B.** Utilizing racemic ligand conditions on an *o*-electron rich arene model.

To modulate the rate of oxidative addition, we opted to employ aryl iodides and use racemic dtbbpy previously employed by the Macmillan group to access a broad range of electron-rich and deficient arenes (**Scheme 5.4A**).[12] Following their strategy, we were able to replicate their model system using proline (**5.10**) and effectuate cross-coupling to an *ortho*-protected phenol (**5.11**) to yield cross-coupled product (**5.12**). Given these results, we opted to employ these conditions to serine/phenol, as well as serine/tyrosine (**Scheme 5.5 A&B**). We opted to employ benzyl-protected serine (**5.13**) in line with the substrate scope utilized by the Macmillan group.

A.

5.13 **5.11**

10.0 mol% NiCl$_2$ glyme
15.0 mol% dtbbpy
0.1 mol% [Ir{dF(CF$_3$)ppy$_2$(dtbpy)PF$_6$

1.8 equiv Cs$_2$CO$_3$
DMF, 72 h, blue LEDs

5.14
20% yield[a]

B.

5.13 **5.8**

10.0 mol% NiCl$_2$ glyme
15.0 mol% dtbbpy
1.0 mol% [Ir{dF(CF$_3$)ppy$_2$(dtbpy)PF$_6$

1.8 equiv Cs$_2$CO$_3$
DMF, 72 h, blue LEDs

5.15
Trace, identifed by MS
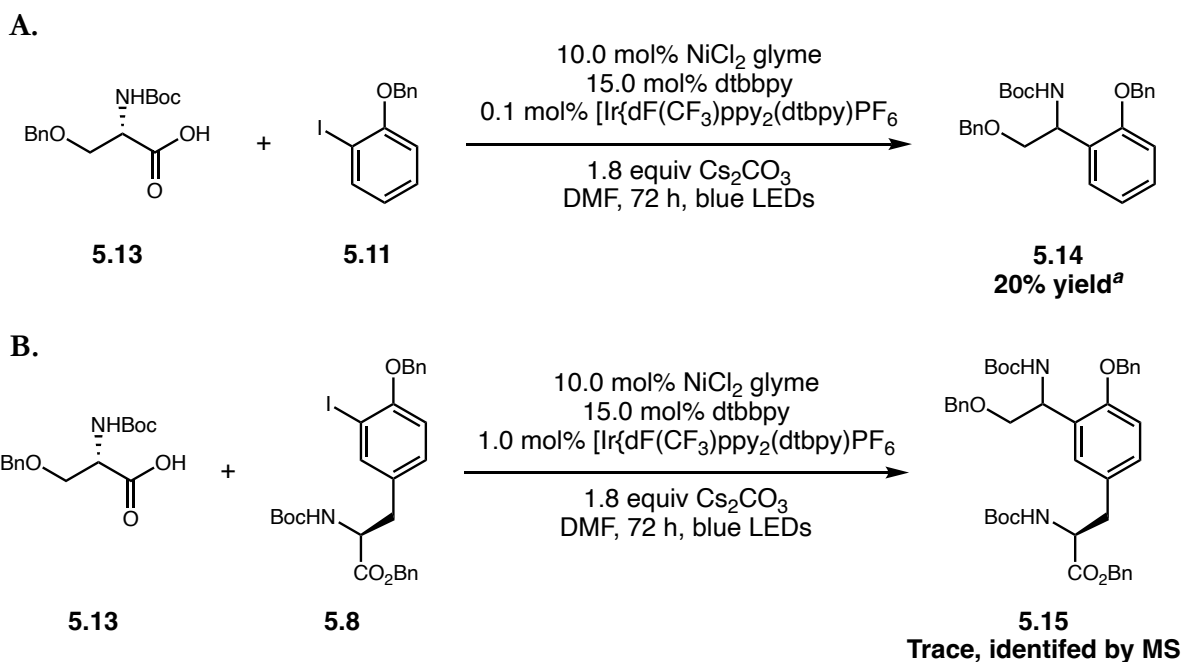
Scheme 5.5 A&B Racemic ligand cross-coupling of Ser/phenol and Ser/Tyr. **A.** Model *o*-iodo-

phenol and serine substrates. **B.** Symmetric cross-coupling of Ser/Tyr. [a]NMR yield.

We observed a significant reduction in yield of product (**5.14**) when moving from proline to serine.

With regards to cross-coupling to tyrosine (**5.8**), although we were unable to identify the cross-coupled

product by NMR, we did observe a mass that potentially correlates to formation of the desired product

(**5.15**). Given the significant challenges we faced attempting to even effectuate a symmetric cross-

coupling, we decided to pursue an alternative route that would be more amenable to our substrate

scope.

5.2 Synthetic strategy leveraging *o*-hydroxylation of Tyr precursor

5.2.1 Background on *o*-hydroxylation of aryl halides

Transition-metal mediated C-H hydroxylation of arenes is an important transformation to access a wide variety of *ortho*-substituted phenols. Seminal work by Fujiwara and co-workers demonstrated the competence of palladium to effectuate hydroxylation of benzene, albeit under harsh conditions and low yields.[14] Since then, various studies have developed mild transformations utilizing a variety of hydroxylating reagents and transition metals, including ruthenium,[15-18] iridium,[19] copper,[20, 21] and palladium.[22-25] A report by Zhao and co-workers revealed that Cbz-protected benzylamines can serve as a directing group to effectuate palladium-catalyzed *ortho*-selective hydroxylation over a broad arene scope (**Scheme 5.6**).[26]
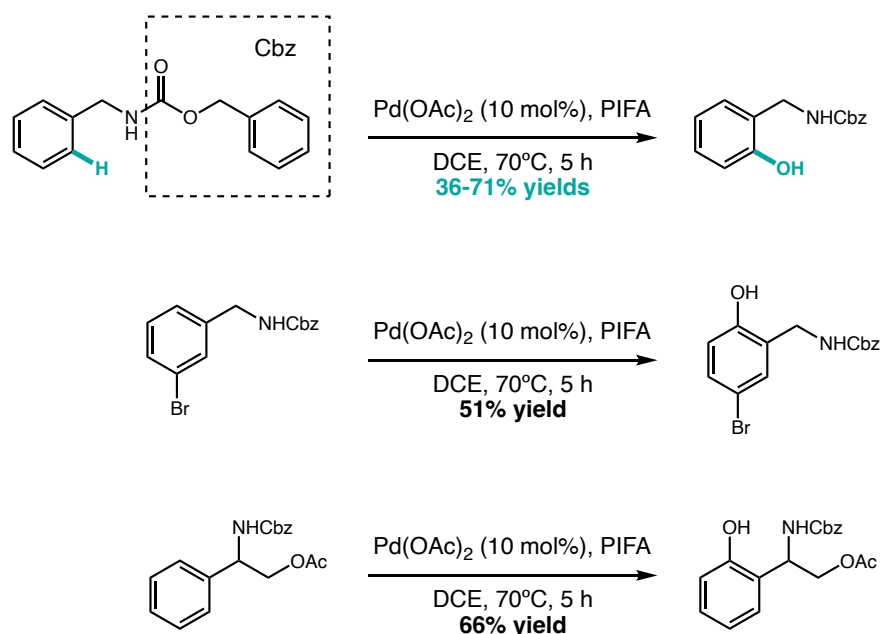
Scheme 5.6 *ortho*-hydroxylation of Cbz-benzylic amines developed by Zhao & co-workers. Select examples from their scope are shown.
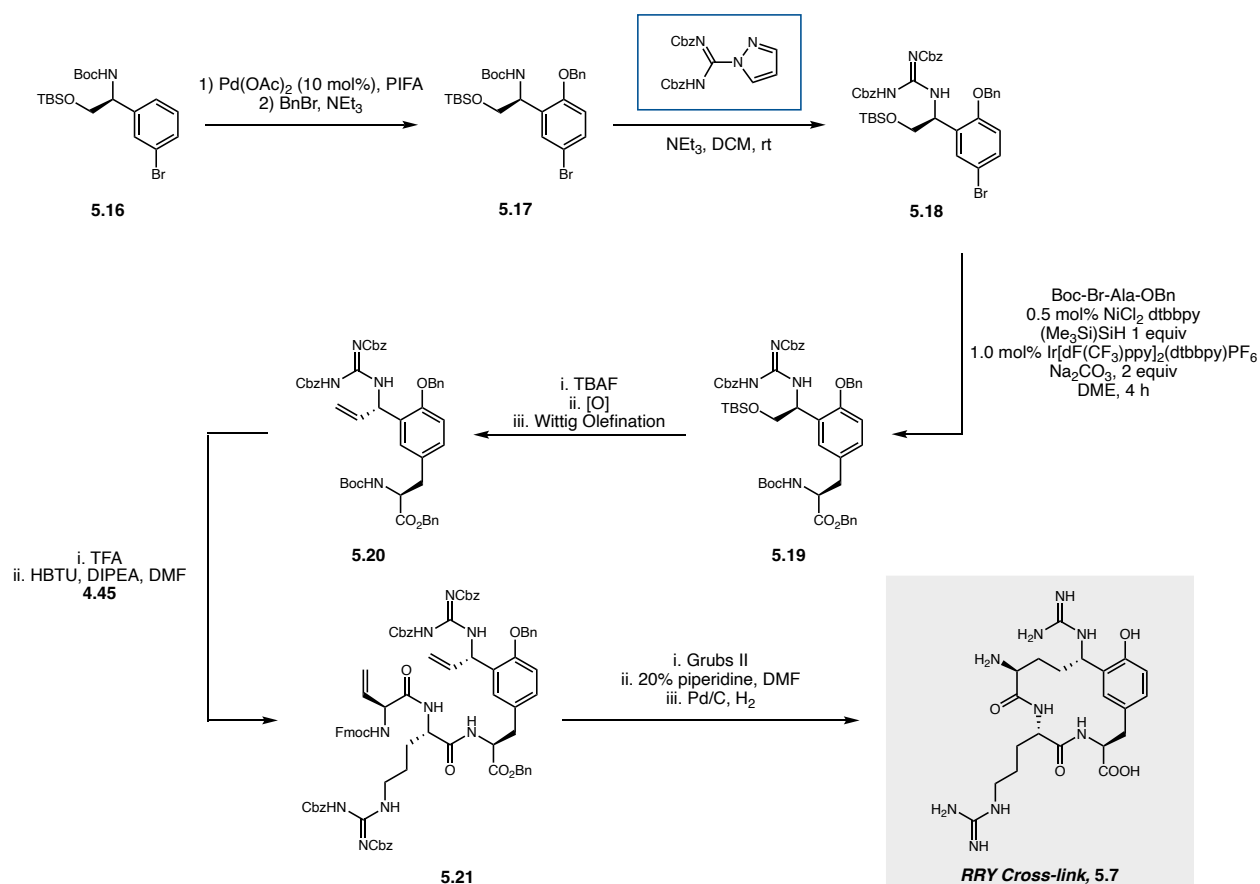
Scheme 5.7 Re-worked total synthesis of the ryptide core, starting with *ortho*-hydroxylation of a protected glycinol derivative. XEC is proposed to furnish the desired tyrosine derivative.

Taking inspiration from their work, we envisioned an alternative strategy (**Scheme 5.7**) starting with a phenylalanine precursor possessing the desired C-C crosslink (**5.16**), then performing an *ortho*-selective hydroxylation to furnish the phenol **5.17**. Given the tolerance of this chemistry with various aryl halides, we considered simplifying the substrate from an amino acid to an aryl precursor possessing a handle to later append the amino acid backbone. In this regard, we modified the existing forward synthesis around a substituted aryl halide possessing the desired amine and alcohol functionalities (**5.16**). Both enantiomers of starting material **5.16** can be purchased for ~$50/gram from Ambeed. After protection of the alkyl alcohol, *ortho*-selective hydroxylation would generate the

desired phenol. Benzylation of the phenol followed by guanidinylation would furnish the top piece of the desired tyrosine fragment (**5.18**).
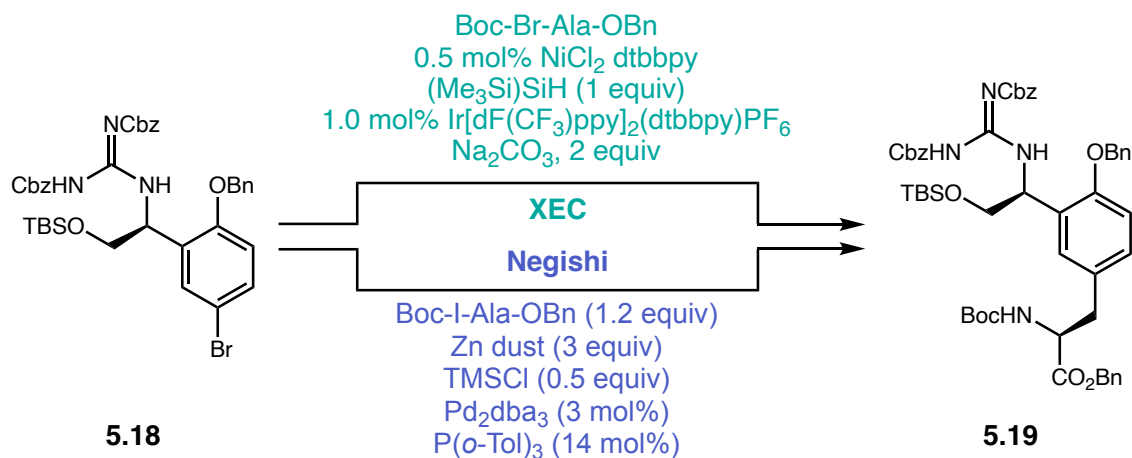
Scheme 5.8 Potential entries (XEC or Negishi) to access the tyrosine fragment to furnish the Ryptide RRY macrocycle.

From this point, we envisioned two potential entries to complete the tyrosine fragment: XEC[27] with a protected bromo-alanine or Negishi cross-coupling with an *in situ* organozinc alanine (**Scheme 5.8**).[28] As a starting point, we initially planned to first test XEC and utilize Negishi cross-coupling as an alternative route. From this point, the forward synthesis is identical to the initial proposed strategy; deprotection, oxidation, and Wittig olefination to generate the olefin handle (**5.20**), peptide coupling to the VGly-Arg dimer (**4.45**) to yield the trimer **5.21**, then RCM and global deprotection to furnish the ryptide macrocycle (**5.7**).

5.2.2 *ortho*-hydroxylation chemistry towards ryptide macrocycle

Although our strategy utilizes a substituted-Boc-glycinol substrate (**5.16**) in the *ortho*-hydroxylation, initial investigations by Zhao and co-workers found that sterically demanding carbamates resulted in diminished *ortho*-functionalization in their model system, noting a significant reduction in yields when switching from Cbz (79% yield) to Boc (35% yield).[29] Thus, we began our investigations employing their model substrate (**5.22**), as well as our model system utilizing a di-Cbz-guanidine benzylamine precursor (**5.24**) (**Scheme 5.9 A&B**).
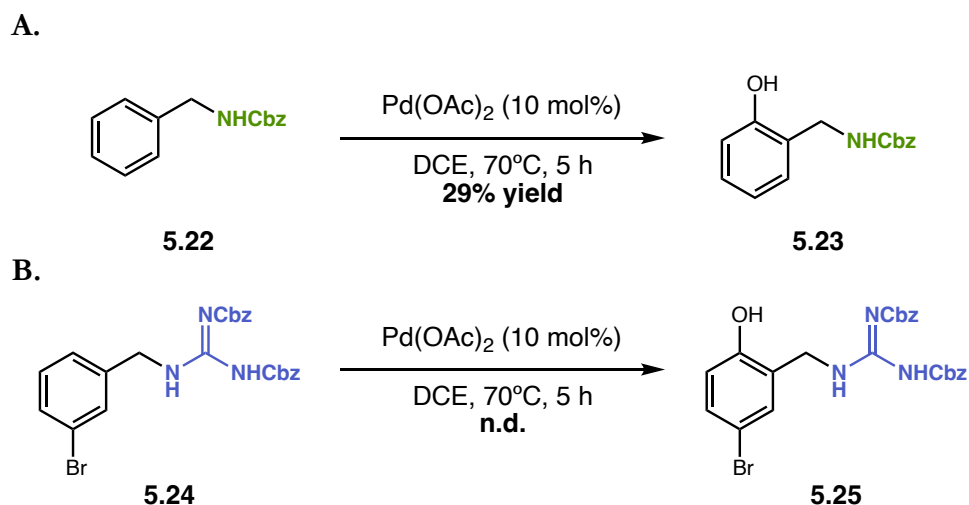
Scheme 5.9 A&B Our initial investigations of *ortho*-hydroxylation on benzylamine model systems. **A.** Our attempts to replicate the model reaction proposed by Zhao et al. **B.** Our proposed model system.

Although we attempted to replicate the model system, we initially observed only trace yields relative to the literature precedent, despite trying different palladium sources and distilled DCE. We noticed impurities present in the ^{1}HNMR of our PIFA source and sought to recrystallize PIFA via

acetone/petroleum ether and from TFA. We decided to run a screen of the literature conditions using our various PIFA sources (**Table 5.1**).
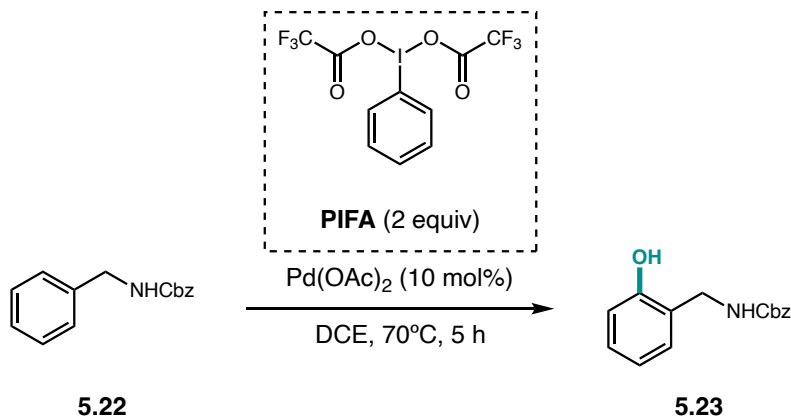
PIFA source	% yield[a] of **5.22**
From bottle	Trace
Recrystallized (Acetone/Pet. Ether)	25
Recrystallized (TFA)	29

[a]NMR yield

Table 5.1 PIFA screen of the *ortho*-hydroxylation model reaction.

While we were able to obtain a significant improvement in yield when employing recrystallized PIFA, we were still observing significantly diminished yields relative to the reported yield in literature (78% NMR yield, 70% isolated yield).[26] Additionally, while we were able to generate hydroxylated product **5.25** in our model system, there were significant difficulties in the purification, and we obtained product as an inseparable mixture with starting material (**5.24**). Given these initial difficulties and the lack of additional literature surrounding *ortho*-selective hydroxylation leveraging benzylamines, we opted to re-design our route once more. The challenges associated with the *ortho*-substituted phenol

coupled with our desire to leverage RCM led us to investigate strategies that would enable a synthon possessing both an olefin and a pre-installed *ortho*-phenol moiety for later installation of the arginine side chain.

5.3 Synthetic strategy leveraging allylic amination towards a Tyr precursor

5.3.1 Background on stereoselective allylic amination
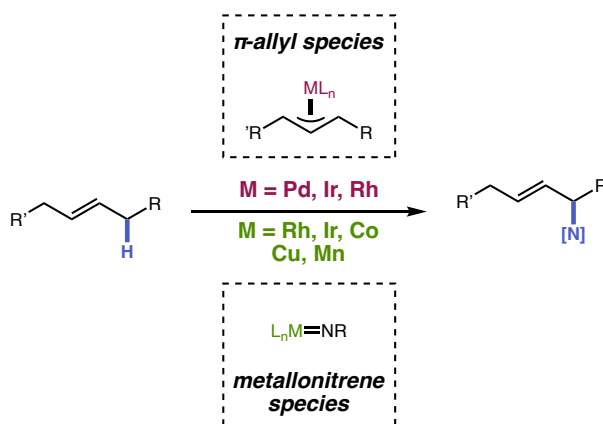
Figure 5.1 Simplified schematic depicting approaches towards allylic C-H amination.

C-H allylic bonds have been previously leveraged in catalysis to enable late-stage amination of natural products, thereby introducing functionality that can alter their biological profiles. Metal-catalyzed C(sp^3)-H activation via π-allyl metal intermediates such as Pd,[30] Ir,[31, 32] and Rh[33, 34] are well-documented in the literature to effectuate amination of allylic terminal olefins (**Figure 5.1**).[35] Furthermore, group transfer reactions via metal-nitrenes have also been employed in allylic aminations.[36, 37] Asymmetric transformations of allylic C-H bonds have been well-documented and constitute one of the most convenient approaches to access optically active allylic amines.[38, 39] Enantioselective transformations

typically rely on either addition of organometallic reagents to imines and subsequent displacement of allylic esters, alcohols, or carbonates; or through stereospecific substitution of asymmetric carbonates, imidodicarboxylates, and alcohols via nucleophilic amine species.[35]
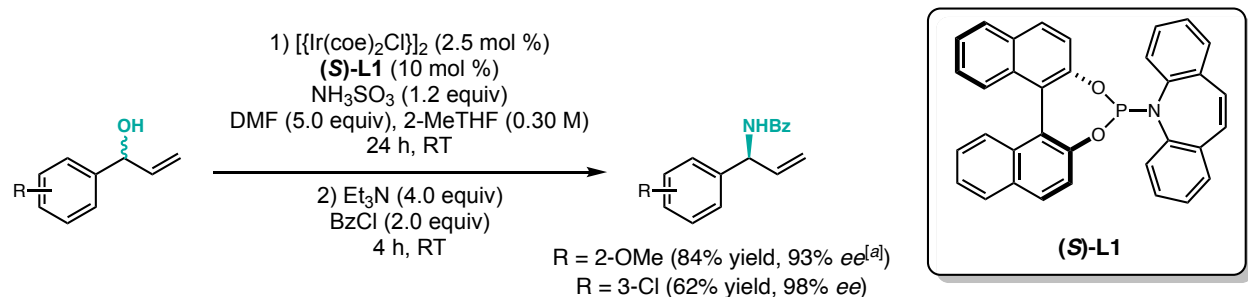
Scheme 5.10 Strategy to access asymmetric allylic aminations of 2° racemic allyic alcohols developed by Carreira and co-workers. [a]CHCl3 was used as the additive in place of 2-MeTHF.

The Carreira group further expands this transformation via enantioselective displacement of 2° racemic allylic alcohols with sulfamic acid to deliver optically active allylic amines (**Scheme 5.10**).[40] Their synthetic strategy broadly tolerates substitution of benzylic allylic alcohols, namely *ortho*-substituted anisole and *meta*-substituted haloarenes. We envisioned that this strategy could be leveraged in our route to the ryptide macrocycle, playing a key role towards the synthesis of our desired tyrosine fragment (**Scheme 5.11**).
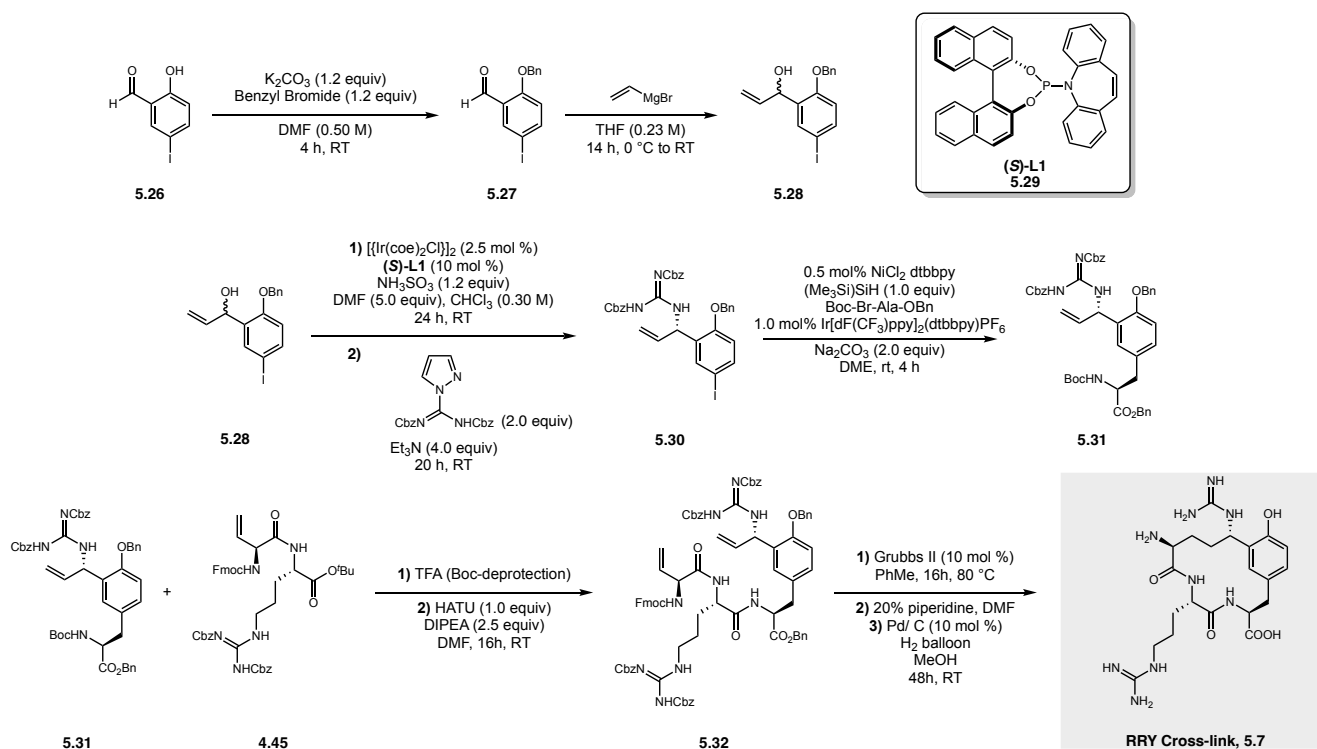
Scheme 5.11 Revised total synthesis of ryptide macrocyclic core leveraging enantioselective allylic amination.

In our revised synthesis, we envisioned that racemic allylic alcohol **5.28** could be accessed in two steps from commercially available 2-hydroxy-5-iodobenzaldehyde **5.26**. Because the Carreira strategy employs an *in-situ* protection of the amine post displacement of the allylic alcohol, we proposed an *in-situ* guanidinylation could be utilized to furnish the arginine side chain in an early stage. This is advantageous to late-stage installation because the immediate introduction of the Cbz-guanidine would enable differential protection of the N-terminus of the RRY macrocycle, enabling selective coupling to the remaining ryptide sequence if desired. In our exploration of the ryptide macrocycle, we plan to utilize both enantiomers of ligand **5.29** to deliver both potential stereocenters of the key Ryptide crosslink. Similar to our revised strategy focusing on *ortho*-hydroxylation, we aim to employ either XEC or Negishi cross-coupling to forge the desired tyrosine fragment **5.31**. Once complete,

peptide coupling to VGly-Arg dimer (**4.45**), RCM, and global deprotection would furnish the ryptide macrocyclic core (**5.7**).

5.3.2 Allylic amination chemistry towards Ryptide macrocycle

To start the synthesis towards the tyrosine fragment, 2-hydroxy-5-iodobenzaldehyde **5.26** underwent benzylation to furnish the protected aldehyde intermediate **5.27** in 69% yield. Grignard addition of vinylmagnesium bromide into the aldehyde furnished the racemic benzyl-protected allylic alcohol **5.28** in excellent yields. For the subsequent step, we chose to employ chloroform as a co-solvent because the Carreira group demonstrated its importance as an additive to improve enantioselectivity of the *ortho*-substituted anisole substrate. Furthermore, to effectuate the guanidinylation, we chose to extend the reaction time by 24 hours. In our initial attempts towards asymmetric allylic amination/guanidinylation, we observed a return of starting material with no formation of product or amine. Because we were following the reaction by TLC, we hypothesized that iterative piercing of the septa was allowing escape of the ammonia generated *in-situ*. Simply allowing the reaction to progress without TLC analysis allowed us to form the desired product **5.28** in 55% yield over two steps.
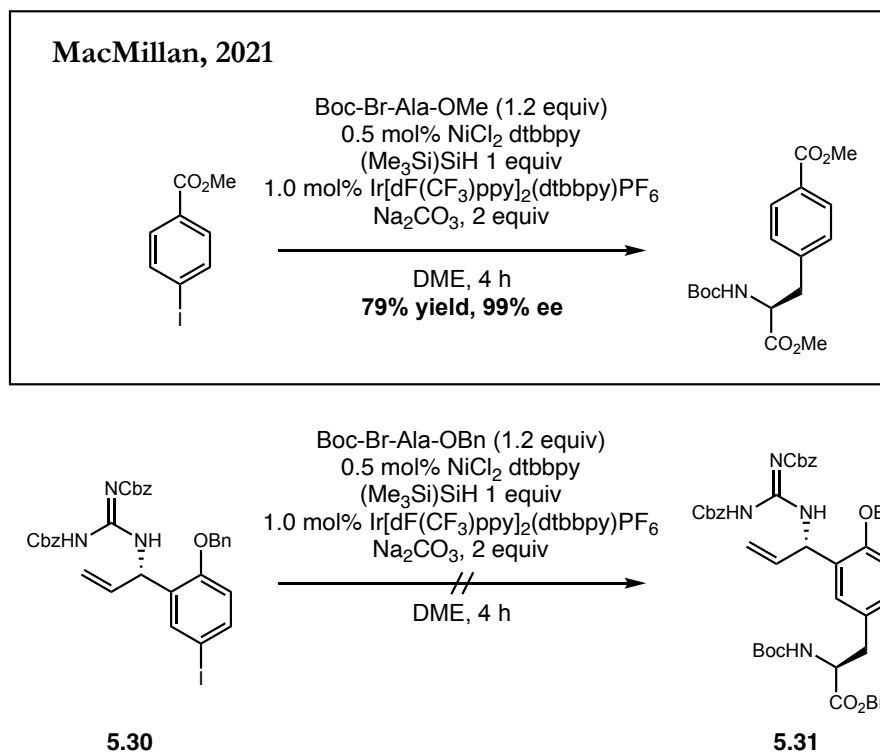
Scheme 5.12 Macmillan and co-workers' metallophotoredox XEC strategy to access aryl amino acids. Implementation of this strategy on our substrate did not yield desired product.

With the desired top piece of the tyrosine fragment in hand, we sought to explore synthetic strategies to furnish the tyrosine fragment. We were initially intrigued by Macmillan and co-workers' metallophotoredox XEC, wherein they were able to access a wide variety of enantiopure aryl amino acids under mild conditions.[27] Following their precedent, we sought to furnish the tyrosine fragment (**5.31**) via XEC of Boc-Br-Ala-OBn with iodoarene **5.30** (**Scheme 5.12**). Unfortunately, we were unable to identify production formation by ^{1}HNMR or MS, of which only dehalogenated alkyl and aryl starting material were detected. We then turned our attention towards Negishi cross-coupling.
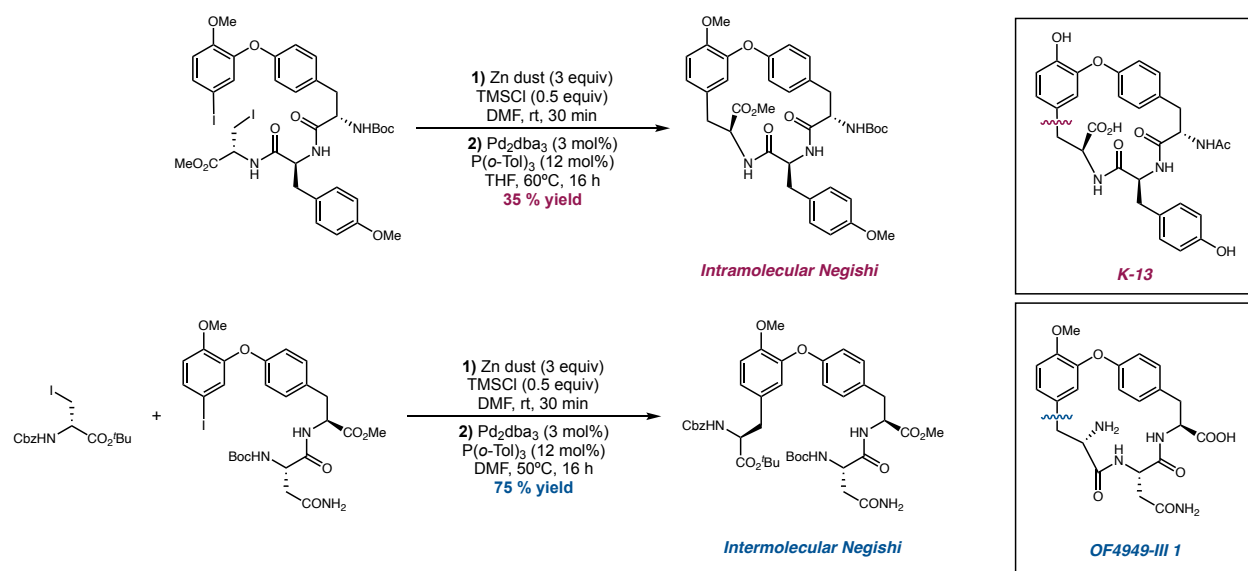
Scheme 5.13 Jackson and co-workers' utility of both inter- and intramolecular Negishi cross-coupling to forge cyclic peptides.

Negishi cross-coupling has previously been used to couple serine-derived organozinc substrates with aryl halides to furnish phenylalanine analogues in highly variable yields (10-67%).[41] Jackson and Mowbray have made significant contributions to this area of chemistry, developing an improved and reliable strategy to access these derivatives via improved zinc activation protocols.[28, 42] Furthermore, the Jackson group not only have translated this chemistry to access tyrosine analogs but have also demonstrated the utility of Negishi in late-stage peptide modification toward their synthesis of cyclic tripeptides OF4949-III and K-13 (**Scheme 5.13**).[43] Using their improved zinc activation strategy of iodoalanine, they were able to forge an intermolecular Negishi between a protected dimer and iodoalanine to generate a linear tyrosine-containing trimer in excellent yields (75%). Furthermore, they demonstrate the competency of their strategy by utilizing Negishi as the ring closing step for one of their analogs, furnishing the macrocycle albeit in reduced yields (35%). Thus, Negishi-cross coupling has substantial promise to enable our synthesis of the ryptide tyrosine fragment.
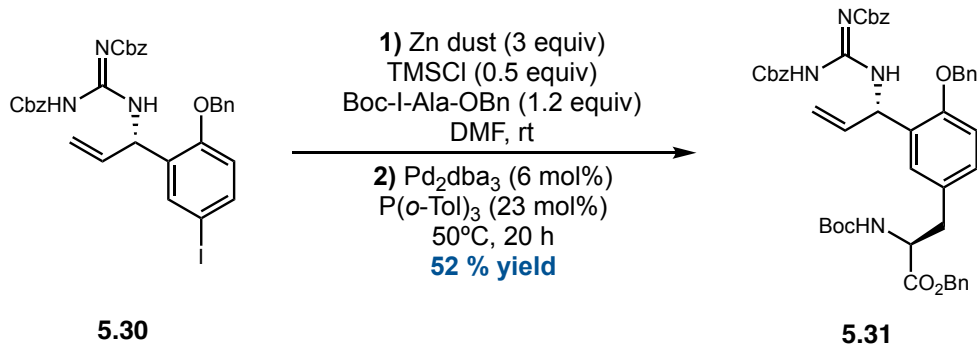
Scheme 5.14 Our utility of Negishi cross-coupling to furnish protected allylic guanidine derived tyrosine.

After a few attempts employing the strategy developed by Jackson and co-workers, we were pleased to obtain the desired tyrosine fragment **5.31** from Boc-I-Ala-OBn and allylic guanidine **5.30** in 52% yield. Despite this success, we identified an iodoalanine-dimer impurity via ^{1}HNMR and mass that co-elutes with **5.31**, which was later be removed in the subsequent steps.

5.4 Synthesis towards dipeptide fragment for ring closing metathesis

5.4.1 Synthesis of vinylglycine

Unsaturated amino acids such as allylglycine, vinylglycine, dehydrobutyrine, and dehydroalanine are well-studied in literature, and synthetic routes have leveraged these residues to access macrocycles and amino acid derivatives.[44-48] To access vinylglycine, several synthetic strategies have been developed that rely on either methionine, homoserine, or glutamate as starting chirons (**Scheme 5.15 A-C**).
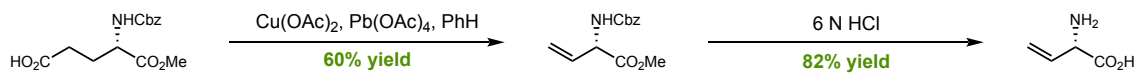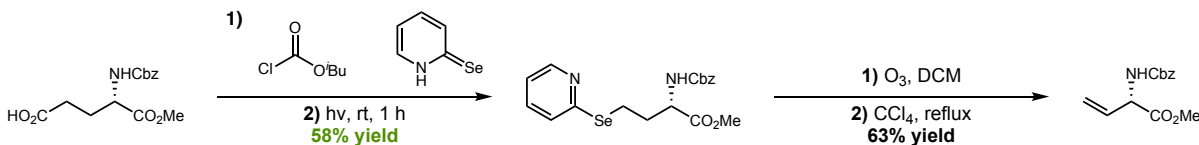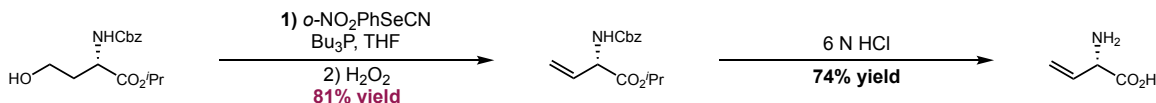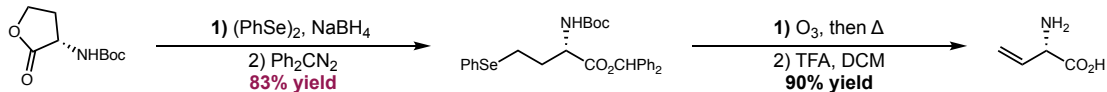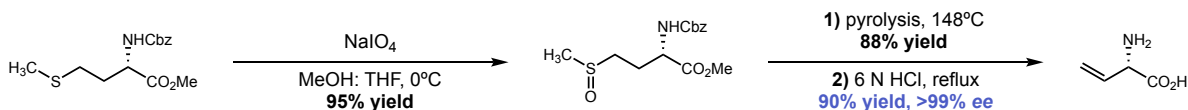
Scheme 5.15 A-C Different synthetic strategies developed towards *L*-vinylglycine (VGly) via chrions. **A.** Synthesis of VGly from *L*-Glutamate. **B.** Synthesis of VGly from *L*-Homoserine. **C.** Synthesis of VGly from *L*-Methionine.

Hanessian and co-workers employed a Cu(II)/Pb(IV)-mediated decarboxylation of the glutamate side chain to install the vinyl group and access vinylglycine (**Scheme 5.15A**).[49] A complementary approach employs a Barton decarboxylation of glutamate to deliver an aryl selenide poised for elimination to

vinylglycine.[50] Strategies developed by Berkowitz and Pellicciari rely on selenoxide elimination chemistry of either homoserine or homoserine lactone (**Scheme 5.15B**).[51, 52] With regards to methionine, a classic route developed by Afzali-Ardakani and Rapport utilized *L*-methionine oxidation to the sulfoxide, following with pyrolysis to generate vinylglycine (**Scheme 5.15C**). Subsequent deprotection forged *L*-vinylglycine in 99% *ee*.[53]
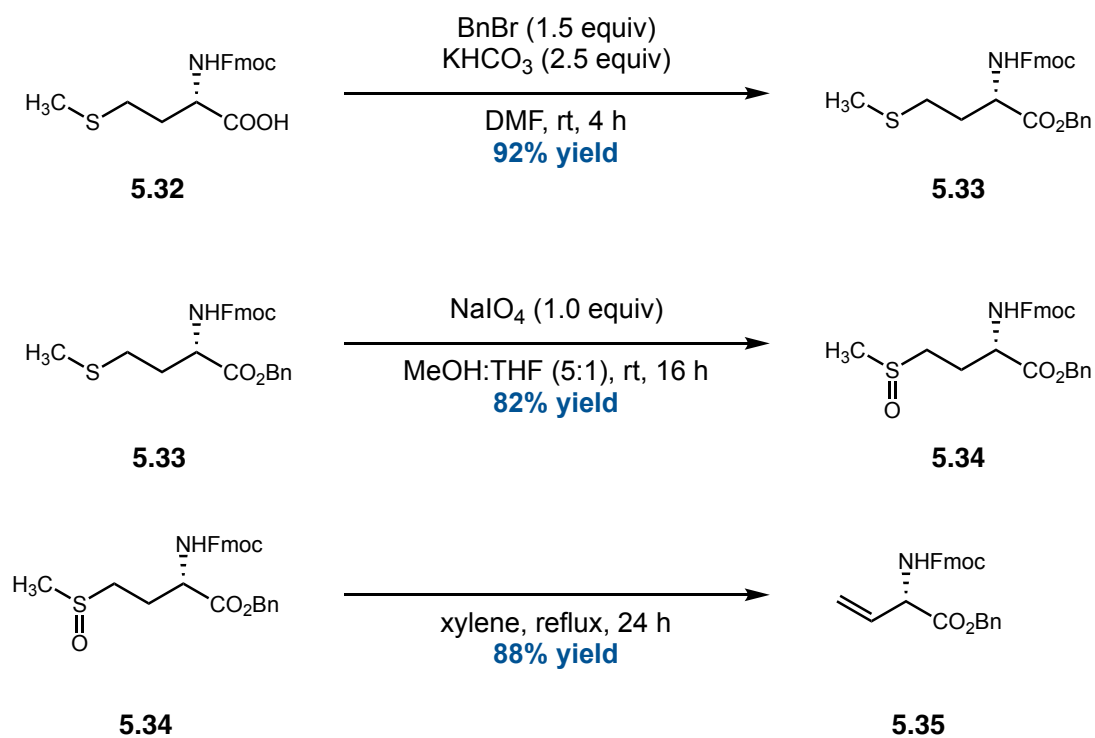
Scheme 5.16 Our attempts to access protected *L*-vinlyglycine via *L*-methionine as the starting chiron.

We chose to employ *L*-methionine as the starting chiron towards our synthesis of Fmoc-*L*-vinylglycine (**Scheme 5.16**). Starting from the readily available Fmoc-*L*-Methionine (**5.32**), benzyl protection (**5.33**) and subsequent oxidation (**5.34**) proceeded in excellent yields. For the pyrolysis, we initially

sought to reflux the sulfoxide **5.34** as precedented in literature.[54] However, we confirmed formation

of the isomerized side product dehydrothreonine by ^{1}HNMR, which eluted closely with vinylglycine

(**5.35**).[55] Ultimately, we found that performing pyrolysis in a pressure tube at gentle reflux was the

most optimal setup, enabling excellent recovery of the desired vinylglycine (**5.35**) in 88% yield.
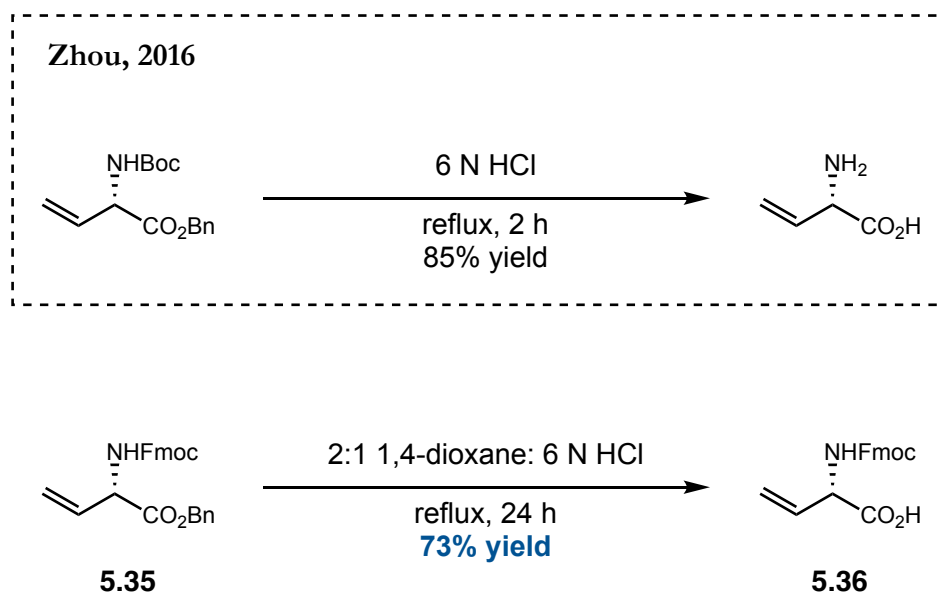
Scheme 5.17 Acidolysis of differentially protected benzyl ester vinylglycine derivatives.

With the protected vinylglycine in hand, we sought to develop hydrolytic conditions to selectively

remove the C-terminus benzyl group without affecting the β-γ unsaturated moeity. Although acid-

mediated hydrolysis has been utilized to deprotect Boc-VGly-OBn derivatives[48] (**Scheme 5.17**), such

procedures only necessitate aqueous conditions due to facile removal of the Boc group, exposing the

polar N-terminus. Because Fmoc is inert to these conditions, we employed 1,4-dioxanes as a co-

solvent to aid solubility of our substrate. Although inclusion of a co-solvent at a 2:1 ratio to acid was

able to fully solubilize **5.35**, we were still unable to generate our desired product (**5.36**) after 2 hours

at reflux, and only recovered starting material. Extending the reflux to 24 hours enabled the deprotection, delivering the product **5.36** in 73% yield.
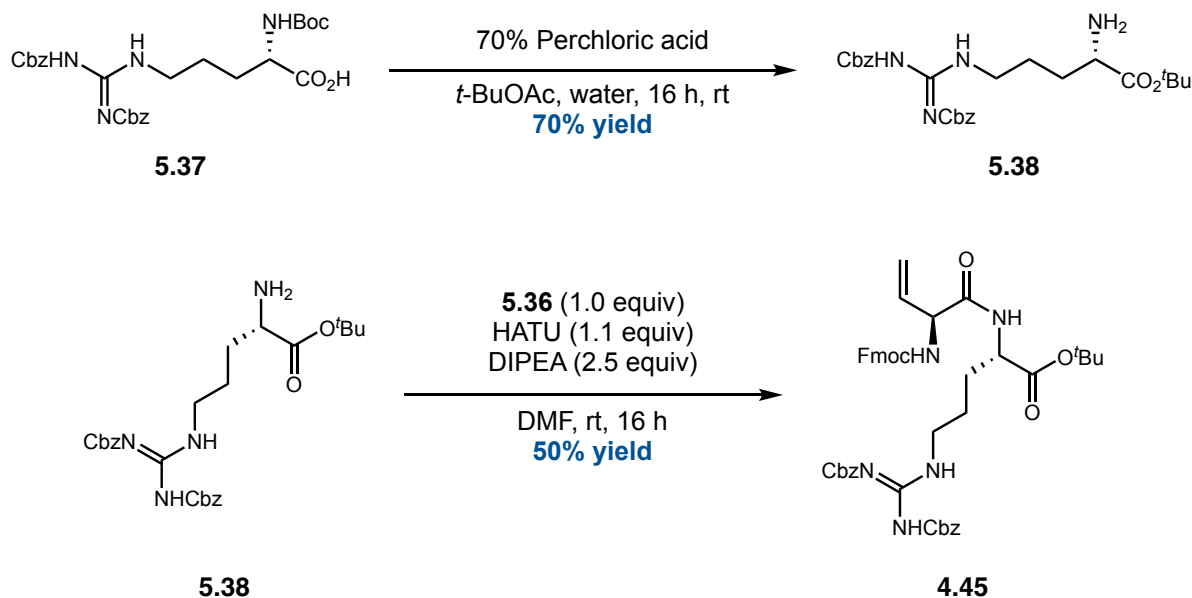
Scheme 5.18 Our synthetic attempts to access the dipeptide vinylglycine-arginine fragment.

With N-terminus protected vinylglycine in hand, we sought to generate the dipeptide necessary for the Ryptide macrocycle (**Scheme 5.18**). Starting from commercially available Boc-Arg(Z)$_2$-OH (**5.37**), we leveraged a dual deprotection/protection strategy to easily access H$_2$N-Arg(Z)$_2$-O^{t}Bu (**5.38**) in one step. From there, a standard peptide coupling using HATU/DIPEA forged the dipeptide **4.45** in 50% yield. Subsequent TFA deprotection of both the tyrosine and dimer fragments, followed by peptide coupling, forged the linear ryptide trimer **5.32** poised for macrocyclization.

## 5.4.2 Background on RCM to generate macrocyclic peptides
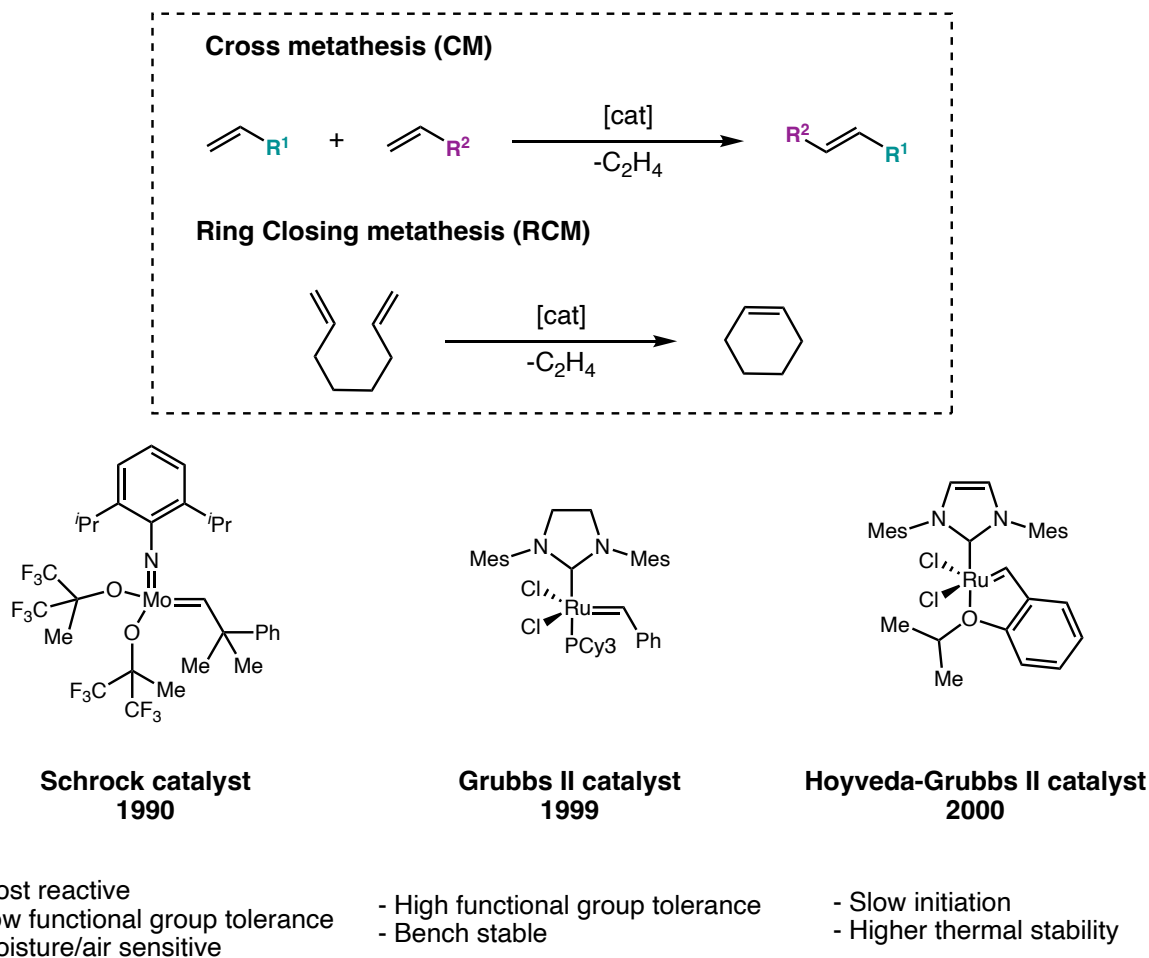
Figure 5.2 Predominant olefin metathesis catalysts used in CM and RCM.

Olefin metathesis has become an essential tool to access C-C macrocyclic peptide scaffolds. Seminal mechanistic studies by Chauvin[5, 56] and catalyst development by Grubbs[7, 57] and Schrock[6, 58, 59] have enabled the successful application of this chemistry in commercial-scale total synthesis of various natural products. While olefin metathesis can be divided into several categories, cross-and ring closing metathesis (CM and RCM, respectively) are the most predominant subclasses used in natural product total syntheses, differing primarily upon reaction dilution to avoid unwanted homo-couplings in RCM. Furthermore, both cross and ring closing metathesis typically rely on either Schrock or Grubbs'

catalysts (**Figure 5.2**). Schrock and co-workers pioneered the development of molybdenum (VI), tungsten (VI)[58, 59], and Re (VII)[60] catalysts to effectuate olefin metathesis. The most active Schrock catalyst shown in **figure 5.2** boasts high reactivity towards a broad range of substrates, at the cost of poor functional group tolerance and air/moisture sensitivity. In contrast to Schrock's catalysts, Grubbs and co-workers have established Ru-based catalysts known for their functional group tolerance and bench stability, making this class of catalysts more popular for utilization in late-stage transformations. The most commonly used Grubb's catalyst is the second-generation catalyst shown in **figure 5.2**. This catalyst is improved over the first generation via incorporation of a N-heterocyclic carbene (NHC) ligand, of which its σ-donor capabilities stabilize a 14 e$^-$ Ru intermediate in the catalytic cycle and make the catalyst more effective. Another popular catalyst for these transformations includes Hoyveda-Grubbs' catalysts, which incorporates a chelating ligand such as 2-isopropoxystyrene that functions to tune catalytic properties. This subclass of Grubbs' catalyst typically exhibits slow initiation, but higher thermal stability compared to traditional Grubbs' first- and second-generation catalysts (**Figure 5.2**). Although these reactions typically generate a mixture of E and Z olefins, more recent progress has been made towards E/Z selective catalytic transformations.[61]

With regards to cross metathesis, olefin substrates can be classified based upon their reactivity under Schrock (highly reactive) or Grubbs' (less reactive) catalysts. Type I olefins undergo rapid cross metathesis and are prone to homodimerization; this class typically include sterically unhindered olefins such as unsubstituted terminal alkenes. Furthermore, the homodimers of this type are reactive and can undergo polymerization. Type II olefins undergo homodimerization, but these side products are largely unreactive. Type III olefins generate the desired cross-coupled product but are not prone to homodimerization. Lastly, type IV olefins are spectators and inert towards cross metathesis. This class typically encompasses sterically encumbered substituted olefins.

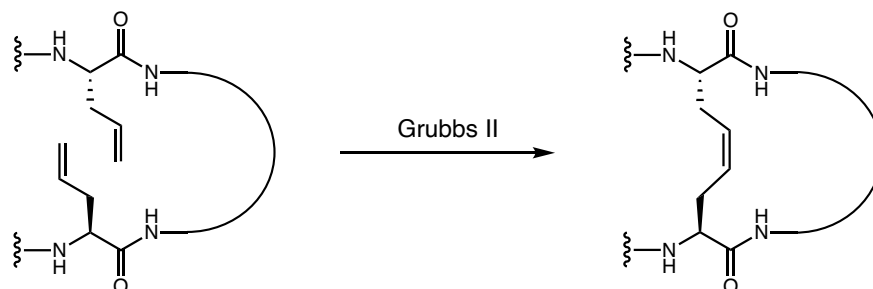**Verdine, 2000**
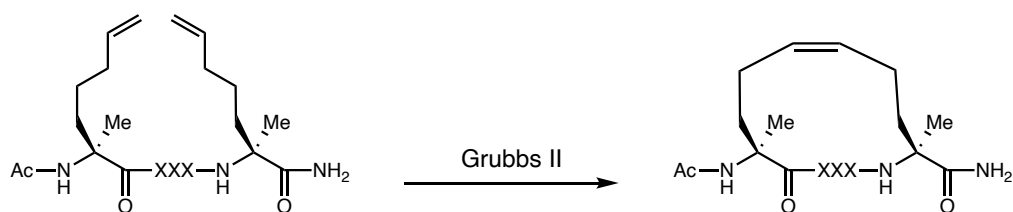
Grubbs, 1995

Figure 5.3 Pentenyl-alanine (top) and allylglycine (bottom) are commonly employed in RCM of peptides, unlike vinylglycine.

In the literature, peptide macrocyclization via ring closing metathesis literature typically rely on either Grubbs II or Hoyveda-Grubbs II catalysts due to their high functional group tolerance.[46] Due to the compatibility of these catalysts with common solvents used for resin swelling, RCM can be utilized either in solution phase or on solid phase of the protected peptide. Two predominant olefins are utilized to effectuate this transformation; in the case of peptide stapling, 4-n-pentenylalanine (S5) is commonly employed at *i,i*+4 intervals to promote α-helicity in peptides.[62] For other macrocyclizations, allylglycine is typically used (**Figure 5.3**).[63] Seminal work by Miller and Grubbs demonstrates the competency of allylglycine with their catalytic design to generate cyclic peptide fragments.[64] Since their discovery, allylglycine and homoallylglycine variants have been utilized to furnish late-stage ring closing metathesis.
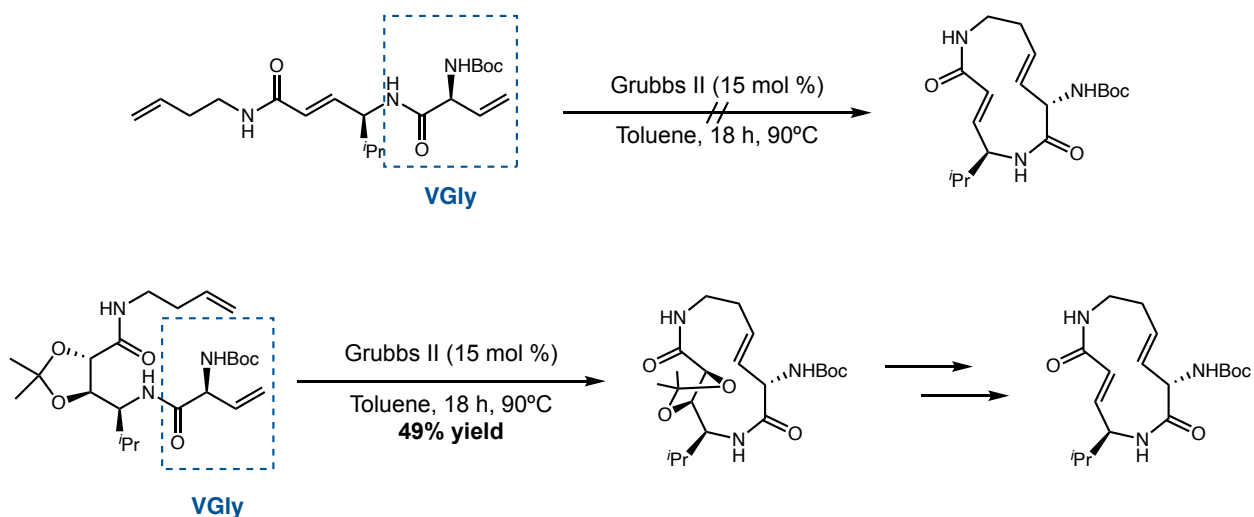
Scheme 5.19 Total synthesis of Syringolin A utilizes a vinylglycine to furnish the macrocycle via RCM. This synthesis required preorganization to facilitate RCM.

Compared to allylglycine, vinlyglycine has seen limited utility in ring closing metathesis, presumably due to its significant lack of reactivity compared to allylglycine. Initial studies by Grubbs and co-workers found that a vinylglycine derivative did not undergo RCM with their catalyst, of which they attribute lack of reactivity to the propensity of the acidic α-proton to undergo isomerization to the α, β-unsaturated olefin, which was unreactive under their conditions. In contrast, the allylglycine derivative proceeded to generate the RCM product under the same conditions.[65] Furthermore, cross-metathesis of allylglycine with vinylglycine has been reported, of which the allylglycine was shown to undergo homodimerization unlike vinylglycine. To ameliorate this, excess vinylglycine was necessary to achieve high conversion to the desired cross-coupled product. Despite these complications, Kaiser and co-workers utilized vinylglycine towards their synthesis of Syringolin A (**Scheme 5.19**).[66] Their initial attempts to effectuate RCM between the vinylglycine and a homoallylic amine moiety were

unsuccessful, achieving only homodimerization adducts. They hypothesized that conformational rigidity was needed to poise the olefins for RCM and modified their synthesis to incorporate a temporary acetal for preorganization. After a series of optimizations, they were able to generate the desired RCM metathesis product in moderate yields, and a Corey-Winter elimination was leveraged to reinstate the unsaturation.

**5.4.3 Exploration of ring closing and cross metathesis of dipeptide and tyrosine fragments**
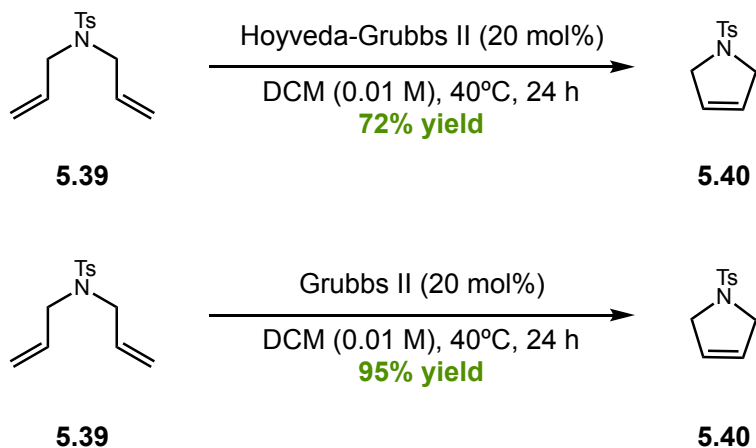
Scheme 5.20 Our model systems for RCM.

In our attempts to close the linear Ryptide trimer **5.32**, we initially sought to develop a model system, then employ the most optimal conditions onto our substrate. Using tosyl-protected diallyl amine as our model substrate (**5.39**), we tested Grubbs II and Hoyveda Grubbs II in our synthesis. We observed that when using Grubbs II we achieved a cleaner crude ^{1}HNMR and almost quantitative conversion of our model substrate to **5.40**.
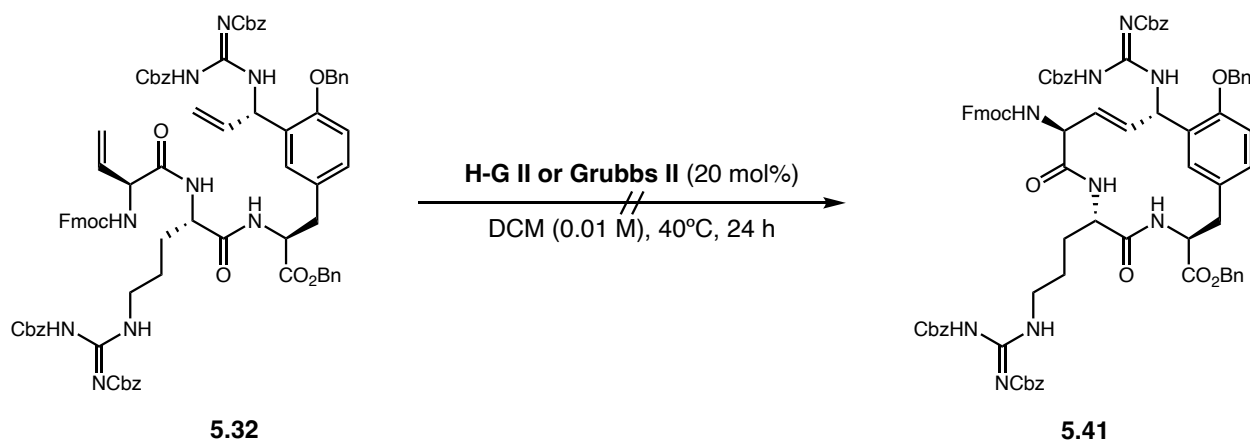
Scheme 5.21 Our investigation of RCM towards the protected and unsaturated Ryptide macrocycle.

When employing these conditions with Grubbs II on linear Ryptide **5.32**, we were unable to achieve any conversion of starting material as evidenced by TLC and ^{1}HNMR analysis (**Scheme 5.21**). We considered that elevated temperatures may facilitate the transformation and attempted to utilize precedent employing microwave conditions. However, even at 120º C for 45 minutes, we were still only seeing starting material by TLC and ^{1}HNMR. No product formation was occurring by MS analysis as well. More forcing conditions did not yield any desired product; however, at 150ºC for 2 hours, we were able to achieve starting material conversion, albeit degradation.
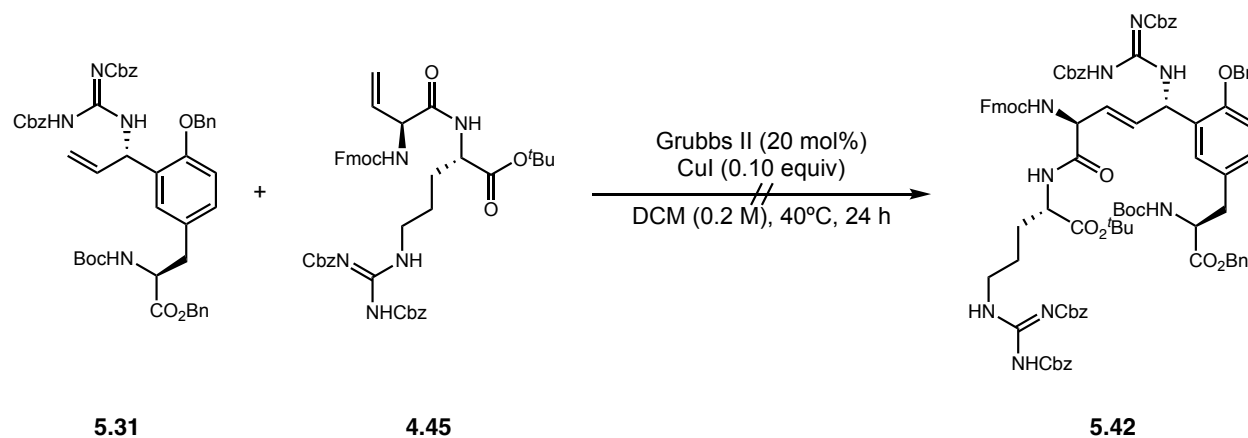
Scheme 5.22 Our investigation of CM to enable lactamization to furnish the protected, unsaturated Ryptide macrocycle.

Because of these initial challenges with RCM and because vinylglycine is significantly more precedented in cross metathesis literature, we opted to simultaneously explore an alternative route that would close the macrocycle via lactamization. Instead of forming the linear ryptide **5.32**, we envisioned initially performing a cross metathesis between VGly-Arg dimer **4.45** and Tyr **5.31** (**Scheme 5.22**). Because of our synergistic protecting group strategy, one pot deprotection with TFA and subsequent peptide coupling would furnish the protected and unsaturated Ryptide macrocycle (**5.41**). For the cross metathesis, we modified our initial model conditions to be more concentrated and to include cuprous iodide due to its significance in the suppression of catalyst toxification and improved conversion in CM reactions.[67] Unfortunately, employing these conditions on dimer **4.45** and tyrosine **5.31** resulted only in return of starting material as evidenced by TLC and ^{1}HNMR. We opted to switch solvents to toluene to accommodate higher temperatures, but again we only saw return of starting material. Furthermore, we attempted both the CM and RCM using the more reactive Grubbs' catalyst Ru-*Z*-DIPP courtesy of the Dai lab. Grubbs and co-workers demonstrated the utility of Ru-*Z*-DIPP to engage challenging olefins, including allylic-substituted olefins and acrylamides.[68] Again, however, we

were unable to effectuate any conversion of starting material when utilizing Ru-*Z*-DIPP in either our

RCM or CM reactions.

Blechert, 1997

Scheme 5.23 Schrock catalysts have been employed to effectuate CM of protected vinylglycine.

Because vinylglycine has been reported to undergo CM in conditions similar to what we have utilized,

we hypothesized that the protected allylic guanidine is hindering conversion to product, which is likely

attributed to steric hindrance. We proposed that this could potentially be remedied by moving to an

olefin metathesis catalyst with higher reactivity and tolerance towards sterically demanding substrates,

such as the Schrock catalysts. Although Schrock catalysts are known to possess low functional group

tolerance, Blechert and co-workers demonstrate the compatibility of protected vinylglycine with

Schrock catalyst (**Scheme 5.23**).[69]

Additionally, because 2° allylic alcohols are classified as type II olefins and should undergo CM, we

decided to try our model conditions on vinylglycine with our allylic alcohol precursor **5.28**.

Gratifyingly, we observed complete consumption of the allylic alcohol, as well as formation of a more

polar product by TLC. While investigations are currently underway, ^{1}HNMR strongly suggests the

formation of desired product, indicating that the allylic guanidine is indeed spectating in our RCM and CM attempts.

5.5 Concluding remarks

In our attempt to access the Ryptide macrocyclic RRY motif, we explored three major synthetic strategies: metallophotoredox cross coupling, *ortho*-hydroxylation, and allylic amination. We were unable to access the desired cross-coupled product when employing the metallophotoredox strategy, which is limited to electron deficient and *para* or *meta* substituted arenes. We faced issues with reproducibility using the *ortho*-hydroxylation strategy and were unable to separate hydroxylated product from starting material. However, we were successful employing stereoselective allylic amination to access the key allylic guanidine tyrosine fragment. Despite this, we faced significant challenges engaging the ring closing metathesis to furnish the macrocycle. We are currently exploring other allylic functionalities for their competency in cross metathesis in the hopes of developing an alternative route to deliver the Ryptide macrocycle.

5.6 References

(1) Zhou, Q. L. Transition-Metal Catalysis and Organocatalysis: Where Can Progress Be Expected? *Angew Chem Int Ed Engl* **2016**, *55* (18), 5352-5353. DOI: 10.1002/anie.201509164 From NLM PubMed-not-MEDLINE.

(2) Knowles, W. S.; Sabacky, M. J. Catalytic asymmetric hydrogenation employing a soluble, optically active, rhodium complex. *Chemical Communications (London)* **1968**, (22), 1445-1446, 10.1039/C19680001445. DOI: 10.1039/C19680001445.

(3) Miyashita, A.; Takaya, H.; Souchi, T.; Noyori, R. 2, 2'-bis(diphenylphosphino)-1, 1'-binaphthyl(binap): A new atropisomeric bis(triaryl)phosphine. synthesis and its use in the rh(l)-catalyzed asymmetric hydrogenation of α-(acylamino)acrylic acids. *Tetrahedron* **1984**, *40* (8), 1245-1253. DOI: https://doi.org/10.1016/S0040-4020(01)82411-X.

(4) Katsuki, T.; Sharpless, K. B. The first practical method for asymmetric epoxidation. *Journal of the American Chemical Society* **1980**, *102* (18), 5974-5976. DOI: 10.1021/ja00538a077.

(5) Jean-Louis Hérisson, P.; Chauvin, Y. Catalyse de transformation des oléfines par les complexes du tungstène. II. Télomérisation des oléfines cycliques en présence d'oléfines acycliques. *Die Makromolekulare Chemie* **1971**, *141* (1), 161-176. DOI: https://doi.org/10.1002/macp.1971.021410112 (acccessed 2024/02/20).

(6) Schrock, R. R. Alkylcarbene complex of tantalum by intramolecular .alpha.-hydrogen abstraction. *Journal of the American Chemical Society* **1974**, *96* (21), 6796-6797. DOI: 10.1021/ja00828a061.

(7) Grubbs, R. H.; Brunck, T. K. Possible intermediate in the tungsten-catalyzed olefin metathesis reaction. *Journal of the American Chemical Society* **1972**, *94* (7), 2538-2540. DOI: 10.1021/ja00762a073.

(8) Miyaura, N.; Yamada, K.; Suzuki, A. A new stereospecific cross-coupling by the palladium-catalyzed reaction of 1-alkenylboranes with 1-alkenyl or 1-alkynyl halides. *Tetrahedron Letters* **1979**, *20* (36), 3437-3440. DOI: https://doi.org/10.1016/S0040-4039(01)95429-2.

(9) Baba, S.; Negishi, E. A novel stereospecific alkenyl-alkenyl cross-coupling by a palladium- or nickel-catalyzed reaction of alkenylalanes with alkenyl halides. *Journal of the American Chemical Society* **1976**, *98* (21), 6729-6731. DOI: 10.1021/ja00437a067.

(10) Heck, R. F. Acylation, methylation, and carboxyalkylation of olefins by Group VIII metal derivatives. *Journal of the American Chemical Society* **1968**, *90* (20), 5518-5526. DOI: 10.1021/ja01022a034.

(11) Tasker, S. Z.; Standley, E. A.; Jamison, T. F. Recent advances in homogeneous nickel catalysis. *Nature* **2014**, *509* (7500), 299-309. DOI: 10.1038/nature13274.

(12) Zuo, Z.; Ahneman, D. T.; Chu, L.; Terrett, J. A.; Doyle, A. G.; MacMillan, D. W. C. Merging photoredox with nickel catalysis: Coupling of α-carboxyl sp3-carbons with aryl halides. *Science* **2014**, *345* (6195), 437-440. DOI: 10.1126/science.1255525 (acccessed 2024/02/21).

(13) Zuo, Z.; Cong, H.; Li, W.; Choi, J.; Fu, G. C.; MacMillan, D. W. Enantioselective Decarboxylative Arylation of alpha-Amino Acids via the Merger of Photoredox and Nickel Catalysis. *J Am Chem Soc* **2016**, *138* (6), 1832-1835. DOI: 10.1021/jacs.5b13211 From NLM Medline.

(14) Jintoku, T.; Nishimura, K.; Takaki, K.; Fujiwara, Y. Palladium Catalyzed Transformation of Benzene to Phenol with Molecular Oxygen. *Chemistry Letters* **1990**, *19* (9), 1687-1688. DOI: 10.1246/cl.1990.1687 (acccessed 2/26/2024).

(15) Thirunavukkarasu, V. S.; Hubrich, J.; Ackermann, L. Ruthenium-Catalyzed Oxidative C(sp2)–H Bond Hydroxylation: Site-Selective C–O Bond Formation on Benzamides. *Organic Letters* **2012**, *14* (16), 4210-4213. DOI: 10.1021/ol3018819.

(16) Liu, W.; Ackermann, L. Ortho- and Para-Selective Ruthenium-Catalyzed C(sp2)–H Oxygenations of Phenol Derivatives. *Organic Letters* **2013**, *15* (13), 3484-3486. DOI: 10.1021/ol401535k.

(17) Yang, X.; Shan, G.; Rao, Y. Synthesis of 2-Aminophenols and Heterocycles by Ru-Catalyzed C–H Mono- and Dihydroxylation. *Organic Letters* **2013**, *15* (10), 2334-2337. DOI: 10.1021/ol400437a.

(18) Yang, Y.; Lin, Y.; Rao, Y. Ruthenium(II)-Catalyzed Synthesis of Hydroxylated Arenes with Ester as an Effective Directing Group. *Organic Letters* **2012**, *14* (11), 2874-2877. DOI: 10.1021/ol301104n.

(19) Wu, Q.; Yan, D.; Chen, Y.; Wang, T.; Xiong, F.; Wei, W.; Lu, Y.; Sun, W. Y.; Li, J. J.; Zhao, J. A redox-neutral catechol synthesis. *Nat Commun* **2017**, *8*, 14227. DOI: 10.1038/ncomms14227 From NLM Medline.

(20) Liu, Q.; Wu, P.; Yang, Y.; Zeng, Z.; Liu, J.; Yi, H.; Lei, A. Room-Temperature Copper-Catalyzed Oxidation of Electron-Deficient Arenes and Heteroarenes Using Air. *Angewandte Chemie International Edition* **2012**, *51* (19), 4666-4670. DOI: https://doi.org/10.1002/anie.201200750 (acccessed 2024/02/26).

(21) Esguerra, K. V. N.; Lumb, J.-P. Synthesis of ortho-Azophenols by Formal Dehydrogenative Coupling of Phenols and Hydrazines or Hydrazides. *Chemistry – A European Journal* **2017**, *23* (36), 8596-8600. DOI: https://doi.org/10.1002/chem.201701226 (acccessed 2024/02/26).

(22) Shan, G.; Yang, X.; Ma, L.; Rao, Y. Pd-Catalyzed C H Oxygenation with TFA/TFAA: Expedient Access to Oxygen-Containing Heterocycles and Late-Stage Drug Modification. *Angewandte Chemie International Edition* **2012**, *51* (52), 13070-13074. DOI: https://doi.org/10.1002/anie.201207458 (acccessed 2024/02/26).

(23) Mo, F.; Trzepkowski, L. J.; Dong, G. Synthesis of ortho-Acylphenols through the Palladium-Catalyzed Ketone-Directed Hydroxylation of Arenes. *Angewandte Chemie International Edition* **2012**, *51* (52), 13075-13079. DOI: https://doi.org/10.1002/anie.201207479 (acccessed 2024/02/26).

(24) Liang, Y.-F.; Wang, X.; Yuan, Y.; Liang, Y.; Li, X.; Jiao, N. Ligand-Promoted Pd-Catalyzed Oxime Ether Directed C–H Hydroxylation of Arenes. *ACS Catalysis* **2015**, *5* (10), 6148-6152. DOI: 10.1021/acscatal.5b01700.

(25) Choy, P. Y.; Kwong, F. Y. Palladium-Catalyzed ortho-CH-Bond Oxygenation of Aromatic Ketones. *Organic Letters* **2013**, *15* (2), 270-273. DOI: 10.1021/ol303088z.

(26) Dai, C.; Han, Y.; Liu, L.; Huang, Z.-B.; Shi, D.-Q.; Zhao, Y. Palladium-catalyzed ortho-selective C–H hydroxylation of carboxybenzyl-protected benzylamines. *Organic Chemistry Frontiers* **2020**, *7* (13), 1703-1708, 10.1039/C9QO01523J. DOI: 10.1039/C9QO01523J.

(27) Faraggi, T. M.; Rouget-Virbel, C.; Rincón, J. A.; Barberis, M.; Mateos, C.; García-Cerrada, S.; Agejas, J.; de Frutos, O.; MacMillan, D. W. C. Synthesis of Enantiopure Unnatural Amino Acids by Metallaphotoredox Catalysis. *Organic Process Research & Development* **2021**, *25* (8), 1966-1973. DOI: 10.1021/acs.oprd.1c00208.

(28) Ross, A. J.; Lang, H. L.; Jackson, R. F. W. Much Improved Conditions for the Negishi Cross-Coupling of Iodoalanine Derived Zinc Reagents with Aryl Halides. *The Journal of Organic Chemistry* **2010**, *75* (1), 245-248. DOI: 10.1021/jo902238n.

(29) Li, G.; Hu, J.; Zeng, R.; Shi, D.-Q.; Zhao, Y. Direct ortho-Selective C–H Functionalization of Carboxybenzyl-Protected Arylalkylamines via Ir(III)-Catalyzed C–H Activation. *Organic Letters* **2018**, *20* (8), 2454-2458. DOI: 10.1021/acs.orglett.8b00797.

(30) Pàmies, O.; Margalef, J.; Cañellas, S.; James, J.; Judge, E.; Guiry, P. J.; Moberg, C.; Bäckvall, J.-E.; Pfaltz, A.; Pericàs, M. A.; et al. Recent Advances in Enantioselective Pd-Catalyzed Allylic Substitution: From Design to Applications. *Chemical Reviews* **2021**, *121* (8), 4373-4505. DOI: 10.1021/acs.chemrev.0c00736.

(31) Lei, H.; Rovis, T. A site-selective amination catalyst discriminates between nearly identical C–H bonds of unsymmetrical disubstituted alkenes. *Nature Chemistry* **2020**, *12* (8), 725-731. DOI: 10.1038/s41557-020-0470-z.

(32) Knecht, T.; Mondal, S.; Ye, J.-H.; Das, M.; Glorius, F. Intermolecular, Branch-Selective, and Redox-Neutral Cp*IrIII-Catalyzed Allylic C−H Amidation. *Angewandte Chemie International Edition* **2019**, *58* (21), 7117-7121. DOI: https://doi.org/10.1002/anie.201901733.

(33) Burman, J. S.; Blakey, S. B. Regioselective Intermolecular Allylic C−H Amination of Disubstituted Olefins via Rhodium/π-Allyl Intermediates. *Angewandte Chemie International Edition* **2017**, *56* (44), 13666-13669. DOI: https://doi.org/10.1002/anie.201707021.

(34) Harris, R. J.; Park, J.; Nelson, T. A. F.; Iqbal, N.; Salgueiro, D. C.; Bacsa, J.; MacBeth, C. E.; Baik, M.-H.; Blakey, S. B. The Mechanism of Rhodium-Catalyzed Allylic C–H Amination. *Journal of the American Chemical Society* **2020**, *142* (12), 5842-5851. DOI: 10.1021/jacs.0c01069.

(35) Ide, T.; Feng, K.; Dixon, C. F.; Teng, D.; Clark, J. R.; Han, W.; Wendell, C. I.; Koch, V.; White, M. C. Late-Stage Intermolecular Allylic C–H Amination. *Journal of the American Chemical Society* **2021**, *143* (37), 14969-14975. DOI: 10.1021/jacs.1c06335.

(36) Zalatan, D. N.; Du Bois, J. A Chiral Rhodium Carboxamidate Catalyst for Enantioselective C−H Amination. *Journal of the American Chemical Society* **2008**, *130* (29), 9220-9221. DOI: 10.1021/ja8031955.

(37) Nishioka, Y.; Uchida, T.; Katsuki, T. Enantio- and Regioselective Intermolecular Benzylic and Allylic C   H Bond Amination. *Angewandte Chemie International Edition* **2013**, *52* (6), 1739-1742. DOI: https://doi.org/10.1002/anie.201208906.

(38) Cai, A.; Guo, W.; Martínez-Rodríguez, L.; Kleij, A. W. Palladium-Catalyzed Regio- and Enantioselective Synthesis of Allylic Amines Featuring Tetrasubstituted Tertiary Carbons. *Journal of the American Chemical Society* **2016**, *138* (43), 14194-14197. DOI: 10.1021/jacs.6b08841.

(39) Wei, Y.; Xiong, F.-Y.; Lu, L.-Q.; Xiao, W.-J. Photoinduced palladium-catalyzed asymmetric allylic C–H amination. *Chem* **2023**, *9* (3), 559-561. DOI: https://doi.org/10.1016/j.chempr.2023.02.007.

(40) Lafrance, M.; Roggen, M.; Carreira, E. M. Direct, Enantioselective Iridium-Catalyzed Allylic Amination of Racemic Allylic Alcohols. *Angewandte Chemie International Edition* **2012**, *51* (14), 3470-3473. DOI: https://doi.org/10.1002/anie.201108287 (acccessed 2024/03/05).

(41) Jackson, R. F. W.; Wishart, N.; Wood, A.; James, K.; Wythes, M. J. Preparation of enantiomerically pure protected 4-oxo .alpha.-amino acids and 3-aryl .alpha.-amino acids from serine. *The Journal of Organic Chemistry* **1992**, *57* (12), 3397-3404. DOI: 10.1021/jo00038a030.

(42) Dexter, C. S.; Jackson, R. F. W.; Elliott, J. Synthesis of Enantiomerically Pure β- and γ-Amino Acid Derivatives Using Functionalized Organozinc Reagents. *The Journal of Organic Chemistry* **1999**, *64* (20), 7579-7585. DOI: 10.1021/jo990941y.

(43) Nolasco, L.; Perez Gonzalez, M.; Caggiano, L.; Jackson, R. F. W. Application of Negishi Cross-Coupling to the Synthesis of the Cyclic Tripeptides OF4949-III and K-13. *The Journal of Organic Chemistry* **2009**, *74* (21), 8280-8289. DOI: 10.1021/jo9018792.

(44) Berkowitz, D. B.; Charette, B. D.; Karukurichi, K. R.; McFadden, J. M. α-Vinylic amino acids: occurrence, asymmetric synthesis, and biochemical mechanisms. *Tetrahedron: Asymmetry* **2006**, *17* (6), 869-882. DOI: https://doi.org/10.1016/j.tetasy.2006.02.026.

(45) Dadová, J.; Galan, S. R. G.; Davis, B. G. Synthesis of modified proteins via functionalization of dehydroalanine. *Current Opinion in Chemical Biology* **2018**, *46*, 71-81. DOI: https://doi.org/10.1016/j.cbpa.2018.05.022.

(46) Gleeson, E. C.; Jackson, W. R.; Robinson, A. J. Ring-closing metathesis in peptides. *Tetrahedron Letters* **2016**, *57* (39), 4325-4333. DOI: https://doi.org/10.1016/j.tetlet.2016.08.032.

(47) Oroz, P.; Navo, C. D.; Avenoza, A.; Busto, J. H.; Corzana, F.; Jiménez-Osés, G.; Peregrina, J. M. Towards Enantiomerically Pure Unnatural α-Amino Acids via Photoredox Catalytic 1,4-Additions to a Chiral Dehydroalanine. *The Journal of Organic Chemistry* **2022**, *87* (21), 14308-14318. DOI: 10.1021/acs.joc.2c01774.

(48) Guo, J.-X.; Zhou, T.; Xu, B.; Zhu, S.-F.; Zhou, Q.-L. Enantioselective synthesis of α-alkenyl α-amino acids via N–H insertion reactions. *Chemical Science* **2016**, *7* (2), 1104-1108, 10.1039/C5SC03558A. DOI: 10.1039/C5SC03558A.

(49) Hanessian, S.; Sahoo, S. P. A novel and efficient synthesis of L-vinylglycine. *Tetrahedron Letters* **1984**, *25* (14), 1425-1428. DOI: https://doi.org/10.1016/S0040-4039(01)80177-5.

(50) Barton, D. H. R.; Crich, D.; Motherwell, W. B. The invention of new radical chain reactions. Part VIII. Radical chemistry of thiohydroxamic esters; A new method for the generation of carbon radicals from carboxylic acids. *Tetrahedron* **1985**, *41* (19), 3901-3924. DOI: https://doi.org/10.1016/S0040-4020(01)97173-X.

(51) Berkowitz, D. B.; Smith, M. K. A Convenient Synthesis of L-α-Vinylglycine from L-Homoserine Lactone. *Synthesis* **1996**, *1996* (01), 39-41. DOI: 10.1055/s-1996-4177.

(52) Pellicciari, R.; Natalini, B.; Marinozzi, M. L-α-Aminoadipic Acid from L-Glutamic Acid. *Synthetic Communications* **1988**, *18* (14), 1707-1714. DOI: 10.1080/00397918808081333.

(53) Afzali-Ardakani, A.; Rapoport, H. L-Vinylglycine. *The Journal of Organic Chemistry* **1980**, *45* (24), 4817-4820. DOI: 10.1021/jo01312a002.

(54) Wu, H.; Zhang, Y.; Li, Y.; Xu, J.; Wang, Y.; Li, X. Chemical Synthesis and Biological Evaluations of Adiponectin Collagenous Domain Glycoforms. *Journal of the American Chemical Society* **2021**, *143* (20), 7808-7818. DOI: 10.1021/jacs.1c02382.

(55) Somlai, C.; Lovas, S.; Forgó, P.; Murphy, R. F.; Penke, B. DEHYDRATION OF THREONINE ESTERS DURING TOSYLATION. *Synthetic Communications* **2001**, *31* (23), 3633-3640. DOI: 10.1081/SCC-100107012.

(56) Chauvin, Y. Olefin Metathesis: The Early Days (Nobel Lecture). *Angewandte Chemie International Edition* **2006**, *45* (23), 3740-3747. DOI: https://doi.org/10.1002/anie.200601234 (acccessed 2024/03/10).

(57) Nguyen, S. T.; Grubbs, R. H.; Ziller, J. W. Syntheses and activities of new single-component, ruthenium-based olefin metathesis catalysts. *Journal of the American Chemical Society* **1993**, *115* (21), 9858-9859. DOI: 10.1021/ja00074a086.

(58) Schrock, R.; Rocklage, S.; Wengrovius, J.; Rupprecht, G.; Fellmann, J. Preparation and characterization of active niobium, tantalum and tungsten metathesis catalysts. *Journal of Molecular Catalysis* **1980**, *8* (1), 73-83. DOI: https://doi.org/10.1016/0304-5102(80)87006-4.

(59) Wengrovius, J. H.; Schrock, R. R.; Churchill, M. R.; Missert, J. R.; Youngs, W. J. Multiple metal-carbon bonds. 16. Tungsten-oxo alkylidene complexes as olefins metathesis catalysts and the crystal structure of W(O)(CHCMe3(PEt3)Cl2. *Journal of the American Chemical Society* **1980**, *102* (13), 4515-4516. DOI: 10.1021/ja00533a035.

(60) Toreki, R.; Schrock, R. R. A well-defined rhenium(VII) olefin metathesis catalyst. *Journal of the American Chemical Society* **1990**, *112* (6), 2448-2449. DOI: 10.1021/ja00162a071.

(61) Dawood, K. M.; Nomura, K. Recent Developments in Z-Selective Olefin Metathesis Reactions by Molybdenum, Tungsten, Ruthenium, and Vanadium Catalysts. *Adv Synth Catal* **2021**, *363* (8), 1970-1997. DOI: https://doi.org/10.1002/adsc.202001117 (acccessed 2024/03/10).

(62) Schafmeister, C. E.; Po, J.; Verdine, G. L. An all-hydrocarbon cross-linking system for enhancing the helicity and metabolic stability of peptides. *Journal of the American Chemical Society* **2000**, *122* (24), 5891-5892. DOI: DOI 10.1021/ja000563a.

(63) Oishi, S.; Shi, Z.-D.; Worthy, K. M.; Bindu, L. K.; Fisher, R. J.; Burke Jr., T. R. Ring-Closing Metathesis of C-Terminal Allylglycine Residues with an N-Terminal β-Vinyl-Substituted Phosphotyrosyl Mimetic as an Approach to Novel Grb2 SH2 Domain-Binding Macrocycles. *ChemBioChem* **2005**, *6* (4), 668-674. DOI: https://doi.org/10.1002/cbic.200400298.

(64) Grubbs, R. H.; Miller, S. J.; Fu, G. C. Ring-Closing Metathesis and Related Processes in Organic Synthesis. *Accounts of Chemical Research* **1995**, *28* (11), 446-452. DOI: 10.1021/ar00059a002.

(65) Miller, S. J.; Blackwell, H. E.; Grubbs, R. H. Application of Ring-Closing Metathesis to the Synthesis of Rigidified Amino Acids and Peptides. *Journal of the American Chemical Society* **1996**, *118* (40), 9606-9614. DOI: 10.1021/ja961626l.

(66) Clerc, J.; Schellenberg, B.; Groll, M.; Bachmann, A. S.; Huber, R.; Dudler, R.; Kaiser, M. Convergent Synthesis and Biological Evaluation of Syringolin A and Derivatives as Eukaryotic 20S Proteasome Inhibitors. *European Journal of Organic Chemistry* **2010**, *2010* (21), 3991-4003. DOI: https://doi.org/10.1002/ejoc.201000317 (acccessed 2024/03/06).

(67) Wang, J.; Lin, D. a.; Liu, M.; Liu, H.; Blasco, P.; Sun, Z.; Cheung, Y. C.; Chen, S.; Li, X. Total Synthesis of Mannopeptimycin β via β-Hydroxyenduracididine Ligation. *Journal of the American Chemical Society* **2021**, *143* (32), 12784-12790. DOI: 10.1021/jacs.1c05922.

(68) Quigley, B. L.; Grubbs, R. H. Ruthenium-catalysed Z-selective cross metathesis of allylic-substituted olefins. *Chemical Science* **2014**, *5* (2), 501-506, 10.1039/C3SC52806E. DOI: 10.1039/C3SC52806E.

(69) Brümmer, O.; Rückert, A.; Blechert, S. Olefin Cross-Metathesis with Monosubstituted Olefins. *Chemistry – A European Journal* **1997**, *3* (3), 441-444. DOI: https://doi.org/10.1002/chem.19970030316.

5.7 Supporting Information

5.7.1 General Information

^{1}H and ^{13}C nuclear magnetic resonance (NMR) spectra were recorded on a Varian INOVA 500 spectrometer (^{1}H 400 MHz, ^{13}C 126 MHz); Bruker AVANCE NEO 400 (^{1}H 400 MHz ; Bruker AVANCE III 600 (^{1}H 600 MHz, ^{13}C 151 MHz); and Bruker AVANCE NEO 800 (^{1}H 800 MHz) at room temperature in CDCl$_3$ unless otherwise indicated. Chemical shifts are reported in ppm and coupling constants (*J*) in Hz. Multiplicities are reported using the following abbreviations: s = singlet, d = doublet, t = triplet, q = quartet, qn = quintet, m = multiplet, and b = broad. Analytical thin-layer chromatography (TLC) was carried out utilizing glass-backed Silicycle TLC plates and visualized with UV light, KMnO$_4$, or ninhydrin unless otherwise indicated. Flash chromatography was performed using Silicycle SilaFlash® F60 silica gel (40-63 µm) on a Biotage Isolera One system. Silica gel chromatography was performed using Silicycle SilaFlash® F60 silica gel (40-63 µm).

All reactions were carried out under nitrogen atmosphere using Schlenk technique unless otherwise noted. Anhydrous tetrahydrofuran (THF), diethyl ether (Et$_2$O), dichloromethane (DCM), hexanes, and toluene were obtained via passage over activated alumina using *Glass Contours* solvent system. Anhydrous dimethylformamide (DMF), dimethoxysulfoxide (DMSO), and 1,4-dioxanes were obtained from Dry-Seal EMD Millipore, subjected to degassing and stored over 4Å molecular sieves. Solvents for work-up procedures and chromatography were obtained from commercial suppliers without additional purification. All reagents were purchased from Ambeed, MilliporeSigma, Strem Chemicals, Oakwood Chemicals, or TCI and were used without further purification.

5.7.2 Procedures

General Procedure A

An oven-dried vial with stir bar was charged with Ir[dF(CF$_3$)ppy]$_2$(dtbbpy)PF$_6$, NiCl$_2$•glyme, 4,4′-di-tert-butyl-2,2′-bipyridyl (dtbbpy), the aryl halide, Boc-protected amino acid, Cs$_2$CO$_3$, and DMF. The reaction mixture was degassed by sonication under vacuum, then irradiated with two 26 W fluorescent lamps (at approximately 2 cm away from the light source). After 72h, the reaction mixture was diluted with saturated aqueous NaHCO$_3$ solution and extracted with Et$_2$O. The combined organic extracts were washed with water, brine, dried over anhydrous MgSO$_4$, and concentrated *in vacuo*. The crude material was purified via SiO$_2$ chromatography.

methyl *N*-(*tert*-butoxycarbonyl)-*O*-(*tert*-butyldimethylsilyl)-*L*-serinate
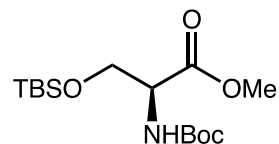
Prepared according to literature procedure.[1] Boc-*L*-Ser-OMe (1.0 equiv, 5.0 mmol) and imidazole (1.2 equiv, 6.0 mmol) were added to a flask and dissolved in DCM (0.25 M). After cooling the reaction in an ice/water bath, TBDMSCl (1.2 equiv, 6.0 mmol) in DCM (10 mL) was added to the reaction dropwise. After complete addition, the reaction was warmed to room temperature and allowed to stir overnight. The reaction was then poured into 1 N HCl (50 mL) and extracted with 2x50 mL DCM. The organic phase were washed with 1 N HCl (50 mL), then H$_2$O (50 mL), brine (50 mL), and dried over anhydrous Na$_2$SO$_4$. The crude material was concentrated *in vacuo* to yield product as a colorless oil (1.65 g, **99% yield**) that was used in the next step without further purification. ^{1}HNMR matched previously reported spectra.[1]

^{1}H NMR (600 MHz, CDCl$_3$) δ 5.33 (d, *J* = 8.8 Hz, 1H), 4.35 (dt, *J* = 8.8, 3.0 Hz, 1H), 4.03 (dd, *J* = 10.0, 2.8 Hz, 1H), 3.81 (dd, *J* = 10.1, 3.1 Hz, 1H), 3.73 (s, 3H), 1.45 (s, 9H), 0.85 (s, 9H), 0.02 (d, *J* = 8.2 Hz, 6H).

5.1 *N*-(*tert*-butoxycarbonyl)-*O*-(*tert*-butyldimethylsilyl)-*L*-serine
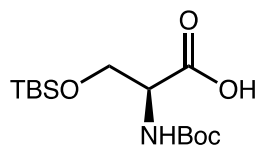
Boc-Ser(OTBS)-OMe (1.0 equiv, 3.0 mmol) was added to a flask and dissolved in MeOH (0.5 M). LiOH (2.0 equiv, 6.0 mmol) was added, and the reaction was stirred at room temperature for 8 hours. The reaction was concentrated *in vacuo* to afford product as a colorless oil that was used without further purification. ^{1}HNMR matched previously reported spectra.[2]

^{1}H NMR (600 MHz, CDCl$_3$) δ 5.34 (d, *J* = 8.4 Hz, 1H), 4.42 – 4.33 (m, 1H), 4.10 (dd, *J* = 10.0, 2.9 Hz, 1H), 3.87 – 3.79 (m, 1H), 1.45 (s, 9H), 0.91 – 0.86 (m, 9H), 0.11 – 0.02 (m, 6H).

5.8 benzyl (*S*)-3-(4-(benzyloxy)-3-iodophenyl)-2-((*tert*-butoxycarbonyl)amino)propanoate
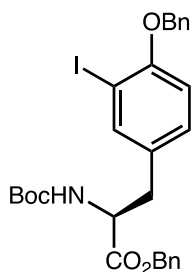
Prepared according to literature procedure.[3] To a solution of Boc-I-Tyr-OH (1.0 equiv, 3.8 mmol) in acetone (0.32 M), K$_2$CO$_3$ (3.0 equiv, 11.5 mmol) and benzyl bromide (2.2 equiv, 8.4 mmol) were added. The reaction was refluxed for 5 hours. After the reaction was cooled to room temperature, the reaction was concentrated *in vacuo* and the residue was dissolved in EtOAc and washed with saturated NaHCO$_3$ (3x80 mL), dried over anhydrous Na$_2$SO$_4$ and concentrated *in vacuo* to afford product as a colorless oil (1.7 g, **76% yield**) used without further purification. ^{1}HNMR matched previously reported spectra.[3]

^{1}H NMR (400 MHz, CDCl$_3$) δ 7.56 (s, 1H), 7.54 – 7.47 (m, 2H), 7.45 – 7.30 (m, 7H), 6.95 (d, *J* = 8.3 Hz, 1H), 6.70 (d, *J* = 8.4 Hz, 1H), 5.15 (d, *J* = 10.4 Hz, 1H), 5.12 (s, 2H), 5.02 (d, *J* = 8.2 Hz, 1H), 4.58 (d, *J* = 7.8 Hz, 1H), 3.01 (qd, *J* = 14.0, 6.0 Hz, 2H), 1.45 (s, 9H).

5.11 1-(benzyloxy)-2-iodobenzene
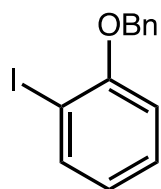
A solution of 2-iodophenol (1.0 equiv, 8.0 mmol) and K_2CO_3 (1.5 equiv, 12 mmol) in acetone (0.09 M) was stirred for 10 minutes at room temperature. Benzyl bromide (1.1 equiv, 8.8 mmol) was added dropwise to the solution. The reaction was then refluxed overnight. After cooling to room temperature, the reaction was diluted in EtOAc (50 mL) and washed with saturated $NaHCO_3$ (2x50 mL). The organic phase was dried over anhydrous $MgSO_4$ and concentrated *in vacuo*. The crude material was purified via chromatography (SiO_2, 0-10% EtOAc in Hex) to yield product as an orange/brown oil (1.73 g, **70% yield**). ¹HNMR matched previously reported spectra.[4]

¹H NMR (600 MHz, CDCl₃) δ 7.83 – 7.79 (m, 1H), 7.53 – 7.49 (m, 2H), 7.40 (dd, *J* = 8.3, 6.9 Hz, 3H), 7.35 – 7.26 (m, 2H), 6.87 (dd, *J* = 8.3, 1.4 Hz, 1H), 6.73 (td, *J* = 7.6, 1.3 Hz, 1H), 5.16 (s, 2H).

5.12: *tert*-butyl 2-(2-(benzyloxy)phenyl)pyrrolidine-1-carboxylate
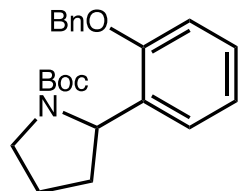
General procedure **A** was applied to Boc-Pro-OH (1.5 equiv, 0.15 mmol), 1-iodo-4-methoxybenzene (1.0 equiv, 0.10 mmol), NiCl₂glyme (0.1 equiv, 0.01 mmol), dtbbpy (0.15 equiv, 0.015 mmol), [Ir{dF(CF₃)ppy}₂(dtbpy)PF₆ (0.01 equiv, 0.0001 mmol), CsCO₃ (1.5 equiv, 0.15 mmol) in degassed DMF (0.02 M) to yield product as an orange amorphous solid (**40% yield[a]**).

[a]NMR yield determined using dibromomethane as a standard. **¹H NMR** (600 MHz, CDCl₃) δ 7.44 (d, *J* = 7.7 Hz, 2H), 7.39 (q, *J* = 9.0, 8.3 Hz, 2H), 7.32 (dt, *J* = 12.0, 7.5 Hz, 1H), 7.19 – 7.02 (m, 2H), 6.95 – 6.88 (m, 2H), 5.37 – 5.19 (m, 1H), 5.18 – 5.04 (m, 2H), 3.66 – 3.42 (m, 2H), 2.34 – 2.20 (m, 1H),

1.85 (tq, J = 19.2, 5.6 Hz, 3H), 1.47 (s, 3H), 1.21 (d, J = 1.7 Hz, 6H). **MS** (ESI+) calculated 353.46, found 354 [M+H]$^{1+}$.

5.14 *tert*-butyl (2-(benzyloxy)-1-(2-(benzyloxy)phenyl)ethyl)carbamate
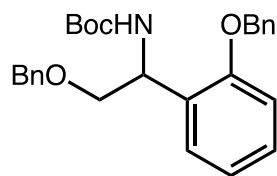
General procedure **A** was applied to Boc-Pro-OH (1.5 equiv, 0.15 mmol), 1-(benzyloxy)-2-iodobenzene (1.0 equiv, 0.10 mmol), NiCl₂glyme (0.1 equiv, 0.01 mmol), dtbbpy (0.15 equiv, 0.015 mmol), [Ir{dF(CF₃)ppy}₂(dtbpy)PF₆ (0.01 equiv, 0.0001 mmol), CsCO₃ (1.5 equiv, 0.15 mmol) in degassed DMF (0.02 M) to yield product as an orange amorphous solid (**20% yield** ^{a}).

^{a}NMR yield determined using dibromomethane as a standard. **^{1}H NMR** (600 MHz, CDCl₃) δ 7.37 – 7.29 (m, 10H), 7.00 – 6.95 (m, 4H), 5.44 (d, J = 8.7 Hz, 1H), 5.07 (s, 2H), 5.05 (d, J = 2.2 Hz, 2H), 4.74 (dt, J = 8.7, 3.8 Hz, 1H), 4.41 (s, 2H), 3.94 (dd, J = 9.6, 4.0 Hz, 1H), 3.78 (dd, J = 9.6, 3.4 Hz, 1H), 1.46 (s, 11H). **MS** (ESI+) calculated 433.55, found 434.2927 [M+H]$^{1+}$.

5.23 benzyl (2-hydroxybenzyl)carbamate
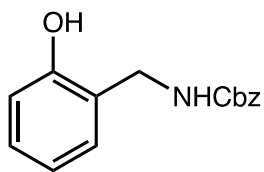
Prepared according to literature procedure.[5] A solution of benzyl benzylcarbamate **5.23** (1 equiv, 0.1 mmol), PIFA (1.22 equiv, 0.12 mmol), and Pd(OAc)₂ (0.10 equiv, 0.01 mmol) in DCE (0.1 M) was heated to 70°C under air with vigorous stirring for 5 hours. After cooling to room temperature, the solution was diluted with EtOAc and passed through a celite plug. The filtrate was concentrated *in vacuo* and purified via SiO₂ chromatography (EtOAc:Pet Et₂O, 1:20 to 1:10) to give the corresponding product (11.2 mg, **29% yield** ^{a}) ^{1}HNMR matched previously reported spectra.[5] ^{a}NMR yield determined using dibromomethane as a standard.

5.24 1-(3-bromobenzyl)-(Z)$_2$-guanidine
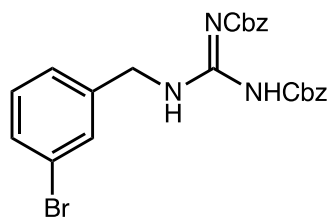
Benzyl (*E*)-((((benzyloxy)carbonyl)amino)(1*H*-pyrazol-1-yl)methylene)carbamate (1.0 equiv, 2.15 mmol) in a flask was dissolved in DCM (0.46 M). 3-bromobenzylamine (1.0 equiv, 2.15 mmol) was added to the reaction, and the reaction was allowed to stir at room temperature for 18 hours. After complete consumption of SM by TLC, the reaction was diluted with EtOAc and the organic layer was washed with brine. The organic phase was dried over anhydrous MgSO$_4$ and concentrated *in vacuo* to deliver product as a colorless oil used without further purification (960.2 mg, **90% yield**).

^{1}H NMR (400 MHz, CDCl$_3$) δ 11.78 (s, 1H), 8.62 (t, *J* = 5.6 Hz, 1H), 5.18 (s, 1H), 5.14 (s, 1H), 4.61 (d, *J* = 5.5 Hz, 1H). **MS** (ESI+) calculated 495.08, found 495.9597 [M+H]$^{1+}$.

5.25 1-(5-bromo-2-hydroxybenzyl)-(Z)$_2$-guanidine
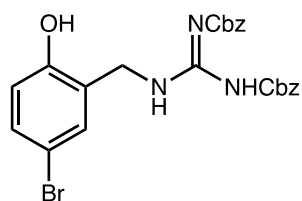
A solution of 1-(3-bromobenzyl)-(Z)$_2$-guanidine **5.23** (1 equiv, 0.1 mmol), PIFA (1.22 equiv, 0.12 mmol), and Pd(OAc)$_2$ (0.10 equiv, 0.01 mmol) in DCE (0.1 M) was heated to 70ºC under air with vigorous stirring for 5 hours. After cooling to room temperature, the solution was diluted with EtOAc and passed through a celite plug. The filtrate was concentrated *in vacuo* and purified via SiO$_2$ chromatography (EtOAc:Pet Et$_2$O, 1:20 to 1:10) to give an inseparable mixture of **5.24** and **5.25**.

MS (ESI+) calculated 511.07, found 512.0630 [M+H]$^{1+}$.

5.27 2-(benzyloxy)-5-iodobenzaldehyde
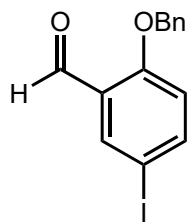
To 2-hydroxy-5-iodobenzaldehyde (1.0 equiv, 16.5 mmol) dissolved in DMF (0.5 M), BnBr (1.2 equiv, 19.7 mmol) and K_2CO_3 (1.2 equiv, 19.7 mmol) were added. The reaction was stirred at room temperature for 4 hours. The reaction was washed with saturated LiCl solution (3x100 mL), then brine (100 mL) and dried over anhydrous $MgSO_4$. The crude material was concentrated *in vacuo* and purified via chromatography (SiO_2, 10% EtOAc in Hex) to afford product as an off-white solid (3.83 g, **69% yield**). ^{1}HNMR matched previously reported spectra.[6]

^{1}H NMR (400 MHz, CDCl₃) δ 10.42 (s, 1H), 8.12 (d, *J* = 2.4 Hz, 1H), 7.78 (dd, *J* = 8.8, 2.4 Hz, 1H), 7.46 – 7.32 (m, 5H), 6.84 (d, *J* = 8.8 Hz, 1H), 5.18 (s, 2H).

5.28 1-(2-(benzyloxy)-5-iodophenyl)prop-2-en-1-ol
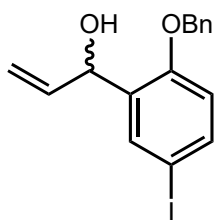
2-(benzyloxy)-5-iodobenzaldehyde (1.0 equiv, 5.7 mmol) was added to a flask and dissolved in THF (0.25 M). The flask was cooled in an ice/water bath and vinylmagnesium bromide (3 equiv, 17 mmol) was added. The reaction was warmed to room temperature and stirred overnight. The reaction was quenched with NH₄Cl, and the reaction was transferred to a separatory funnel. The organic phase was removed, and the aqueous phase was washed with EtOAc (2x). The organic phase was washed with brine, dried over anhydrous Na₂SO₄, then concentrated *in vacuo*. The crude material was purified via chromatography (SiO_2, 10-12% EtOAc in Hex) to afford product as a white solid (1.84 g, **88% yield**).

^{1}H NMR (400 MHz, CDCl₃) δ 7.68 – 7.61 (m, 1H), 7.52 (dd, *J* = 8.6, 2.3 Hz, 1H), 7.41 – 7.32 (m, 5H), 6.71 (d, *J* = 8.6 Hz, 1H), 6.07 (ddd, *J* = 17.2, 10.4, 5.5 Hz, 1H), 5.44 (tt, *J* = 5.5, 1.5 Hz, 1H), 5.31

(dt, J = 17.2, 1.5 Hz, 1H), 5.19 (dt, J = 10.4, 1.4 Hz, 1H), 5.08 (s, 2H), 2.56 (d, J = 5.5 Hz, 1H). ^{13}C

NMR (101 MHz, CDCl$_3$) δ 155.56, 138.79, 137.38, 136.22, 136.06, 133.76, 128.79, 128.31, 127.40,

115.22, 114.31, 83.82, 70.42, 70.37. MS (ESI-) calculated 366.20, found 365.0023 [M-H]$^-$.

5.30 (*S*)-1-(1-(2-(benzyloxy)-5-iodophenyl)allyl)-Cbz-guanidine
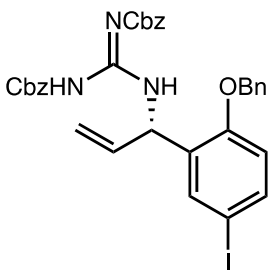
[Ir(COE)$_2$Cl$_2$]$_2$ (0.025 equiv, 0.013 mmol), (*S*)-ligand (0.1 equiv, 0.05 mmol), 5.29 (1 equiv, 0.5 mmol) and sulfamic acid (1.2 equiv, 0.6 mmol) were placed in a screw-capped vial charged with a stir bar. The vial was backfilled with N$_2$ three times, then anhydrous DMF (5.0 equiv, 0.2 mL) followed by

chloroform (1.7 mL) were added. The reaction was stirred for 24 hours at room temperature. To the

reaction, TEA (4.0 equiv, 2 mmol) was added and stirred. After 10 minutes, pyrazol(Z)2 N,N'-Bis-Z-

1-Guanylpyrazole (2 equiv, 1 mmol) was added, and the reaction was left to stir for 24 hours at room

temperature. The reaction was concentrated *in vacuo* and the crude material was purified via

chromatography (SiO$_2$, 8-10% EtOAc in Hex) to afford product as a white foam (185.2 mg, **55%**

yield).

^{1}H NMR (800 MHz, CDCl$_3$) δ 11.76 (s, 1H), 9.20 (d, J = 8.4 Hz, 1H), 7.56 (d, J = 2.2 Hz, 1H), 7.50

(dd, J = 8.6, 2.3 Hz, 1H), 7.42 – 7.27 (m, 15H), 6.68 (d, J = 8.7 Hz, 1H), 6.06 – 5.99 (m, 2H), 5.20 –

5.09 (m, 9H). ^{13}C NMR (201 MHz, CDCl$_3$) δ 163.91, 156.35, 155.31, 153.69, 137.97, 137.84, 136.99,

136.41, 136.21, 134.80, 130.69, 128.87, 128.80, 128.65, 128.62, 128.53, 128.19, 128.07, 127.99, 127.33,

115.81, 115.01, 83.37, 70.56, 68.16, 67.38, 53.56. MS (ESI+) calculated 675.52, found 676.2156

[M+H]$^{1+}$.

Boc-Br-Ala-OBn
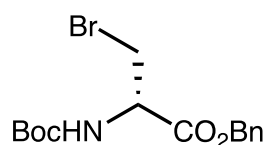
Procedure adapted from literature.[7] To Boc-Ser-OBzl (1.0 equiv, 2.54 mmol) and CBr$_4$ (1.5 equiv, 3.81 mmol) dissolved in DCM (0.12 M) and cooled over an ice/water bath, PPh$_3$ (2.0 equiv, 5.1 mmol) was added. The reaction was allowed to stir at 0°C for 20 minutes until TLC indicated complete consumption of starting material. The reaction was treated with Et$_2$O (20 mL), and the precipitate was filtered and washed with additional Et$_2$O. The filtrate was washed with saturated NaHCO$_3$ (50 mL), brine (50 mL), then dried over anhydrous MgSO$_4$ and concentrated *in vacuo*. The crude material was recrystallized with hexanes to afford product as white needles (0.62 g, **69% yield**). ^{1}HNMR matched previously reported spectra.[7]

^{1}H NMR (400 MHz, CDCl$_3$) δ 7.37 (d, J = 1.4 Hz, 5H), 5.42 (d, J = 7.8 Hz, 1H), 5.26 – 5.17 (m, 2H), 4.79 (dt, J = 7.6, 3.3 Hz, 1H), 3.84 (dd, J = 10.5, 3.3 Hz, 1H), 3.71 (dd, J = 10.5, 3.5 Hz, 1H), 1.45 (s, 9H).

Boc-I-Ala-OBn
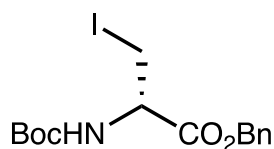
Procedure adapted from literature.[8] To Boc-Ser-OBzl (1.0 equiv, 2.56 mmol) and PPh$_3$ (1.25 equiv, 3.19 mmol) dissolved in anhydrous DCM (0.17 M) cooled in an ice/water bath, imidazole (1.25 equiv, 3.19 mmol) was added, followed by iodine (1.25 equiv, 3.19 mmol) in three portions. The reaction mixture was warmed to room temperature and allowed to stir for 2.5 hours. The reaction was filtered through SiO$_2$ using 1:1 Et$_2$O:Pet ether, and the filtrate was concentrated *in vacuo*. Et$_2$O (15 mL) was added to crash out phosphine oxide, and the filtrate was passed through a celite plug with Et$_2$O. The crude material was concentrated *in vacuo* and was purified via chromatography (SiO$_2$, 10-15% Et$_2$O in Pet ether) to afford product as a white solid (1.033 g, **quant**). ^{1}HNMR matched previously reported spectra.[9]

¹H NMR (400 MHz, CDCl₃) δ 7.37 (d, *J* = 2.4 Hz, 5H), 5.36 (d, *J* = 7.7 Hz, 1H), 5.27 – 5.16 (m, 2H), 4.55 (dt, *J* = 7.7, 3.9 Hz, 1H), 3.58 (qd, *J* = 10.3, 3.9 Hz, 2H), 1.45 (s, 9H).

5.31 benzyl (*S*)-3-(4-(benzyloxy)-3-((*S*)-1-((*Z*)-2,3 bis ((benzyloxy)carbonyl)guanidino)allyl)phenyl)-2-((*tert*-butoxycarbonyl)amino)propanoate
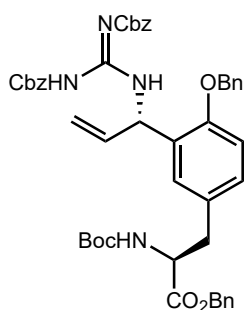
To an oven dried HPLC vial charged with a stir bar, Zn dust (5.8 equiv, 1.20 mmol) was added. The vial was flame-dried and back-filled with N₂ three times. Anhydrous DMF (0.1 mL) was added followed by TMSCl (0.026 mL). The mixture was vigorously stirred for 15 minutes at room temperature. Stirring was then stopped, and solvent was removed *in vacuo* using a heat gun. Anhydrous DMF (0.4 mL) was again added to the vial, followed by Boc-I-Ala-OBn (1.26 equiv, 0.260 mmol). The reaction was allowed to stir vigorously at room temperature until TLC indicated complete consumption of the amino acid (20% EtOAc in Hex, Ninhydrin). Pd₂(dba)₃ (0.063 equiv, 0.013 mmol), P(*o*-Tol)₃ (0.3 equiv, 0.062 mmol), and a stock of aryl iodide **5.30** (1.0 equiv, 0.207 mmol) were added, and the reaction was allowed to vigorously stir at 50ºC overnight. After cooling to room temperature, the reaction was diluted with 10 mL EtOAc and passed through a celite plug. The crude material was extracted with saturated LiCl₂ solution (2x20 mL). The aqueous phase was extracted with EtOAc (2x20 mL), and the combined organic phase were dried over anhydrous Na₂SO₄ and concentrated *in vacuo*. The crude material was purified via chromatography (SiO₂, 10-35% EtOAc in Hex) to yield product as a yellow/orange oil (89 mg, **52% yield**).

¹H NMR (400 MHz, CDCl₃) δ 11.72 (s, 1H), 9.29 (d, J = 8.4 Hz, 1H), 7.44 – 7.22 (m, 28H), 7.02 – 6.85 (m, 2H), 6.77 (d, J = 8.4 Hz, 1H), 6.11 – 5.92 (m, 2H), 5.21 – 5.01 (m, 12H), 4.98 (d, J = 8.4 Hz, 1H), 4.56 (q, J = 6.5 Hz, 1H), 3.00 (d, J = 6.0 Hz, 2H), 1.41 (d, J = 7.5 Hz, 13H). **¹³C NMR** (101 MHz, CDCl₃) δ 171.84, 163.99, 155.28, 153.58, 137.07, 136.94, 136.90, 135.32, 134.88, 130.59, 128.84, 128.78, 128.70, 128.64, 128.59, 128.55, 128.52, 128.46, 128.25, 127.97, 127.92, 127.34, 115.23, 112.82, 80.07, 70.48, 68.04, 67.30, 67.17, 54.67, 28.84, 28.42. **MS** (ESI+) calculated 826.95, found 827.22 [M+H]¹⁺.

5.33: Fmoc-*L*-Met-OBn
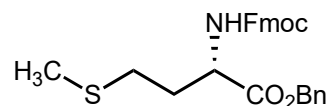
KHCO₃ (2.5 equiv, 13.8 mmol) was slowly added to a mixture of Fmoc-Met-OH (1.0 equiv, 5.52 mmol) and BnBr (1.5 equiv, 8.28 mmol) in anhydrous DMF (1.1 M). The reaction was allowed to stir for 4 hours at room temperature. The reaction was then diluted with EtOAc (500 mL) and washed with 1 N HCl (3x100 mL) then brine (100 mL). The organic phase was dried over anhydrous Na₂SO₄ and concentrated *in vacuo*. The crude material was purified via chromatography (SiO₂, 6:1 Hex:EtOAc) to afford product as a white solid (2.36 g, **92.5% yield**). ¹HNMR matched previously reported spectra.[10]

¹H NMR (500 MHz, CDCl₃) δ 7.77 (d, J = 7.5 Hz, 2H), 7.59 (d, J = 7.5 Hz, 2H), 7.44 – 7.28 (m, 8H), 5.44 (d, J = 8.3 Hz, 1H), 5.20 (h, J = 12.5 Hz, 2H), 4.55 (td, J = 7.8, 4.8 Hz, 1H), 4.41 (d, J = 7.1 Hz, 2H), 4.22 (t, J = 7.1 Hz, 1H), 2.55 – 2.41 (m, 2H), 2.23 – 2.12 (m, 1H), 2.09 – 1.93 (m, 2H).

5.34 Fmoc-*L*-Met(S=O)-OBn
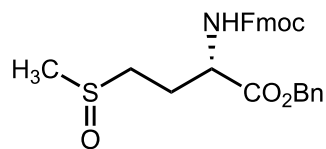
NaIO$_4$ (1.0 equiv, 0.542 mmol) slurried in H$_2$O (0.37 mL) was slowly added to Fmoc-Met-OBn (1.0 equiv, 0.542 mmol) in MeOH (2.7 mL) and THF (0.54 mL) in an ice bath. After addition, the ice bath was removed and the reaction was allowed to stir overnight at room temperature. The reaction mixture was concentrated *in vacuo* then diluted with DCM (14 mL) and washed with 1 N HCl (2x10 mL) and brine (10 mL). The organic phase was dried over anhydrous Na$_2$SO$_4$ and concentrated *in vacuo*. The crude material was purified via chromatography (SiO$_2$, 18:1 DCM:MeOH) to yield product as a white solid (213 mg, **82% yield**). ^{1}HNMR matched previously reported spectra.[10]

^{1}H NMR (500 MHz, CDCl$_3$) δ 7.75 (d, *J* = 7.6 Hz, 2H), 7.60 (td, *J* = 7.1, 3.0 Hz, 2H), 7.44 – 7.21 (m, 9H), 6.24 (dd, *J* = 23.5, 8.0 Hz, 1H), 5.23 – 5.12 (m, 2H), 4.50 (td, *J* = 8.5, 4.4 Hz, 1H), 4.39 (qd, *J* = 10.7, 9.7, 5.6 Hz, 1H), 4.19 (td, *J* = 7.1, 3.4 Hz, 1H), 2.77 – 2.58 (m, 1H), 2.45 (d, *J* = 7.7 Hz, 2H), 2.42 – 2.31 (m, 1H), 2.17 (dq, *J* = 9.7, 4.7 Hz, 1H).

5.35 Fmoc-*L*-VGly-OBn
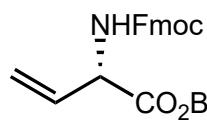
Procedure adapted from literature.[10, 11] To an oven-dried pressure tube, Fmoc-Met(S=O)-OBn (200 mg, 0.420 mmol) was added. *m*-xylenes was added to the solid (0.2 M). The reaction was heated to 150°C over 24 hours with no stirring. After cooling the reaction to room temperature, the reaction was purified by chromatography (SiO$_2$, 20% EtOAc in Hex) to yield product as a white solid (153 mg, **88% yield**). ^{1}HNMR matched previously reported spectra.[10]

¹H NMR (400 MHz, CDCl₃) δ 7.77 (d, *J* = 7.5 Hz, 2H), 7.61 (d, *J* = 7.5 Hz, 2H), 7.45 – 7.27 (m, 9H), 5.94 (ddd, *J* = 16.4, 10.3, 5.4 Hz, 1H), 5.51 (d, *J* = 8.2 Hz, 1H), 5.43 – 5.25 (m, 2H), 5.22 (s, 2H), 5.04 – 4.96 (m, 1H), 4.42 (d, *J* = 6.9 Hz, 2H), 4.23 (t, *J* = 7.1 Hz, 1H).

5.36 Fmoc-*L*-VGly-OH
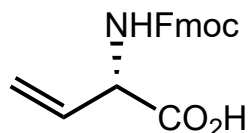
To a flask containing Fmoc-VGly-OBn (294 mg, 0.712 mmol) was added a 2:1 mixture of 1,4-dioxanes: 6 N HCl (90 mM). Using a condenser, the reaction was refluxed under air for 24 hours. After cooling the reaction to room temperature, the reaction was basified (pH 9) with saturated NaHCO₃ and extracted with 3x10 mL DCM. The aqueous phase was re-acidified (pH 1) with 1 N HCl and extracted with 3x10 mL DCM. The organic phase was dried over anhydrous Na₂SO₄ and concentrated *in vacuo* to afford product as a white solid (167.1 mg, **73% yield**) that was used forward without further purification. ¹HNMR matched previously reported spectra.[12]

¹H NMR (400 MHz, CDCl₃) δ 7.76 (d, *J* = 7.5 Hz, 2H), 7.58 (s, 2H), 7.39 (t, *J* = 7.4 Hz, 2H), 7.30 (t, *J* = 7.4 Hz, 2H), 5.96 (s, 1H), 5.47 (d, *J* = 7.6 Hz, 1H), 5.44 – 5.26 (m, 1H), 4.96 (s, 1H), 4.43 (d, *J* = 7.1 Hz, 2H), 4.22 (t, *J* = 7.0 Hz, 1H).

5.38 H₂N-*L*-Arg(Z)₂-O*t*Bu
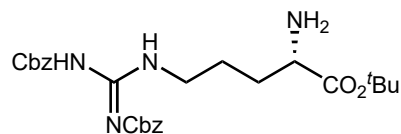
Procedure adapted from literature.[13] Boc-Arg(Z)₂-OH (1.0 equiv, 3.02 mmol) was added to a vial containing *t*BuAc (0.15 M), followed by perchloric acid (70%, 3.0 equiv, 9.05 mmol). The mixture was allowed to stir overnight at room temperature. The reaction was then extracted with H₂O (100 mL) and 0.5 N HCl (150 mL). The aqueous phase was bascified with 10% (w/v) aq. K₂CO₃ (pH 9). The aqueous layer was washed with

DCM (4x100 mL), and the organic phase was dried over anhydrous Na_2SO_4 and concentrated *in vacuo* to afford product as a colorless oil (1.00 g, **70% yield**) used without further purification.

^{1}H NMR (400 MHz, CDCl$_3$) δ 9.44 (s, 1H), 9.25 (s, 1H), 7.39 – 7.26 (m, 10H), 5.21 (s, 2H), 5.12 (s, 2H), 4.04 – 3.91 (m, 2H), 3.29 (dd, *J* = 7.6, 4.3 Hz, 1H), 1.74 – 1.59 (m, 3H), 1.49 – 1.46 (m, 1H), 1.39 (s, 9H). **^{13}C NMR** (101 MHz, CDCl$_3$) δ 175.15, 163.99, 160.60, 155.95, 137.00, 134.73, 128.92, 128.69, 128.59, 128.53 –127.76, 82.23, 68.99, 67.07, 54.46, 44.41, 28.12, 28.06, 27.97. **MS** (ESI+) calculated 498.58, found 499.2604 [M+H]$^{1+}$.

4.45 Fmoc-VGly-Arg(Z)$_2$-O^{t}Bu
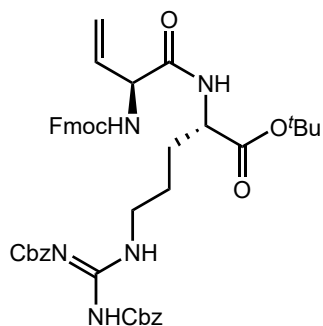
Fmoc-VGly-OH (1.0 equiv, 0.11 mmol) and H$_2$N-Arg(Z)$_2$-O^{t}Bu (1.0 equiv, 0.11 mmol) were dissolved in DMF (0.1 M). To the resulting mixture, DIPEA (2.5 equiv, 0.29 mmol) and HATU (1.1 equiv, 0.13 mmol) were added. The reaction was stirred at room temperature overnight. After completion, Et$_2$O (25 mL) and H$_2$O (25 mL) were added and transferred to a separatory funnel. The aqueous layer was extracted with Et$_2$O (3x25 mL) and the combined organic phase were washed with brine (50 mL), dried over MgSO$_4$, and concentrated *in vacuo*. The crude material was purified via chromatography (SiO$_2$, 20-50% EtOAc in Hex) to yield product as a white solid (45.7 mg, **50% yield**).

^{1}H NMR (800 MHz, CDCl$_3$) δ 9.48 (d, *J* = 22.0 Hz, 1H), 9.27 (d, *J* = 20.9 Hz, 1H), 7.76 (d, *J* = 7.6 Hz, 2H), 7.60 (dd, *J* = 8.8, 5.1 Hz, 2H), 7.43 – 7.27 (m, 14H), 6.73 (d, *J* = 7.6 Hz, 1H), 5.87 – 5.78 (m, 1H), 5.78 – 5.69 (m, 1H), 5.39 – 5.25 (m, 2H), 5.24 – 5.20 (m, 2H), 5.14 (q, *J* = 12.5 Hz, 2H), 4.74 (dt, *J* = 24.2, 6.9 Hz, 1H), 4.54 – 4.44 (m, 1H), 4.43 – 4.32 (m, 2H), 4.21 (t, *J* = 7.2 Hz, 1H), 3.97 (ddt, *J* =

24.5, 14.3, 6.8 Hz, 2H), 1.86 – 1.78 (m, 1H), 1.73 – 1.59 (m, 3H), 1.39 (d, J = 2.6 Hz, 9H). **^{13}C NMR**

(201 MHz, CDCl₃) δ 170.71, 169.15, 163.94, 160.72, 155.91, 144.03, 143.93, 141.41, 136.98, 134.71,

133.87, 129.01, 128.94, 128.54, 128.38, 128.19, 128.01, 127.81, 127.18, 120.09, 82.50, 69.06, 67.20,

67.11, 60.51, 57.40, 52.96, 47.26, 44.35, 28.01, 24.57. **MS** (ESI+) calculated 803.91, found 804.37

$[M+H]^{1+}$.

5.32 Linear ryptide trimer
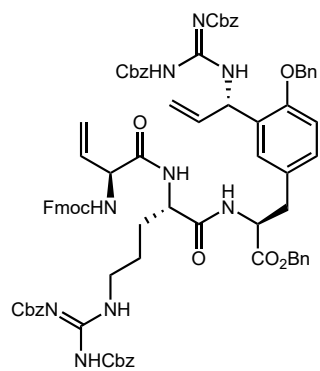
4.45 (1.0 equiv, 5.78 µmol) and **5.31** (1.0 equiv, 5.78 µmol) were treated with 1:1 DCM:TFA for 1 hour at room temperature. The mixture was concentrated *in vacuo*, and CHCl₃ was used to azeotrope off residual TFA. To the crude deprotected **4.45** and **5.31** dissolved in DMF (0.1 M), DIPEA (10 equiv, 57.8 µmol) and HATU (1.1 equiv, 6.36 µmol) were added. The reaction was stirred at room temperature overnight. After completion, Et₂O (5 mL) and

H₂O (5 mL) were added and transferred to a separatory funnel. The aqueous layer was extracted with

Et₂O (3x5 mL) and the combined organic phase were washed with brine (50 mL), dried over MgSO₄,

and concentrated *in vacuo*. The crude material was purified via chromatography (SiO₂, 20-75% EtOAc

in Hex) to yield product as a white solid (4.1 mg, **49% yield**).

^{1}H NMR (800 MHz, CDCl₃) δ 11.69 (s, 1H), 9.43 (s, 1H), 9.27 (t, J = 11.0 Hz, 2H), 7.75 (d, J = 7.5

Hz, 2H), 7.57 (d, J = 7.5 Hz, 2H), 7.43 – 7.20 (m, 40H), 7.15 (d, J = 7.5 Hz, 2H), 7.05 (s, 1H), 6.90 (s,

1H), 6.86 – 6.78 (m, 2H), 6.71 (d, J = 8.4 Hz, 1H), 6.05 – 5.92 (m, 2H), 5.80 – 5.67 (m, 2H), 5.28 (d, J

= 17.2 Hz, 1H), 5.20 (s, 3H), 5.15 – 4.98 (m, 13H), 4.65 (d, J = 7.5 Hz, 1H), 4.61 – 4.48 (m, 2H), 4.36

(tt, J = 19.5, 8.5 Hz, 2H), 4.19 (t, J = 7.1 Hz, 1H), 4.02 – 3.83 (m, 2H), 2.88 (d, J = 12.8 Hz, 2H), 1.78

– 1.70 (m, 1H), 1.63 (d, J = 7.0 Hz, 2H), 1.59 – 1.55 (m, 1H). **^{13}C NMR** (201 MHz, CDCl₃) δ 170.98,

170.88, 169.68, 163.96, 163.57, 161.06, 155.90, 155.85, 155.59, 155.27, 153.57, 144.00, 143.91, 141.43, 141.42, 136.99, 136.90, 136.88, 136.80, 135.21, 134.87, 134.70, 133.51, 130.34, 130.00, 129.05, 129.03, 128.97, 128.95, 128.81, 128.76, 128.67, 128.65, 128.61, 128.57, 128.55, 128.50, 128.45, 128.34, 128.26, 128.18, 128.14, 127.97, 127.94, 127.90, 127.84, 127.44, 127.21, 125.24, 125.21, 120.11, 118.91, 115.26, 112.63, 70.43, 69.15, 68.03, 67.28, 67.26, 67.21, 67.18, 67.11, 57.46, 54.46, 53.97, 53.10, 47.26, 44.05, 38.76, 36.84, 36.63, 29.84, 28.42, 24.82. **MS** (ESI+) calculated 1455.59, found 1456.5925 [M+H]$^{1+}$ & 728.80064 [M+2H]$^{2+}$

5.39 Tosyl-protected diallylamine
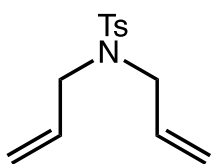
Procedure adapted from literature.[14] TsCl (1.0 equiv, 5.0 mmol) was added to a solution of diallylamine (1.0 equiv, 5.0 mmol) in TEA (1.0 equiv, 5.0 mmol) in DCM (0.3 M). The reaction was stirred at room temperature for 2 hours. Saturated NaHCO$_3$ (75 mL) was added to the reaction, and the organic phase was separated and washed with brine (25 mL) then dried over anhydrous MgSO$_4$. The crude material was concentrated *in vacuo* and purified via chromatography (SiO$_2$, 15% EtOAc in Hex) to yield product as a colorless oil (1.052 g, **84% yield**). ^{1}HNMR matched previously reported spectra.[14]

^{1}H NMR (400 MHz, CDCl$_3$) δ 7.72 – 7.64 (m, 2H), 7.32 – 7.23 (m, 2H), 5.58 (ddt, J = 17.6, 9.8, 6.3 Hz, 2H), 5.13 (dq, J = 5.4, 1.4 Hz, 2H), 5.09 (t, J = 1.6 Hz, 2H), 3.77 (dt, J = 6.3, 1.4 Hz, 4H), 2.39 (s, 3H).

5.40 1-tosyl-2,5-dihydro-1*H*-pyrrole
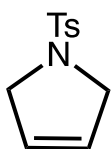
To either Grubbs II or Hoyveda-Grubbbs II (0.20 equiv, 0.02 mmol) dissolved in DCM, a stock of tosyl-protected diallylamine (1.0 equiv, 0.99 mmol) in DCM was added. DCM was added to make a 0.01 M solution. The reaction was stirred at 30°C overnight. After cooling to room temperature, the reaction was concentrated *in vacuo* and purified via chromatography (SiO$_2$, 5-75% EtOAc in Hex) to afford product as a light brown solid (Grubbs II – 21 mg, **95% yield**; Hoyveda-Grubbs II – 13.5 mg, **61% yield**). ^{1}HNMR matched previously reported spectra.[14]

¹H NMR (400 MHz, CDCl$_3$) δ 7.76 – 7.67 (m, 2H), 7.35 – 7.29 (m, 2H), 5.65 (s, 2H), 4.12 (s, 4H), 2.42 (s, 3H).
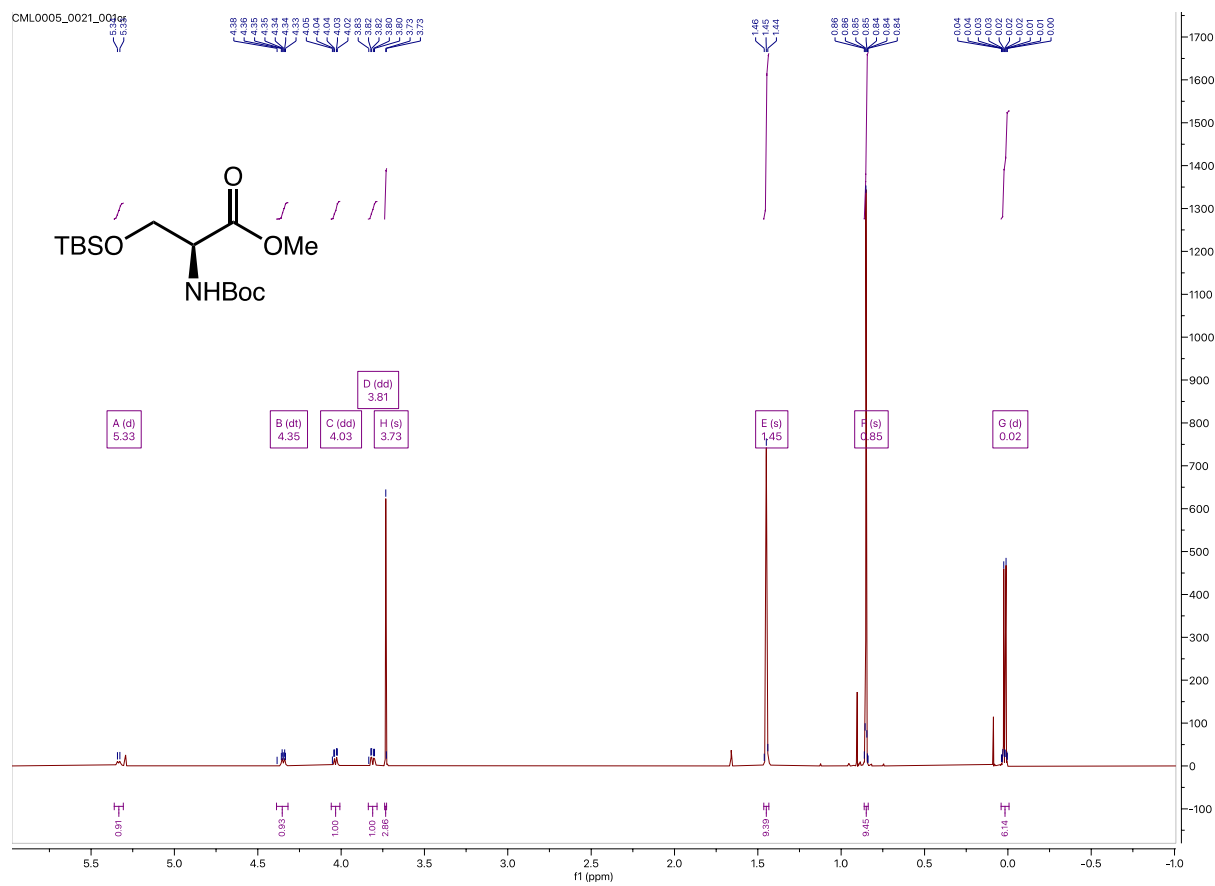
5.1: ^{1}H NMR 600 MHz, CDCl$_3$

5.8 ^{1}H NMR 400 MHz, CDCl₃

5.11 ^{1}H NMR 600 MHz, CDCl$_3$

A (m)
7.81

B (m)
7.51

C (dd)
7.40

D (m)
7.30

G (td)
6.73

E (dd)
6.87

F (s)
5.16
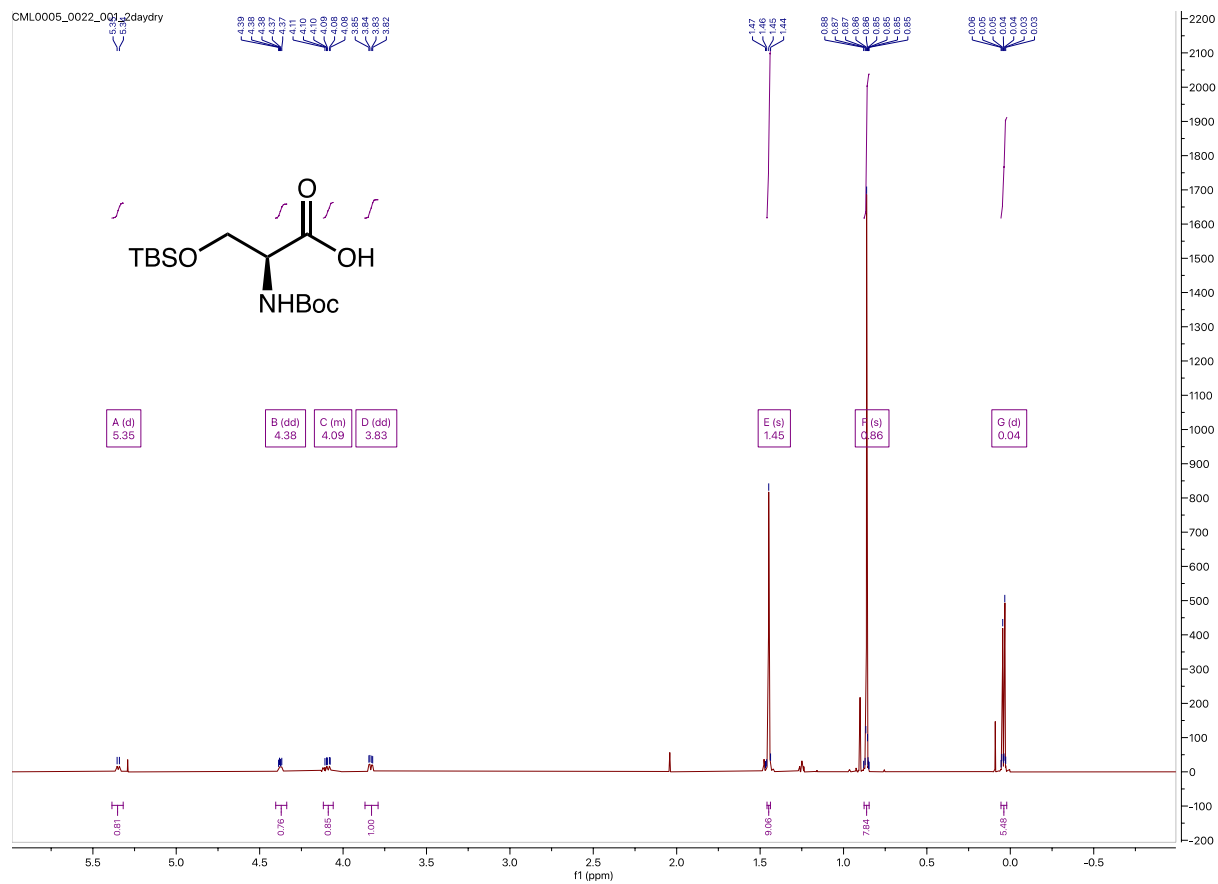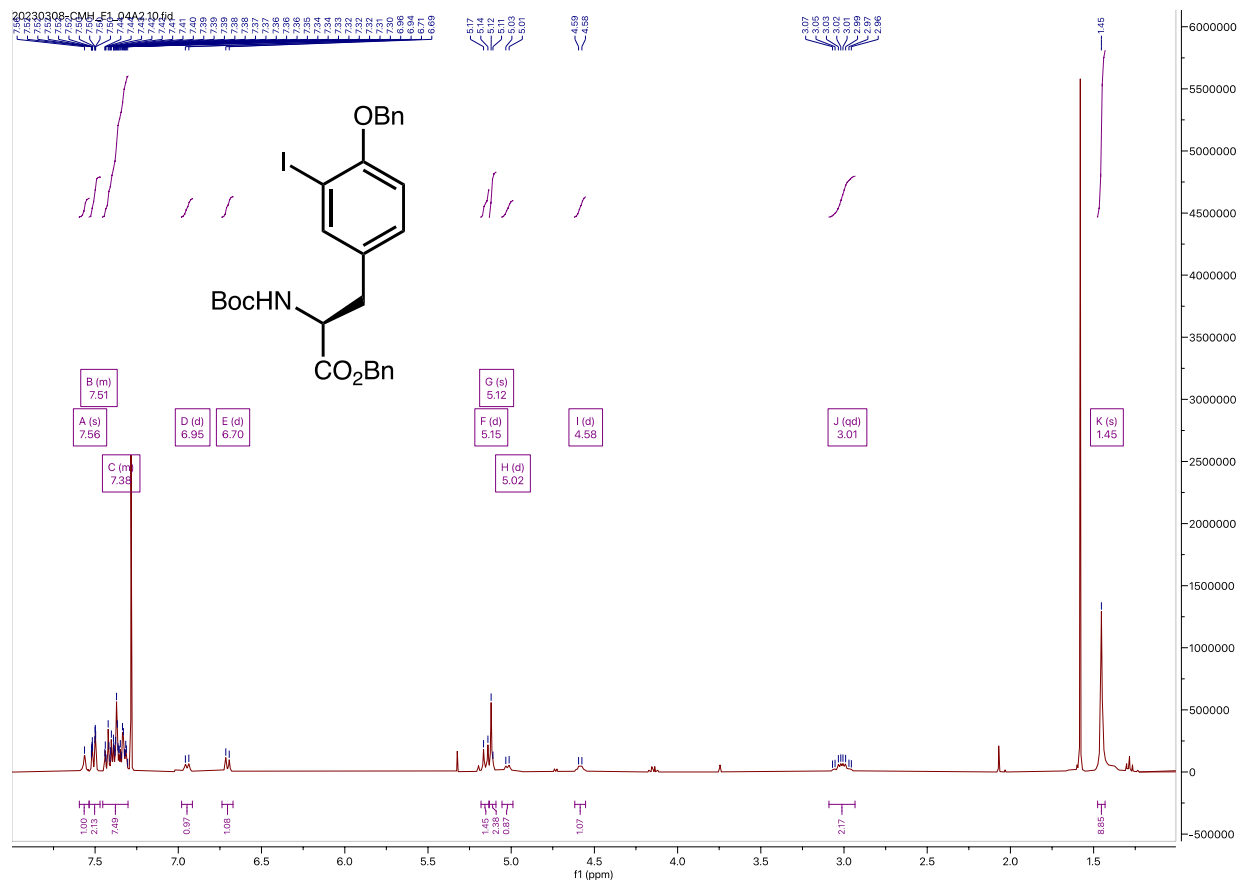
5.12 ^{1}H NMR 600 MHz, CDCl$_3$

5.24 ^{1}H NMR 400 MHz, CDCl$_3$

KD02-03-2Recol.10.fid

5.27: ^{1}H NMR (400 MHz, CDCl$_3$)
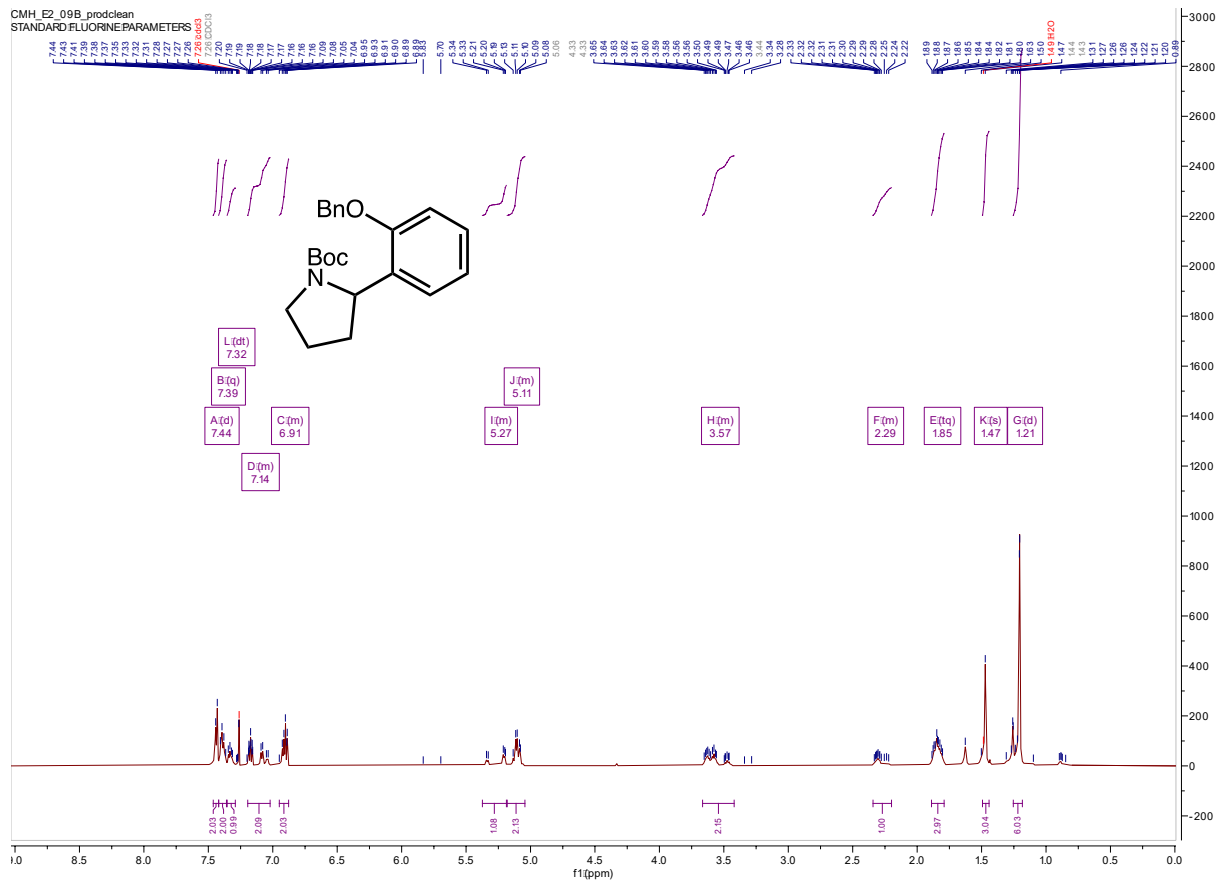
5.28: ^{1}H NMR (400 MHz, CDCl$_3$)
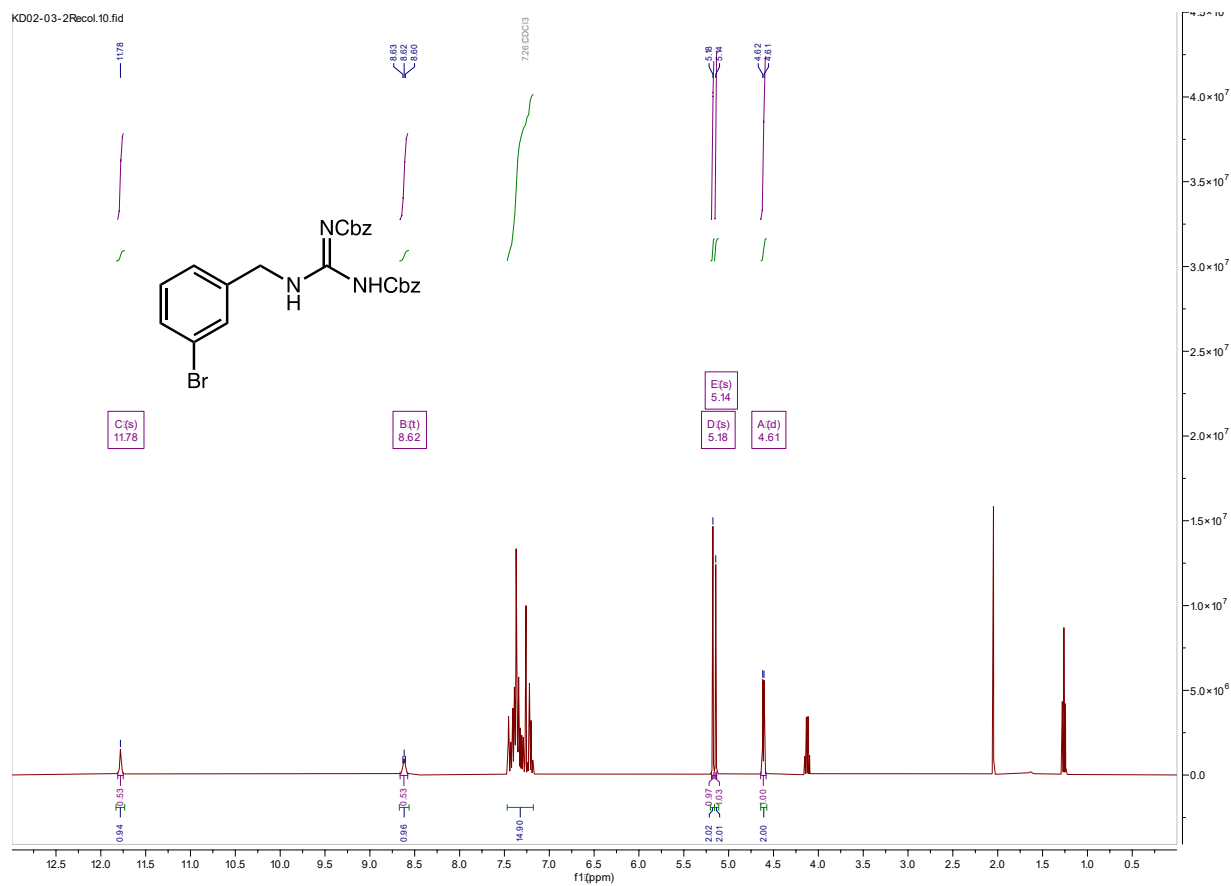
5.28 ^{13}CNMR 101 MHz, CDCl$_3$

20240304-CML2-26-3.2.fid
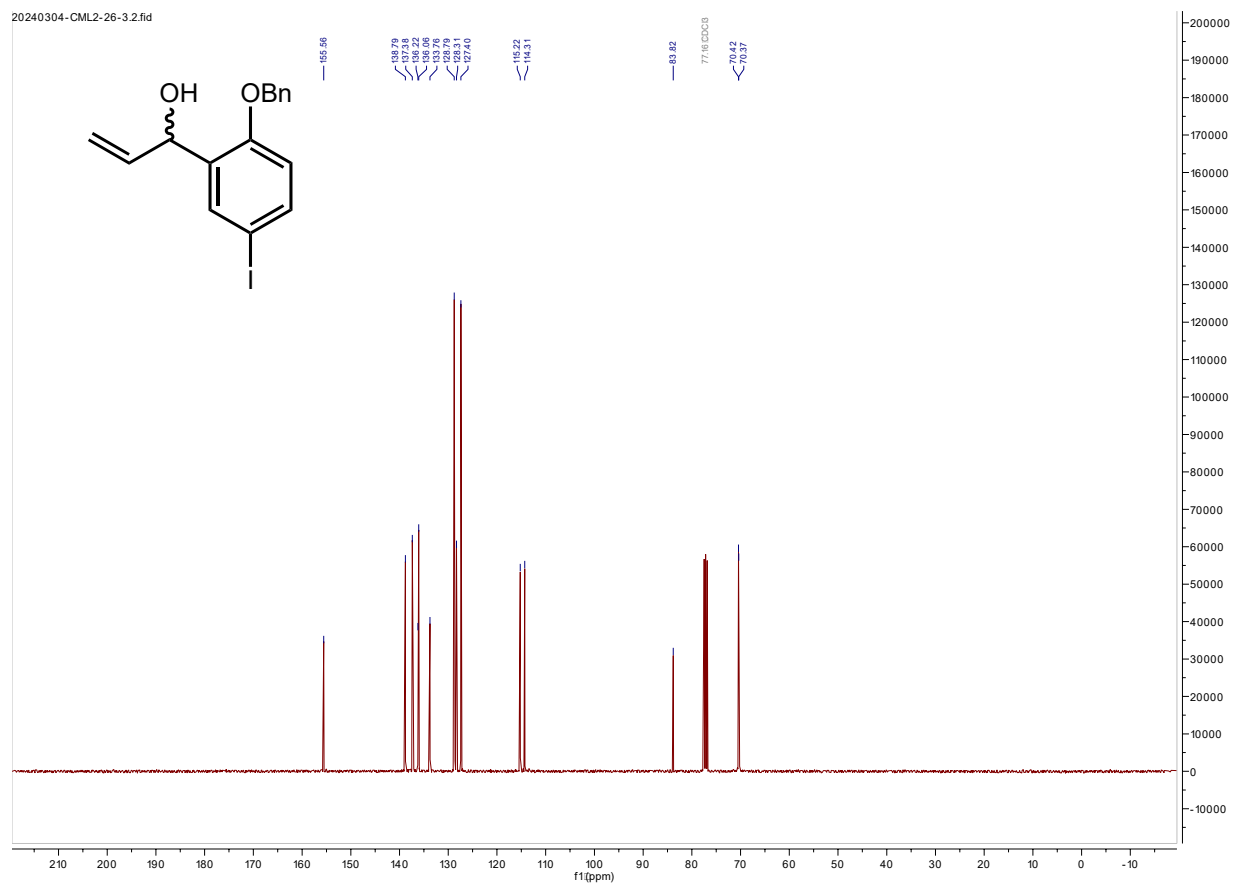
5.30: ^{1}H NMR 800 MHz, CDCl$_3$
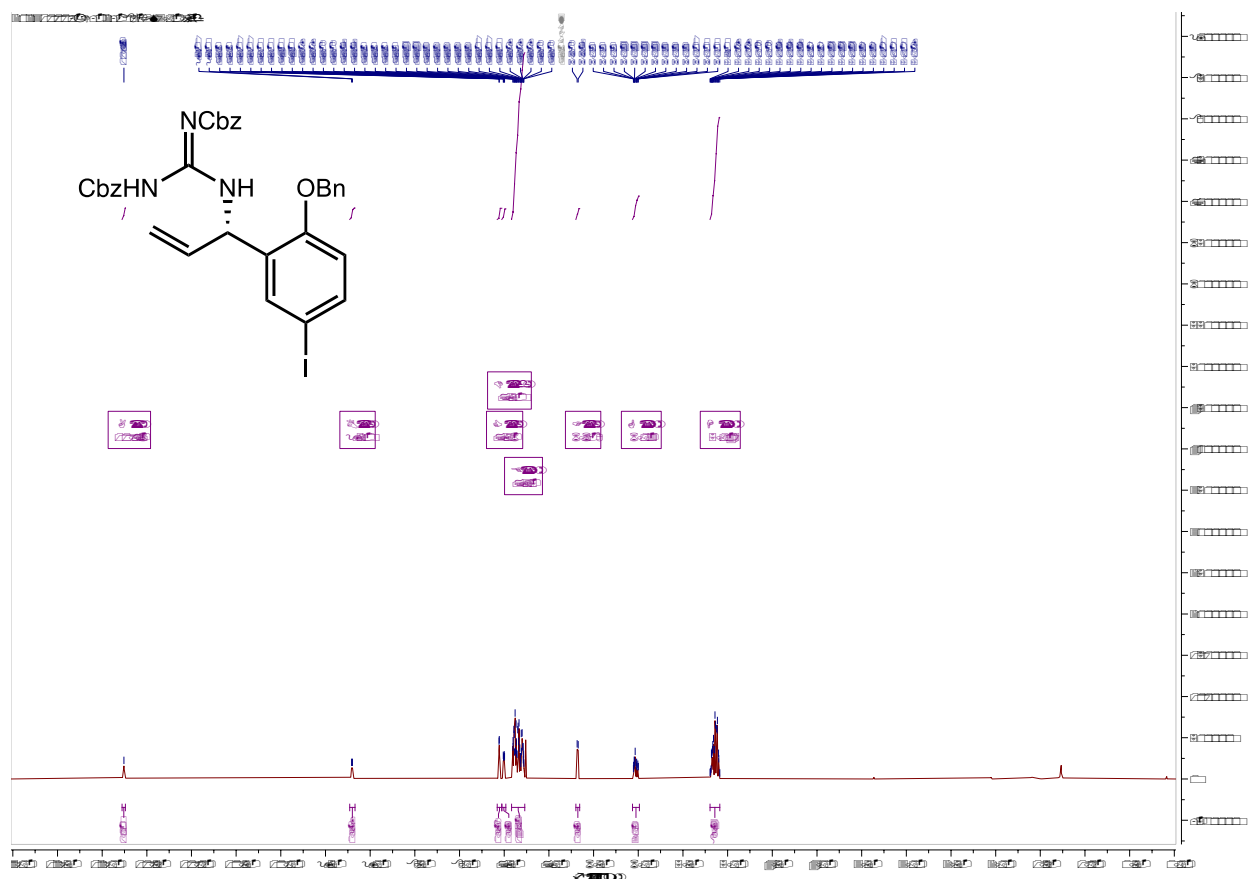
5.30: ^{13}C NMR 201 MHz, CDCl$_3$
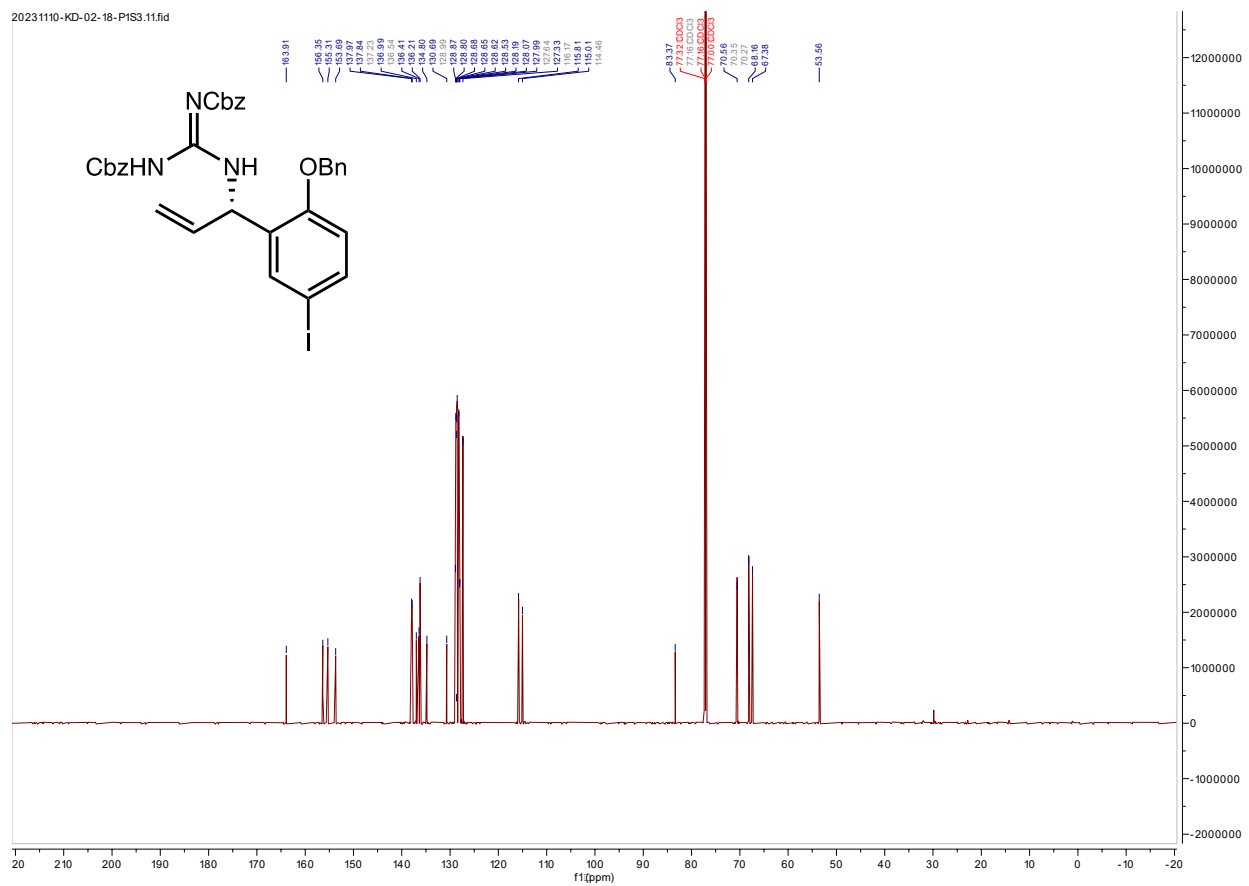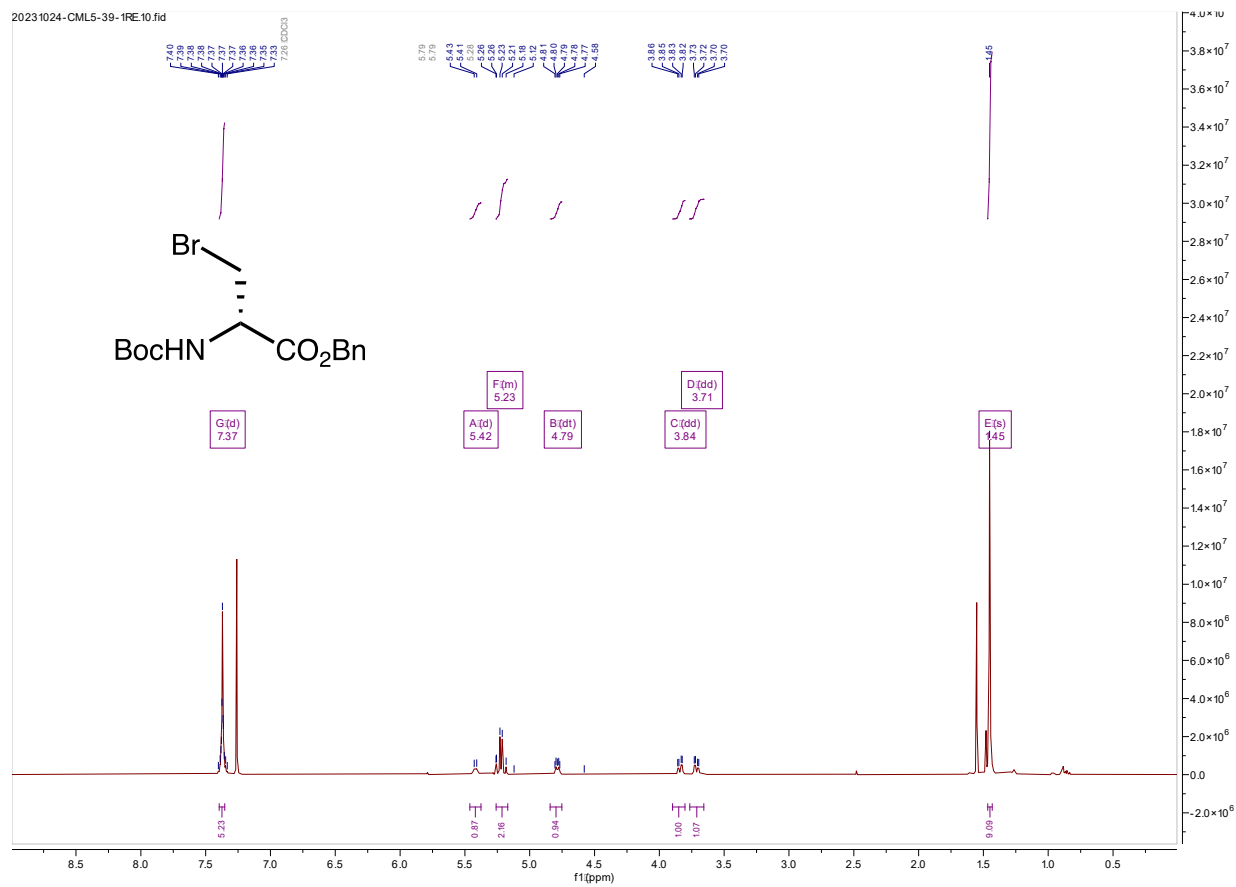
¹H NMR 400 MHz, CDCl₃

5.31: [^1]H NMR 400 MHz, CDCl$_3$

20240111-CML5-43B118.1.fid

5.31 ^{13}C NMR 101 MHz, CDCl$_3$

20240307-KD02-24-4Carbons.11.fid

5.33: ^{1}H NMR 500 MHz, CDCl$_3$

CML0005-001-001
Gradient Shimming

| A (d) 7.77 | C (m) 7.37 |
| B (d) 7.59 | |

| E (h) 5.20 |
| D (d) 5.44 |

| H (d) 4.41 |
| F (td) 4.55 | G (t) 4.22 |

| K (m) 1.99 |
| I (m) 2.47 | J (m) 2.17 |
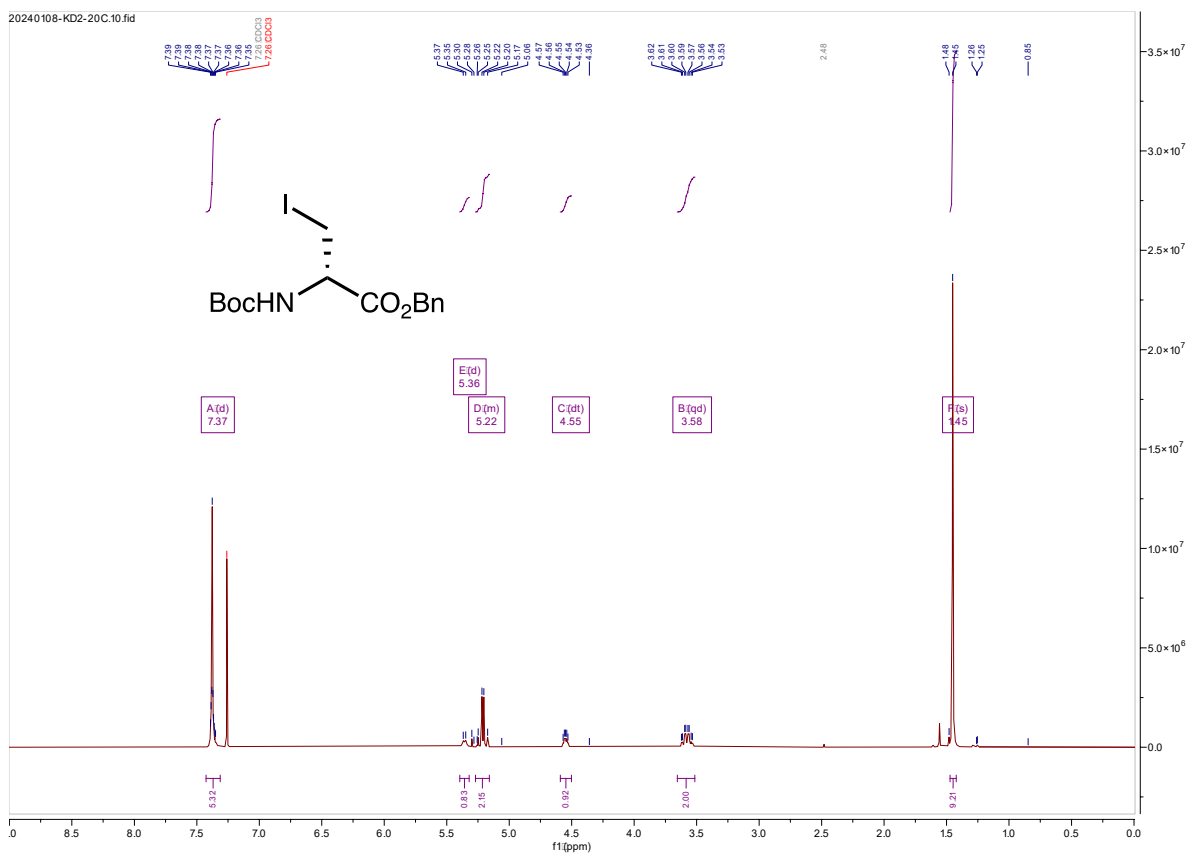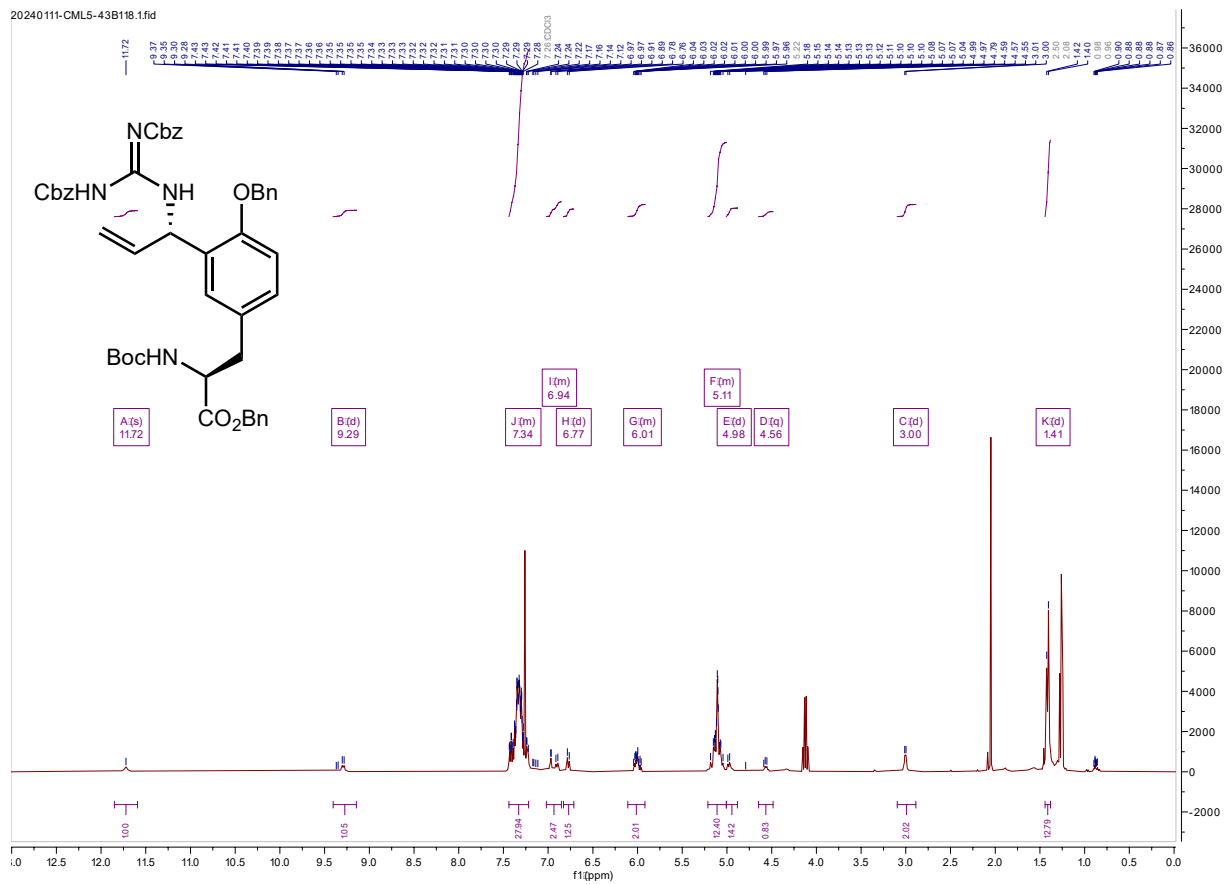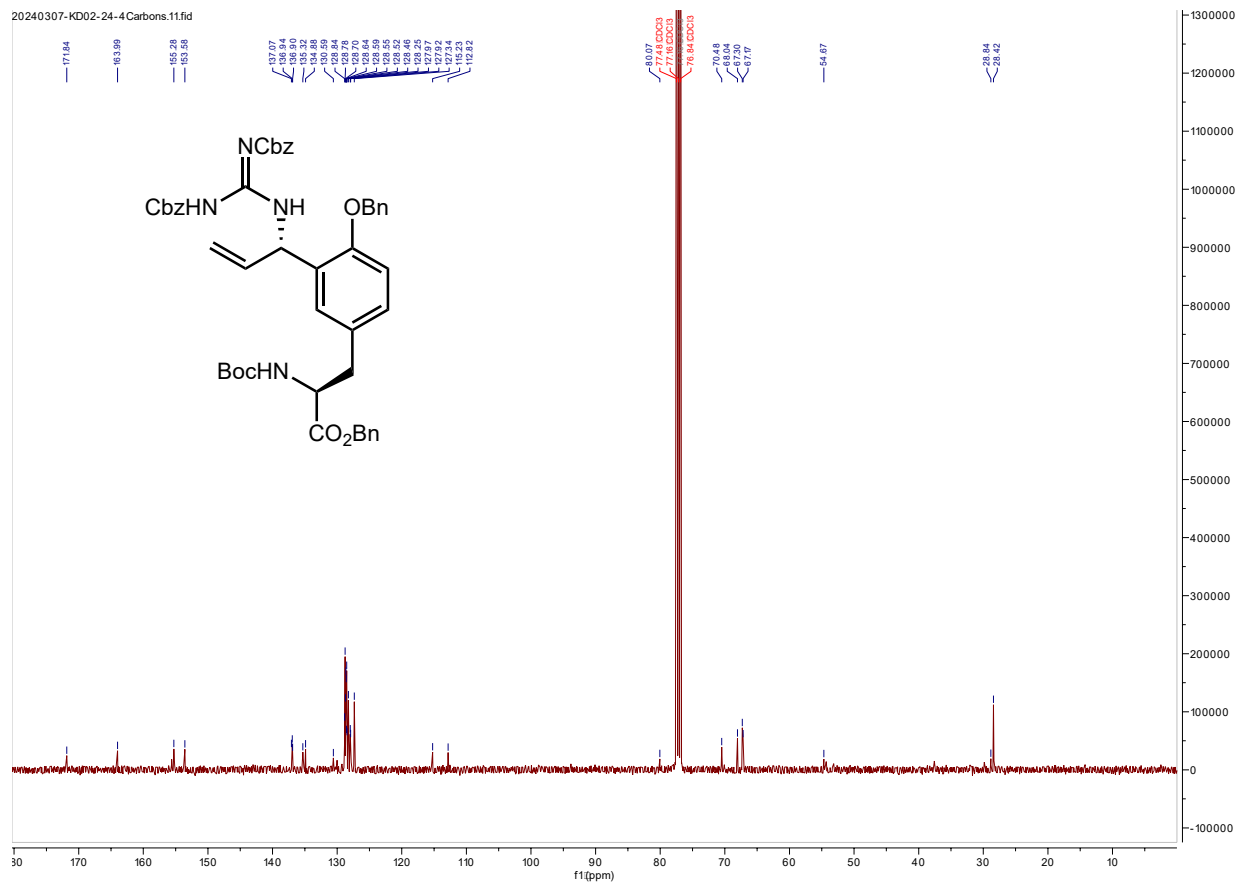
5.34: ^{1}H NMR 500 MHz, CDCl$_3$
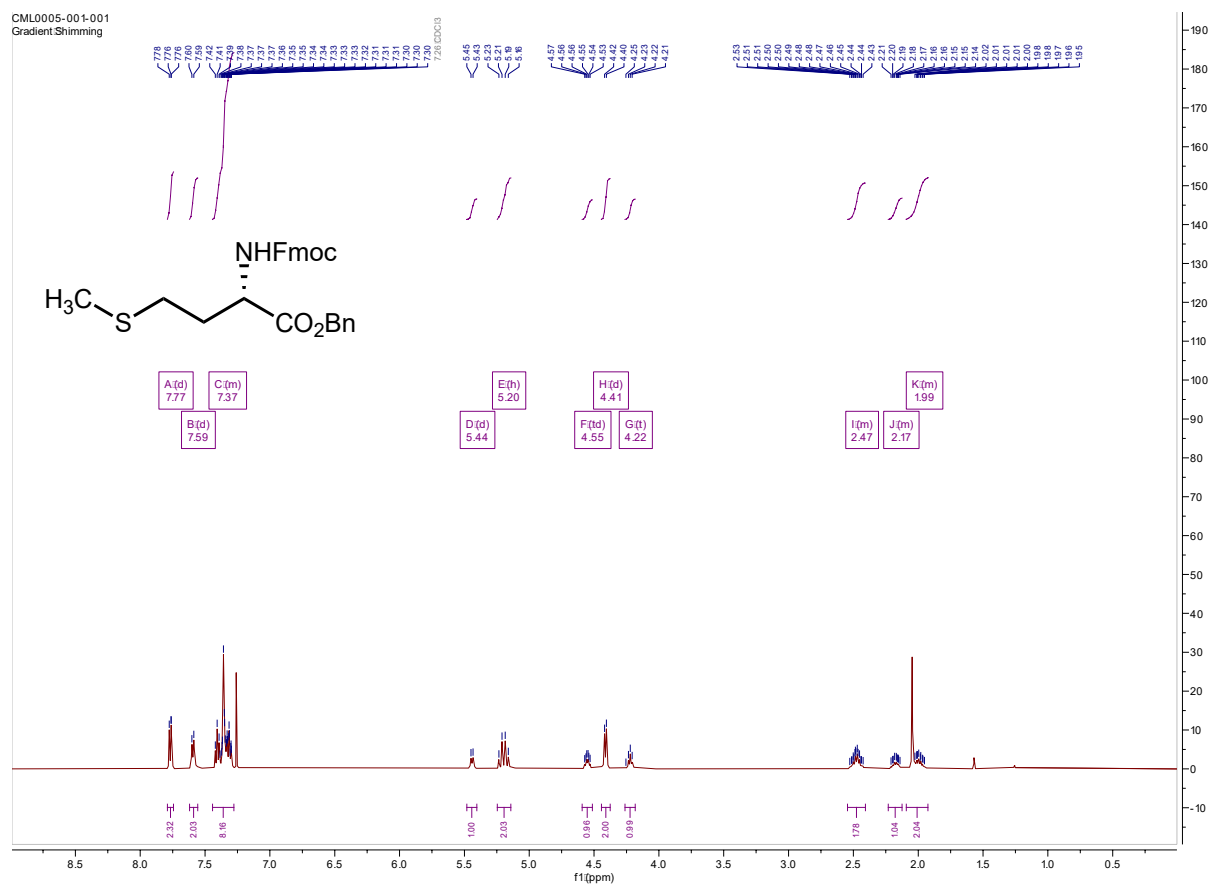
5.35: ^{1}H NMR 400 MHz, CDCl$_3$
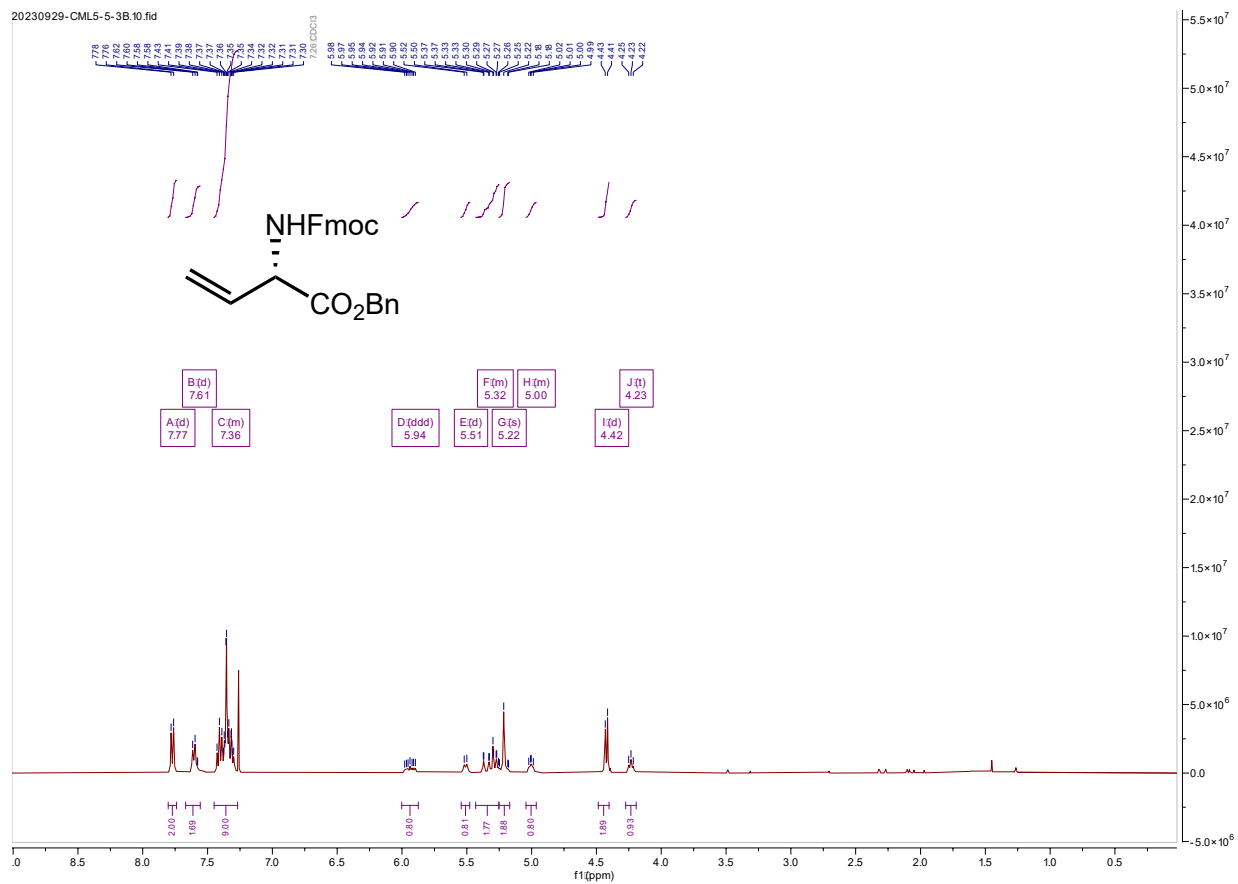
5.36: ^{1}H NMR 400 MHz, CDCl$_3$
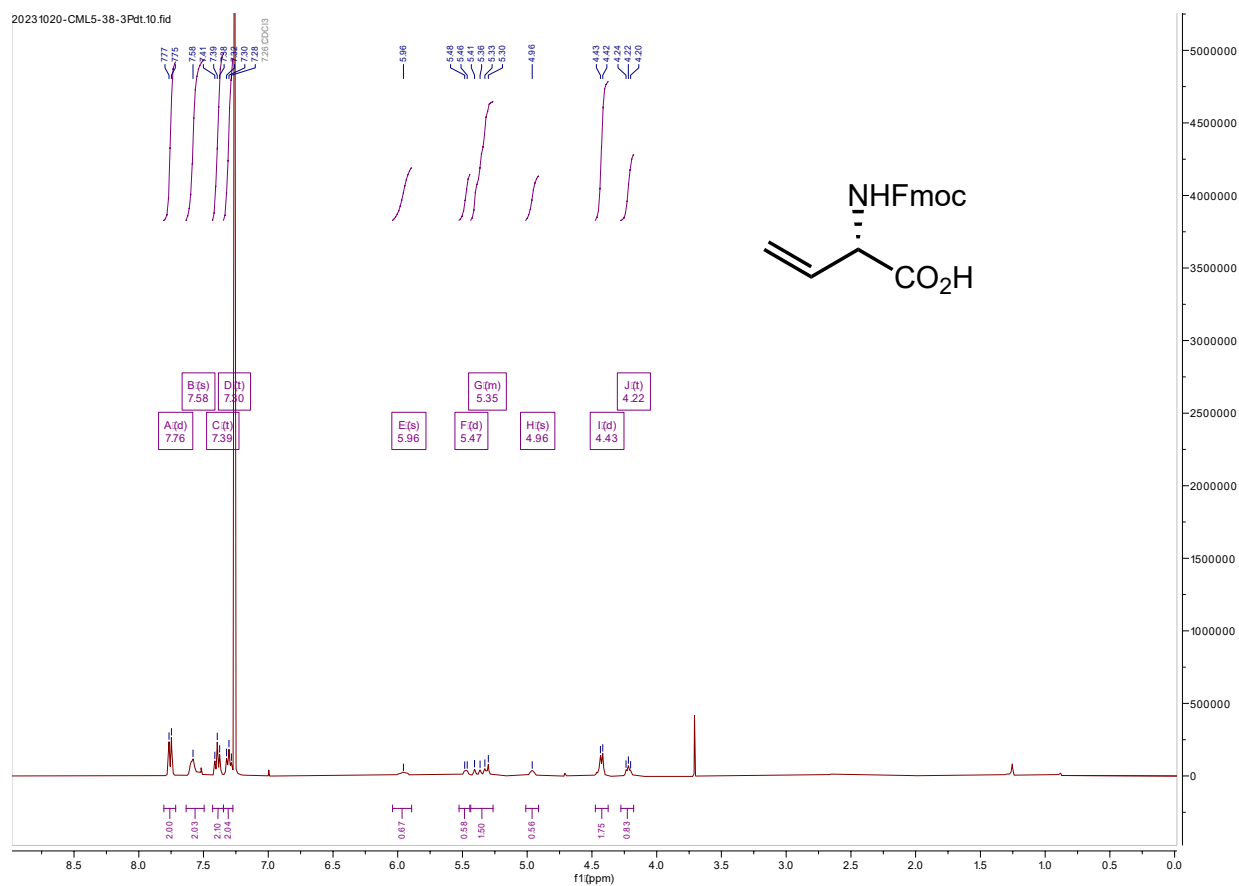
5.38: ^{1}H NMR 400 MHz, CDCl$_3$

5.38 ^{13}C NMR 201 MHz, CDCl$_3$

20231211-CML5-44pk3.11.fid
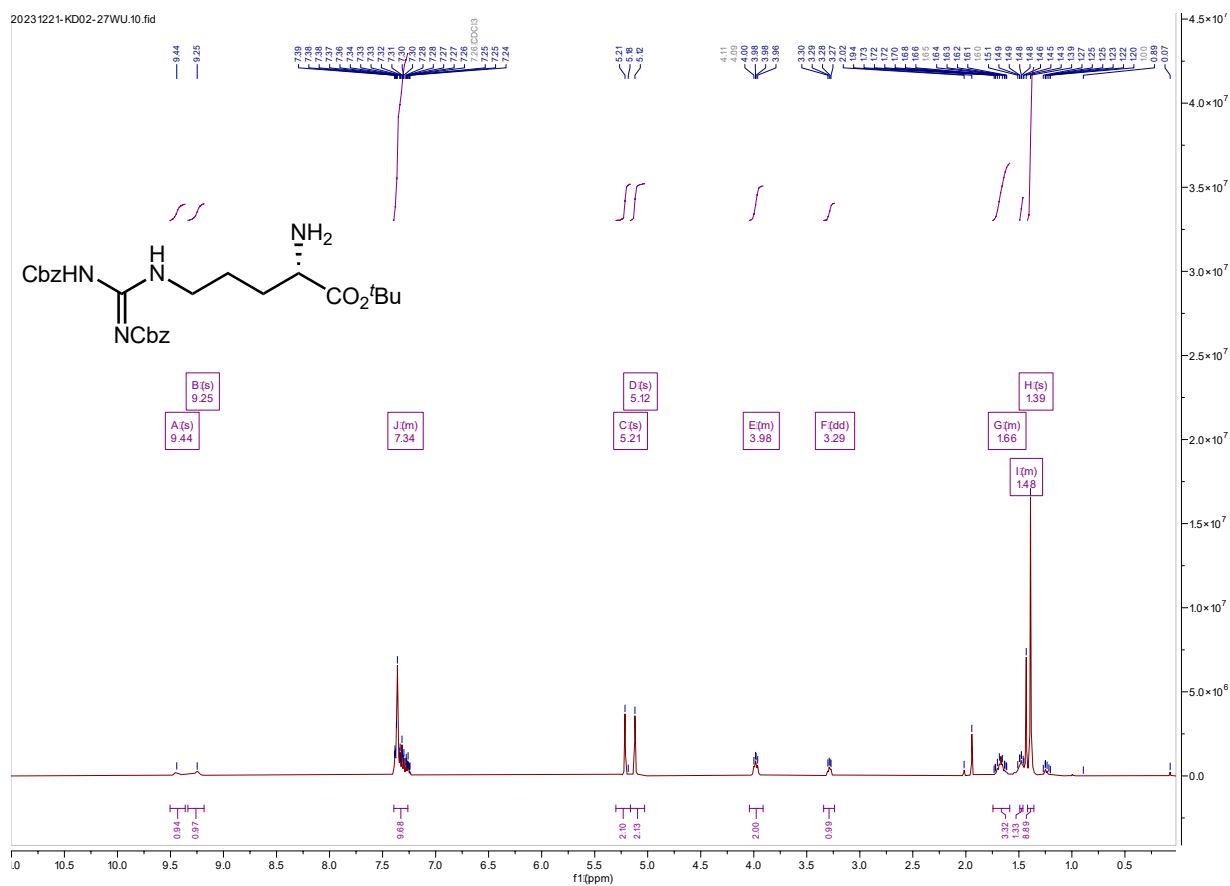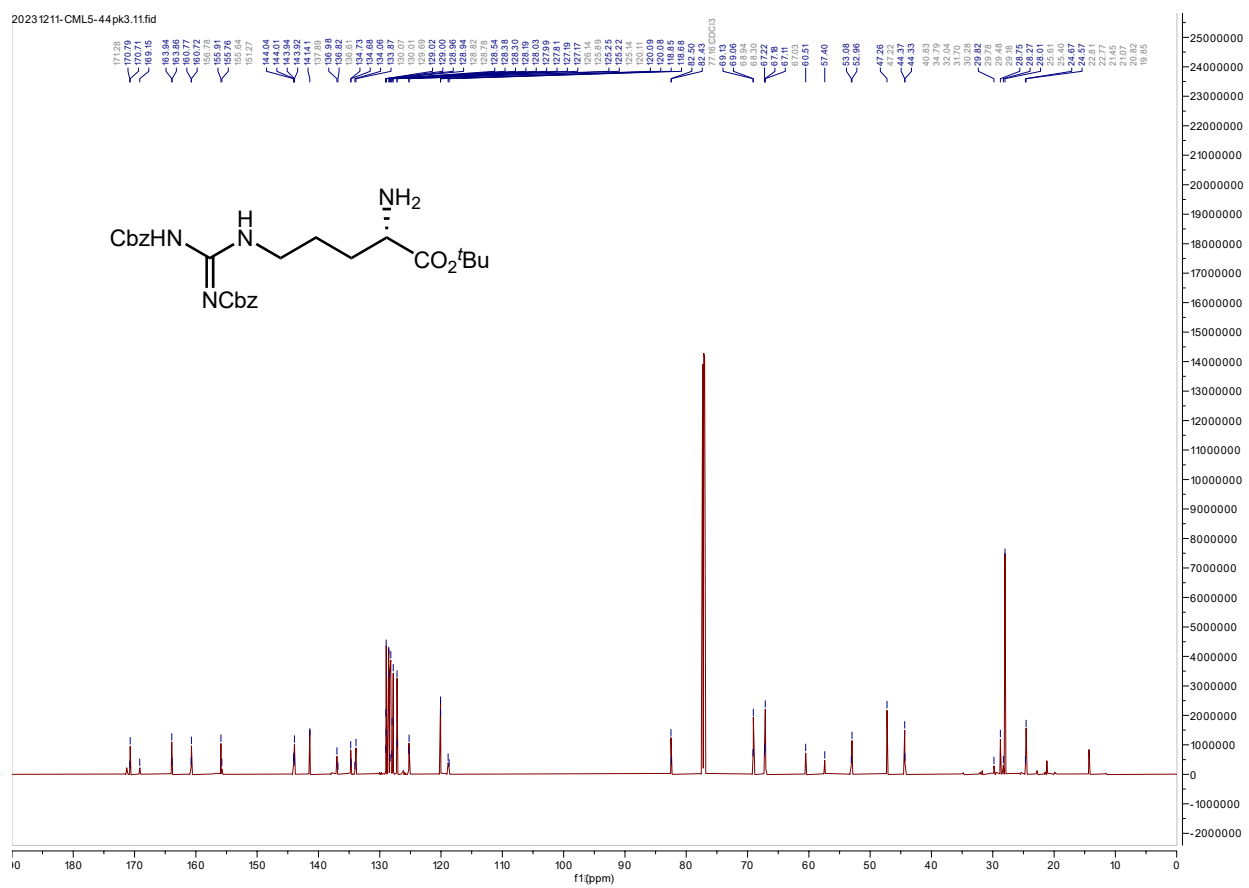
4.45: ^{1}H NMR 800 MHz, CDCl$_3$
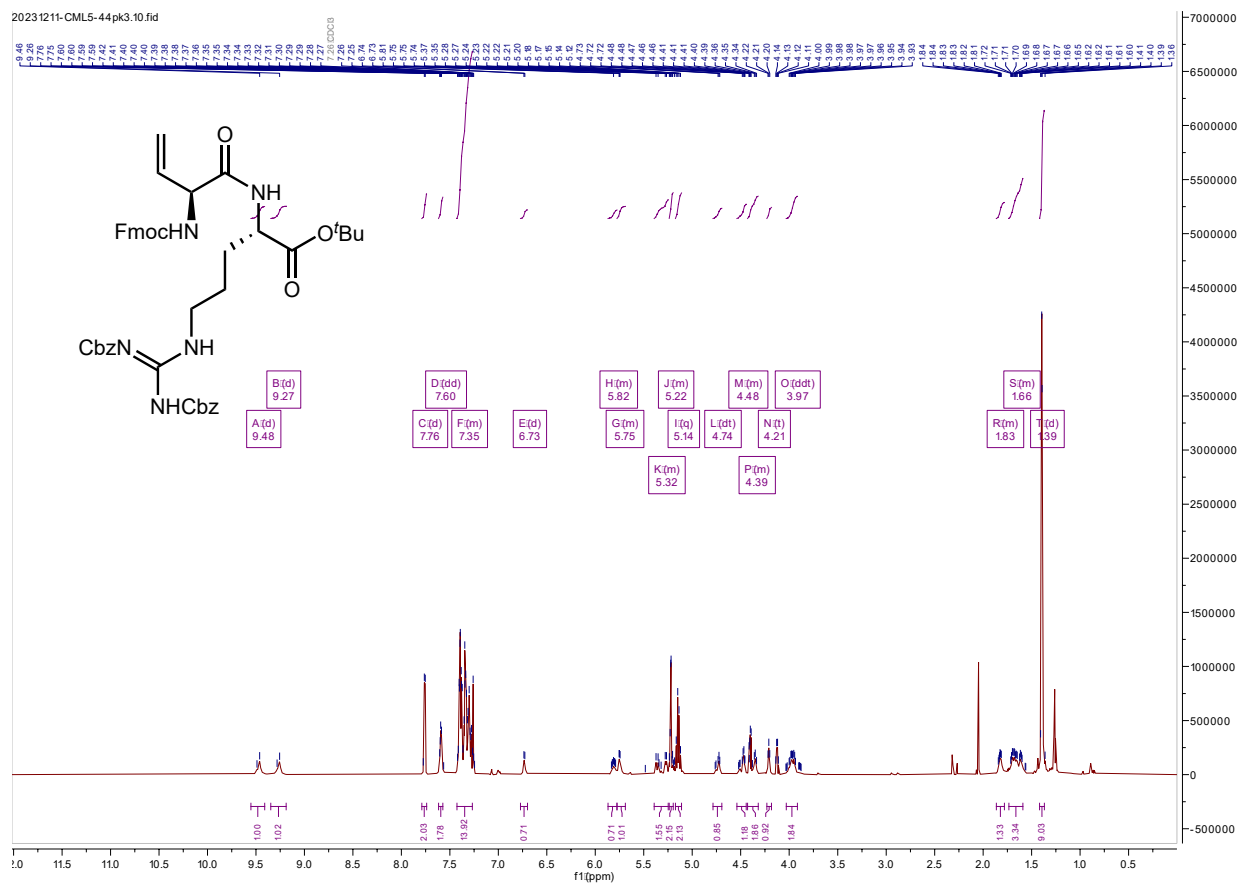
4.45: ^{13}C NMR 201 MHz, CDCl$_3$

20231211-CML5-44pk3.11.fid
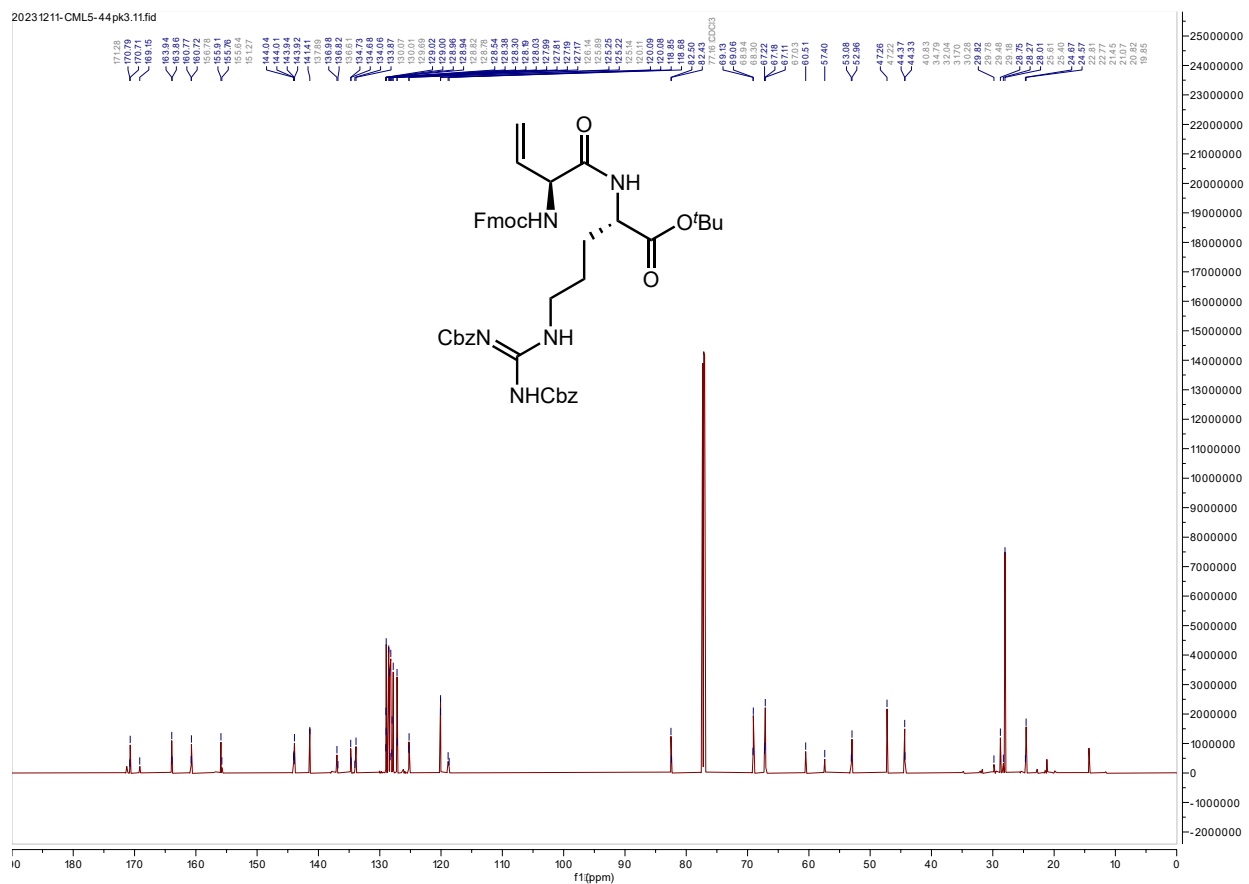
5.32: ^{1}H NMR 800 MHz, CDCl$_3$
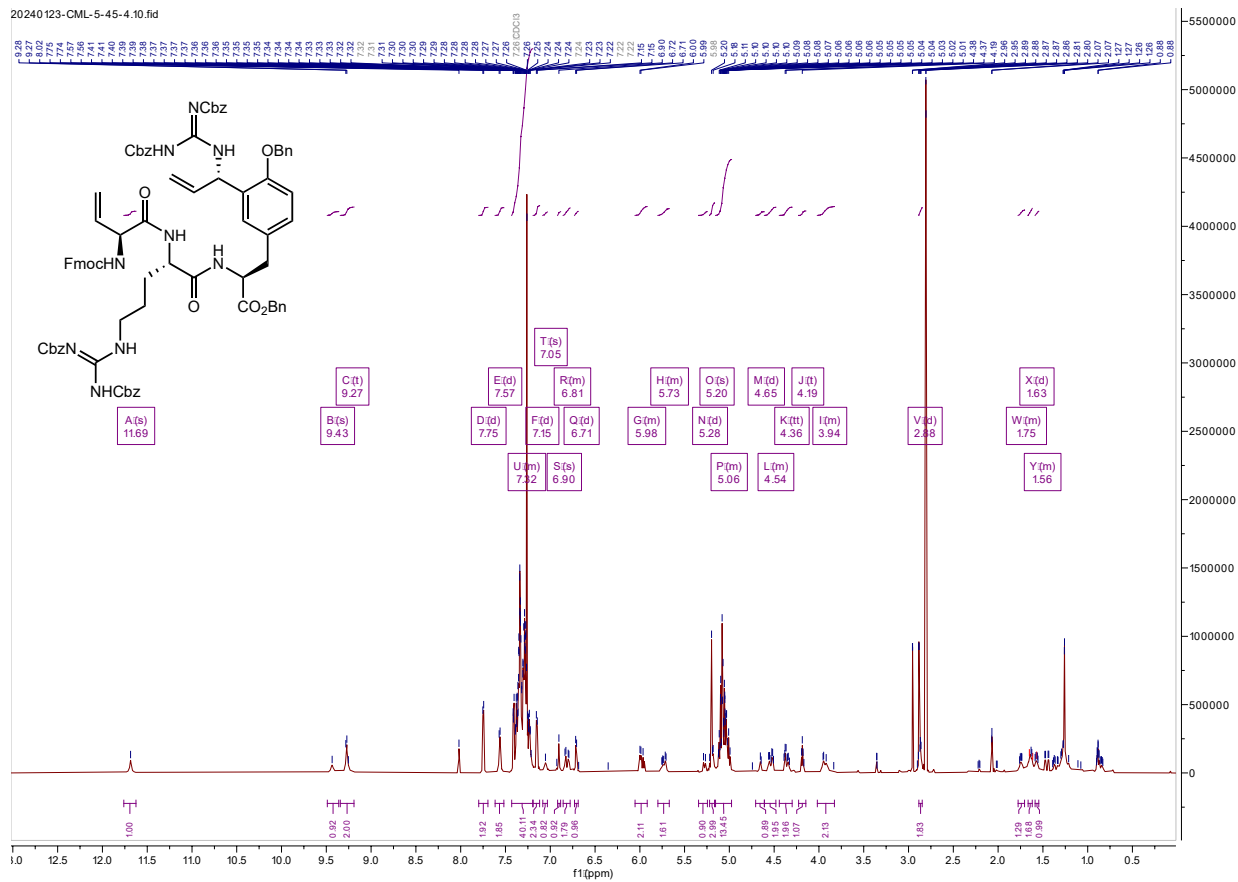
5.32: ^{13}C NMR 201 MHz, CDCl$_3$
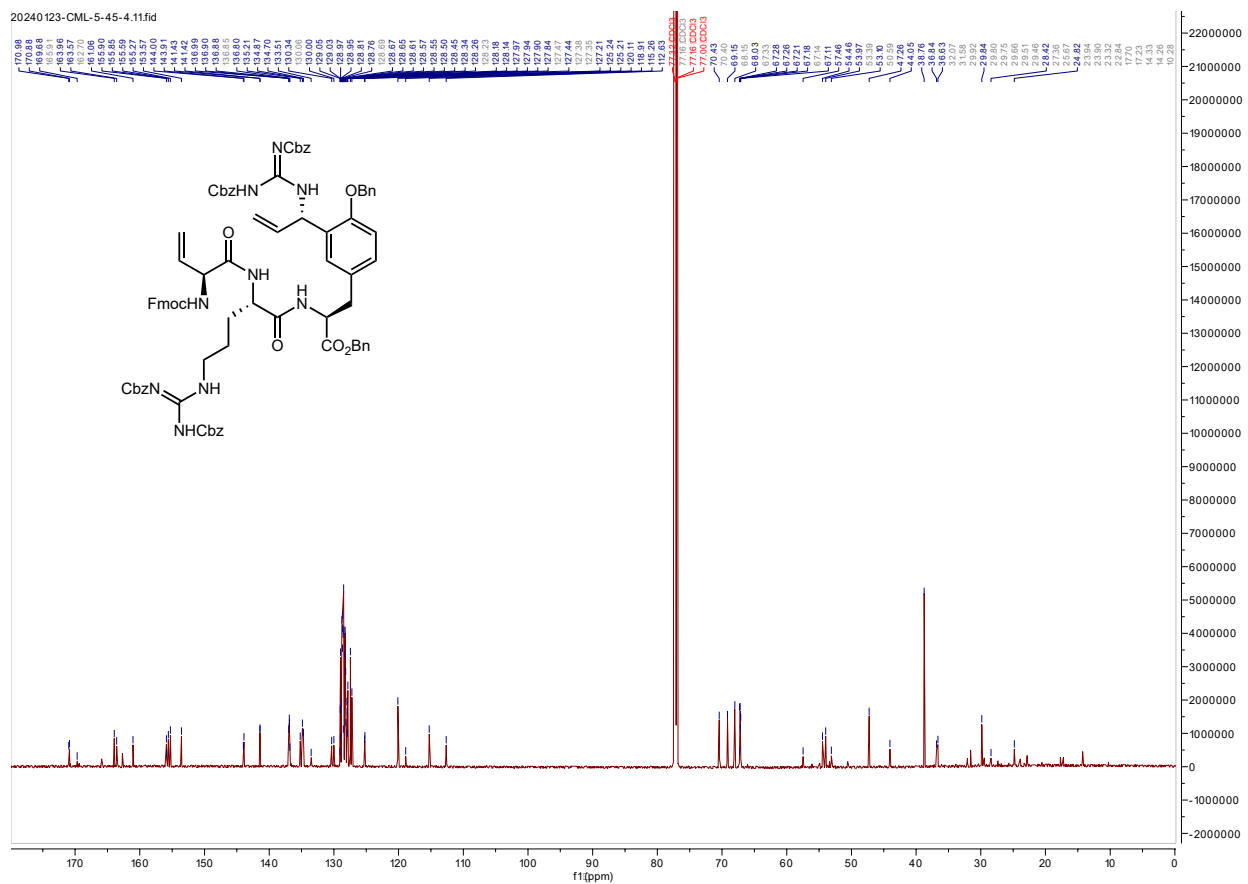
5.39 ^{1}H NMR 400 MHz, CDCl$_3$
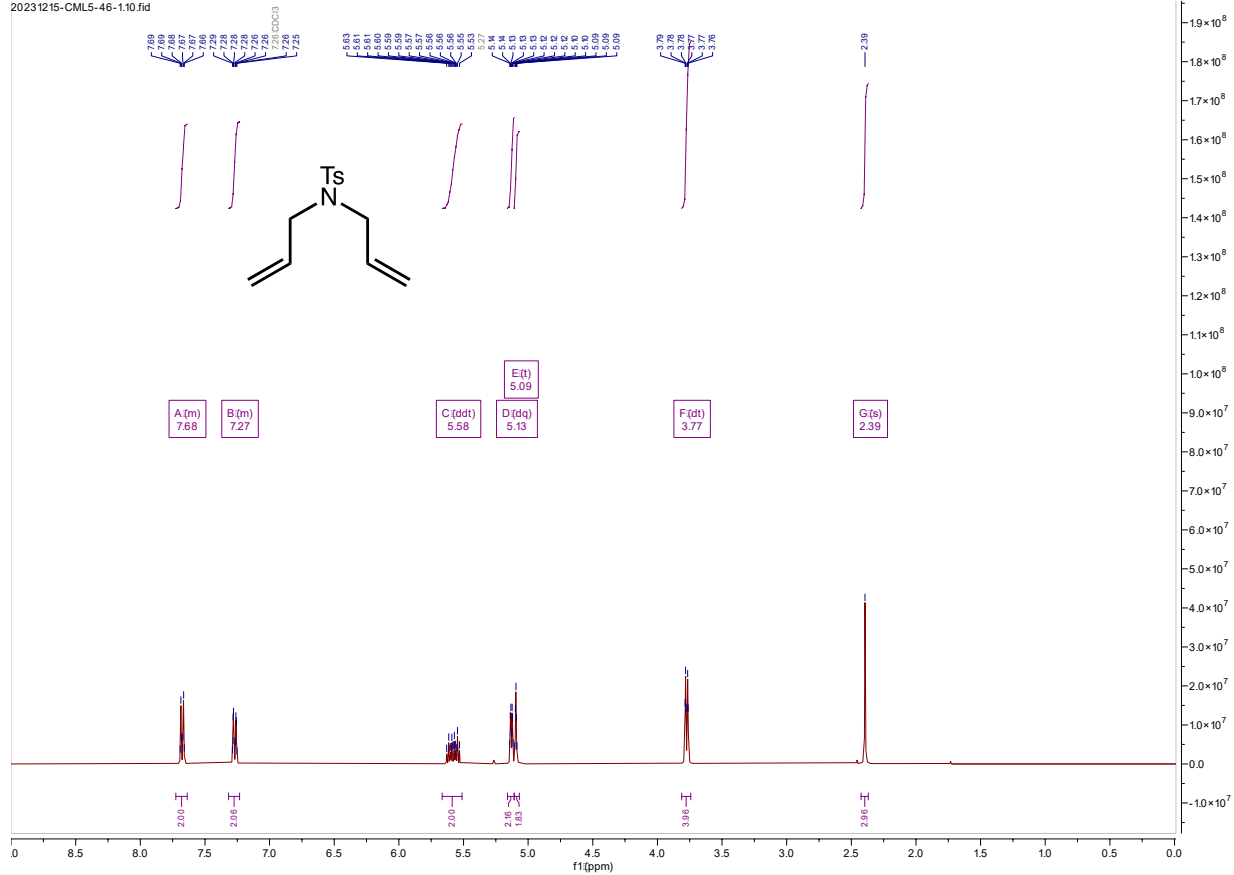
5.40 ^{1}H NMR 400 MHz, CDCl$_3$
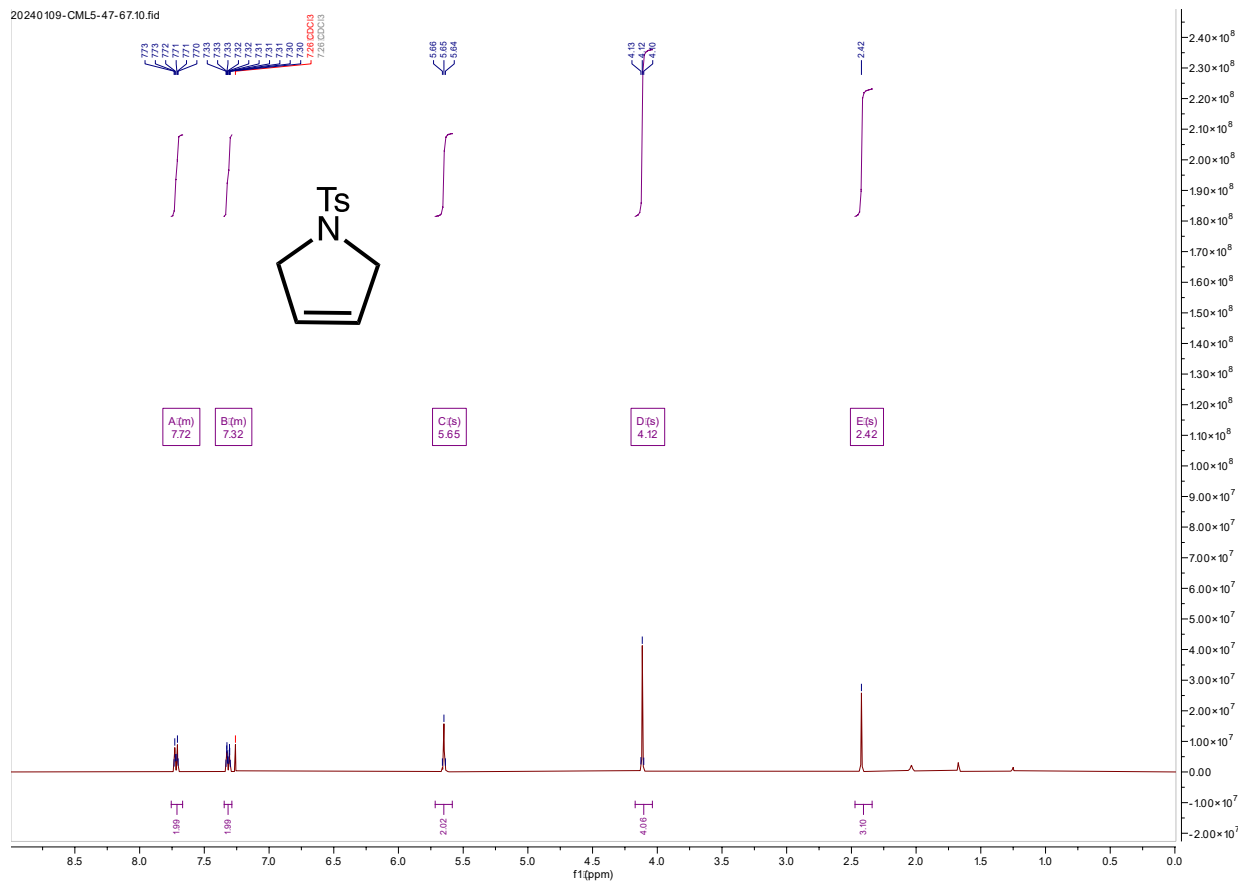
5.7.3 References

(1) Kundu, I.; Maitra, R.; Jana, M.; Chattopadhyay, S. K. A Stereodivergent Route to Four Stereoisomeric 3'-Acetoxycyclopentenylglycine Derivatives. *Synthesis* **2012**, *44* (02), 304-310. DOI: 10.1055/s-0031-1289645.

(2) Saha, P.; Madhavan, N. Macrocyclic Transmembrane Anion Transporters via a One-Pot Condensation Reaction. *Organic Letters* **2020**, *22* (13), 5104-5108. DOI: 10.1021/acs.orglett.0c01699.

(3) Knör, S.; Laufer, B.; Kessler, H. Efficient Enantioselective Synthesis of Condensed and Aromatic-Ring-Substituted Tyrosine Derivatives. *The Journal of Organic Chemistry* **2006**, *71* (15), 5625-5630. DOI: 10.1021/jo060704c.

(4) Kosuge, S.; Araki, Y.; Tsuge, K.; Sugimoto, K.; Matsuya, Y. One-Pot Synthesis of Pentasubstituted Pyridines following the Gold(I)-Catalyzed Aza–Enyne Metathesis/6π-Electrocyclization–Aromatization Sequence. *The Journal of Organic Chemistry* **2023**, *88* (11), 6973-6986. DOI: 10.1021/acs.joc.3c00270.

(5) Dai, C.; Han, Y.; Liu, L.; Huang, Z.-B.; Shi, D.-Q.; Zhao, Y. Palladium-catalyzed ortho-selective C–H hydroxylation of carboxybenzyl-protected benzylamines. *Organic Chemistry Frontiers* **2020**, *7* (13), 1703-1708, 10.1039/C9QO01523J. DOI: 10.1039/C9QO01523J.

(6) Nguyen, T. X.; Abdelmalak, M.; Marchand, C.; Agama, K.; Pommier, Y.; Cushman, M. Synthesis and Biological Evaluation of Nitrated 7-, 8-, 9-, and 10-Hydroxyindenoisoquinolines as Potential Dual Topoisomerase I (Top1)–Tyrosyl-DNA Phosphodiesterase I (TDP1) Inhibitors. *Journal of Medicinal Chemistry* **2015**, *58* (7), 3188-3208. DOI: 10.1021/acs.jmedchem.5b00136.

(7) Zhu, X.; Schmidt, Richard R. Efficient Synthesis of Differently Protected Lanthionines via β-Bromoalanine Derivatives. *European Journal of Organic Chemistry* **2003**, *2003* (20), 4069-4072. DOI: https://doi.org/10.1002/ejoc.200300336 (acccessed 2024/03/04).

(8) Trost, B. M.; Rudd, M. T. Chemoselectivity of the Ruthenium-Catalyzed Hydrative Diyne Cyclization: Total Synthesis of (+)-Cylindricine C, D, and E. *Organic Letters* **2003**, *5* (24), 4599-4602. DOI: 10.1021/ol035752n.

(9) Li, D.; Zhang, X.; Ma, X.; Xu, L.; Yu, J.; Gao, L.; Hu, X.; Zhang, J.; Dong, X.; Li, J.; et al. Development of Macrocyclic Peptides Containing Epoxyketone with Oral Availability as Proteasome Inhibitors. *Journal of Medicinal Chemistry* **2018**, *61* (20), 9177-9204. DOI: 10.1021/acs.jmedchem.8b00819.

(10) Wu, H.; Zhang, Y.; Li, Y.; Xu, J.; Wang, Y.; Li, X. Chemical Synthesis and Biological Evaluations of Adiponectin Collagenous Domain Glycoforms. *Journal of the American Chemical Society* **2021**, *143* (20), 7808-7818. DOI: 10.1021/jacs.1c02382.

(11) Masuda, Y.; Maruyama, C.; Kawabata, K.; Hamano, Y.; Doi, T. Synthesis of (2S,3R,4R)-3,4-dihydroxyarginine and its inhibitory activity against nitric oxide synthase. *Tetrahedron* **2016**, *72* (36), 5602-5611. DOI: https://doi.org/10.1016/j.tet.2016.07.050.

(12) Kastrinsky, D. B.; Kumar, P.; Marriner, G. A.; Barry, C. E., III. A Convergent Synthesis of Chiral Diaminopimelic Acid Derived Substrates for Mycobacterial l,d-Transpeptidases. *Synthesis* **2012**, *44* (19), 3043-3048. DOI: 10.1055/s-0032-1316774.

(13) Schnell, S. D.; Hoff, L. V.; Panchagnula, A.; Wurzenberger, M. H. H.; Klapötke, T. M.; Sieber, S.; Linden, A.; Gademann, K. 3-Bromotetrazine: labelling of macromolecules via monosubstituted bifunctional s-tetrazines. *Chemical Science* **2020**, *11* (11), 3042-3047, 10.1039/C9SC06169J. DOI: 10.1039/C9SC06169J.

(14) Kawauchi, D.; Noda, K.; Komatsu, Y.; Yoshida, K.; Ueda, H.; Tokuyama, H. Aerobic Dehydrogenation of N-Heterocycles with Grubbs Catalyst: Its Application to Assisted-Tandem

Catalysis to Construct N-Containing Fused Heteroarenes. *Chemistry – A European Journal* **2020**, *26* (68), 15793-15798. DOI: https://doi.org/10.1002/chem.202001961 (acccessed 2024/03/06).